

THE APPLICATION OF MECHANISTIC MODELLING AS A TOOL IN  
DRUG DISPOSITION AND RISK ASSESSMENT

ZARIL HARZA ZAKARIA

Doctor of Philosophy

ASTON UNIVERSITY

June 2018

© Zaril Harza Zakaria, 2018

Zaril Harza Zakaria asserts his moral right to be identified as the author of this  
thesis

This copy of the thesis has been supplied on condition that anyone who consults  
it is understood to recognise that its copyright rests with its author and that no  
quotation from the thesis and no information derived from it may be published  
without appropriate permission or acknowledgement.

## THESIS SUMMARY

New molecular entities entering the pharmaceutical market are required to adhere to stringent safety, efficacy and quality requirements that often lead to delays in the early-phases of drug development. Pharmacokinetic modelling approaches, such as physiologically-based pharmacokinetic (PBPK) modelling, can cater to most of the critical PK issues and at the same time optimise the utilising of resources. The overall aim of this work was to illustrate, explore and facilitate the application of PBPK modelling in the context of drug disposition and risk assessment. In Chapter 2 of this thesis, we illustrated the concept of developing customisable pharmacokinetic models through the development of a region-specific CNS PBPK model to assess the rodent hippocampus and frontal cortex pharmacokinetics using MATLAB. We then extrapolated the model to predict human regional brain pharmacokinetics, using morphine as a case study for comparison. This successfully proposed a simplified first-principle approach to the development of a regional brain central nervous system (CNS) PBPK model. This approach has significant implications for assessing drug disposition across the human CNS and provides an opportunity for exploring the relationship between regional brain drug concentration, pharmacodynamics effects, and interspecies extrapolation.

In Chapter 3 of this thesis, our goal was to develop a population-based PBPK modelling that could explore the potential risk of drug-drug interactions (DDIs) in adults and paediatric populations. We developed a model capable of predicting the impact of efavirenz-mediated DDIs on the pharmacokinetics of the antimalarial drug lumefantrine in Ugandan paediatric population groups, whilst also accounting for the polymorphic nature of CYP2B6. We demonstrated that an extension of the current artemether-lumefantrine treatment regimen from 3-days to 7-days would counteract the reduction in efavirenz metabolism common with the  $*6/*6$  genotype and hence enhance the attainment of the target day-7 lumefantrine concentration in both  $*1/*1$  and  $*6/*6$  genotype groups, thereby reducing the risk of malaria parasite recrudescence. This study demonstrated the capability of PBPK modelling in predicting PK profiles in special population such as paediatrics and dealing with complex DDIs associated with genotype specific effects.

The final part of this work, Chapter 4, focussed on demonstrating the capability of PBPK modelling in addressing inter-ethnicity variability and risk assessments within a mixed population group. We explored the application of PBPK models for specific population data analyses in the context of CYP2C19 polymorphism on clopidogrel in the multi-ethnic populations of Malaysia. We demonstrated a statistically significant difference in the peak concentrations of the active metabolite, clopi-H4, between the extensive metaboliser (EM) and poor metaboliser (PM) phenotypes with either Malay or Malaysian Chinese population groups. The study directly addresses this inter-ethnicity variability and provide a research tool that brings together the complexity of systems-biology with the ease-of-use applicability of pharmacokinetic modelling to provide a robust predictive platform which can easily be adapted and developed as required within a population.

### **Keywords:**

PBPK; CNS; malaria; HIV; paediatrics; clopidogrel; Malaysian

## **ACKNOWLEDGEMENTS**

First and foremost, all my praise goes to God, the Most Gracious, the Most Merciful.

Deepest gratitude to my supervisor Dr. Raj K. S. Badhan for your tireless efforts and guidance throughout these years. You are, without a doubt, an excellent supervisor and teacher.

To my associate supervisors, Professor Gavin Woodhall, and Dr Alan Fong, thank you for your facilitation throughout this stage of the project.

Thank you to the Ministry of Health Malaysia, for the approval of my sponsorship to undertake my studies at Aston University.

To my mentor, Dr. Kamaruzaman Saleh, I am grateful for all the guidance and support that you gave me. It has been a pleasure working with you.

To both my parents, I am proud to be your son. Thank you for bringing me up to this world and all the life lessons that you have given me.

There is ordinary, and then there is you, my dear wife, Noraziemah. I'm so grateful for your tireless support through thick and thin of this journey. And, last but not least, to my daughter Haifa, you complete me...I love you both.

## TABLE OF CONTENTS

<b>THESIS SUMMARY</b> .....	<b>2</b>
<b>ACKNOWLEDGEMENTS</b> .....	<b>3</b>
<b>LIST OF ABBREVIATIONS</b> .....	<b>7</b>
<b>LIST OF FIGURES</b> .....	<b>11</b>
<b>LIST OF TABLES</b> .....	<b>14</b>
<b>LIST OF PUBLICATIONS</b> .....	<b>16</b>
<b>CHAPTER 1 Introduction to mechanistic pharmacokinetic approaches</b> .....	<b>18</b>
1.1 BACKGROUND .....	19
1.1.1 Modelling and simulation in drug development .....	20
1.2 PHARMACOKINETIC MODELLING .....	24
1.2.1 Compartmental modelling .....	25
1.2.2 Non-compartmental analysis .....	31
1.2.3 Population pharmacokinetics .....	34
1.3 ALLOMETRIC SCALING IN PHARMACOKINETICS MODELLING .....	35
1.4 MECHANISTIC APPROACHES: PBPK MODELLING .....	37
1.4.1 PBPK modelling equations and assumptions .....	42
1.4.2 <i>In vitro</i> to <i>in vivo</i> scaling in PBPK modelling .....	44
1.5 PBPK AND POPULATION VARIABILITY .....	50
1.5.1 Absorption .....	52
1.5.2 Distribution .....	53
1.5.3 Metabolism .....	54
1.5.4 Elimination .....	55
1.6 STRATEGIES FOR DEVELOPING A PBPK MODEL .....	56
1.6.1 Development of tentative models .....	57
1.6.2 Designing and performing experiment .....	58
1.6.3 Exploring data .....	58
1.6.4 Model fitting .....	59
1.6.5 Analysing outputs .....	60
1.7 PBPK MODELLING SOFTWARE .....	62
1.8 ROLE OF PREDICTIVE MODELS FOR DRUG DELIVERY .....	63
1.8.1 Regulatory Perspectives .....	65
1.9 AIMS AND OBJECTIVES .....	77
<b>CHAPTER 2 Target tissue pharmacokinetics: the application of PBPK modelling to predict regional brain pharmacokinetics</b> .....	<b>80</b>
2.1 INTRODUCTION .....	81
2.1.1 Background .....	81
2.1.2 Brain penetration .....	81
2.1.3 Quantifying CNS drug delivery .....	86
2.2 METHODS .....	96
2.2.1 Step 1: a whole-body physiologically based pharmacokinetic (PBPK) CNS model .....	97
2.2.2 Step 2: development of a rat regional brain PBPK sub-model .....	107

2.2.3	Step 3: development of a human regional brain PBPK sub-model .....	111
2.2.4	Data and statistical analysis .....	114
2.3	RESULTS .....	114
2.3.1	Step 1: Validation of the PBPK Model.....	114
2.3.2	Step 2: development of a rat regional brain PBPK sub-model.....	115
2.3.3	Step 3: development of a human regional brain PBPK sub-model .....	122
2.4	DISCUSSION .....	126
2.4.1	Validation of the PBPK Model.....	126
2.4.2	Prediction of regional brain concentrations in rats .....	127
2.4.3	Prediction of regional brain concentrations in humans .....	128
2.5	CONCLUSIONS.....	130
<b>CHAPTER 3 Utility of PBPK modelling in dose optimisation for complex drug-drug interactions in HIV- and malaria- infected children .....</b>		<b>132</b>
3.1	INTRODUCTION.....	133
3.1.1	Background .....	133
3.1.2	Malaria .....	133
3.1.3	Human Immunodeficiency Virus (HIV).....	135
3.1.4	Malaria and HIV co-infection.....	137
3.1.5	Genetic polymorphisms .....	141
3.1.6	<i>CYP2B6</i> polymorphisms.....	143
3.1.7	Efavirenz and <i>CYP2B6</i> polymorphisms.....	144
3.2	METHODS .....	146
3.2.1	Compounds selection and development .....	146
3.2.2	Model development .....	148
3.2.3	Predictive performance .....	154
3.2.4	Data analysis .....	154
3.3	RESULTS .....	155
3.3.1	Characterisation of selected population .....	155
3.3.2	Step 1: Adult simulations with efavirenz.....	162
3.3.3	Step 2: Adult simulations with lumefantrine-efavirenz drug-drug interactions .....	167
3.3.4	Step 3: Paediatric simulations with efavirenz.....	172
3.3.5	Step 4: Paediatric simulations with lumefantrine-efavirenz drug-drug interactions.....	181
3.3.6	Step 5: Paediatric dose evaluation prediction .....	185
3.4	DISCUSSION .....	190
3.4.1	Characterisation of selected populations .....	191
3.4.2	Model validation and DDI dose evaluation in paediatric populations.....	192
3.5	CONCLUSION .....	196
<b>CHAPTER 4 The application of PBPK modelling to address the impact of inter-ethnic variability on the pharmacokinetics of drugs in Malaysian subjects.....</b>		<b>197</b>
4.1	INTRODUCTION.....	198
4.2	METHODS .....	202
4.2.1	Model development .....	203

4.2.2	Data analysis .....	208
4.2.3	Predictive performance .....	208
4.2.4	Visual predictive checks .....	209
4.3	RESULTS .....	209
4.3.1	Step 1: Malaysian population group development .....	209
4.3.2	Step 2: Adult simulation with repaglinide and tramadol .....	214
4.3.3	Step 3: Prediction of the impact of CYP2C19 polymorphisms on clopidogrel pharmacokinetics in Malaysians .....	220
4.3.4	Step 4: Sensitivity analysis for CYP2C19 hepatic abundances .....	226
4.3.5	Step 5: Dose optimization in CYP2C19 poor metabolisers.....	229
4.4	DISCUSSION .....	229
4.4.1	Step 1: Malaysian population development.....	232
4.4.2	Step 2: Adult simulations with repaglinide and tramadol.....	233
4.4.3	Step 3: Prediction of the impact of CYP2C19 polymorphisms on clopidogrel pharmacokinetics in Malaysians .....	234
4.4.4	Step 4: Sensitivity analysis for CYP2C19 hepatic abundances .....	236
4.4.5	Step 5: Dose optimization in CYP2C19 poor metabolisers.....	237
4.4.6	Study limitations and future directions for clopidogrel use in Malaysia.....	237
4.5	CONCLUSIONS.....	238
	<b>CHAPTER 5 Conclusions .....</b>	<b>239</b>
5.1	CONCLUSIONS.....	240
5.2	FUTURE WORK.....	243
	<b>REFERENCES.....</b>	<b>244</b>
	<b>APPENDIX A .....</b>	<b>280</b>
	<b>APPENDIX B .....</b>	<b>281</b>
	<b>APPENDIX C .....</b>	<b>283</b>
	<b>APPENDIX D .....</b>	<b>284</b>
	<b>APPENDIX E .....</b>	<b>286</b>

## LIST OF ABBREVIATIONS

AAG	Alpha-1-Acidic Glycoprotein
ABPI	Association of the British Pharmaceutical Industry
ACAT	Advanced Compartmental Absorption and Transit
ACT	Antimalarial Combination Therapy
ADAM	Advanced, Dissolution, Absorption and Metabolism
ADME	Absorption, Distribution, Metabolism, Excretion
AFE	Average Fold-Error
AIDS	Acquired Immune Deficiency Syndrome
ANDA	Abbreviated New Drug Applications
AUC	Area Under the Curve
AUMC	Area Under the First Moment of The Systemic Drug Concentration Curve
AZT	Zidovudine
B:P	Blood to Plasma Ratio
BB	Intravascular Blood (Brain Blood)
BBB	Blood Brain Barrier
BC	Intracellular Brain Space
BCEC	Primary or Low Passage Brain Capillary Endothelial Cells
BCRP	Breast Cancer Resistance Protein
BCS	Biopharmaceutical Classification System
BCSFB	Blood Cerebrospinal Fluid Barrier
BEI	Brain Efflux Index
BLA	Biologics License Applications
BMI	Body Mass Index
BT	Brain Tissue
BUI	Brain Uptake Index
BW	Body Weight
$C_{AR}$	Arterial Drug Input
CDC	Centres for Disease Control and Prevention
$C_{ev}$	Concentration in Extravascular Space
CF	Correction Factor
CL	Clearance
$CL_H$	Hepatic Clearance
$CL_{int}$	Intrinsic Clearance
$CL_{intapp}$	Apparent <i>in vitro</i> $CL_{int}$
$CL_{intscaled}$	Scaled <i>in vivo</i> $CL_{int}$
$CL_R$	Renal Clearance
CM	Cisterna Magna
$C_{max}$	Maximum (or peak) serum concentration that a drug achieves
CNS	Central Nervous System
CPTR	Critical Path to Tuberculosis Drug Regimens
CSF	Cerebrospinal Fluid
$C_T$	Drug Concentration of the Respective Tissues

C <sub>v</sub>	Concentration of Drug at Venous
CVD	Cardiovascular Disease
CYP	Cytochrome
DDI	Drug-Drug Interactions
ECF	Extra Cellular Fluid
ECF	Extracellular Fluid
EFV	Efavirenz
EM	Extensive Metabolisers
EMA	European Medicines Agency
EMA	European Agency for The Evaluation of Medicinal Products
ESAM	Endothelial-Specific Adhesion Molecule
ETV	Etravirine
EU	European Union
FC	Frontal Cortex
FD&C	Food, Drug and Cosmetics
FE	Fold-Error
FIH	First in Human
f <sub>up</sub>	Fraction Unbound of Drug in Plasma
f <sub>ut</sub>	Unbound Fraction of Drug at Tissue
g	Gram
GCP	Good Clinical Practice
GFR	Glomerular Filtration Rate
GLP	Good Laboratory Practice
GOF	Gain of Function
GST	Glutathione S-Transferase
HAART	Highly Active Antiretroviral Therapy
HBD	Hydrogen-Bonded Donors
HC	Hippocampus
HEK	Human Embryonic Kidney
HHS	Health and Human Services
HIV	Human Immunodeficiency Virus
HPGL	Hepatocellularity Per Gram of Liver
HSA	Human Serum Albumin
IAM	Immobilized Artificial Membrane Chromatography
ICF	Intracellular Fluid
IM	Intermediate Metabolisers
IND	Investigational New Drug
ISF	Interstitial Fluid
IUD	Intra-Uterine Device
IV	Intravenous
IVF	Intravascular Fluid
IVIVC	<i>In vitro-in vivo</i> Correlation
JAAME	Japan Association for The Advancement of Medical Equipment
JAM	Junctional Adhesion Molecules

K <sub>p</sub>	Tissue Partition Coefficient
LD	Loading Dose
LOF	Loss of Function
LogD	Log Distribution Coefficient
LogP <sub>OCT</sub>	Octanol/Water Partition Coefficient
LPV	Lopinavir
LUM	Lumefantrine
LV	Lateral Ventricle
LW	Liver Weight
MAA	Marketing Authorisation Application
MAT	Mean Absorption Time
MD	Multiple Dose
MD	Maintenance Dose
MDCK	Madin-Darby Canine Kidney
MDR	Multiple Drug Resistance
MHRA	Medicines and Healthcare Products Regulatory Agency
MPPGL	Milligrams of Microsomal Protein Per Gram
MRI	Magnetic Resonance Imaging
MRP	Multidrug Resistance Protein
MRT	Mean Residence Time
MSP	Microsomal Protein
MW	Molecular Weight
NAD	Naïve Averaged Data
NCA	Non-Compartmental Analysis
NCVD	National Cardiovascular Disease Database
NDA	New Drug Application
NME	New Molecular Entity
NNRTI	Non-Nucleoside Reverse Transcriptase Inhibitor
NPD	Naïve Pooled Data
NRTI	Nucleoside Analogue Reverse Transcriptase Inhibitors
NSAID	Non-Steroidal Anti-Inflammatory Drugs
NVP	Nevirapine
ODE	Ordinary Differential Equation
OPSR	Organisation for Pharmaceutical Safety and Research
PAMPA	Parallel Artificial Permeability Assay
P <sub>app</sub>	<i>In vitro</i> Permeability
PBPK	Physiologically-Based Pharmacokinetic
PE	Parameter Estimation
P <sub>eff</sub>	Human Effective Permeability
PET	Positron Emission Tomography
PI	Proteases Inhibitor
PK	Pharmacokinetics
PK/PD	Pharmacokinetic/Pharmacodynamic
PM	Poor Metabolisers

PMDA	Pharmaceuticals and Medical Devices Agency
PMDEC	Pharmaceuticals and Medical Devices Evaluation Centre
PPK	Population Pharmacokinetics
PS	Permeability Surface Area
PSA	Polar Surface Area
PS <sub>T</sub>	Permeability-Surface Area of Tissue
Q <sub>h</sub>	Hepatic Blood Flow
Q <sub>L</sub>	Liver Blood Flow Rate
QSAR	Quantitative Structure-Activity Relationship
Q <sub>T</sub>	Tissue Flow Rate
R <sub>b</sub>	Blood to Plasma Ratio
REF	Relative Expression Factor
RMSE	Root-Mean-Square Error
ROB	Rest of Brain
SAS	Subarachnoid Space
SD	Single Dose
SF	Scaling Factor
SLC	Solute Carrier
SNP	Single Nucleotide Polymorphism
SPECT	Single Photon Computed Tomography
TEER	Trans-Endothelial Electrical Resistance
TFV	Third and Fourth Ventricle
TJ	Tight Junction
T <sub>max</sub>	The time at which the C <sub>max</sub> is observed
UM	Ultra-Rapid Metabolisers
USFDA	United States Food and Drug Administration
VD	Volume of Distribution
VPC	Visual Predictive Checks
V <sub>T</sub>	Tissue Volume
WB-PBPK	Whole-Body Physiologically-Based Pharmacokinetic
WHO	World Health Organisation

## LIST OF FIGURES

Figure 1.1 Application of modelling and simulation during drug development. ....	20
Figure 1.2 Approaches used in pharmacokinetics modelling. ....	24
Figure 1.3 Diagrammatic representation of a one-compartment model and its plasma concentration-time profile. ....	26
Figure 1.4 Diagrammatic representation of a 2-compartment model and its plasma concentration-time profile. ....	29
Figure 1.5 Diagrammatic representation a of 3-compartment model and its plasma concentration-time profile. ....	31
Figure 1.6 Diagrammatic representation of the AUC in the plasma concentration-time profile and AUMC in the plasma concentration*time-time graphs. ....	32
Figure 1.7 Example of allometric scaling for plasma clearance. ....	36
Figure 1.8 Example of allometric scaling for volume of distribution. ....	36
Figure 1.9 Diagrammatic representation of the earliest PBPK models from Teorell, 1937 and the concentration-time profiles estimation in several compartments. ....	38
Figure 1.10 Schematic diagram of PBPK models. ....	41
Figure 1.11 Diagrammatic representation of perfusion vs permeability rate-limited tissue models. ....	42
Figure 1.12 Phase I and II CYP450 metabolism enzymes composition in the liver and intestine of the human body. ....	54
Figure 1.13 Diagrammatic representation of a nephron, delineating an area where active secretion, passive reabsorption, and filtration occur. ....	56
Figure 1.14 Development of a PBPK model: from data to model. ....	57
Figure 1.15 Relationship between the residual error ( $\epsilon$ ), the observed concentration ( $C_{obs}$ ) and the predicted concentration ( $C_{calc}$ ) for PPK model analyses. ....	61
Figure 1.16 The Overview Structure of the EMA. ....	66
Figure 1.17 Areas of PBPK application submissions received by the EMA up to 2015 (n=112). ....	67
Figure 1.18 The structure of the FDA. ....	69
Figure 1.19 Areas of PBPK application submissions received by the USFDA from 2008 to 2012 (n=33). ....	71
Figure 1.20 Biopharmaceutical classification system as defined by the USFDA. ....	72
Figure 1.21 The Structure of the PMDA. ....	74
Figure 1.22 Areas of PBPK application submissions of NME received by the PMDA from 2014 to 2016 (n=17). ....	75
Figure 2.1 The location of brain barriers ....	82
Figure 2.2 BBB transport pathways. ....	84
Figure 2.3 PBPK model of the rat CNS utilised by Badhan <i>et al.</i> (2014). ....	91
Figure 2.4 A hybrid brain PBPK model utilised by Liu <i>et al.</i> (2005). ....	92
Figure 2.5 A whole-body rat PBPK model incorporating a permeability limited brain model as utilised by Ball <i>et al.</i> (2012) ....	93
Figure 2.6 Schematic diagram of Ball <i>et al.</i> (2014) (A) the rat CNS minimal PBPK model and (B) the rat CNS whole-body PBPK model. ....	94

Figure 2.7 A hybrid brain PK model utilised by Yamamoto et al. (2016)	95
Figure 2.8 A generic whole-body PBPK model.	97
Figure 2.9 CNS PBPK brain model.	98
Figure 2.10 5-compartmental rat CNS PBPK brain model.	108
Figure 2.11 Comparisons of predicted and reported $K_{p_{uu,brain}}$ in rat.	115
Figure 2.12 Simulated mean phenytoin plasma concentration-time profiles.	116
Figure 2.13 Simulated mean phenytoin hippocampus and frontal cortex concentration-time profiles.	117
Figure 2.14 Simulated mean carbamazepine plasma and hippocampus concentration-time profiles.	119
Figure 2.15 Model sensitivity analysis of brain PS on $C_{max}$ .	121
Figure 2.16 Simulated human morphine concentration-time profiles.	124
Figure 3.1 Life cycle of the plasmodium species.	134
Figure 3.2 HIV replication cycle.	136
Figure 3.3 Structure of chromosome, DNA, and gene.	141
Figure 3.4 SNP schematic illustrating changes of a nucleotide at a single base-pair location on DNA.	143
Figure 3.5 Model development strategy.	149
Figure 3.6 Age-weight relationship comparison between adult Ugandan and Caucasian males (A) and females (B).	157
Figure 3.7 Age-weight relationship comparison between paediatric Ugandan and Caucasian males (A) and females (B).	161
Figure 3.8 Simulated single dose plasma concentration-time profiles of efavirenz in healthy volunteer adults.	163
Figure 3.9 Simulated multidose plasma concentration-time profile of efavirenz in a Ugandan population group	165
Figure 3.10 Simulated lumefantrine plasma concentration following co-administration with efavirenz in a healthy volunteer population group	168
Figure 3.11 Simulated drug-drug interaction between lumefantrine and efavirenz in a South African population groups.	170
Figure 3.12 Simulated efavirenz plasma concentration-time profile in a Ugandan paediatric population group.	173
Figure 3.13 Simulated plasma concentration-time profile of body weight efavirenz dosing in Healthy Volunteers (10-15 kg and 15-20 kg).	175
Figure 3.14 Simulated plasma concentration-time profile of efavirenz dosed at 25 mg/kg to 2-3 years old Ugandan children.	178
Figure 3.15 Simulated plasma concentration-time profile of efavirenz in South African children stratified by genotype.	180
Figure 3.16 Simulated median plasma concentration-time profile of lumefantrine administered to Ugandan children in the absence and presence of efavirenz (5-15 kg).	182
Figure 3.17 Simulated mean plasma concentration-time profile of lumefantrine administered in a 5-day to Ugandan children.	186
Figure 4.1 Model development strategy	204

Figure 4.2 Visual predictive checks on the comparison between predicted and observed (NCVD) age-weight relationship for the Malay male (n=18601) (A) and female (n=4513) (B) populations. ....	212
Figure 4.3 Visual predictive checks on the comparison between predicted and observed (NCVD) age-weight relationship for the Chinese male (n=7445) (A) and female (n=2484) (B) population. ....	213
Figure 4.4 Simulated plasma concentration-time profile of repaglinide in healthy adults.....	214
Figure 4.5 Simulated plasma concentration-time profile of repaglinide following single and multiple oral doses in healthy adults.....	215
Figure 4.6 Simulated plasma concentration-time profile of repaglinide in healthy Malaysian Chinese adults. ....	216
Figure 4.7 Simulated plasma concentration-time profile of repaglinide in healthy Malay adults.....	217
Figure 4.8 Simulated plasma concentration-time profile of tramadol intravenous bolus dosing in Malay and Malaysian Chinese subjects.....	218
Figure 4.9 Visual predictive check of clopidogrel in CYP2C19-PM, -IM, -EM and -UM. ..	221
Figure 4.10 Visual predictive check of clopi-H4 (active metabolite) in CYP2C19-PM, -IM, -EM and -UM. ....	222
Figure 4.11 Impact of clopidogrel standard dose regimens on final dose clopi-H4 plasma in Malay and Malaysian Chinese.....	225
Figure 4.12 Impact of clopidogrel standard dose regimens on final dose clopi-H4 plasma in Malay subjects .....	227
Figure 4.13 Impact of clopidogrel standard dose regimens on final dose clopi-H4 plasma in Chinese subjects.....	228
Figure 4.14 Impact of clopidogrel high dose regimen on clopi-H4 plasma $C_{max}$ in Malay and Malaysian Chinese subjects. ....	230

## LIST OF TABLES

Table 1.1 Typical steps, values and units used for the microsomes and hepatocytes assay scaling factors. ....	49
Table 1.2 Implementation of PBPK modelling in drug development and regulatory authorities policies. ....	64
Table 2.1 System-related parameters used for the rat whole-body PBPK model.....	100
Table 2.2 <i>In vitro</i> permeability data.....	101
Table 2.3 Model predicted versus literature reported in situ permeabilities .....	102
Table 2.4 Physicochemical parameters used to calculate partition coefficients.....	103
Table 2.5 Protein binding and metabolic clearance .....	104
Table 2.6 Renal Clearance .....	105
Table 2.7 System-related parameters used for the brain PBPK model.....	112
Table 2.8 Physicochemical parameters for the human regional brain model.....	113
Table 2.9 Summary of predicted and observed pharmacokinetic parameters of phenytoin in plasma, hippocampus and frontal cortex in rats. ....	118
Table 2.10 Summary of predicted and observed pharmacokinetic parameters of carbamazepine in plasma and hippocampus brain regions in rats. ....	120
Table 2.11 Summary of predicted and observed pharmacokinetic parameters of morphine in plasma and regional brain compartments in humans.....	125
Table 3.1 Summary of lumefantrine pharmacokinetics.....	139
Table 3.2 Summary of efavirenz pharmacokinetics .....	140
Table 3.3 Compound-specific parameters for lumefantrine and efavirenz .....	147
Table 3.4 Weight-based dosing regimens for lumefantrine and efavirenz .....	148
Table 3.5 List of published papers utilised for validation purposes .....	150
Table 3.6 Malaria population biochemistry .....	152
Table 3.7 Summary of predicted and observed pharmacokinetic parameters of efavirenz in adults with CYP2B6*1/*1 and CYP2B6*6/*6 genotypes in a Healthy Volunteer population .....	164
Table 3.8 Summary of predicted and observed efavirenz plasma concentrations in Ugandan adults with CYP2B6*1/*1 and CYP2B6*6/*6 genotypes.....	167
Table 3.9 Summary of predicted and observed PK parameters of lumefantrine in the absence and presence of efavirenz in healthy adults. ....	168
Table 3.10 Summary of the simulated lumefantrine pharmacokinetics parameters in the absence and presence of efavirenz in South African adults with CYP2B6*1/*1 and CYP2B6*6/*6 genotypes.....	171
Table 3.11 Summary of predicted and observed efavirenz pharmacokinetics parameters in HIV-infected Ugandan children.....	173
Table 3.12 Summary of predicted pharmacokinetic parameters of efavirenz in Ugandan children. ....	178
Table 3.13 Summary of predicted pharmacokinetic parameters of efavirenz in South African children. ....	179

Table 3.14 Summary of simulated lumefantrine pharmacokinetic parameters in the absence and presence of efavirenz in children with CYP2B6 *1/*1 and CYP2B6 *6/*6 genotypes. ....	184
Table 3.15 Summary of the percentage of subjects attaining a lumefantrine Cd7 > 280 ng/mL .....	188
Table 3.16 Summary of predicted mean day 7 lumefantrine concentrations during a 5 and 7-day treatment schedule in children stratified for CYP2B6*1/*1 and CYP2B6*6/*6 genotypes (n=100). ....	189
Table 4.1 Malay and Malaysian Chinese blood biochemistry .....	205
Table 4.2 Summary demographic data from the NCVD database .....	210
Table 4.3 Summary of predicted and observed pharmacokinetic parameters of repaglinide and tramadol. ....	219
Table 4.4 Summary of simulated clopidogrel and clopi-H4 pharmacokinetic parameters at Day 1 (300 mg loading dose) and Day 5 (75 mg last maintenance dose) in Healthy adult Volunteers with CYP2C19 EM, CYP2C19 PM, CYP2C19 IM and CYP2C19 UM phenotypes. ....	223

## LIST OF PUBLICATIONS

### Peer reviewed published articles:

1. **Zakaria Z**, Badhan R. Development of a Region-Specific Physiologically Based Pharmacokinetic Brain Model to Assess Hippocampus and Frontal Cortex Pharmacokinetics. *Pharmaceutics*. 2018;10(1):14.
2. **Zakaria, Z.** and R. K. Badhan. The impact of CYP2B6 polymorphisms on the interactions of efavirenz with lumefantrine: Implications for paediatric antimalarial therapy. *European Journal of Pharmaceutical Sciences*. 2018; 119: 90–101
3. Badhan R, **Zakaria Z**, Olafuyi O. The repurposing of ivermectin for malaria: a prospective pharmacokinetics-based virtual clinical trials assessment of dosing regimen options, *Journal of Pharmaceutical Sciences*. 2018, doi: 10.1016/j.xphs.2018.03.026.
4. **Zaril Zakaria**, Alan Y.Y. Fong and Raj K. S. Badhan. Clopidogrel pharmacokinetics in Malaysian population groups: the impact of inter-ethnic variability. *Pharmaceutics*. 2018; 11:74.

### Conference Proceedings:

1. **Zaril Zakaria**, Gavin Woodhall and Raj K Singh Badhan, 2016. A Mechanistic Pharmacokinetic Approach to the Development of Predictive Models for Central Nervous System Drug Delivery. LHS PG Research day, Aston University, Birmingham, UK.
2. **Zaril Zakaria**, Gavin Woodhall and Raj K Singh Badhan, 2016. PBPK Method to the Development of Predictive Models for Central Nervous System Drug Delivery. MathSys Summer School, University of Warwick, UK.
3. **Zaril Zakaria**, Gavin Woodhall and Raj K Singh Badhan, 2016. Bridging the gaps in CNS Drug Delivery: PBPK Method to the Development of Predictive Models. 7<sup>th</sup> APS International PharmSci Conference, University of Strathclyde, Glasgow, UK.
4. **Zaril Zakaria**, Gavin Woodhall and Raj K Singh Badhan, 2016. PBPK in the CNS Drug Delivery: Drug Disposition across the BBB, BCSFB, Hippocampus and Frontal Cortex. PKUK Conference, London UK.
5. **Zaril Zakaria** and Raj K Singh Badhan, 2017. A Mechanistic Pharmacokinetic Approach to the Development of Predictive Models in HIV-malaria Co-infection in Children Accounting for Induction of CYPs 3A4 and 2B6 – a Lumefantrine and Efavirenz Case Study. 26<sup>th</sup> PAGE Meeting, Budapest, Hungary.

6. **Zaril Zakaria** and Raj K Singh Badhan, 2017. A PBPK Approach to the Development of Predictive Models in HIV-malaria Co-infection in Children. LHS PG Research day, Aston University, Birmingham, UK.
7. **Zaril Zakaria** and Raj K Singh Badhan, 2017. Impact of *CYP2B6* polymorphisms on the interactions of efavirenz with lumefantrine: implications for paediatric antimalarial therapy. PKUK Conference, Great Malvern, UK. (**Best Poster Award**)

# **CHAPTER 1**

## **Introduction to mechanistic pharmacokinetic approaches**

## 1.1 BACKGROUND

New drug products that enter the pharmaceutical market are required to adhere to stringent safety, efficacy and quality requirements. These requirements are becoming increasingly apparent with the emergence of high profile cases of drug product safety issues arising following marketing authorisation. Ever since the thalidomide controversy, a drug which was marketed in Europe indicated for morning sickness, which led to thousands of babies with birth defects in 1957, the United States Food and Drug Administration (USFDA) has made major amendments in its drug registration policies in 1962 (1, 2). Such amendments include the mandatory requirement of establishing proof of efficacy and safety through recognised well-controlled studies.

Another recent case that has posed stricter safety regulation was rofecoxib, a non-steroidal anti-inflammatory drug (NSAID) under the brand name Vioxx<sup>®</sup>, indicated for the treatment of osteoarthritis, acute pain conditions, and dysmenorrhea. Registered by USFDA in 1999, this drug has been used by almost 80 million people (3). In a USFDA safety analysis, it was estimated 88,000-139,000 Americans had heart attacks and strokes because of taking rofecoxib (4, 5). Such alarming findings have led to the drug's withdrawal in September 2004 (4, 6). Consequently, regulatory authorities such as the USFDA and European Medicines Agency (EMA) have imposed several measures to monitor these trends including, but not limited to, a requirement in obtaining rapid information regarding the pharmacokinetics (PK) of new drug candidates. This requirement might lead to a bottleneck in the early-phase of drug development since a considerable amount of resources are required to assess the pharmacokinetics profile of a drug.

In order to optimise the resources for assessing this, predictive PK modelling has becoming a growing interest among researchers to predict PK behaviour of drug molecules, thereby aiding in facilitating the selection of suitable candidates for further development and rejecting those molecules which have a low probability of success (7). Furthermore, predictive PK modelling could also be beneficial in assessing the safety of established drugs by predicting possible drug-drug interaction (DDI) that could occur in specific population groups such as paediatrics,

geriatrics and patients with co-infected diseases (8). Optimal prediction of a drug’s PK properties will ultimately be a pre-cursor towards better treatment optimisation to improve drug safety and efficacy without jeopardising patients’ safety.

### 1.1.1 Modelling and simulation in drug development

Prior to drug product marketing authorisations, drug discovery and development processes are rigorous, taking 12-15 years from the discovery phase up to obtaining market authorisation with an associated development cost of up to \$48 billion (9, 10). With the advancement of *in-silico* capabilities, modelling and simulation techniques have become an essential element of drug development strategies, particularly in pre-clinical and clinical trials setting (Figure 1.1). Since such settings are subjected to rigorous regulatory requirements such as Good Laboratory practice (GLP) for pre-clinical studies, and Good Clinical Practice (GCP) for the clinical studies, the application of modelling simulation have been utilised in each of the phases in drug development in order to efficiently manage the risks towards human and animal subjects.

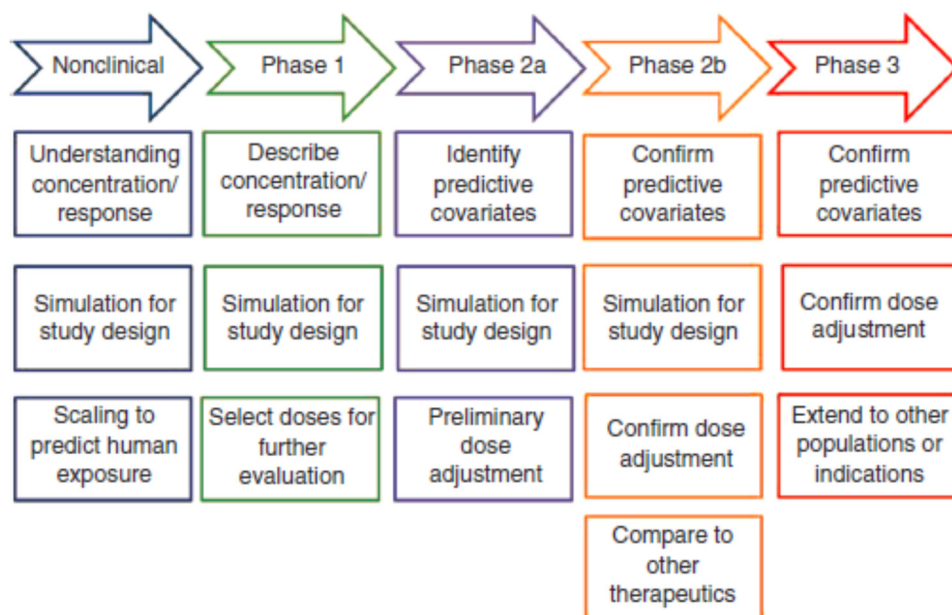


**Figure 1.1 Application of modelling and simulation during drug development.**

Reproduced from Mould *et al.* (2012) (11)

#### **1.1.1.1 Pre-clinical testing**

Every new candidate compound is required to undergo pre-clinical testing in order to determine its toxicology and pharmacological profile prior to first-in-human (FIH) studies, as required by international regulations and standards (12, 13). The range of tests includes both rodent and non-rodent species with the aim to investigate the maximum-tolerated dose in single and multiple dose administration, carcinogenicity, mutagenicity, fertility, teratogenicity, and reproduction. The number of animals which are involved in the studies usually varies depending on the type of studies and the data that has been generated from these types of studies will be extrapolated to predetermine the safety and efficacy aspects of the compound in human subjects.

In this very early phase, mechanistically relevant pharmacokinetic/pharmacodynamic (PK/PD) data derived from modelling and simulation can be utilised to understand the response and concentration of the drug molecule in animal models. Results generated can be used to extrapolate to humans and aid in giving preliminary data for risk assessment of the drug and selecting appropriate dose ranges (14). After the required amount of data has been generated to justify the safety, efficacy, and quality of the compound in animal studies, subsequent steps expose the new compound to human subjects.

#### **1.1.1.2 Phase I studies**

After the compound has been subjected to pre-clinical testing and the maximum-tolerated dose in human has been determined, it then goes through FIH trials whereby human subjects (usually healthy ones) will be exposed to the drug to determine its pharmacology, safety, and tolerability aspects. This phase has its unpredicted risks even with the progressive advancement of pharmaceutical technology (9). Due to the risks involved, pharmacokinetic modelling and simulation can be the first-line assessment towards describing the dose-concentration response and also dose selection for further assessment at phase II clinical trials.

According to Aarons *et al.* (2001) (14), even though modelling and simulations were utilised in only a small number of phase I clinical trials, the application of this approach was significant

in numerous scenarios including estimating exposure-response relationship, characterisation of non-linearity, sparse sampling studies, special population studies, filtering investigational molecule due to assay limitation, combined analyses, integrating PK/PD knowledge for decision making, formulation development, bridging studies, sparse sampling studies and predicting multiple dose profile from single dose.

### **1.1.1.3 Phase II studies**

During phase II trials, the drug is subjected to the first assessment of its safety, tolerability and preliminary efficacy in a patient population. Its dose range will also be assessed as a basis for the confirmatory phase III studies. The number of subjects is also substantially increased (approximately 100 to 300 patients) as compared with phase I studies to obtain the power needed for statistically significant results. As the desired therapeutic outcomes of many new drugs were usually long term especially for anticancer treatments, many of the phase II trials use surrogate markers (biomarkers) as primary endpoints. This emerging trend has met with scepticism with regards to the actual efficacy of the drug in phase III trials (15). Therefore, given this issue, preliminary analysis can be implemented using modelling and simulation in identifying as well as confirming dose adjustment that is required to be exposed to subjects in phase III clinical trial, further minimising the risk towards safety and provides a suitable starting point for an efficacious dose.

During this phase, specifically in dose-ranging studies, a model based simulation may provide a quantitative understanding as well as useful insights towards the selection of doses that have been derived from a phase II studies (16). Furthermore, a comparison study using other drug molecules for the same indication could also be conducted using virtual trials that are available in modelling and simulation software. Such comparison can be made to determine its safety and efficacy in virtual subjects as a preliminary representative towards phase III study involving actual subjects that will be conducted.

#### **1.1.1.4 Phase III studies**

Phase III clinical trials typically involve thousands of patients and can amount to significant financial investment. This phase is where the clinical efficacy and safety aspects of the drug are determined in a patient population as it includes the ‘real’ endpoints required by many regulatory authorities such as survival rate, lowering of blood glucose levels or myocardial infarction rather than using surrogates, such as HbA1c or lowering of plasma cholesterol. As discussed by Richards (2008) (9), the challenge that the pharmaceutical industry needs to overcome in this phase is the extent of information that is required by regulatory authorities which require that the results of these studies be specific to their regions such as in China and Japan. This scenario will also lead to studies being conducted in that particular region after the product has obtained its authorisation globally which will further escalate the drug development time and cost. Modelling and simulation may facilitate in this aspect since clinical trials simulation can be utilised to include the specific virtual population such as the Chinese and Japanese to provide an accurate estimation that occurred for these populations. Similar to phase II studies, modelling and simulation approaches in phase III could also confirm the dose adjustment, dose-response and the predictive covariates that have been made by utilising virtual clinical trials to assess that information.

Further, a dose-response model of a clinical response can be developed using data derived from phase II analyses. Simulations can be conducted to assess the robustness of the on-going phase III studies by comparing data that has been derived from the simulation with the actual on-going phase III results regarding ‘true’ dose-response, and patient’s variability in dose-response severity, thereby, minimising uncertainty. Also, a comparison can be made between the range of possible outcomes generated by the simulation with the on-going phase III data to provide an informed decision-making process with regards to the fate of the investigational drug encompassing its safety, efficacy and registerability with respective regulatory authorities (17).

Following generation of supporting data to justify a drug’s safety, efficacy and quality aspects at this stage, a compilation of data which includes information from pre-clinical, phase I, phase

II and phase III studies will be made available for the submission to the relevant regulatory authorities to be assessed for marketing authorisation.

## 1.2 PHARMACOKINETIC MODELLING

There are several approaches to PK modelling and simulations dependent upon the complexity and types of data that are available (Figure 1.2). Empirical or *top-down* approaches include compartmental and non-compartmental modelling which require the availability of clinical data (18, 19). On the other hand, mechanistic or *bottom-up* approaches such as physiologically-based pharmacokinetic (PBPK) modelling often do not rely on clinical and pre-clinical data to adequately extrapolate the intended drug molecules to predict its absorption, distribution, metabolism, and excretion (20-22).

Finally, population PK is often utilised in clinical trials with poor sampling and a large number of patients to predict the optimum dosing for the subgroup populations (23, 24), allowing for the inclusion of patient covariates to describe population variability in clinical drug concentrations/response.

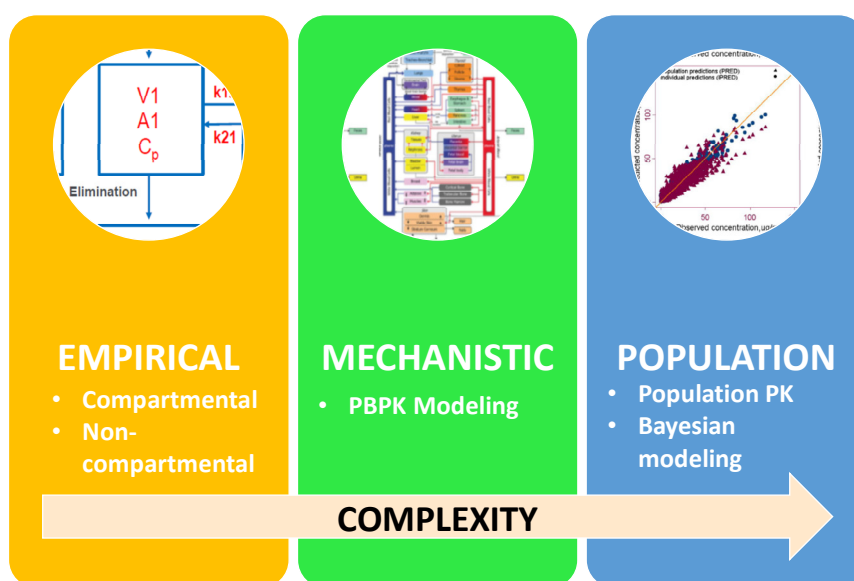


Figure 1.2 Approaches used in pharmacokinetics modelling.

### 1.2.1 Compartmental modelling

Compartmental modelling integrates the concept of pharmacokinetics (absorption, distribution, metabolism and elimination) into logical mathematical terms. Such integrations enable this approach to model complex physiological processes by condensing the body into smaller and manageable number of mathematical terms which allows prediction of drug PK as well as determining the parameter of that system. In general, compartmental modelling will allow pharmacometricians to determine parameters such as volume of distribution, half-life, area under the curve (AUC) and elimination rates (25). One of the earliest compartmental models in history was developed by Widmark in 1924 whereby he modelled the distribution of alcohol in the human body (26).

In compartmental modelling, a compartment is termed as an imaginary unit or boxes which represents a group of tissues that have similar rates of drug distribution such as rapid or slowly perfused (27). Assumptions must be made that the drug concentration is homogeneous in all the compartments and it does not represent any specific tissues. In order to predict the PK parameters, the model requires *a priori* plasma concentration data available, and typically, the number of compartments is dictated by the plasma concentration profile.

The number of compartments in a PK analysis will be dependent on the drug's physicochemical characteristics as numerous processes involving drug movement around the body are not saturated at normal therapeutic dose levels (28). Compartment 1 represents the central (tissue or plasma) compartment in which the drug molecule rapidly absorbs. The addition of extra compartment will be determined whenever there is a slow distribution of drugs to other tissues. Conceptually, the elimination typically will occur from Compartment 1, but it could also occur in another compartment as well, depending on the characteristics of the molecule (29).

#### 1.2.1.1 1-compartment model

For 1-compartmental model, the assumption is made that the whole body is considered as a single compartment and that drug is rapidly distributed to tissues (Figure 1.3). The route of administration for this model is usually intravenous bolus administration, considering the body

to behave as a single compartment and due to its simplest route of drug administration. Because of rapid drug equilibration between the tissues and blood, drug distribution and elimination happen as if the dose is all dissolved in a single compartment whereby the drug is eliminated (30). However, there are certain cases whereby a 1-compartment model has been applied to an orally administered drug due to sparse sampling method which limits the calculation of full PK parameters of each patient (31). An example of drugs that follows the 1-compartment model are aminoglycosides when given as IV bolus whereby its distribution phase is only 15 to 30 minutes (32).

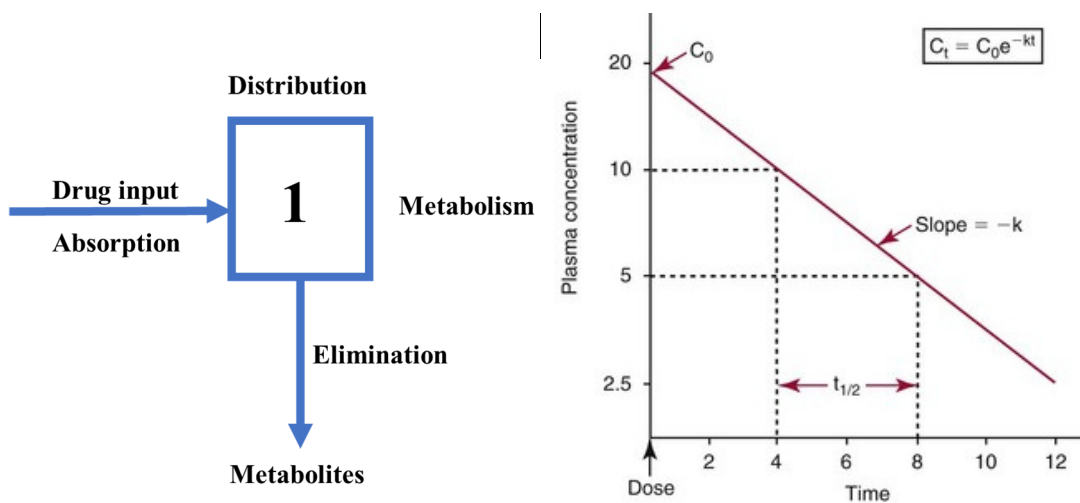


**Figure 1.3 Diagrammatic representation of a one-compartment model and its plasma concentration-time profile.**

Mono-exponential (single  $k$  term) decline from the original concentration ( $C_0$ ) is defined by the elimination constant ( $k$ ), which is related to the drug half-life ( $t_{1/2}$ ). Drug concentration at any time ( $C_t$ ) can be estimated with knowledge of  $C_0$ ,  $k$ , and the time ( $t$ ) (33).

The drug half-life ( $t_{1/2}$ ) is determined by the following equation;

$$t_{1/2} = \frac{0.693}{k} \quad (1.1)$$

where  $k$  is the elimination constant.

This model relies on a simple mass balance equation;

$$\frac{dC}{dt} = -k_{el}C(t) \quad (1.2)$$

where  $k_{el}$  is the elimination constant, and  $C(t)$  is the drug concentration.

At  $t = 0$ ;

$$C_0 = \frac{Dose}{V} \quad (1.3)$$

where  $V$  is the compartment volume.

Therefore;

$$C = C_0 e^{-k_{el}t} \quad (1.4)$$

To account for differences in the extent of distribution, a volume of distribution ( $V_D$ ) can be determined for each compound. The  $V_D$  is represented by the association between a single dose ( $D_0$ ) and the plasma concentration ( $C_0$ ) observed after dosing as well as corrected for bioavailability ( $F$ ). Such relationship can be summarised in the following equation;

$$V_D = \frac{D_0 \times F}{C_0} \quad (1.5)$$

where  $V_D$  is the volume of distribution.

The  $V_D$  is not an actual physiologic volume; on the contrary, it is a calculated parameter that can be much larger than the volume of a human body.  $V_D$  could be described as the volume of fluid theoretically required to dilute a given dose to its known concentration if the drug were present only in the blood. A higher calculated  $V_D$  means a low plasma concentration due to most of the drugs enter tissue. Therefore, a large  $V_D$  represents an extensive distribution, whereas a

small  $V_D$  suggests that the drug is retained in the plasma vasculature. The value of  $V_D$  in an individual depends on many of the factors including protein binding, drug lipophilicity and body composition which also represents inter-individual variability.  $V_D$  can be expressed as a volume such as litres or as a volume per unit body weight such as L/kg. The  $V_D$  is an essential parameter for predicting the clearance rate of a drug as well as estimating plasma concentrations after dosing.

When a drug is taken orally as a tablet, the 1-compartment model equation is modified to accommodate a first-order transfer kinetics, representing the absorption of drug through the gut. In this instance, an absorption constant ( $k_a$ ) is introduced to represent drug input in the following equation (first-order absorption);

$$\frac{dC}{dt} = k_a D - k_{el} C \quad (1.6)$$

$$C = C_0 e^{-k_a t} \quad (1.7)$$

Therefore;

$$C = \frac{k_a C_0}{V(k_{el} - k_a)} [1 - e^{-k_a t}] \quad (1.8)$$

### 1.2.1.2 2-compartment model

In the 2-compartment model, the human body is divided into two compartments, namely the central and peripheral. For the central compartment, the drug is distributed rapidly, which is in contrast with the peripheral compartment that distributed at a slow rate (Figure 1.4). These assumptions create two distinct plasma curves which represent the distribution of drug through peripheral compartment and its elimination.

In this model, the initial plasma concentration of drug declines rapidly as the compound equilibrates between the two compartments (distribution phase). When approaching equilibrium between the two compartments, the dominant kinetic mechanism becomes the elimination of the drug from the plasma (elimination phase). Generally, the elimination process occurred by the necessity for the drug to leave the tissue compartment before it can be eliminated

from the body. The slopes at the two phases represent the distribution ( $\alpha$ ) and elimination ( $\beta$ ) macroconstants, which determine corresponding half-lives for each phase. The distribution half-life is called the alpha half-life, and the elimination half-life is the beta half-life. An example of a drug which follows the 2-compartment model is vancomycin whereby its distribution phase, when given as IV bolus, is 1 to 2 hours (34).

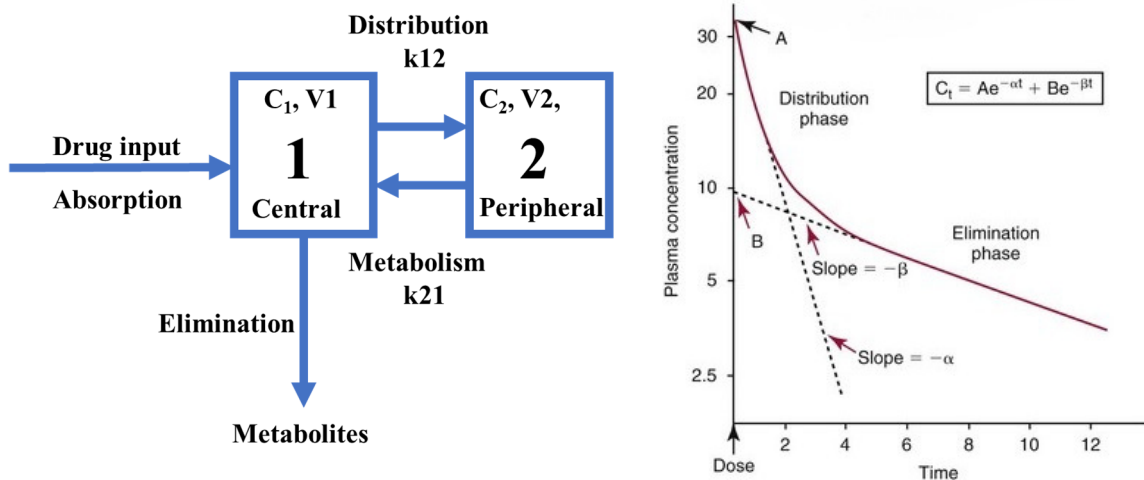


**Figure 1.4** Diagrammatic representation of a 2-compartment model and its plasma concentration-time profile.

Bi-exponential decline from the original concentration ( $C_0$ ) is influenced by both the distribution phase (characterised by the constant  $\alpha$ ) and the elimination phase (characterised by the constant  $\beta$ ) (33).

The kinetic equations for this model are as follows;

$$\frac{1}{V_1} \cdot \frac{dC_1}{dt} = \frac{-k_{12} \cdot C_1}{V_1} - \frac{k_{10} \cdot C_1}{V_1} + \frac{k_{21} \cdot C_2}{V_2} \quad (1.9)$$

and,

$$\frac{1}{V_2} \cdot \frac{dC_2}{dt} = \frac{-k_{21} \cdot C_2}{V_2} + \frac{k_{12} \cdot C_1}{V_1} \quad (1.10)$$

At  $t = 0$ ,  $C_1 = \frac{D}{V_1}$ ,  $C_2 = 0$ , which gives,

$$C_1 = \frac{D}{V_1} \cdot \frac{(k_{21} - \alpha)e^{-\alpha t}}{(\beta - \alpha)} + \frac{(k_{21} - \beta)e^{-\beta t}}{(\alpha - \beta)} \quad (1.11)$$

and,

$$C_2 = \frac{D}{V_2} \cdot \frac{k_{12}}{(\alpha - \beta)} [e^{-\beta t} - e^{-\alpha t}] \quad (1.12)$$

Therefore, to represent integration between the two compartments,

$$C_t = Ae^{-\alpha t} + Be^{-\beta t} \quad (1.13)$$

whereby A and B represent the intercepts as in Figure 1.4.

### 1.2.1.3 3-compartment model

The 3-compartment model is an extension of 2-compartment model, with an additional deep tissue compartment as an extension (Figure 1.5). In certain situations, whenever there is a drug that distributes very slowly to poorly perfused tissues such as at the bone and fat area or for strongly lipophilic drugs distributed into adipocytes, extra compartments can be added to illustrate such conditions. A drug that is in the peripheral compartment can also return to the central compartment. The kinetic equations are similar with 2-compartment model with the addition of the third compartment and the gamma phase. The tissue release phase (gamma phase) usually occurs 16 hours post-infusion whereby drug that is tissue bound at various organs is released. Even though the amount of drug that is release is in a small volume, the accumulation of the drug over time could lead to aminoglycosides toxicity (35).

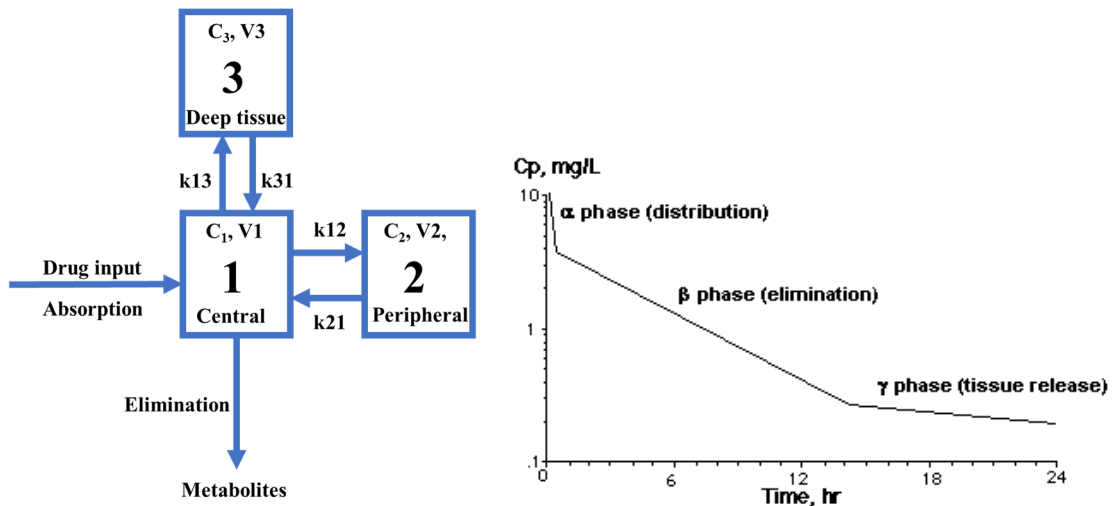


**Figure 1.5 Diagrammatic representation a of 3-compartment model and its plasma concentration-time profile.**

Tri-exponential decline from the original concentration ( $C_0$ ) is influenced by the distribution phase (characterised by the constant  $\alpha$ ), the elimination phase (characterised by the constant  $\beta$ ) and the tissue release phase (characterised by the constant  $\gamma$ ).

### 1.2.2 Non-compartmental analysis

Similar to compartmental modelling, non-compartmental analysis (NCA) or model-independent method is an empirical approach that relies on a compilation of clinical data of individuals (36). NCA has several advantages over compartmental modelling as it requires less restrictive assumptions to be made to conduct the modelling approach in which there is no compartment that needs to be assumed to suit the drug PK profile (26). The process for model development is also more straightforward and manageable for less experienced modellers. Furthermore, regarding clinical data, NCA requires fewer plasma samples and sampling time may not be as critical as compared to the compartmental modelling.

The aim of NCA is to estimate essential parameters such as mean residence time (MRT), mean absorption time (MAT) and area under the first moment of the systemic drug concentration curve (AUMC).

Similar with the area under the curve (AUC), AUMC can be determined by the trapezoidal rule equation, whereby the plasma concentration-time profile is divided into individual trapezoids, and the AUC of these trapezoids are added, for example;

$$AUC_{t_1-t_2} = \left(\frac{C_1+C_2}{2}\right) \cdot (t_2 - t_1) \quad (1.14)$$

whereby time is represented by t and concentration is represented by C

Therefore,

$$AUC_{t_1-t_2} + AUC_{t_2-t_3} + AUC_{t_3-t_4} \dots \dots \dots AUC_{t_{last}} \quad (1.15)$$

The AUMC is a product of the AUC and time (Figure 1.6).

$$AUMC_{t-\infty} = \frac{C_{last} \cdot t_{last}}{k_{el}} + \frac{C_{last}}{(k_{el})^2} \quad (1.16)$$

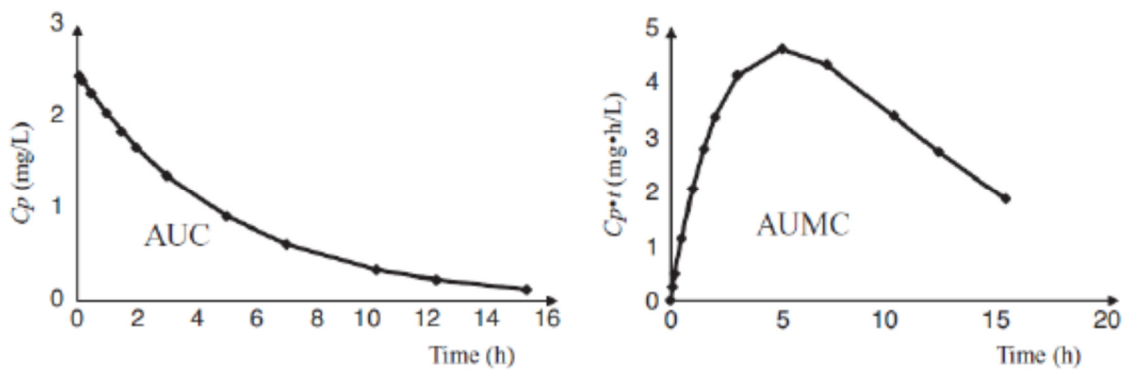


**Figure 1.6 Diagrammatic representation of the AUC in the plasma concentration-time profile and AUMC in the plasma concentration\*time-time graphs.**

MRT mainly reflects the elimination rates process in the body since it is calculated for a drug after intravenous bolus injection.

$$MRT = \frac{AUMC}{AUC} \quad (1.17)$$

MAT is the difference between the oral MRT and intravenous MRT.

$$MAT = MRT_{oral} - MRT_{iv} \quad (1.18)$$

Following determination of the MRT, other PK parameters such as clearance (CL), elimination rate ( $k_{el}$ ) and the volume of distribution at steady state ( $V_{ss}$ ) can be calculated from IV data, can be derived from the following equation (26);

For volume of distribution at steady state ( $V_{ss}$ ), the relationship between the AUC, AUMC, MRT and CL are as follows;

$$CL = \frac{Dose}{AUC} \quad (1.19)$$

Therefore;

$$V_{ss} = CL \cdot MRT = \frac{Dose \cdot MRT}{AUC} \quad (1.20)$$

Results derived from NCA are usually a generalisation from a compartmental analysis and is still useful in providing a general overview extrapolation of the drug PK profile especially in its early stage of development (25). An example would be the evaluation of drug absorption data whereby the more prolonged the MRT, the more sustained or prolonged the drug absorption.

### **1.2.3 Population pharmacokinetics**

Population pharmacokinetics (PPK) is a study of the variability in plasma drug concentrations between individuals whenever standard dosage regimens are administered and its effects towards absorption, distribution, metabolism, and excretion (37). The covariates in question can include gender, weight, age, creatinine clearance, liver function markers or other disease biomarkers. The interest in PPK stems from a concern that new drugs that are developed might not have been studied in different or relevant populations or that patients have not been introduced to the new drugs at the early stage of drug development (38). The latter concern is more related to obtaining as much information as possible regarding the safety and efficacy of the new drugs. To date, most PPK studies are conducted in clinical setting as well as for drug development programme (39-41).

Variability in pharmacokinetics is influenced by several factors which include, but not limited to, demographics (sex, gender, ethnicity, body surface area and body weight), drug-drug interactions (DDI), genetic phenotypes which affect the clearance of drugs (polymorphism), physiologic (pregnancy, renal and hepatic impairment or other disease states), and environmental factors (diet and smoking) (39, 42). The effect of this population variability on pharmacokinetics will be discussed further in the following section of this thesis.

PPK has several characteristics which differ from traditional PK evaluation (41). Such characteristics include the ability to incorporate and explain the source of variabilities such as demographics, DDI, pathophysiology and environmental factors which contributes to the PK of the drugs. In addition, a PPK approach could recognise the source of variability including inter- and intra-subjects as well as inter-occasions which are essential factors during drug development. PPK also can obtain relevant PK information which is specific to specific populations that are intended to be treated with the new drug. Finally, PPK could quantitatively predict the unexplained aspects of the variability that occurs in the specific population. This characteristic will further enhance the safety and efficacy of the new drug in evaluation as the lower the magnitude of unexplained variability, the higher the estimated safety and efficacy.

Once a PPK analysis has been completed, simulation results derived from the analyses can be utilised to predict ‘what-if’ scenarios such as dose optimisation in achieving a therapeutic goal and the extent of dosage that will give a toxic effect to the patients as well as the optimum dosage that will have minimal adverse effects. Ultimately, PPK analyses can lead to improved patient care and facilitate drug development processes.

### 1.3 ALLOMETRIC SCALING IN PHARMACOKINETICS MODELLING

Allometric scaling or pharmacokinetic interspecies scaling is used to scale pharmacokinetic parameters from animals to humans. It is based on the relationship that shows the ratio of organ weights compared to body weight is similar across species. Allometric scaling in combination with preclinical pharmacodynamics may provide a more meaningful clinical data that allows a greater predicting accuracy regarding the efficacy and toxicity of new chemical entities in humans (43).

Allometric scaling of PK parameters such as clearance and volume of distribution, is generalised as non-linear regression equations:

$$Y = a(BW)^b \quad (1.21)$$

which can be transformed to a linear functions;

$$\log(Y) = \log a + b(\log W) \quad (1.22)$$

These can then be plotted in a linear graphical format such as Figure 1.7 for clearance and Figure 1.8 for volume of distribution;

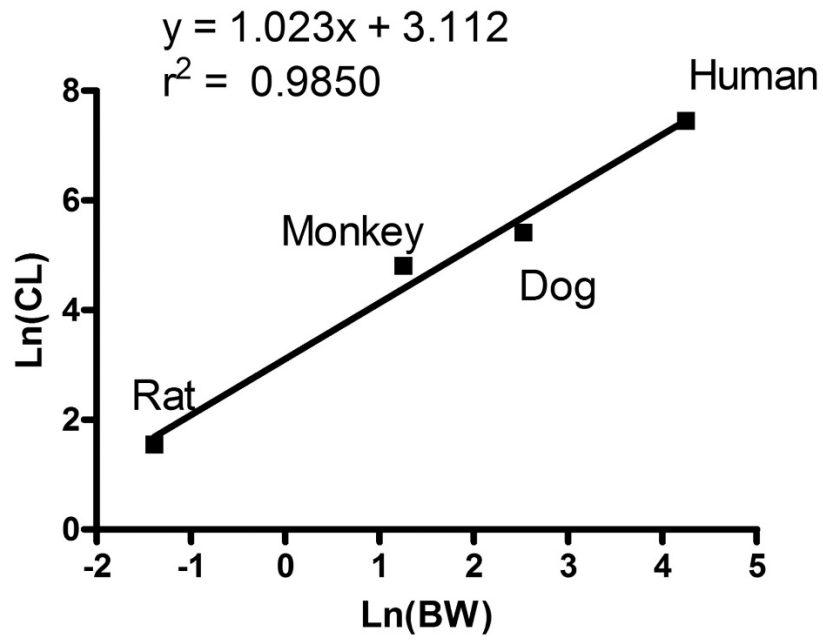


**Figure 1.7 Example of allometric scaling for plasma clearance.**

Reproduced from Zhang *et al.* (2011) (44).

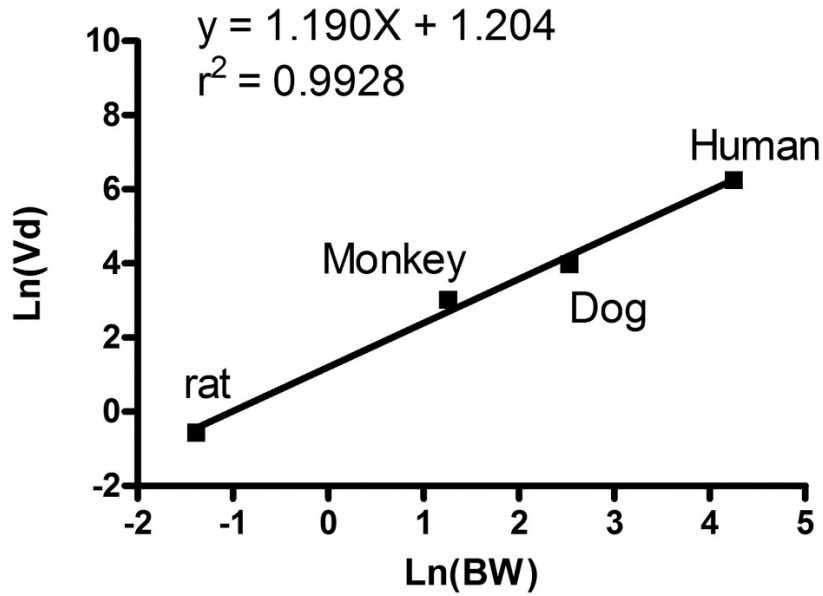


**Figure 1.8 Example of allometric scaling for volume of distribution.**

Reproduced from Zhang *et al.* (2011) (44).

In this approach,  $Y$  represents PK parameter,  $BW$  represents body weight,  $a$  represents the allometric constant and  $b$  is the allometric scaling exponent (45). The value of  $a$  is dependent on the PK parameter, and the compound, whereas  $b$  is specific to the PK parameter. There are five principles that delineate the allometric scaling exponent,  $b$  (46): 1. When  $b = 0$ , then  $Y$  is independent of  $BW$ , such as hematocrit and body temperature; 2. When  $b < 0$ , then  $Y$  decreases with the increase in  $BW$ , such as heart rate; 3. When  $b > 1$ , then  $Y$  increases faster than  $BW$ , such as skeleton weight; 4. When  $b = 1$ , then  $Y$  increases proportionally with  $BW$ , such as blood volumes and 5. When  $0 < b < 1$ , then  $Y$  does not increase as fast as  $BW$ , such as heart beat.

The volume of distribution, half-life and clearance are the three most frequently extrapolated parameters. Physiological flow rates and clearance usually have an exponent of 0.75, signifying that clearance increases as species get larger, but not as rapidly as body weight (46). Also, for clearance scaling, only unbound clearance is taken into consideration since plasma protein binding of many drugs varies between species and only unbound drug can be eliminated (47). At least five animal species (mouse, rat, rabbit, dogs and monkey) have to be taken into account to generate correlation of the changes in  $BW$  versus the PK parameter. The accurate value of allometric scaling is considered to be prominent in therapeutic proteins as opposed to small molecules due to the limited role of the hepatic enzymes that are highly species-variable and limited non-specific distribution (48).

#### **1.4 MECHANISTIC APPROACHES: PBPK MODELLING**

PBPK modelling is another unique type of compartmental model that does not rely on prior clinical or pre-clinical data to adequately extrapolate drug distribution. The model's characteristics are in contrast with the previously described compartmental models which rely heavily on the empirical data for prediction. PBPK model structures include multiple compartments representing tissue/organs supplemented by the incorporation of its physiological parameters values, and these approaches have been utilised extensively in drug development. The application of predictive pharmacokinetics modelling to drug discovery and development has increased over the past decade and has become routine aspects of all clinical

trials phases to both extrapolate dose to optimal therapy in population groups and to also identify covariates which may contribute to the variability in clinical response to drugs.

Integration of knowledge regarding physiological processes with physicochemical attributes or other information regarding specific compounds to simulate complex physiological system is the primary aim of PBPK modelling (48). Such approach provides a superior platform with which to both predict temporal tissue concentration profiles and also to conduct interspecies scaling of pharmacokinetics.

The earliest known PBPK model was developed by the ‘father’ of pharmacokinetics, Torsten Teorell in 1937 (49, 50). In this model, blood circulation is represented by a circle of water pipeline that is in contact with several compartments of tissues which have different volumes according to the representative organs (Figure 1.9). Drug molecules are transported *via* subcutaneous routes (rate constant  $k_1$ ) and then circulated throughout the body through blood circulation.

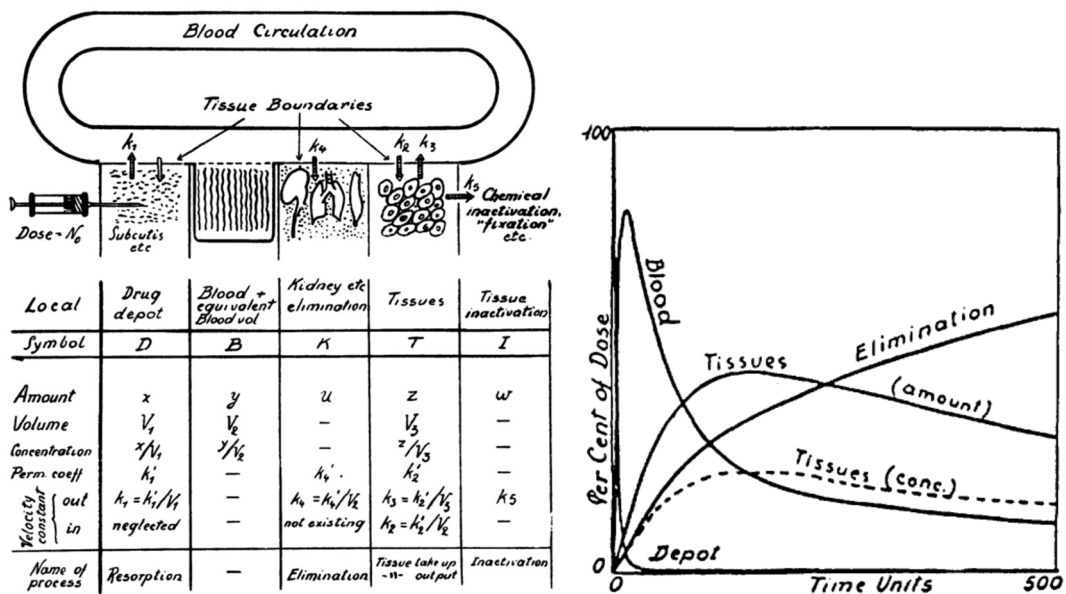


**Figure 1.9** Diagrammatic representation of the earliest PBPK models from Teorell, 1937 and the concentration-time profiles estimation in several compartments.

Reproduced from Teorell *et al.* (1937) (49, 50)

Transportation of drug molecules to different tissues are represented by the rate constant into respective tissues and out of it. Teorell then developed differential equations to illustrate the process and established concentration-time curve profiles that expressed the peak concentration of the drug. Due to the technology at that time, this model was not fully utilised to its full potential. This early model provided a stepping stone for other researchers and gave overviews of the processes of the drug in the human body. However, in this time the term 'pharmacokinetic' has yet to be define, and it was only in 1953 where it was introduced by a German Professor, F.H Dost (51).

As technology progresses and computing abilities became feasible, this first concept was developed further by Bischoff and Brown in 1967 (52) whereby multicompartment models based on known physiology were formulated using compartment as an actual tissue region, as proposed by Bellman *et al.* (53). To date, many hundreds of published PBPK models exist to describe drug distribution and this approach has received recognition by several prominent regulatory authorities including United States Food and Drug Administration (USFDA), European Medicines Agency (EMA) and Pharmaceuticals and Medical Devices Agency, Japan (PMDA).

For any drug of interest, PBPK approaches require the use of drug-specific parameters or 'compound data' which describe the pharmacokinetics of the drug, namely absorption (lipophilicity, hydrogen-bonded donors (HBD) and polar surface area (PSA)), distribution (size, log P, pKa, blood to plasma ratio (B:P or  $R_b$ ), and unbound tissue partition coefficients ( $K_p$ )), metabolism and elimination (intrinsic clearance) data, while also taking into account the physiology of the population group within which the drug will be used (48). In addition to 'compound data', PBPK model also requires 'system data' consisting of physiological (organ volumes, organ perfusion rates, glomerular filtration rates, fat content, body weight and alveolar ventilation) and biochemical attributes (transporter abundance and enzyme abundance) representing relevant species (45). Such approaches allow the scientist to develop population-based predictions, where the physiology of the subject (e.g., tissue volumes, cardiac output, tissue perfusions, and enzyme abundances) are varied within a defined range (dictated by prior literature knowledge) to enable predictions of plasma concentration-time profiles to be made

which will include the typical variability observed within real population groups. Further, this approach allows the extensive extrapolation of pharmacokinetics to special population groups such as paediatrics and those with organ impairments (54, 55). Additionally, we can address ethnic differences in both the abundance and genotype of metabolic enzymes and drug transporter proteins to drive predictions of drug plasma concentrations in non-Caucasian population groups (56).

PBPK modelling approaches mathematically model the biophysical and physical processes that determine the fate of a compound in the body. Therefore, PBPK models are often represented in various ordinary differential equations according to organs such as lungs, arterial blood, venous blood, stomach, gut, brain, and others. The schematic diagram of a 'typical' PBPK model is illustrated in Figure 1.10.

Typically, 14-compartments are used to represent major tissue/organs in the human body and include the lung, heart, brain, muscle, adipose, skin, spleen, pancreas, liver, stomach, gut, bone, kidney and thymus (48). Much of the physiological data required for operation of a PBPK model was collated by Brown *et al.* (1997) (45), and includes values such as organ volumes and organ perfusion rates for adrenals, adipose tissue, bone, brain, gastrointestinal tract, heart, kidneys, liver, lung, muscle, pancreas, skin, spleen, and thyroid in four species (rats, mice, dogs and humans).

The physiological parameter values delineated by Brown *et al.* (1997) (45) also include biological and experimental variability associated with the data and provides modellers with information on the variability associated with each parameter as well as factors that may influence the values selected for the respective parameter. Once developed, the generic whole-body PBPK modelling will be able to simulate the concentration-time profiles in any species whether intravenously, orally or any other route of interest through measurement of physicochemical properties such as solubility, pKa, Log P, permeability, intrinsic clearance and protein binding.

Compound-dependent parameters can also be altered in PBPK model through sensitivity analysis, to provide further understanding and achieve the desired pharmacokinetic properties. Also, extrapolations of data from preclinical to clinical, from one route of administration to another, and from different populations are the most critical applications of PBPK modelling (20, 45).

As with other *in silico* methods, quality and validity of the simulations need to be emphasised. Results obtained in the simulation should be supported by experimental data and should not replace data that has been established from well-conducted experiments to be used as primary evidence (57).

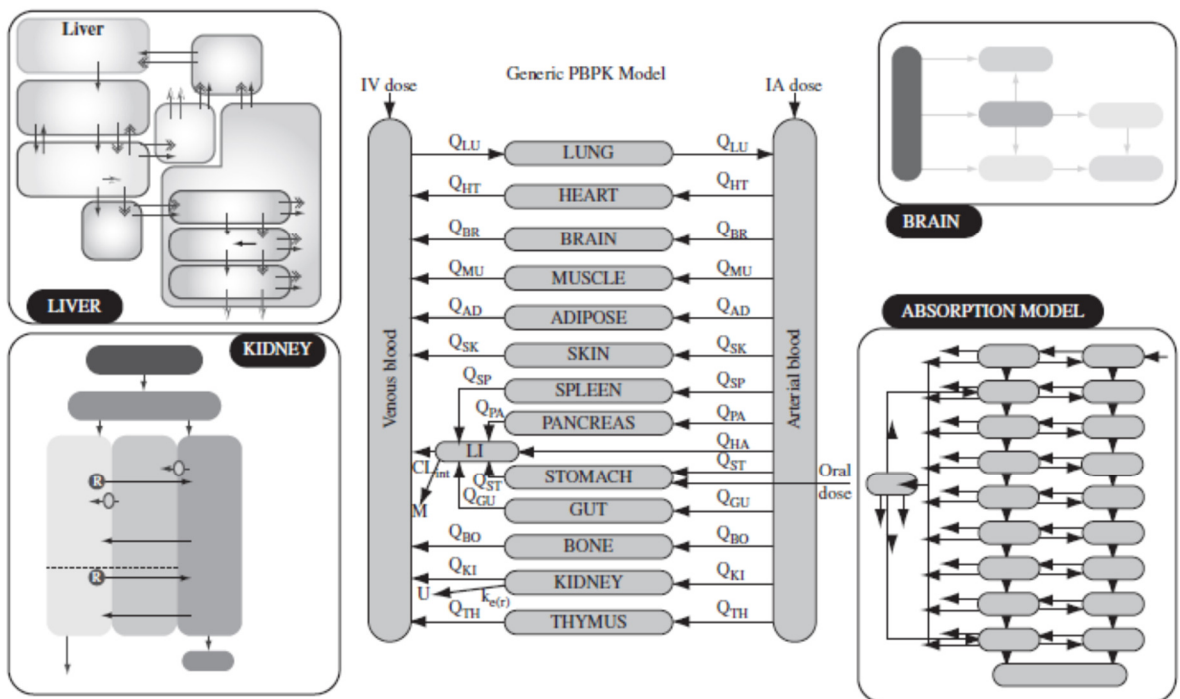


**Figure 1.10 Schematic diagram of PBPK models.**

Reproduced from Peters *et al.* (2012) (48).

### 1.4.1 PBPK modelling equations and assumptions

PBPK models represent several tissue compartments connected by the circulating blood system. Each tissue compartment is represented by a volume ( $V_T$ ), which is often obtained from retrospectively published literature (58-61). Transfer of drug from one compartment to another is defined by a flow rate ( $Q_T$ ). Partitioning of drug into tissue compartments are defined by the tissue partition coefficient of the drug ( $K_p$ ), fraction unbound of drug in plasma ( $f_{up}$ ), and a permeability-surface area metric ( $PS_T$ ), which is obtained from the *in-vitro* permeability ( $P_{app}$ ) and corrected for the surface area that is available for absorption at the respective tissue site (62).

Typically, the tissues in the PBPK model can be described as either permeability rate limited or perfusion rate limited (Figure 1.11) (63). Generic PBPK models generally assumes perfusion rate-limited kinetics (21). In a perfusion rate-limited tissue, the kinetics usually occur for small lipophilic compounds whereby the blood flows to the tissues is the limiting process.

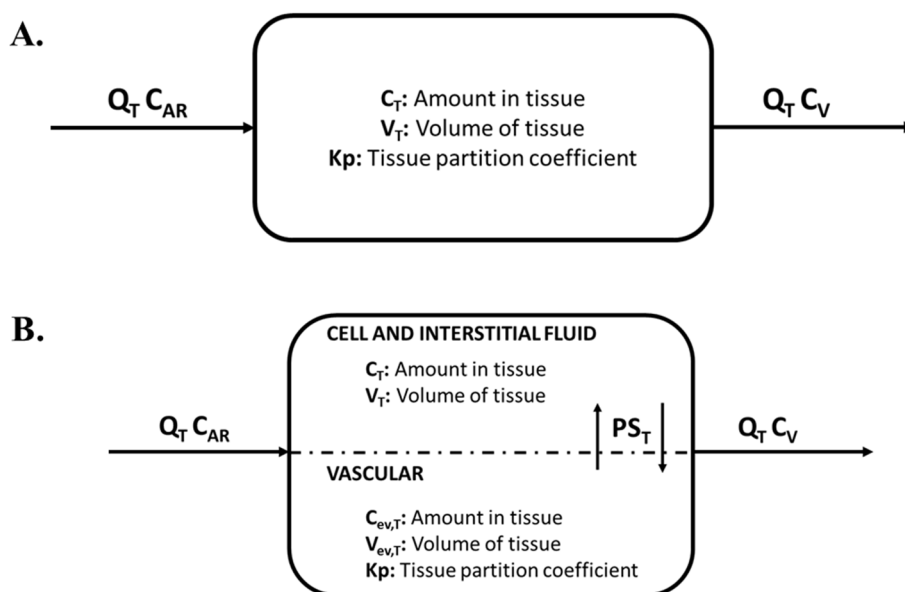


**Figure 1.11 Diagrammatic representation of perfusion vs permeability rate-limited tissue models.**

(A) Perfusion rate limited and (B) Permeability rate limited.

At a steady state, the total drug concentration in the blood circulation is in equilibrium with the total drug concentration in the tissue as determined by the drug-specific  $K_p$  value and the free drug concentrations (unbound) are equal (64). The time taken to reach steady state is determined by the  $K_p$  value, tissue volume, and blood flow rate for the respective tissue. Generally, a poorly perfused tissue will reach steady state slower compared with a highly perfused tissue. The mass balance differential equation representing these perfusion rate-limited non-eliminating tissues is represented as;

$$\frac{dC_T}{dt} = \left[ \frac{1}{V_T} \times Q_T \times C_{AR} \right] - \left[ \frac{1}{V_T} \times Q_T \times \left( \frac{C_T}{f_{up} \times K_p} \times R_b \right) \right] \quad (1.23)$$

where  $C_T$  is the drug concentration of the respective tissues,  $t$  is for time,  $Q_T$  is the blood flow rate of the tissue,  $C_{AR}$  is the arterial drug input,  $V_T$  is the volume of the respective tissue compartment,  $f_{up}$  is the fraction unbound of drug in plasma,  $K_p$  is the tissue-to-plasma partition coefficient, and  $R_b$  is the blood-to-plasma ratio of the drug.

For eliminating tissues, the mass balance differential equation is as follows;

$$\frac{dC_T}{dt} = \left[ \frac{1}{V_T} \times Q_T \times C_{AR} \right] - \left[ \frac{1}{V_T} \times Q_T \times \left( \frac{C_T}{f_{up} \times K_p} \times R_b \right) \right] - \left[ \frac{1}{V_T} \times CL_{int} \times C_{uT} \right] \quad (1.24)$$

where  $CL_{int}$  represents the *in-vitro* intrinsic clearance of the compound and  $u$  represents unbound. The  $CL_{int}$  here refers to the *in-vitro* intrinsic capability of a compound (unbound) to be metabolised by related enzymes in the absence of extrinsic factors such as blood flow and protein binding.

Likewise, in a permeability rate-limited tissues, the tissue for this kinetic reaction is divided into two compartments namely, the extracellular and intracellular space, separated by a cell membrane that forms a diffusional barrier. At a steady state, like perfusion rate-limited kinetics, this model will reach its equilibrium state whenever the unbound drug concentration is equal. Nevertheless, the time to equilibrium is highly dependent on compound permeability across the

barrier membrane, as opposed to blood flow. These drug-specific permeability values are used to estimate the permeability rate constant that affects the equilibrium across the membrane between the intracellular and extracellular concentrations. Whenever there is an active transport process, the unbound drug concentrations in the intracellular space may become lower or higher than the extracellular space depending on the exit or entry of the compound from the intracellular area (62). The mass balance differential equation representing these permeability rate-limited tissues is represented as;

*Tissue:*

$$\frac{dC_T}{dt} = (PS_T \times C_{ev}) - \left(PS_T \times \frac{C_T}{Kp}\right) \quad (1.25)$$

where  $PS_T$  is permeability-surface area metric and  $C_{ev}$  is drug concentration within the extravascular space.

*Extravascular (tissue blood):*

$$\frac{dC_T}{dt} = Q_T \times (C_{AR} - C_V) + PS_T \times \left(\frac{C_T}{Kp} - C_{ev}\right) \quad (1.26)$$

where  $C_V$  is the concentration of drug with the venous circulation.

#### **1.4.2 *In vitro* to *in vivo* scaling in PBPK modelling**

In order to simulate oral and intravenous plasma concentration-time profiles using PBPK modelling, additional drug-specific inputs such as intestinal effective permeability ( $P_{eff}$ ), the apparent permeability ( $P_{app}$ ), partition coefficient ( $Kp$ ) and intrinsic clearance ( $CL_{int}$ ) values are required. The following section portrays how these input parameters are extrapolated from *in vitro* derived inputs, into parameters reflecting the equivalent *in vivo* processes for use within PBPK models.

### 1.4.2.1 Absorption

The permeation of drug compound through cell membranes involve two main pathways: transcellular and paracellular processes. Transcellular pathways involve the diffusion of drug molecules through the lipid bilayer and have an affinity towards hydrophobic or lipophilic compounds of small molecular weight. Paracellular pathways comprise of the movement of typically small hydrophilic compound through small aqueous channels within the membrane.

A key input parameter for absorption is the human jejunum effective permeability ( $P_{eff}$ ), which can be predicted from *in silico* methods or *in vitro* high-throughput assays such as the human epithelial colorectal adenocarcinoma cells (Caco-2) or Madin-Darby canine kidney (MDCK-II) studies (65).

*In vitro* values must be scaled to *in vivo*  $P_{eff}$  values in order to utilise these values in a PBPK model. In Caco-2 model, the *in vitro* permeability values, or also defined as the apparent permeability ( $P_{app}$ ), are usually obtained during preclinical screening. Linear regression has been applied previously by Sun *et al.* (2002) to develop correlations between  $P_{app}$  and  $P_{eff}$  (66). In their study, *in vivo*  $P_{eff}$  drug permeability measurements were obtained through single-pass intestinal perfusion in human subjects, and correlated with *in vitro* Caco-2 transport permeability. The resultant regression expression for this correlation can be used to estimate  $P_{eff}$  from  $P_{app}$ : (66);

$$\text{Log}(P_{eff}) = 0.6532 \text{Log}(P_{app}) - 0.3036 \quad (1.27)$$

Similarly, *in silico* method can also be applied utilising the quantitative structure-activity relationship (QSAR) parameters namely the molecular polar surface area (PSA) and the number of hydrogen bond donors (HBD) with the following equation (67);

$$\text{Log}(P_{eff}) = 4 - 2.546 - 0.11\text{PSA} - 0.278\text{HBD} \quad (1.28)$$

The above equation has been utilised by Winiwarter *et al.* (1998) (67) in a study to predict passive absorption of 34 structurally diverse drugs in the human intestine using projections to latent structures method to correlate between  $P_{eff}$  and the physicochemical data.

### 1.4.2.2 Distribution

Another important drug-specific parameter is the  $Kp$  value which is used to characterise the distribution of the drug into different tissues in the body (68).  $Kp$  values are the ratio of total concentration of compound in the tissue to total concentration of compound in the plasma at steady state. In other words,  $Kp$  values represent the tissue accumulation resulted from processes which include lipid dissolution and protein binding;

$$Kp = \frac{C_{tissue}}{C_{plasma}} \quad (1.29)$$

In recent years,  $Kp$  values can be obtained through mechanistic methodologies which have proven to be cost-effective when compared with obtaining  $Kp$  experimentally in preclinical studies (68). Utilising *in vitro* data (binding characteristics of compounds to lipids and proteins) and physicochemical properties, these models could estimate the tissue distribution of the drug compound;

$$Kp = \frac{fu_t}{fu_p} \quad (1.30)$$

where  $fu_t$  is the unbound fraction of drug at tissue and  $fu_p$  represents the unbound fraction of drug in plasma.

Poulin and Theil (2000) (69) and Rodgers and Rowland (70-72) have developed this concept further through advanced mechanistic equations that incorporate the following considerations: (i) dissolution of ionised and unionised drug in tissue water; (ii) partitioning of unionised drug into neutral lipids and neutral phospholipids; (iii) interactions with extracellular protein for neutrals, weak bases and acids and (iv) electrostatic interactions between ionised drug and acidic phospholipids for strong ionised bases (See appendix A for a full description of the associated mechanistic equations).

These mechanistic equations are capable of predicting the steady-state tissue to plasma water unbound drug concentration ratio ( $Kp_u$ ) for moderate to strong bases and for acids, very weak bases, neutrals and zwitterions drugs, further defined  $Kp$  values into more logical PK interpretation whereby typically, it is the unbound drug that can partition into tissues;

$$Kp_u = \frac{Kp}{fu_p} \quad (1.31)$$

Furthermore, through these tissue composition-based equations,  $Kp_u$  values can now be calculated with only four drug-specific parameters namely  $LogP$ ,  $pKa$ ,  $Rb$  and  $fu_p$ , further facilitating early phase drug development.

### 1.4.2.3 Metabolism

*In vitro* metabolic clearances can be determined in model systems which include recombinant CYP systems, primary hepatocytes, and microsomes (73, 74). Recombinant CYP assays are utilised using incubations with baculovirus-expressed recombinant CYP enzymes forming certain metabolite representing participation of specific CYP isoforms that are well characterised (74). Primary hepatocyte assays are perhaps the most commonly used method due to the use of whole intact hepatocyte cellular systems which incorporate both drug metabolism and drug active transport (biliary secretion) (73).

Hepatocytes are isolated from human liver. Since hepatocytes contain both phase I and phase II drug metabolising enzymes, the assay can be utilised to determine the *in vitro* intrinsic clearance of a drug, as well as prediction of *in vivo* hepatic clearance.

Finally, microsomes are isolated from cellular fraction, specifically the endoplasmic reticulum, and are popular due to their simplicity in isolation and cost-effectiveness when compared to other cell models. However, due to the poor predictive utility of microsomal data hepatocytes are preferred. This is often a result of wide variability in quality which is often laboratory-dependent, and the fact that microsomes only contain phase I enzymes as compared to primary hepatocytes assay in which hepatocellularity is not an experimental variable and contains both phase I and phase II enzymes (73, 75).

Since *in vitro* metabolic clearance data generated by these *in vitro* assays are mainly related to the unit of enzyme content, extrapolation is required to an unbound human hepatic intrinsic clearance ( $CL_H$ ). The scaling of  $CL_{int, in vitro}$  to  $CL_{int, in vivo}$  involves the inclusion of microsomal

recovery that consists of the microsomal protein content or hepatocellularity (74, 76, 77) and the liver weight of species (76). These scaling factors can be summarised in two key equations representing the microsomes (equation 1.32) and the hepatocytes (equation 1.33) (62);

$$CL_{int, scaled} = \frac{CL_{int, app}}{f_{u, inc}} \times MPPGL \times LW \quad (1.32)$$

$$CL_{int, scaled} = \frac{CL_{int, app}}{f_{u, inc}} \times HPGL \times LW \quad (1.33)$$

where  $CL_{int, scaled}$  represents the scaled *in vivo*  $CL_{int}$  in ml/min,  $CL_{int, app}$  represents the apparent *in vitro*  $CL_{int}$  ( $\mu$ l/min/mg for microsomes and  $\mu$ l/min/million cells for hepatocytes),  $f_{u, inc}$  represents the fraction unbound in the *in vitro* system,  $MPPGL$  represents the milligrams of microsomal protein (MSP) per gram of liver (mg/g),  $LW$  represents liver weight (kg), and  $HPGL$  represents the hepatocellularity per gram of liver ( $10^6$ /g).

Using a well-stirred liver model, the unbound hepatic plasma clearance of a drug is then calculated with the following equation;

$$CL_H = \frac{f_{u, p} \times CL_{int, in vivo} \times Q_H}{Q_L + f_{u, p} \times CL_{int, in vivo} / R_b} \quad (1.34)$$

where  $CL_H$  represents the unbound hepatic plasma clearance,  $f_{u, p}$  represents the fraction unbound of drug in plasma,  $CL_{int, in vivo}$  represents the *in vivo* intrinsic metabolic clearance,  $Q_H$  represents the blood flow rate of the liver tissue and  $R_b$  is the blood-to-plasma ratio of the drug.

Table 1.1 highlights the typical values and units used for the hepatocytes and microsomes assay scaling factors.

**Table 1.1 Typical steps, values and units used for the microsomes and hepatocytes assay scaling factors.**

<b>Microsomes Assay</b>			
<b>Step</b>	<b>Value</b>	<b>Unit</b>	<b>Note</b>
1	<i>a</i>	pmol/min/mg MSP	V <sub>max</sub> <i>in vitro</i> value
2	<i>a</i> x 20.8	mg MSP/g liver	MPPGL (78)
3	<i>b</i> x 1820	g	Liver Weight
4	<i>c</i> x 10 <sup>9</sup>	mmol/nmol	pmol to mmol conversion
5	<i>d</i> / MW	mg/mmol	Molecular Weight (MW)
6	<i>e</i> x 60	min/hr	Minutes to hour conversion
<b>7</b>	<b><i>f</i></b>	<b>mg/hr</b>	<b>V<sub>max</sub> <i>in vivo</i> value</b>
8	<i>g</i>	mg/hr/kg body weight (BW)	V <sub>max</sub> scalar in PBPK model (for 70kg human)
<b>Primary Hepatocytes Assay</b>			
1	<i>a</i>	nmol/hr/10 <sup>6</sup> cells	V <sub>max</sub> <i>in vitro</i> value
2	<i>a</i> x 137	10 <sup>6</sup> cells/g liver	HPGL (79)
3	<i>b</i> x 0.026 x 70 x 10 <sup>3</sup>	g	Liver Weight 2.6% of BW, BW=70kg
4	<i>c</i> / 10 <sup>3</sup>	μmol/nmol	nmol to μmol
<b>5</b>	<b><i>d</i></b>	<b>μmol/hr</b>	<b>V<sub>max</sub> <i>in vivo</i> value</b>
6	<i>e</i>	μmol/hr/kg BW <sup>0.7</sup>	V <sub>max</sub> scalar in PBPK model (for 70kg human)

Scaling factors are based on the assumption that the content of enzyme present in each system is proportional to the amount of the functional unit of the given system. Enzyme activity is expressed as the amount of product formed/unit such as nmol/min.

*a* – value extracted from *in vitro* assay; *b*, *c*, *d*, *e*, *f*, *g* – values calculated

#### **1.4.2.4 Renal or biliary excretion**

Numerous approaches can be used to predict *in vivo* intrinsic organ clearance for organs other than the liver such as renal and biliary. However, these approaches are still under scrutiny and development (21, 80-82). An example of a more recent approach for renal excretion is the extrapolation of animal renal clearance such as in rodents to human *in vivo* values as well as utilising allometric method including the use of glomerular filtration rate (GFR) (83).

## 1.5 PBPK AND POPULATION VARIABILITY

Population-based PBPK modelling is a platform and integration of database that links mechanistic modelling and simulation of ADME processes of drug compounds in healthy and disease population. This platform is an invaluable tool to simulate and predicts population variability in terms of metabolically-based DDIs and also multi-ethnic polymorphism (84).

As previously highlighted, developing a PBPK model requires three types of data for it to be functioning as intended, namely, the ‘compound-data’, the model structure which comprises of tissues and organs arrangement, and the ‘systems-data’ (biochemical, anatomical and physiological data) (85). The integration of these data allows the understanding and prediction of concentration-time profiles in tissues and plasma as well as the PK behaviour of the drug compounds. PBPK model can also extrapolate across the mammalian species such as rat, mouse, and human due to the generic structures of the model and if an appropriate system data is utilised.

Since PBPK modelling involves system’s data such as blood flow and organ volumes of animal or human, it is expected that population variability or inter-individual differences in physiology and biochemistry occurs. This variability can affect the susceptibility of individual towards drug compounds especially its PK profiles (absorption, distribution, metabolism, and elimination) which in turn, has an impact towards the efficacy and safety of drugs.

Within the context of PBPK modelling, the incorporation of such variability is possible through defining boundary limits on ‘system-data’ parameters, often within a plausible range (coefficient of variation [CV]) of 30 % (48). Thereafter, in simulating multiple subjects, a Monto-Carlo approach can be implemented to allow random between-subject variability in specific ‘systems-data’) to mimic the variability in pharmacokinetics observed in clinical studies.

To explore this population variability, two modelling approaches have been developed: *a priori* (bottom-up) and *a posteriori* (top-down).

In *a priori* (based solely on theory) approach, variability can be modelled in two separate models or a combination of stochastic simulations (Monte-Carlo methods) and deterministic description of the determinants of variability (48). Mechanistic PBPK modelling belongs to this group. These methods aim to estimate the overall variability of the concentration-time profile which is then used to compare with the observed variability data, independent of experience such as clinical trials. The Monte-Carlo approach involves computation and generation of multiple sampling of purely random statistical distribution to generate 90% or 95% confidence interval of multiple parameters such as the volume of distribution and clearance. This method can sometimes be considered as ‘random guessing’ of parameters since it only provides purely statistical distribution even for a simple PK-determined parameter such as time, age and sex that can be easily obtainable from literature. However, Monte-Carlo method can be beneficial to estimate drug disposition in complex organs such as the central nervous system which can prove to be difficult to obtain any observed data. In deterministic modelling approaches, the concept of this method revolves around the fact that some of the inter-individual variability is due to gender, growth or age-related changes which can be modelled in a specific lifetime PBPK models such as paediatric, geriatric, pregnant, disease states and gender-specific models (86, 87).

For *a posteriori* (observational) models, the approach to obtain an estimate of the inter-individual variability is through data based on clinical trials or empirical evidence. This is where empirical compartmental PK models (population PK) plays a part in providing a plausible explanation of covariates in observed variability (88, 89). This model aims to determine scenarios such as the impact of variability in metabolic rate, renal clearance or bioavailability has on the variability of plasma concentration of drug molecules inter-individually. This model can also be used to predict various clinical treatment scenarios provided that the determinants of variability have been obtained. Population variability can be observed within phases of PK which is discussed below.

### 1.5.1 Absorption

The most convenient and common route of drug administration is the oral route albeit with its issues of high inter-individual variability and low bioavailability. Several factors could affect oral absorption of drug molecules. Such factors can be classified into two main categories which are the drug-related (physicochemical) and system (physiological) factors. Inter-individual effects mainly involve the system factors, and it includes the intestinal residence time, transporters contribution, gastrointestinal pH and gastric emptying time.

Drugs with low permeability characteristics often contribute to the effect of intestinal residence time, hence, lead to high inter-individual variability (90). Studies have shown that intestinal residence time can vary between one to six hours in 400 subjects and it appears to be independent between solid and liquid dosage forms as well as the presence of food (90-92). Regarding membrane localised drug efflux/influx transporters, inter-individual variability can be observed along the basolateral and apical membranes of the intestinal cells whereby most of the affected transporters are expressed (93-95). The expression of these transporters has been found to be varied across the gastrointestinal tract (96). Most of the studies seem to be revolved around the efflux transporters such as *BCRP (ABCG2)*, *MRP2, (ABCC2)* and *MDR1 (ABCB1)* located at the apical membrane of the intestine due to its characteristics in limiting intestinal drugs absorption when administered orally.

Drug solubility and dissolution can also be influenced by the pH along the gastrointestinal tract (97, 98). Also, drug permeability can also be affected by the gastrointestinal pH since the latter can influence the balanced between non-ionised and ionised moieties. The inter-individuality of the gastrointestinal pH can vary up to two pH units at the same time, and this observation has been reported by Fallingborg *et al.* (1989) (97). Presence of food in the gastrointestinal tract could also raise the gastrointestinal pH in the proximal part of the small intestine and the stomach due to the buffering capacity of proteins. Oral drug absorption can also be affected by gastric emptying time of the drug in the stomach in which variability can also occur with the drug's absorption rates (99-101).

### 1.5.2 Distribution

Drug distribution can be defined as a reversible transfer of molecule from one location to another within the body (102). Several factors could affect the distribution of the drug which includes the binding of the drug within blood and tissues, partitioning of molecule into fat, tissue uptake, the ability of the drug molecule to cross tissue membranes and the delivery of drug to tissue by blood (103, 104). Physiological factors that introduce variability in the drug distribution include expression of transporter proteins, plasma protein concentrations, tissue composition, tissue volumes, haematocrit and blood perfusion rates to the tissues.

Several drug transporters can be found in the membranes of tissues which can influence drug distribution especially for the low passive permeability drug such as valsartan, methotrexate, and digoxin (105). Polymorphism has also been reported occurred in transporters which may affect the drug distribution variability among individual (106). In order to be considered a polymorphism, the minority or variant allele's frequency should be at a minimal 1 % (107).

Tissue composition also plays a role in the variability of drug distribution. In blood, the volume of haematocrit is influenced by several factors such as physical activity, seasonal influence, sex and age (108-110). The reported value of haematocrit ranges from 40 % - 54 % in males and 38 % - 47 % in females. The three essential plasma proteins responsible for binding of drugs are albumin, alpha1-acid glycoprotein (AAG), and lipoproteins (111). Of those three, albumin levels have been reported to generally decreased with age (112).

Tissue volumes and blood flows have been reported to influence inter-individual variability in a PBPK modelling study which shows the importance of modelling and simulation in detecting inter-individual variability in human pharmacokinetics (113). This model included physiological parameter values approximately 31,000 database records which include information regarding volumes and masses of selected organs and tissues as well as blood flows to the organs and tissues.

### 1.5.3 Metabolism

Ethnicity within a population plays a role in metabolic variability due to differences in biological parameters such as enzymatic abundance which can differ between ethnic population (114, 115). Drug metabolism occurs in many organs; however, the liver has been established to be the primary site of metabolism in many drugs. Cytochrome P450 (CYP450) is a family of enzymes that catalyse the biotransformation of drugs (Figure 1.12). It was observed that the African and South Asian population have lower CYP3A4 activities when compared to the Caucasians, further, the Africans also have lower CYP2D6 levels compared to the Caucasians (116). Consequently, age-related differences also contributed to the variability in drug metabolism due to the low levels of activity of CYP1A2, CYP3A4 and glucuronidating enzymes in paediatrics and the slower activity or expression of CYP2C19, CYP2D6 and CYP3A4 in the elderly population (117). The impaired functionality of the liver due to liver cirrhosis could also potentially affect the first-pass metabolism of drugs which contributes to the metabolic variability in a subpopulation (55).

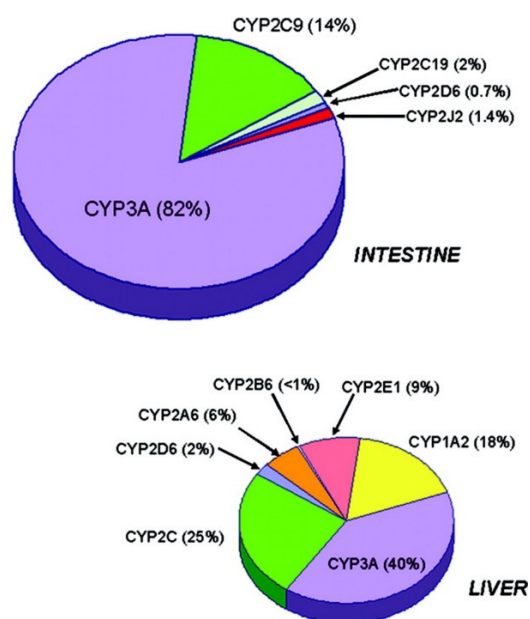


**Figure 1.12 Phase I and II CYP450 metabolism enzymes composition in the liver and intestine of the human body.**

Reproduced from Paine *et al.* (2006) (118).

#### 1.5.4 Elimination

Variability in elimination phase occurs due to several factors including genetic polymorphism of renal transporters, glomerular filtration rate variation due to disease such as hypertension and diabetes as well as variation in the bile flow due to cholestasis (48). Drug excretion or elimination is defined as an irreversible loss of chemically unchanged drug from the body (119). In many drugs, elimination is primarily mediated by the kidneys, but there are some drugs which are excreted predominantly *via* the bile (and faecally eliminated). Drug elimination could also happen *via* sweat, lungs, breast milk and saliva but at limited rates. There are three processes involved when drugs are eliminated via kidneys: 1. Tubular secretion, 2. Tubular reabsorption and 3. Glomerular filtration (Figure 1.13). Tubular secretion is mediated by transporters and happens mostly at the proximal tubule area. Tubular reabsorption is active and passive processes. The former occurs around the nephron whereas the latter at the proximal tubule (transporter-dependent) and usually associated with drug interactions (120). Renal elimination is dependent on plasma protein binding, renal blood flow, renal transporters, urine pH, and urine flow (121, 122). Variability in renal elimination depends on the genetic variations that occur in transporters and affects renal secretion as well as reabsorption (123).

Besides kidneys, biliary elimination also plays a part in excretion of drugs and drug metabolites (124). It requires active transporters to allow drug molecules to cross the biliary epithelium against a concentration gradient and it is often that a drug will undergo reabsorption (enterohepatic circulation) when eliminated via the bile. Similar to kidney excretion, variability in biliary excretion also depends on the genetic variations due to the transporters (proteins) involved in its mechanism (125).

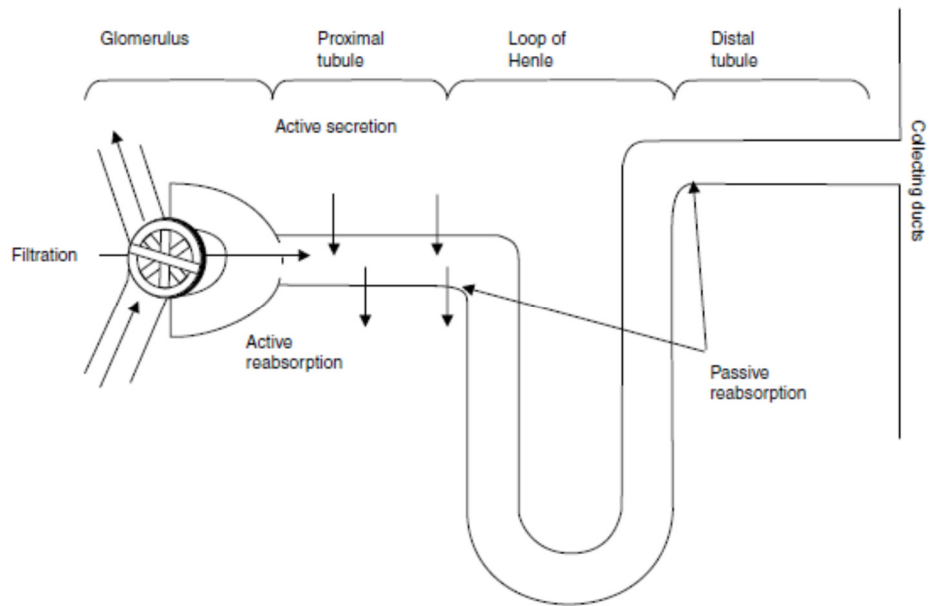


**Figure 1.13 Diagrammatic representation of a nephron, delineating an area where active secretion, passive reabsorption, and filtration occur.**

Reproduced from Tett *et al.* (2003) (120).

## 1.6 STRATEGIES FOR DEVELOPING A PBPK MODEL

Developing a PBPK model requires intuition, experience, patience and solid theoretical background. Troubleshooting skill is also necessary for solving difficult problems, especially in model fitting. Gabrielsson and Weiner (2010) (126) have established several guidelines that can be utilised as a strategy when developing a PBPK or PPK models (Figure 1.14).

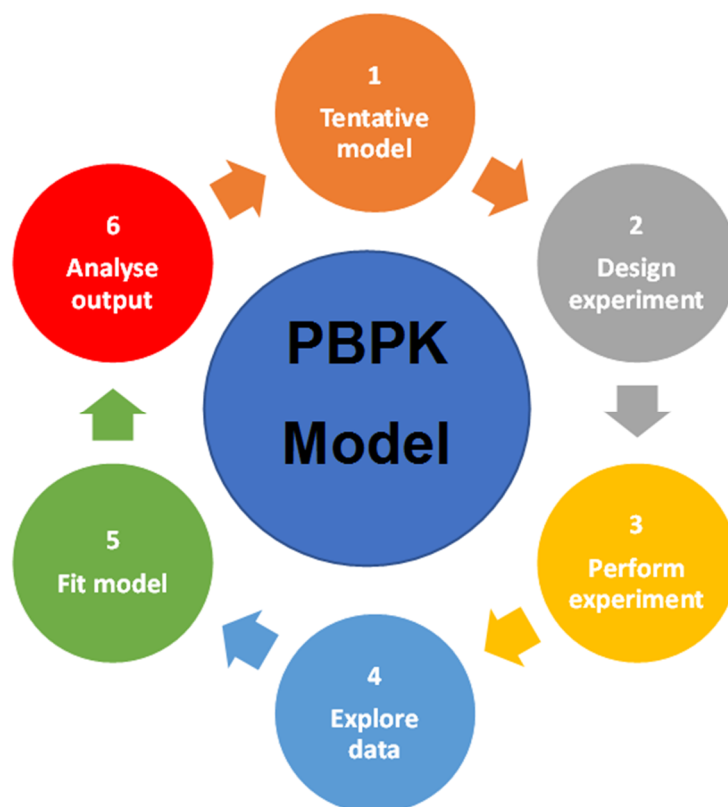


**Figure 1.14 Development of a PBPK model: from data to model.**

The initial starting point is developing a tentative model (1) and designing/selecting experiment to obtain parameters, e.g. effect at various concentrations (2). Next, obtaining the parameters required (3) and exploring the data by analysing it (4). After that, fitting the model if necessary (5) and finally, analysing the data output after fitting has been done (6). Then, the cycle restarts to obtain more precise and accurate simulations.

### **1.6.1 Development of tentative models**

According to Gabrielsson and Weiner (2010) (126), understanding of pharmacological effects and underlying kinetics are one of the initial steps for model selection. For example, the modeller needs to determine if the response that they observed is the result of stimulation or inhibition. Regarding kinetics, the linearity and non-linearity should be taken into consideration. As for the compound, the physicochemical characteristics such as the clearance and half-life should be known first-hand if there is any plasma profiles to be analysed. In other

words, the kinetics or turnover of the compound should be examined including the routes of elimination and time to reach steady state.

### **1.6.2 Designing and performing experiment**

As stated previously, before designing and conducting an experiment, prior information regarding kinetics, dynamics or turnover needs to be taken into accounts. The data that has been gathered from all these parameters will be used to make an initial simulation. This is done to obtain initial design points for sampling (minimum/maximum plasma concentrations or time points) from the concentration-time plot using the estimation of the tentative parameter of the proposed model. After all of these strategies were performed, the proposed experiment can be conducted for the proposed model testing or validation.

### **1.6.3 Exploring data**

Once the tentative model, experimental design, and data collection have been conducted, the experimental data needs to be explored and prepared. For this stage, it is recommended to begin by pooling data from several subjects as well as inspecting data from each subject. Data pooling is essential whenever there is an insufficient data density from individuals to be analysed or when the data has high variability. Two approaches can be used for data, the Naïve Pooled Data (NPD), whereby model fitting is done simultaneously to all individual data observations and Naïve Averaged Data (NAD) whereby the data are averaged, and model fitting is done to the mean data. These two approaches will give identical estimates with the condition that the number of observations at each time point is the same. However, pooling methods could only be used as a general overview as it may expose the risk of masking individual data or behaviour.

Obtaining initial estimates is also part of data exploration. These initial estimates are integral whenever the data does not fit the model, and there is much scattering. Numerous methods can be conducted to obtain initial estimates such as non-compartmental analysis, convolution-deconvolution methods and graphical methods and linear regression. Knowledge of the compound should be obtained as early as possible, and any regression methods that have been utilised should have a clear objective to achieve the desired modelling outcome.

#### 1.6.4 Model fitting

After data exploring, model fitting is used to fit the proposed model to the available data. The rationale for this approach is to reduce the variability of the observed and predicted data by way of parameter estimation (PE), or ‘model fitting’. PE is also conducted whenever there is the need to quantify physiological process that involves sophisticated system-related parameter such as absolute abundances of hepatic transporters in which it is relatively difficult to obtain its published values. However, before any attempt to parameter estimated the unknown parameter, a sensitivity analysis is recommended to be conducted to determine whether the output is sensitive to the respective unknown model parameter. Sensitivity analysis is a method whereby the variation of the specific output in the model is examined quantitatively or qualitatively to different sources of variation (127). Nestorov *et al.* (1997) (128) and Gueorguieva *et al.* (2006) (129) made comprehensive reviews on numerous methods that can be utilised and technical issues regarding the implementation of sensitivity analysis in PBPK modelling. Results from sensitivity analysis can be used to justify any output that has been parameter estimated due to its robust calculations of obtaining variability in different scenarios. Such approach can also provide uncertainty analysis by providing an overview of which parameter that is needed to be determined to improve the predictability of the PBPK model.

PE approaches can be challenging due to sparse observed data availability and a large number of parameters that are usually involved. Hence, various approaches have been developed in order to fit the model to observed data. As mentioned previously (Section 1.5), one of the most widely used approaches is using Monte-Carlo optimisation which searches optimisation randomly for adequate fits and also to address uncertainties in parameters (130). In Monte-Carlo optimisation for uncertainty analysis, the simulation will randomly samples model parameters from defined distributions (e.g., normal, log-normal) with defined variability (131). Using this method, parameter values are chosen using random selection scheme. These parameter values are then simulated in a huge number (amounting to thousands of iterations) to generate values of the output variables which are then saved for analysis. These output variables represent the distribution of the model output as well as estimation of its level of uncertainties (132). It is important to note that using Monte-Carlo approaches could sometimes

lead to unrealistic parameter values in some well-defined physiological parameters such as volumes and flows in certain organs. Therefore, it is recommended that any results obtained by Monte-Carlo analysis should always be validated with physiological values that are plausible within their 'true' physiological space.

In general, it is advisable to do several simulations with variable parameters representing the different effect in calculated curves with various degrees of parameter values. It is also highly recommended to use upper and lower bound of the parameters (e.g., 5<sup>th</sup> and 95<sup>th</sup> percentile of the population) to correlates with better numerical stability. The visual inspection between the predicted and observed values is essential as the parameter values from the compound must be consistent with the predicted and observed data to indicate their value towards the proposed model.

### **1.6.5 Analysing outputs**

The final step of the modelling approach is the analysis of the output and assessment of goodness-of-fit which is related to the fitted curve of the data distribution. The evaluation of goodness-of-fit is very subjective to the modeller as it requires the modeller to make superimposed comparisons between fitted curve plots and the observed data. For PPK models, it is recommended to use residual plots to analyse the goodness-of-fit. Residuals are errors which the model could not explain and can be defined as the vertical difference between the observed and predicted concentration (Figure 1.15). The residual values ( $\epsilon$ ) can be positive or negative. A positive value means that the residual point is above the curve whereas, for a negative value, it is below the curve. In general, it is preferable that the residuals be randomly distributed around the predictive curve to indicate a good fit in a PPK model. In other words, if the model fit to the data were correct, the residuals would approximate the random errors that make the relationship between the explanatory variables and the response variable a statistical relationship. Consequently, if the residuals appear to act randomly, it suggests that the model fits the data well. In contrast, if non-random structure is apparent in the residuals, it indicates that the model fits the data poorly (133).

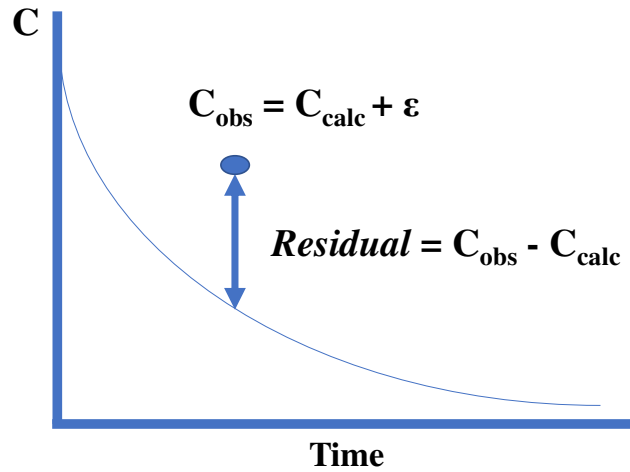


**Figure 1.15 Relationship between the residual error ( $\epsilon$ ), the observed concentration ( $C_{obs}$ ) and the predicted concentration ( $C_{calc}$ ) for PPK model analyses.**

In a PBPK model, assessment of the goodness-of-fit and accuracy can be determined by two approaches: the assessment of mean fold error and the reduced mean squared error ( $X^2$ ) statistic method (134). For the mean fold error assessment, a ratio of predicted and observed values can be taken into account as such the value will always be more than 1. This equation can be summarised as follows:

$$Mean\ fold\ error = 10^{\left[\frac{1}{n} \sum \log(fold\ error)\right]} \quad (1.35)$$

where  $n$  represents the number of observations. The closer the number of mean fold error to 1, the higher probability that the prediction can be accepted.

In the  $X^2$  statistic assessment, this approach can be utilised whenever there are standard deviations or standard deviations of multiple observations at each timepoint. The equation is as follows:

$$X^2 = \frac{1}{N} \sum_{i=1}^N \left( \frac{\Delta_i^2}{\sigma_i^2} \right) \quad (1.36)$$

where  $N$  represents the number of observations,  $\Delta$  represents the difference between the observed and simulated concentrations at the same timepoints, and  $\sigma$  represents the standard

deviation at the corresponding timepoints. The closer the value of  $X^2$  to 1, the higher probability that the prediction can be accepted.

For a model to be accepted or rejected with a known level of confidence, statistical tests should also be conducted to any goodness-of-fit value as an essential complement to visual inspection. Generally, a mean fold error of less than 2 is considered an acceptable range for a good prediction. Such error range is commonly reported by other researchers and is considered appropriate for a predictive model (87, 135-138).

## **1.7 PBPK MODELLING SOFTWARE**

Several commercial software have been developed to cater for different applications in PBPK modelling. Typically there are two types of software available; general mathematical and engineering modelling software and PBPK specialised software (57, 139). General mathematical and engineering modelling software includes acsIX®, Berkeley Madonna® and Matlab® (140). This software provides not only programming language and numerical solution of the system of the model but also a graphical output of the simulation results and offers much flexibility to the modellers. However, advanced programming, modelling skills, and experience are required which makes this software unsuitable for beginners.

For PBPK specialised software such as Simcyp® (141), PK-Sim® (142) and GastroPlus® (143), even though this software provides less flexibility in modelling development, it required less experience and modelling skill from the modeller. In addition, these software offers additional features such as simulation for virtual populations (obese, pediatric, renal impairments, and others), simulation of complex PK involving multiple metabolite profiles and drug interactions as well as clearance prediction model (57). It also needs to be mentioned that although this software requires less experience and modelling skills, users need to understand the fundamentals of PK and background of clinical pharmacology to determine the appropriate models and understand the difference between various models offered in the software that is used in the PK analysis.

## **1.8 ROLE OF PREDICTIVE MODELS FOR DRUG DELIVERY**

Advancement in computing technologies has made it possible for PBPK modelling to explore more complex scenarios including simulating complex absorption models such as the advanced compartmental absorption and transit (ACAT) (144) and the advanced, dissolution, absorption and metabolism (ADAM) models (20). These two models have been used extensively in complex scenarios such as simulation of drug-drug interactions (139, 145, 146), changes of PK characteristics (ADME) in different age groups and special populations, i.e. pregnant women, renal and hepatic impairments and also children (147-151). Also, PBPK approach has shown to be useful in predicting drug disposition in complex organs such as the central nervous system (152).

Regulatory authorities have also taken an interest in applying PBPK modelling in their routine evaluation of submission of drugs for marketing authorisation and have also utilised such approach when implementing or developing new policies of drug utilisations (153-156). For example, European Medicines Agency (EMA) has published several guidelines related to the application of PBPK modelling in its investigational new drugs (IND) and new drug applications (NDA) as well as in special populations such as hepatic impairment and DDIs (157, 158). Likewise, the United States Food and Drug Administration (USFDA) has also established their version of guidelines related to PBPK modelling in pharmacogenetics, paediatrics and also predicting optimal dose and design of clinical studies, specifically, the first in human (FIH) trials (159-161) (Table 1.2).

**Table 1.2 Implementation of PBPK modelling in drug development and regulatory authorities policies.**

<b>SCENARIO</b>	<b>IMPLEMENTATION</b>	<b>EXAMPLE</b>
<b>Specific Patient Population</b>	<ul style="list-style-type: none"> <li>• Paediatrics and Geriatrics</li> <li>• Hepatic and Renal Impairment</li> </ul>	<p><u>Paediatrics</u> Skyla® IUD (progestin-containing IU system for prevention of pregnancy)</p> <ul style="list-style-type: none"> <li>• The simulated pediatric PK of levonorgestrel in pediatric subjects supported the use of this product in a paediatric trial for females postmenarcheal to 18, an age group for which there is currently no data (156).</li> </ul>
<b>Drug-drug Interactions</b>	<ul style="list-style-type: none"> <li>• Drug as Enzyme Substrate</li> <li>• Drug as Enzyme Perpetrator</li> <li>• Transporter-mediated Interaction</li> </ul>	<p><u>DDI</u> Cabazitaxel (hormone-refractory metastatic prostate cancer)</p> <ul style="list-style-type: none"> <li>• PBPK analysis indicated minimal effect on the exposure of midazolam (a CYP3A probe) in humans – resulted in USFDA to request a post-marketing requirement study to evaluate a possible interaction between cabazitaxel and CYP3A substrates in humans (156).</li> </ul>
<b>Other Situations</b>	<ul style="list-style-type: none"> <li>• Tissue concentration</li> <li>• PK prediction in humans: FIH studies</li> </ul>	<p><u>FIH studies</u> Pfizer – PF-02413873 (non-steroidal progesterone receptor antagonist)</p> <ul style="list-style-type: none"> <li>• Simulations were performed in human using CL values estimated from human liver microsomes and the dog CL (153).</li> </ul>

## **1.8.1 Regulatory Perspectives**

### **1.8.1.1 European Medicines Agency (EMA)**

The increasing demand on developing medicines (for human or animal use) adhering to high standards of safety, efficacy and quality as well as constant monitoring of medicines following its approval led to the establishment of the European Agency for the Evaluation of Medicinal Products (EMEA) in 1995 for the purpose of harmonising and integrating the function of existing medicines regulatory authorities within the European Union (EU). The name was subsequently changed to European Medicines Agency (EMA) in December 2009 as part of strengthening its communication materials to the public and giving more explicit messages about the agency's roles and activities (162). EMA is organised into five main Units which are the Human Medicines Development and Evaluation, Patient Health Protection, Veterinary Medicines and Product Data Management, Information and Communications Technology and Administration Unit. All these Units are headed by the Executive Director who is appointed by Agency's Management Board. Figure 1.16 shows the overview of the primary organisation structure.

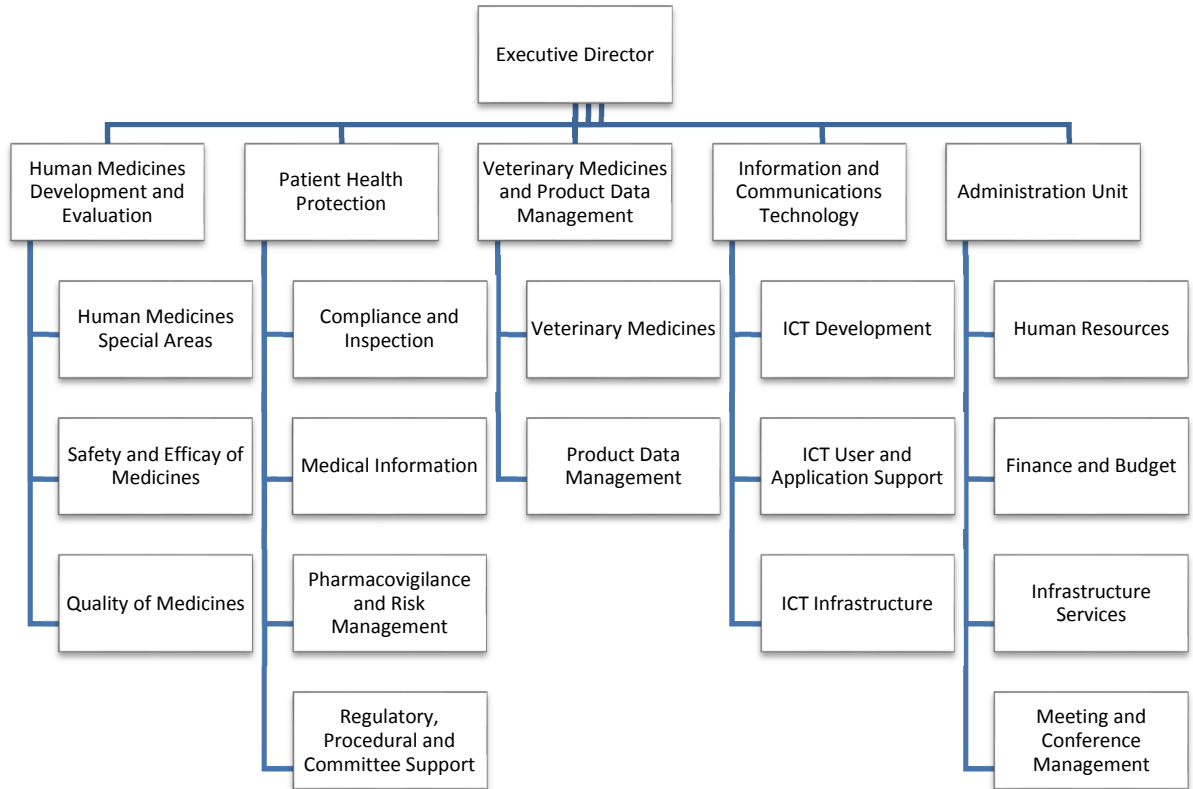


**Figure 1.16 The Overview Structure of the EMA.**

Diagrammatic representation of the overview structure of EMA showing the various units and the subunits of the organisation.

*EMA viewpoint on PBPK modelling*

In response to narrowing the knowledge gaps between ethical and practical issues in drug development, especially when it is related to conduct of clinical trials and its benefit-risk evaluations, the EMA has begun to implement virtual trials or PBPK modelling as part of its strategic plan for regulatory science (163). Draft guidance on the qualification and reporting of PBPK modelling and simulation has been established on July 2016 to address issues such as the ability of the platform to adequately perform a simulation of the predetermined type, and drug model specific issues (157). The scope of the guideline revolves on the qualification of the PBPK platform and the reporting of PBPK modelling and simulation. To date, numerous marketing authorisation application (MAA) containing PBPK as part of the dossier is

increasingly submitted and requested. These submission and requests have comprised mainly of drug-drug interactions (DDI), paediatric dose selection and first in human trials (Figure 1.17). Such information has been included in EMA’s European Public Assessment Reports and European Summaries of Product Characteristics for several products such as Imbruvica<sup>®</sup> (ibrutinib - anticancer), Opsumit<sup>®</sup> (macitentan - pulmonary arterial hypertension), Cerdelga<sup>®</sup> (eliglustat tartrate - lysosomal storage disorders), Zykadia<sup>®</sup> (ceritinib - anticancer), and Odomzo<sup>®</sup> (sonidegib phosphate - anticancer) (164).

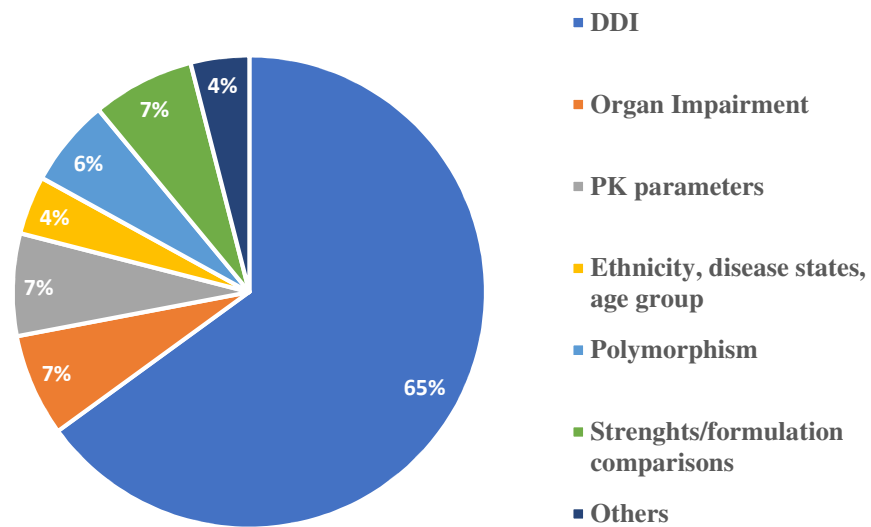


**Figure 1.17 Areas of PBPK application submissions received by the EMA up to 2015 (n=112).**

A forum was held on 30 June 2014 between the Association of the British Pharmaceutical Industry (ABPI) and United Kingdom Medicines and Healthcare products Regulatory Agency (MHRA), representing EMA to explore PBPK simulation and modelling and its regulatory applications (165). In that meeting, MHRA, which represents the European regulatory perspective, has made several recommendations towards a better implementation of PBPK platforms towards regulatory submissions. The key recommendations were for companies to

agree and adopt common reference standards especially with regards to methodologies when conducting PBPK modelling since different companies were developing methodologies which include various reference standards that prove to be challenging to validate across companies. This led to difficulties in assessing and validating the models by the evaluators. Furthermore, to address critical parameters that are required for PBPK modelling especially those that involve DDI, specific populations and biopharmaceutics, a consensus should be developed to compile essential input parameters that cater for these conditions to provide appropriate data standards to the regulatory authorities.

The EMA also has provided guidance on the verification of drug specific input parameters especially the range of values in sensitivity analysis around the chosen parameters (158). To address this issue, it was recommended that general guidance regarding the choice of parameters and the range of values in sensitivity analysis should be developed based on the experimental system and physicochemical properties of the drug molecule. Companies were also advised to not solely depend on sensitivity analysis to resolve parameters uncertainty, instead it was recommended that they need to resolve that uncertainty by experimental methods wherever possible.

In terms of establishing a PBPK report, EMA inferred that a specific plan to extrapolate the PBPK modelling to clinical pharmacology program should be developed to provide an integrated approach towards drugs quantitative disposition. Also, a clear statement of assumptions underlying the development of the modelling should be accounted and integrated with the impact on the prediction so that the rationale of the model can be justified (158).

In summary, EMA's viewpoints towards PBPK modelling shows that standardisation and rationalisation are paramount in determining the acceptability of the PBPK evaluations towards the MAA. Also, EMA's willingness to develop policy guidance in PBPK modelling proved that this area is evolving rapidly and is expected to show its full potential regarding model-informed drug development in the very near future.

### 1.8.1.2 United States Food and Drug Administration (USFDA)

The USFDA is one of the oldest establishments of regulatory authorities dating back to 1862. Its primary roles are the evaluation and monitoring of most of food products (excluding meat and poultry), drugs for the use of human and animal, biological therapeutic agents, medical devices, radiation-emitting products for medical, occupational and consumer use and cosmetics as well as animal feed in accordance with the Federal Food, Drug, and Cosmetic Act (FD&C Act). The FDA also regulates the distribution, marketing, and manufacture of tobacco products (166, 167). The organisation is an agency within the Department of Health and Human Services and consists of nine Centres and Offices as shown in Figure 1.18.



**Figure 1.18 The structure of the FDA.**

Diagrammatic representation of the structure of FDA showing the hierarchy, the centres, and the offices. The Office of the Commissioner is overseen by two other principal offices; Office of the Chief Counsel which report to the General Counsel of Department of Health and Human Services (HHS) and gives advises to the Commissioner of Food and Drugs and Office of the Administrative Law Judge which reports directly to the Secretary of HHS.

### *USFDA policy on PBPK modelling*

USFDA is one of the early adopters of PBPK approaches based on its various strategic plans for regulatory science promoting innovation in drug development (159). The earliest known PBPK application on drug approvals by USFDA was in the 1990s whereby a compound known as tretinoin was approved as an active ingredient in topical anti-wrinkle cream (168). The USFDA requested a PBPK simulation to be conducted to determine the risk of congenital disabilities and foetal exposure due to the teratogenic effect of the compound. The simulation concluded that the risk was minimal and the PBPK model has managed to provide an estimation of maternal and foetal plasma concentration accurately for the regulatory decision to be made. This first case study has become a stepping stone towards encouraging more companies to utilise PBPK modelling to determine the best dosing strategy (169).

In-line with the recommendations, the USFDA has developed several guidelines related to the application of PBPK modelling such as in clinical lactation studies, paediatric medicines development, drugs interaction evaluations, generic drugs and recently, specific guidance for industry on PBPK analyses (160, 161, 170-172). The latter, being the most recent draft guidance, have covered several types of drugs applications which include investigational new drug (INDs) applications, new drug applications (NDAs), biologics license applications (BLAs), and abbreviated new drug applications (ANDAs). The guidance's primary aim is to standardise the content and format of PBPK study reports that are submitted to the USFDA hence, facilitating assessments efficiency. Similar with EMA, this guidance delineates several aspects to consider when submitting PBPK reports to USFDA for assessment including an overview of modelling strategy, modelling parameters, simulation design, software, model verification and modification, and model application. From 2008 to 2012, USFDA has received 33 PBPK submissions in IND or NDA from pharmaceutical companies which shows higher acceptance towards this approach in drug evaluations (Figure 1.19).

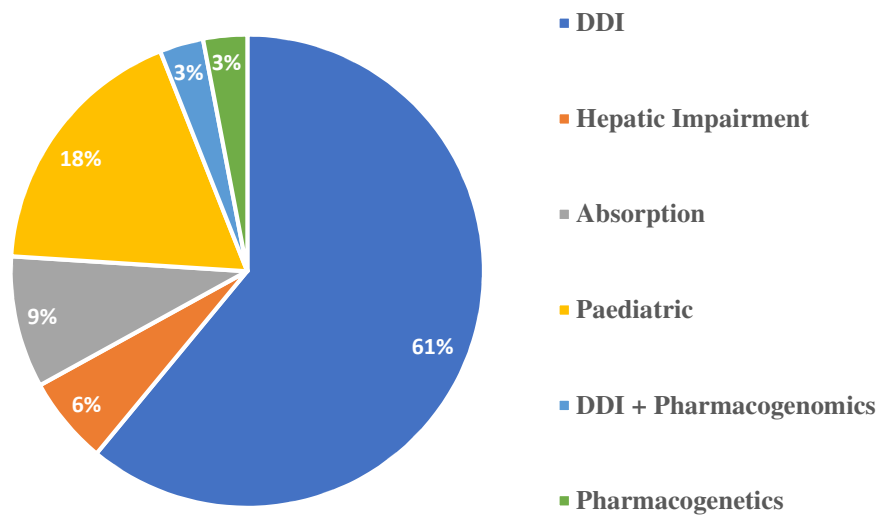


**Figure 1.19 Areas of PBPK application submissions received by the USFDA from 2008 to 2012 (n=33).**

An example of the approach of PBPK modelling actively being utilised in USFDA assessment is in the generic drug review section whereby this approach has been implemented to assess biowaivers for Biopharmaceutical Classification System (BCS) Class 2 (low solubility and high permeability) and 3 (high solubility low permeability) drugs (Figure 1.20) in which these drugs usually display multiple concentration peaks (typical representative of enterohepatic recirculation) such as propofol, acebutolol, digoxin, nevirapine, ranitidine and valproic acid (173).

	High Solubility	Low Solubility
High Permeability	<b>Class 1</b> High Solubility High Permeability (Rapid Dissolution for Biowaiver)	<b>Class 2</b> Low Solubility High Permeability
Low Permeability	<b>Class 3</b> High Solubility Low Permeability	<b>Class 4</b> Low Solubility Low Permeability

**Figure 1.20 Biopharmaceutical classification system as defined by the USFDA.**

Furthermore, the PBPK approach is also used to improve upon a drugs *in vitro-in vivo* correlation (IVIVC), in locally acting gastrointestinal drugs, nanotechnology, formulations evaluation, topical and pulmonary routes of administration among others (174). Recently, another emerging area in which USFDA routinely applied PBPK approach in drug evaluations is in DDI predictions, including the effects on multiple CYP enzyme inducers, inhibitors, and transporters as well as in extreme genetic polymorphisms (175, 176).

A pertinent example in this scenario is in the assessment of pharmacokinetic inhibition of CYP3A substrates by ketoconazole (177). In this assessment, PBPK modelling approaches were used to determine the impact of single dose (SD) versus multiple doses (MD) ketoconazole at 400 mg using CYP3A substrates with a broad range of pharmacokinetic characteristics ( $t_{1/2}$  and bioavailability, F), the impact of multiple dosing regimen of ketoconazole on the inhibition of CYP3A, and the effect of timing of the administration of the substrate when SD ketoconazole is given. In this study, the SD ketoconazole has shown to provide maximal inhibition towards substrate of low F and short  $t_{1/2}$ . Also, MD ketoconazole 200 mg given two times daily provides a higher degree of inhibition when compared with 400 mg daily as it shows sustained CYP3A4

inhibition when compared with the last dose. The results of this simulation have shown the importance of considering the pharmacokinetic characteristics of both inhibitor and drug substrate when designing an *in vivo* DDI study involving *CYP3A* inhibition.

Consequently, USFDA's policy in PBPK will continue to expand to cope with future technological advancement as this approach will further evolve to predict complex situations such as the impact of specific diseases whether in individual, populations or clinical and preclinical trials.

### **1.8.1.3 Pharmaceuticals and Medical Devices Agency, Japan (PMDA)**

The Pharmaceuticals and Medical Devices Agency (PMDA) was established and came into service on 1 April 2004, under the Act on the Pharmaceuticals and Medical Devices Agency following the government restructuring and reorganisation plan in 2001 (178). The main aim of PMDA is to consolidate three agencies under one roof namely, the Pharmaceuticals and Medical Devices Evaluation Centre of the National Institute of Health Sciences (PMDEC), the Organisation for Pharmaceutical Safety and Research (OPSR), and part of the Japan Association for the Advancement of Medical Equipment (JAAME). PMDA focuses on three areas of services to the Japanese population which is product reviews, safety assessments, and relief services for individuals who are injured by adverse effects resulted from medical products (Figure 1.21).

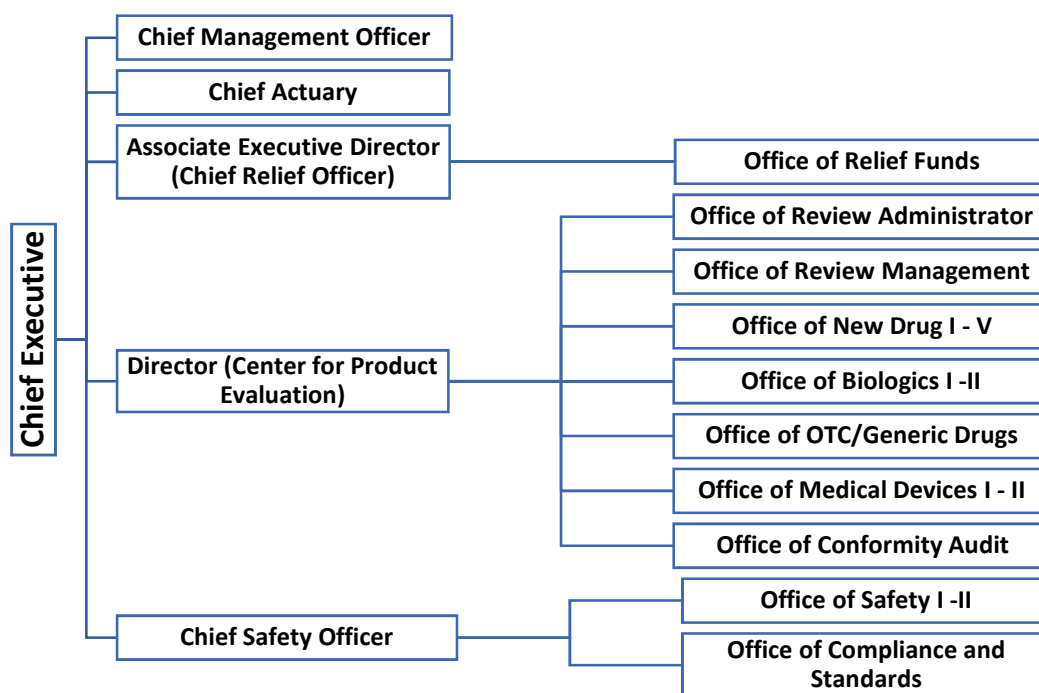


**Figure 1.21 The Structure of the PMDA.**

Diagrammatic representation of the structure of PMDA showing the hierarchy, the centres, and the offices.

*PMDA experience in PBPK*

Albeit being relatively new in the assessment of PBPK modelling and simulation when compared with the previous two regulatory authorities, PMDA has made a commendable achievement regarding assessments and acceptability of submissions related to PBPK. From 2014 to 2016, PMDA has assessed 17 submissions in new drug applications (NDA) of new molecular entities (NME) in the area ranging from DDI, organ impairment, absorption, paediatrics, and DDI and pharmacogenomics (179) (Figure 1.22).

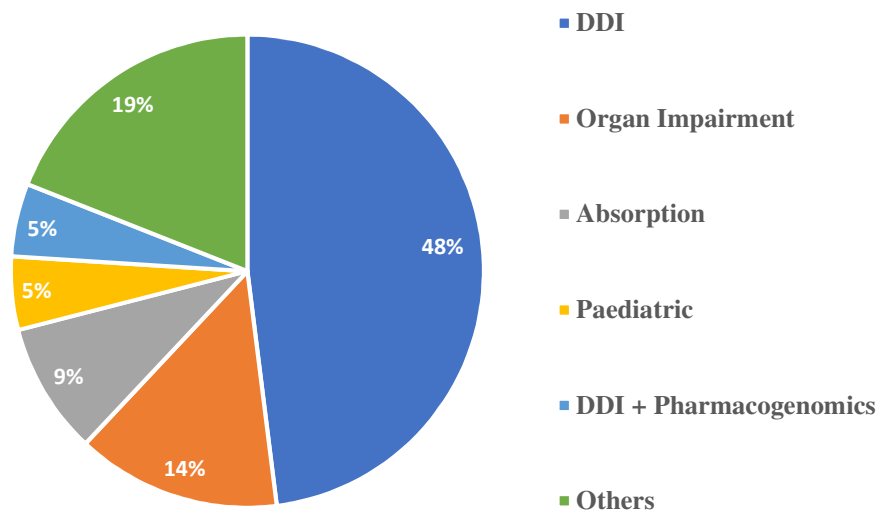


**Figure 1.22 Areas of PBPK application submissions of NME received by the PMDA from 2014 to 2016 (n=17).**

In the evaluation of Cerdelga® (Eliglustat), PBPK assessment was utilised extensively to predict the ADME profile (area under the curve (AUC)) in *CYP2D6* subjects with different genotype (poor metabolisers (PM)) as well as to determine the magnitude of DDI with concomitant treatment of fluconazole, a *CYP3A* inhibitor and terbinafine, a *CYP26* inhibitor (180). Results from the simulations shown that the AUC of eliglustat 100 mg daily dosing in *CYP2D6* PM subjects was comparable with *CYP2D6* intermediate metaboliser (IM) after twice daily dosing. In the DDI simulations, it was observed that the  $C_{max}$  and AUC of eliglustat increased 11.7-fold and 8.85-fold, respectively, in the presence of fluconazole and terbinafine. With these results, PMDA has made two dosage recommendations on the product label of Cerdelga® which were to include contraindication section for co-administration with both the *CYP3A* and *CYP2D6* inhibitors in *CYP2D6* extensive metabolisers (EM) patients and also co-administration with inhibitors of *CYP3A* in *CYP2D6* IM and PM patients.

Another example of a product in which PMDA had utilised the PBPK assessment is Farydak® (panobinostat), an anticancer drug (180). In this assessment, PBPK was used to determine the

magnitude of DDI with rifampin. AUC of panobinostat was simulated and results shown that there was approximately 70% decrease in AUC whenever rifampin is given concomitantly. A strong recommendation was made in the product labelling of Farydak® indicating that dosing with potent inducers of *CYP3A* is not recommended due to a decrease of panobinostat blood concentration that will ultimately result in panobinostat ineffectiveness.

To ensure that the standards of PBPK evaluation are intact and properly conducted, PMDA has taken the initiative to develop a guideline on DDI for drug development and labelling recommendations incorporating PBPK analysis as part of the product assessment. This guideline will encompass input from other regulatory authorities such as USFDA and EMA with regards to modelling and simulation and will be issued in the near future to facilitate PBPK evaluations (164).

## 1.9 AIMS AND OBJECTIVES

The general aim of this thesis is to illustrate, explore and facilitate the application of mechanistic modelling or specifically, PBPK modelling in the context of tissue-specific drug disposition and population data analysis.

This general aim was achieved through the application of PBPK modelling approaches to three distinct research areas:

- i. *Development and application of customised PBPK models to assess hippocampus and frontal cortex drug pharmacokinetics in rodents and humans.*

The first aim is addressed in chapter 2 of this thesis. The study attempted to explore the application of PBPK modelling to simulate target tissue PK, specifically, at the CNS. The rationale for this approach is that CNS diseases warrant effective drug therapy, of which very few exist. The primary cause for this is the difficulty of drug molecules to effectively partition across the blood-brain barrier (BBB) and the blood-cerebrospinal fluid barrier (BCSFB). Both the BBB and BCSFB play a significant role in maintaining the neuroparenchymal microenvironment by protecting the neural tissues from toxins, maintaining the barrier function of the brain and blood as well as buffering variations in blood composition. Incidentally, these same mechanisms that protect the CNS from toxins can also pose significant difficulties in designing effective drugs as most small-molecule drugs do not easily cross the BBB. Due to the high attrition rate for CNS drug development, a new revised approach is urgently needed to improve the research and development of CNS drug therapies. Such an approach can be augmented by the application of PBPK modelling to prospectively assess the CNS pharmacokinetics of drug candidates in humans.

In this chapter, a rat CNS PBPK model was developed to predict pharmacokinetics in brain compartments for the frontal cortex (FC), hippocampus (HC), 'rest-of-brain' (ROB), and cerebrospinal fluid (CSF). The model was also extended to predict human brain morphine concentrations and illustrates how a simplified regional brain PBPK model is useful for

forward prediction approaches in humans for estimating regional brain drug concentrations.

- ii. *To develop a PBPK model with customised virtual population groups to assess the impact of CYP2B6 polymorphisms on the interactions of efavirenz with lumefantrine. Further, this model will be utilised to assess these DDIs implications in paediatric antimalarial therapy, thereby, providing a model informed precision dosing towards this population group.*

The second aim is addressed in chapter 3. The study attempted to explore the application of PBPK modelling to explore the genotype impact on pharmacokinetics of drugs. Lumefantrine is a widely used antimalarial in children in sub-Saharan Africa and is predominantly metabolised by CYP3A4. The concomitant use of lumefantrine with the antiretroviral efavirenz, which is metabolised by CYP2B6 and is an inducer of CYP3A4, increases the risk of lumefantrine failure and can result in an increased recrudescence rate in HIV-infected children. This is further confounded by CYP2B6 being highly polymorphic resulting in a 2–3-fold higher efavirenz plasma concentration in polymorphic subjects, which enhances the potential for an efavirenz-lumefantrine drug-drug interaction (DDI). Due to the complexity and ethical issues of recruitment of paediatrics into complex DDI studies in HIV-infected malaria subjects, PBPK modelling can be used to explore the potential risk of DDIs in adults and paediatric populations. The benefit of this approach is both the ability to model population variability in physiology, but to also specifically develop a modelling approach that is tailored towards a specific geographical population group of interest rather than a standard healthy adult male.

This study developed a population-based PBPK model capable of predicting the impact of efavirenz-mediated DDIs on lumefantrine pharmacokinetics in African paediatric population groups, which also considered the impact of the polymorphic nature of CYP2B6 on pharmacokinetics. Further, this chapter demonstrated the application of PBPK modelling to develop and optimised dosing regimen for paediatric patients who may be exposed to an

antiretroviral-antimalarial DDI, where the DDI is mediated through complex polymorphisms affected processes.

- iii. *Explore the application of PBPK models in the multi-ethnic Malaysian population group to assess inter-individual variability attributed to polymorphisms in CYP2C19 using clopidogrel.*

The final aim of this thesis is addressed in chapter 4. The study attempted to explore the application of PBPK modelling to address inter-ethnicity pharmacokinetics variability in a multi-racial population. Malaysia is a multi-ethnic society whereby the impact of pharmacogenetics between different ethnic groups may contribute significantly to clinical therapy, as in the case of clopidogrel, a second generation thienopyridine antiplatelet drug and its active metabolite, clopi-H4. Since CYP2C19 plays an integral part towards the metabolism of clopidogrel to clopi-H4, genetic polymorphisms in CYP2C19 could potentially influence the attainment of target clopi-H4 plasma concentrations for clinical efficacy. The rationale of this study was to address the inter-ethnicity variability in the Malaysian population by applying pharmacokinetic modelling to address the impact of polymorphism of CYP2C19 on clopi-H4 in the two predominant groups, namely Malays and Malaysian Chinese.

## **CHAPTER 2**

# **Target tissue pharmacokinetics: the application of PBPK modelling to predict regional brain pharmacokinetics**

### **Disclaimer**

Elements of this chapter have been published as follows:

Zakaria, Z & Badhan, R 2018, 'Development of a Region-Specific Physiologically Based Pharmacokinetic Brain Model to Assess Hippocampus and Frontal Cortex Pharmacokinetics' *Pharmaceutics*, vol 10, no. 1.

DOI: [10.3390/pharmaceutics10010014](https://doi.org/10.3390/pharmaceutics10010014)

## **2.1 INTRODUCTION**

### **2.1.1 Background**

Diseases of the central nervous system (CNS) represent a considerable socioeconomic burden in Europe, which are often associated with increased incidences as we age. Data reported by the World Health Organisation (WHO) has shown that brain diseases contribute to 35 % of Europe's total disease burden (181). Brain cancer, stroke, spinal cord and brain trauma are all common examples of CNS diseases that warrants effective drug therapy, of which very few exist (182). The primary cause for this is the difficulty of drug molecules to effectively partition across the blood-brain barrier (BBB) and the blood-cerebrospinal fluid barrier (BCSFB).

Both the BBB and BCSFB play a significant role in maintaining the neuroparenchymal microenvironment by protecting neural tissues from toxins, maintaining the barrier function of the brain and blood as well as buffering variations in blood composition (183). Incidentally, these same mechanisms that protect the CNS from toxins can also pose significant difficulties in designing effective drugs as most small-molecule drugs do not easily cross the BBB (182). Out of over 7,000 drugs in the comprehensive medicinal chemistry database, 5 % of those drugs treat the CNS and limited to only diseases such as insomnia, depression, and schizophrenia (182, 184). Due to a high attrition rate in CNS drug development, a new revised approach is urgently needed to improve the research and development of CNS drug therapies.

### **2.1.2 Brain penetration**

Due to the complex and dynamic nature of the BBB, the presence of intercellular tight junctions (TJ) and abundance of active drug transporter proteins that impair or facilitate drug passage, the penetration of drugs into the brain is challenging. Furthermore, dysfunction of the BBB in pathologies such as multiple sclerosis, Alzheimer's disease, traumatic brain injury and stroke can also lead to a compromise in permeability and transportation which affects drug delivery (185). Therefore, assessment of risks when introducing a compound through the pharmaceutical

development process is paramount in obtaining necessary information for rational drug design to minimise shortcomings when developing medicinal products in the CNS area.

### 2.1.2.1 CNS barriers

In humans, three barrier layers regulate and limit molecular exchange between the neural tissue, its fluid spaces and the blood. These barriers are the blood-brain barrier (BBB) (created by the cerebrovascular endothelial cells between the brain interstitial fluid and the blood), the blood-cerebrospinal fluid barrier (BCSFB) (created by the ventricular spinal fluid facing the epithelial cells of the choroid plexus), and the barrier that is provided by the avascular arachnoid epithelium between the subarachnoid CSF and blood which enclosed the CNS completely (186-188) (Figure 2.1).

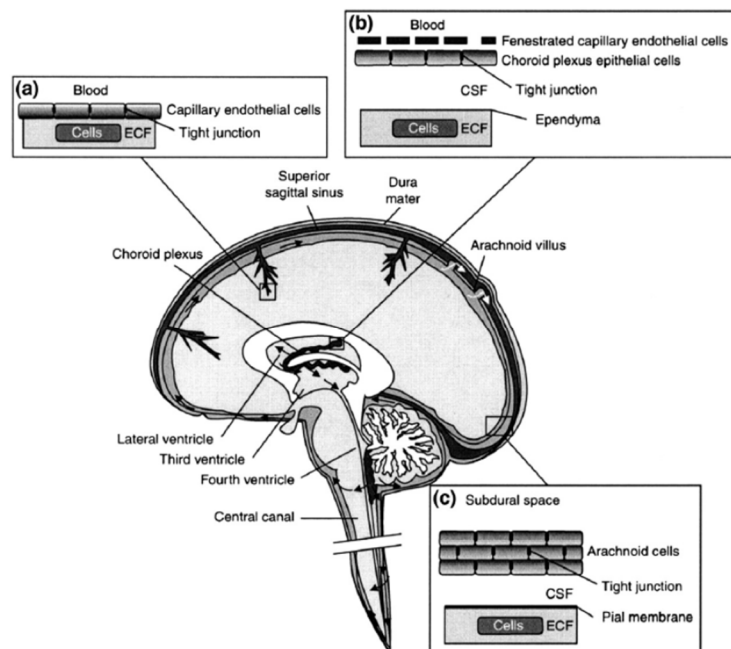


**Figure 2.1** The location of brain barriers

(a) The BBB, which consists of cerebral capillary endothelial cells that form tight junctions. (b) The BCSFB, tight junctions that form between epithelial cells at the apical surface of the epithelium (CSF-facing surface) which is located at the lateral, third and fourth ventricles of the choroid plexus of the brain. (c) The arachnoid barrier. Tight junctions formed by multi-layered epithelium between inner layer cells that create an effective seal. Reproduced from Abbot *et al.* (2010) (187).

### **2.1.2.2 Function of the barriers**

All three barriers function dynamically within three broad scopes; as a transport barrier, physical barrier, and metabolic barrier. In addition, the profoundly negative charge of glycocalyx located at the brain endothelial cells (luminal surface) acts as an additional defence mechanism against molecular permeation (189).

The BBB acts as a transport barrier due to the specific transport system such as the adsorptive and receptor-mediated transendothelial transport, efflux pumps and solute carriers that are present on the abluminal and luminal membranes of endothelial cells which regulate the molecular transcellular traffic (190).

The BBB can also act as a physical barrier, as a result of the complex network of TJ proteins formed between adjacent endothelial cells, and which reduces the movement of molecules paracellularly through the TJ in brain endothelial cells (183, 191).

The BBB can finally act as a metabolic barrier, whereby endothelial cells express several metabolic enzymes. Specific Phase I enzymes (Cytochrome P450 (CYP), CYP1A1, 1B1, 2B6, 2D6, 2E1, 2J2, 2R1, 2S1 and 2U1) and Phase II enzymes (glutathione S-transferase- $\pi$  (GST $\pi$ ), GST $\alpha$ , SULT1A1, SULT1A2, and UDP-glucuronosyl-transferase UGT1A1) are examples of such enzymes (192-197).

### **2.1.2.3 Drug permeation pathways**

At the level of the BBB, six transport pathways of drug compound can be distinguished as it enters this area (Figure 2.2) (189).

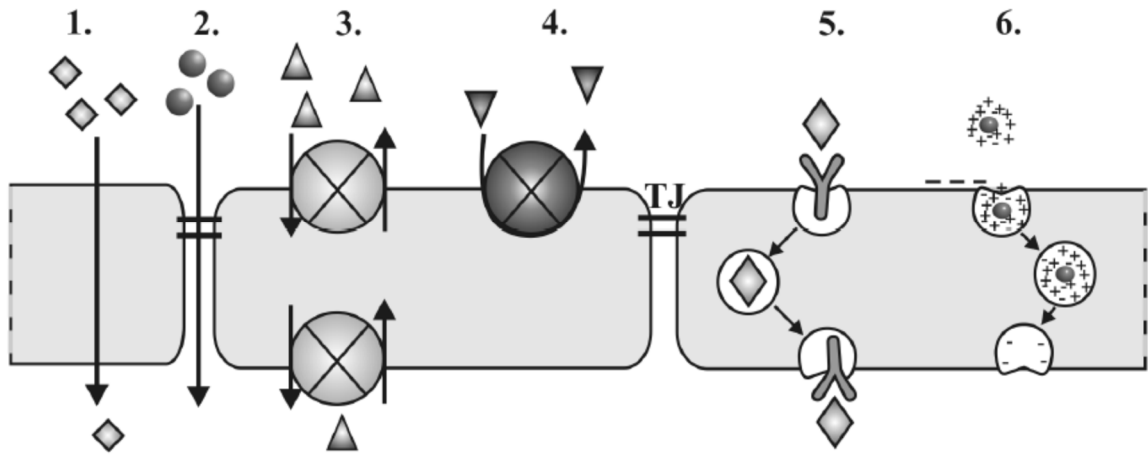


**Figure 2.2 BBB transport pathways.**

1. Passive Transcellular Pathway for Lipophilic Molecules, 2. Passive Paracellular Pathway for Hydrophilic Molecules, 3. Carrier-Mediated Transport, 4. Active Efflux Transport, 5. Receptor-Mediated Transcytosis, and 6. Adsorptive-Mediated Transcytosis. Reproduced from Deli *et al.* (2011) (188, 189).

*i. Passive Transcellular Pathway for Lipophilic Molecules*

Transcellular pathways are often utilised by molecules which are lipophilic ( $\text{LogP} < 5$ ) and a small molecular weight (MW) of  $< 500$  Da (198, 199). These properties typically ensure molecules are able to adequately partition across the lipids bilayer and permeate into the brain parenchyma along a concentration gradient, from a region of high concentration within the microvasculature to a region of lower concentration within the parenchyma.

*ii. Passive Paracellular Pathway for Hydrophilic Molecules*

One of the reasons that most hydrophilic molecules such as peptides, proteins, and polysaccharides cross the BBB poorly is because of the restricted paracellular pathway of the TJs (199). Most of the drugs that have been developed for CNS diseases belong to this category are often hydrophilic which results in low BBB penetration. Due to the structure of BBB which consists mainly of lipid bilayer membranes, it is impermeable to ions such as  $\text{Na}^+$ ,  $\text{K}^+$ ,  $\text{Cl}^-$ , and to polar molecules, even non-charged (non-ionic) molecules such as glucose, and proteins (unless they have special transporters which facilitate their movement across the BBB) (182).

### *iii. Carrier-Mediated Transport*

At the BBB, there exist a bi-directional, saturable transport systems for vitamins, minerals, and nutrients (187, 199). Enerson and Drewes (2006) (200) conducted a serial analysis of gene expression and identified approximately 40 members of the solute carrier (SLC) transporter family in the brain micro vessels. Amongst the SLCs, the most important is that involve in the transport of proteins for glucose which is the primary energy source for the CNS. These SLC proteins include the SLC2A1 (GLUT-1) and SLC2A3 (GLUT-3) glucose transporters and SLC5A2 (SGLT2) sodium glucose co-transporter. The SLC family also involves in transporting amino acids such as system N amino acid transporter SN1 (SLC38A3), system A amino acid transporters 1 and 2 SAT1 (SLC38A1), SAT2 (SLC38A2), the cationic amino acid transporters CAT-1 (SLC7A1) and the large neutral amino acid transporter LAT-1 (SLC7A5). Transporter carriers at the BBB that provide vitamins (SLC5A6 or SMVT), choline (SLC6A8) and long chain fatty acids (SLC27A1 or FATP-1) to the brain can be exploited for drug delivery. An example would be L-Dopa, which crosses the BBB together with LAT-1 and is developed for the treatment of Parkinson's disease. One of the important aspects regarding the rate of uptake of the endogenous ligand of a transporter that crosses the BBB is that it is approximately ten times higher as compared to the same molecule that crosses by transmembrane diffusion (201).

### *iv. Active Efflux Transport*

There is an increasing number of active efflux transporters that have been identified at the BBB (200, 202, 203). Examples of these transporter proteins predominantly include members of the ATP-binding cassette (ABC) transporter family such as MRP-1, -4, -5 and -6 (ABCC1-6), P-glycoprotein (ABCB1) and brain multidrug resistance proteins (BMDP/BCRP/ABCG2). In terms of drug delivery, these efflux transporters act in restricting drug penetration to the brain which caused a decreased effectiveness of drugs used to treat diseases such as brain tumours, neurodegenerative disorders, and stroke (204).

### *v. Receptor-Mediated Transcytosis*

The brain penetration and clearance of proteins and peptides are among the roles of receptor-mediated transport (199, 205). Regulatory proteins (peptide-specific) that are carried using this mechanism includes, but not limited to, insulin, ghrelin, transferrin, leptin, and low-density

lipoprotein (192). This mechanism of transportation can be unidirectional or bidirectional (blood-to-brain and brain-to-blood directions) (199). There are three major steps for this form of transport: (i) receptor-mediated endocytosis at the luminal side of the endothelial cells of the brain, (ii) transcytosis in vesicles through the cytoplasm, and (iii) exocytosis at the abluminal side (199). These pathways have made the delivery of large drug molecules such as nanoparticles and biopharmaceuticals to the CNS area possible (180).

#### *vi. Adsorptive-Mediated Transcytosis*

The transfer and uptake of cationic molecules across the brain endothelial cells followed by abluminal exocytosis is the primary role of this pathway and represent a form of vesicular transport (206).

### **2.1.3 Quantifying CNS drug delivery**

#### **2.1.3.1 *In vitro* methods**

The BBB permeability properties of investigative compounds need to be determined at the early stage of the drug discovery process. High-throughput screening is often employed and Gumbleton and Audus (2001) (207) and Reichel *et al.* (2003) (208) have described in details the basic requirements and properties for a BBB *in vitro* studies whereas Lundquist and Renftel (2002) (209) have listed several advantages of using *in vitro* BBB permeability models.

Such advantages include:

- i. permits the screening of more molecules
- ii. evaluation can be made on the mechanism of transport
- iii. less expensive than *in vivo* studies
- iv. ethical reasons
- v. recording of early signs of toxicity
- vi. evaluation of compounds is less as compared to *in vivo* studies
- vii. supporting the development of structure-transport relationships

viii. inducing of pathological conditions can be made, and molecular mechanisms can be assessed.

Numerous noncell-based and cell-based *in vitro* models have been established for the measurement of the *in vivo* brain uptake which are summarised in Appendix B.

### 2.1.3.2 *In vivo* methods

As stated by Pardridge (1999) (210), *in vivo* methods provide the most reliable assessment of BBB permeability. However, these methods are expensive, low-throughput, requires tracers that are specifically labelled and significant technical expertise (211).

The key outcome of *in vivo* measurements is the determination of the permeability-surface area (PS or LogPS) and the ratio of brain-to-plasma concentration ( $K_p$  or Log BB). At steady state,  $K_p$  is influenced by several factors including the BBB permeability, BBB transporter uptake and efflux, drug binding to plasma proteins and non-specific brain binding, brain tissue and BBB metabolism and the interstitial bulk flow within the brain. To reach brain equilibrium, the ratio of free brain/free plasma concentration plays an essential factor whereas, for the time to reach the brain equilibrium, the PS and the non-specific brain binding are essential (212). To evaluate brain penetration of a compound,  $K_p$  is a widely used parameter and can be defined by the following equations,

$$K_p = \frac{C_{brain}}{C_{plasma}} \quad (2.1)$$

where  $C_{brain}$  is the total brain concentration and  $C_{plasma}$  is total plasma concentration.

Whereas,

$$f_{u,plasma} = \frac{C_{u,plasma}}{C_{plasma}} \quad (2.2)$$

where  $f_{u,plasma}$  is fraction unbound of drug in plasma and  $C_{u,plasma}$  is unbound plasma concentration and:

$$f_{u,brain} = \frac{C_{u,brain}}{C_{brain}} \quad (2.3)$$

where  $f_{u,brain}$  is fraction unbound of drug in the brain.

Furthermore, the ratio of free brain and free plasma concentration at equilibrium can be defined as  $K_{p,uu}$  (213):

$$K_{p,uu} = \frac{C_{u,brain}}{C_{u,plasma}} \quad (2.4)$$

. Therefore,  $K_p$  and  $K_{p,uu}$  can be determined in a relationship as,

$$K_p = \frac{f_{u,plasma}}{f_{u,brain}} \times K_{p,uu} \quad (2.5)$$

This relationship has emphasised the relevance of  $K_{p,uu}$  values in quantifying the presence and absence of active and passive BBB transport in the brain. So far, this  $K_{p,uu}$  values have been shown to vary between 0.02 and 3 (150-fold difference) and has proven that it can be valid representations of the BBB transport of drug molecules (214-217).

However, the  $K_p$  values alone do not necessarily mandate the level of drug penetration at the BBB. As shown by Doran *et al.*(2005) (218) in a study of determining the  $K_p$  values in mice of the 32 most prescribed CNS drugs, the value of  $K_p$  at 0.1 such as sulpiride, can still contribute to a successful CNS drug comparable to  $K_p$  values  $> 10$ . More often however,  $K_{p,uu}$  provides a more suitable quantitative description of the way the BBB transport the drug molecules instead of the  $K_p$  values alone and understanding the impact of the binding in brain and plasma is essential when using  $K_p$  values to optimise drug penetration to the brain.

There are two *in vivo* techniques used to obtain the required *in vivo* parameters for BBB permeability. The invasive techniques include bolus injection, brain uptake index (BUI), brain efflux index (BEI), *in situ* brain perfusion, quantitative autoradiography, intercerebral microdialysis and CSF sampling. As for the non-invasive techniques, it includes magnetic resonance imaging (MRI), near-infrared time-domain optical imaging, positron emission tomography (PET) and single photon computed tomography (SPECT). Appendix C provides

an overview of the *in vivo* methods used and the related parameters established from the techniques.

### **2.1.3.3 *In silico* approaches**

In drug discovery, *in silico* methods provide a high-throughput, economical, and relatively fast method for assessing and establishing the pharmacokinetics of new compounds.

#### *i. Molecular approaches*

Several molecular approaches have been described to assess molecular properties for CNS drug delivery and include quantitative structure-activity relationships (QSAR), molecular descriptors and rule based methods. A full description of these approaches are detailed in Appendix D.

#### *ii. Pharmacokinetics approaches*

PBPK models are capable of making predictions of the extent of CNS drug disposition, which in turn, assists in understanding the characteristics of CNS uptake and reduces the need for complex *in vivo* procedures to quantify CNS drug disposition.

In non-physiological empirical pharmacokinetic models, the CNS is described by either a 1-compartment model (representing brain) or a 2-compartment model (representing brain interstitial fluid and brain intravascular fluid (IVF) with such models often being used in conjunction with brain microdialysis to describe CNS drug disposition (219, 220). Semi-physiological models have also been proposed to describe drug disposition within the brain mechanistically (45, 218, 221-226). However, all current semi-physiological and non-physiological models employed to describe CNS pharmacokinetics fail to consider regional CNS pharmacokinetics within distinct brain sections, which limits the application of such models to the assessment of regional brain extracellular fluid (ECF) drug disposition.

To address this limitation, PBPK can be used to mechanistically describe the drug concentration in tissues with consideration of regional tissue distribution (227, 228). PBPK models are mechanistically driven and developed around accounting for relevant physiological processes which may impact upon the pharmacokinetics of compounds. As opposed to empirical models, the integration between system-dependent (physiological) and compound-dependent parameters of PBPK models in predicting the compound's PK profile have enabled an understanding of the underlying mechanisms of the PK (20, 45) and have recently been applied to model ECF pharmacokinetics of drugs (64, 229, 230).

Several CNS PBPK models have been developed in recent years to predict drug disposition in the brain in rodents and humans. Badhan *et al.* (2014) (64) developed a PBPK model of the rat CNS which formed the foundation for this chapter (Figure 2.3). This model incorporates brain interstitial fluid (ISF), choroidal epithelial and total CSF compartments that were capable of predicting CSF-to-plasma ratios and  $K_{p,uu}$  brain of 90% compounds with diverse pharmacokinetic characteristics using a series of *in vitro* permeability and unbound fraction parameters.

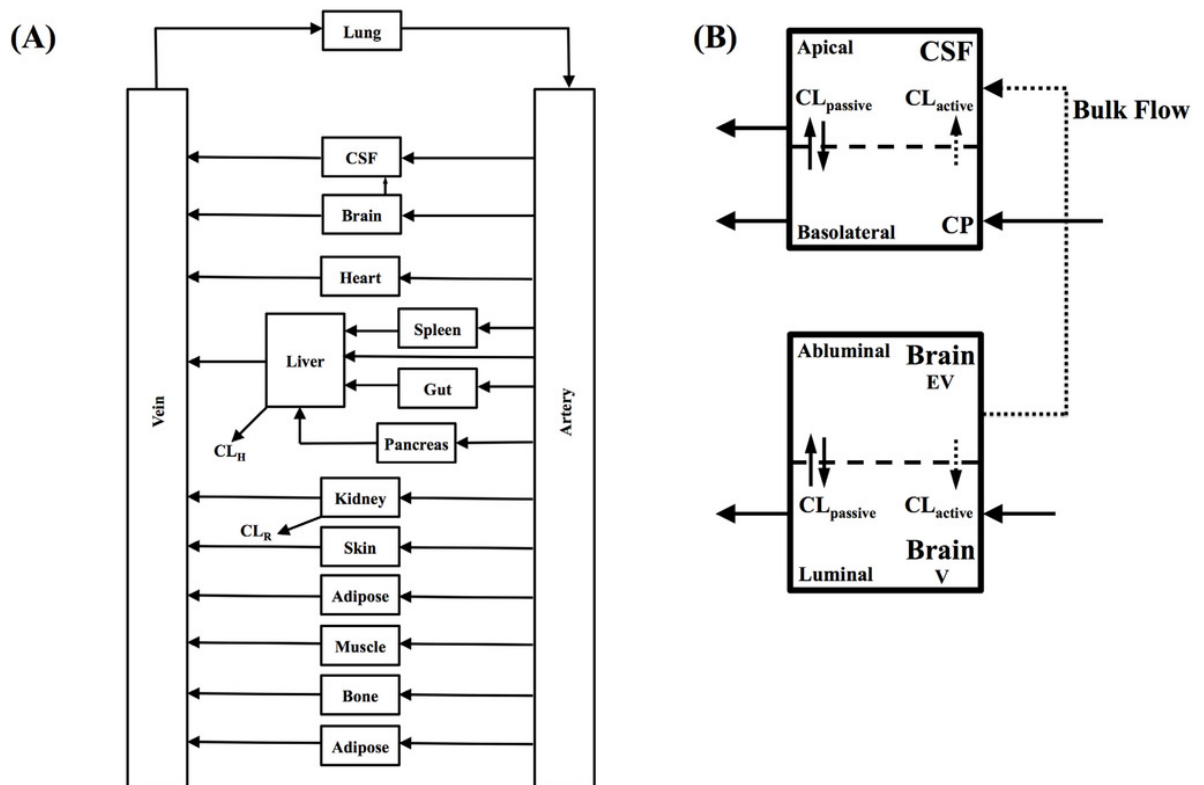


**Figure 2.3 PBPK model of the rat CNS utilised by Badhan *et al.* (2014).**

(A) Whole-body physiologically based pharmacokinetic (PBPK) model. CL: Clearance; CSF: Cerebrospinal fluid; and (B) Brain and CSF compartments. V: vascular compartment; EV: extra-vascular compartment;  $CL_{\text{passive}}$ : passive clearance;  $CL_{\text{active}}$ : active efflux clearance. Reproduced from Badhan *et al.* (2014) (64).

Liu *et al.* (2005) (231) have also developed a semi-mechanistic brain PBPK model and a brain compartmental model to characterise the pharmacokinetics of selected compounds in plasma and brain tissue in order to explore the role of BBB permeability, plasma protein binding, and brain tissue binding on CNS PK (Figure 2.4). They demonstrated that to achieve a rapid brain equilibrium, the two most important aspects that are required are a low tissue binding and a high BBB permeability. However, their brain PBPK model did not take into account the contribution of transporters towards brain drug disposition.

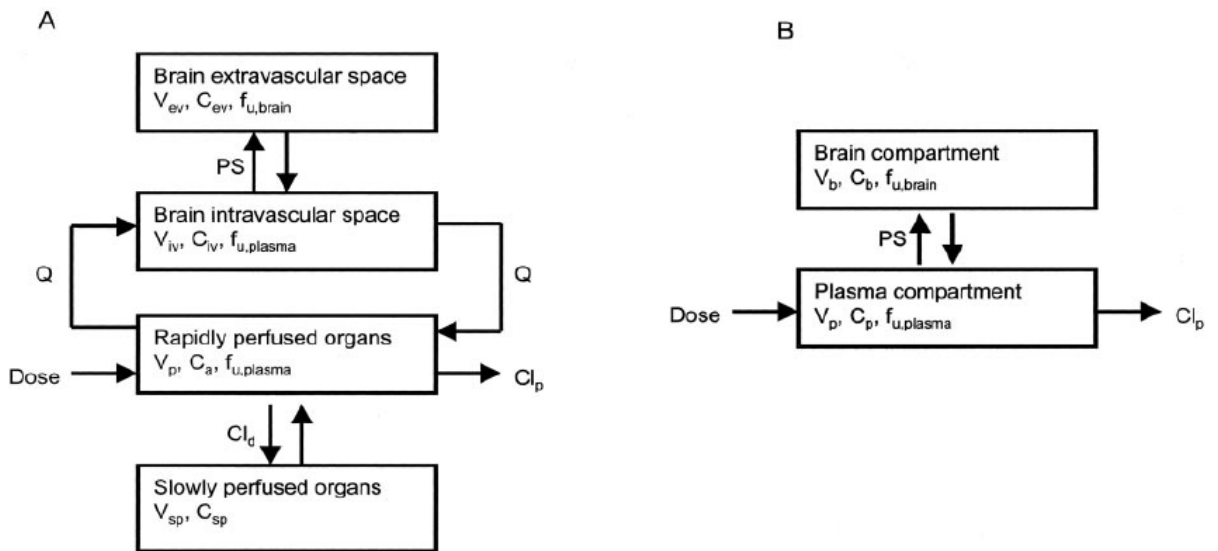


**Figure 2.4** A hybrid brain PBPK model utilised by Liu *et al.* (2005).

$V_p$ : distribution volume of central compartment;  $C_a$ : concentration in central compartment;  $Q$ : cerebral blood flow;  $C_{iv}$ : concentration in the intravascular space in brain;  $V_{iv}$ : physiological volume of intravascular space in brain;  $C_{ev}$ : concentration in extravascular space;  $V_{ev}$ : physiological volume of extravascular space;  $f_{u,brain}$ : unbound fraction in brain tissue;  $f_{u,plasma}$ : unbound fraction in plasma determined using equilibrium dialysis;  $V_{sp}$ : distribution volume of the peripheral compartment;  $C_{sp}$ : concentration in the peripheral compartment;  $Cl_p$ : systemic clearance (A) and a brain compartment model.  $V_b$ : volume of brain tissue;  $C_b$ : concentration in the brain compartment;  $C_p$ : concentration of central compartment (B) were used to characterise the pharmacokinetics in plasma and brain tissues. Reproduced from Liu *et al.* (2005) (231)

Ball *et al.* (2012) (232) established a model to predict morphine, and oxycodone unbound brain concentration profiles by implementing *in vitro* to *in vivo* scaling factors as well as using *in vitro* permeability data for modelling BBB penetration (Figure 2.5). Their brain PBPK model for the rat consists of two compartments which are the brain vasculature and brain tissue.

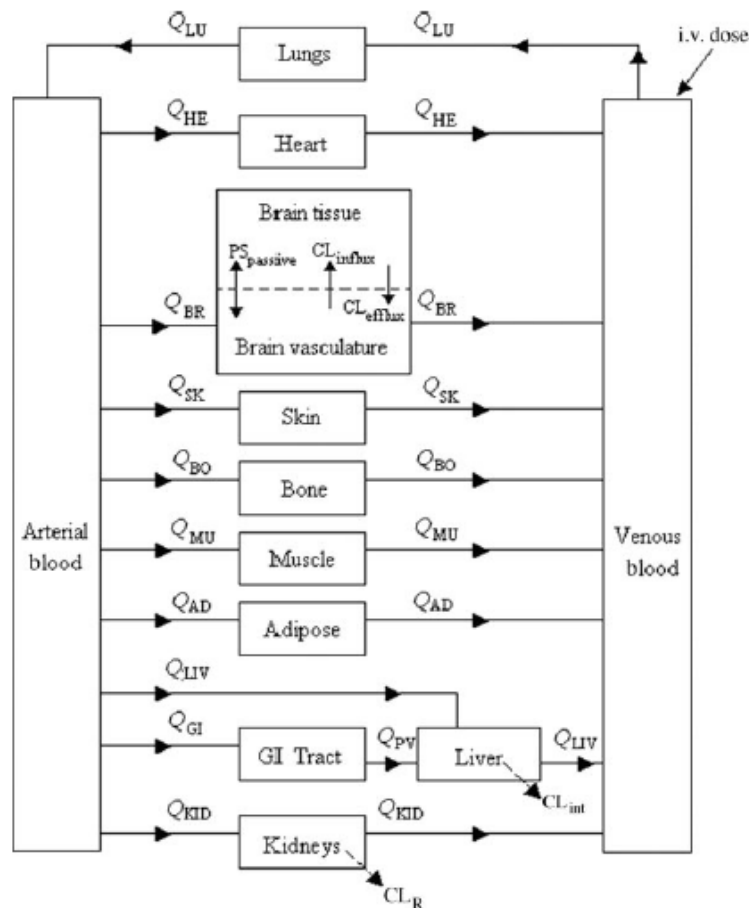


**Figure 2.5 A whole-body rat PBPK model incorporating a permeability limited brain model as utilised by Ball *et al.* (2012)**

Q: blood flow; LU: lungs; HE: heart; BR: brain; SK: skin; BO: bone; MU: muscle; AD: adipose; LIV: liver; GI: gastro-intestinal tract; PV: portal vein; KID: kidneys; CL<sub>int</sub>: intrinsic clearance; CL<sub>R</sub>: renal clearance; PS<sub>passive</sub>: passive permeability surface area product; CL<sub>influx</sub>: active influx clearance; CL<sub>efflux</sub>: active efflux clearance. Reproduced from Ball *et al.* (2012) (232).

In a further study, Ball *et al.* (2014) (233) developed a generic and customisable brain PBPK model of the rat that has shown to be more precise in predicting compounds in the CNS area, specifically the brain permeability of the passively transported drugs (Figure 2.6). The brain PBPK model consists of four compartments: the brain, CSF, brain extracellular fluid (ECF) and the intracellular brain space (BC). The four compartments brain area that was proposed by Ball

*et al.* seems also to be a good framework to be adapted for this study as it shows a good interspecies correlation and all ODEs were customisable and adaptable to different parameters.

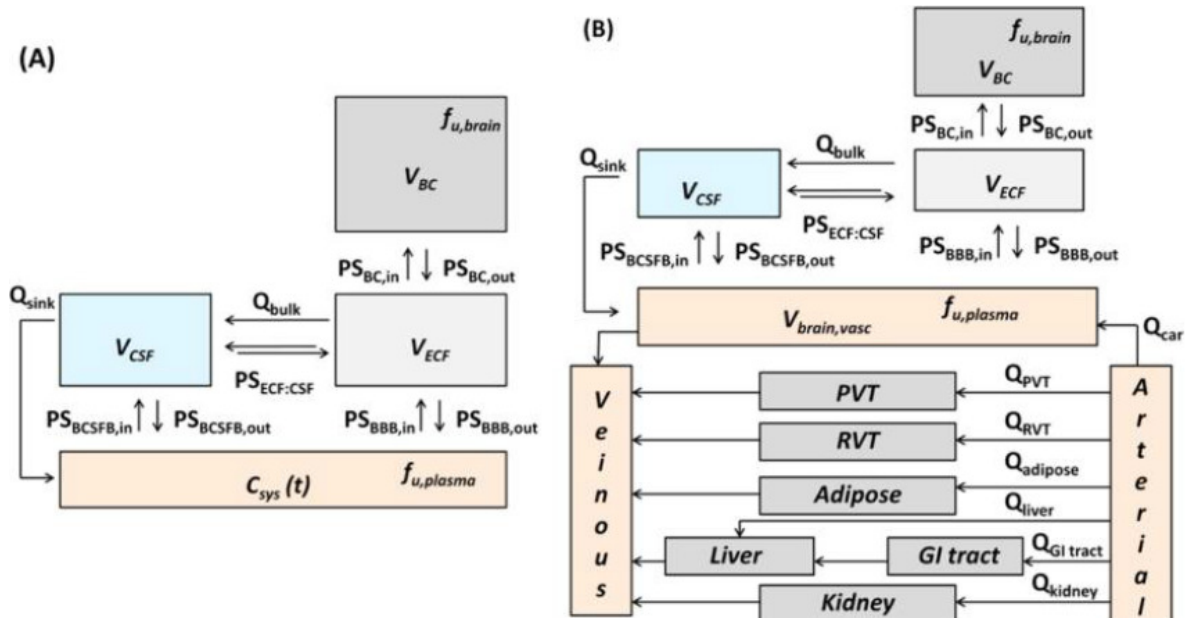


**Figure 2.6 Schematic diagram of Ball *et al.* (2014) (A) the rat CNS minimal PBPK model and (B) the rat CNS whole-body PBPK model.**

Fixed CNS physiological parameters: bulk flow of ECF ( $Q_{bulk}$ ) and sink flow of CSF ( $Q_{sink}$ ), volumes of CSF ( $V_{CSF}$ ), ECF ( $V_{ECF}$ ), and intracellular space ( $V_{BC}$ ). Experimentally measured drug-specific parameters: unbound fractions in plasma ( $f_{u,plasma}$ ) and brain ( $f_{u,brain}$ ). Model-estimated drug-specific parameters: permeability-surface area products across the BBB ( $PS_{BBB,in}$ ,  $PS_{BBB,out}$ ), BCSFB ( $PS_{BCSFB,in}$ ,  $PS_{BCSFB,out}$ ), and BC membrane ( $PS_{BC,in}$ ,  $PS_{BC,out}$ ). Optional model parameter: bidirectional diffusion rate constant between ECF and CSF ( $PS_{ECF:CSF}$ ). Reproduced from Ball *et al.* (2014) (233).

Recently, a series of publications by Yamamoto *et al.* (234-237) have established the basis for some level of mechanistic regional pharmacokinetic modelling of CNS tissues, however this group focussed more on a global regional model of the CNS (i.e. inclusion of regional CSF compartments) which would be more applicable to clinical sampling in humans (i.e. spinal CSF) (Figure 2.7). Furthermore, such models were developed using population-based

compartment modelling pharmacokinetics (e.g., NONMEM (238)), making model portability difficult.

To address this limitation, PBPK can be used to mechanistically describe the drug concentration in tissues with consideration of regional tissue distribution element (227, 228). A key benefit of the application of PBPK models is the ability to amalgamate existing relevant physiological processes, which may impact upon the pharmacokinetics of compounds, alongside a compound's physicochemical properties to both mechanistically describe a compound's pharmacokinetics. Additionally, such approaches allow both interspecies scaling and the prediction of whole organ and organ sub-compartment temporal concentrations profiles. As opposed to empirical models, the integration between system-dependent (physiological) and compound-dependent parameters of PBPK models in predicting the compound's PK profile have enabled an understanding of the underlying mechanisms of the PK (20, 45) and have recently been applied to model ECF pharmacokinetics of drugs (64, 229, 230).

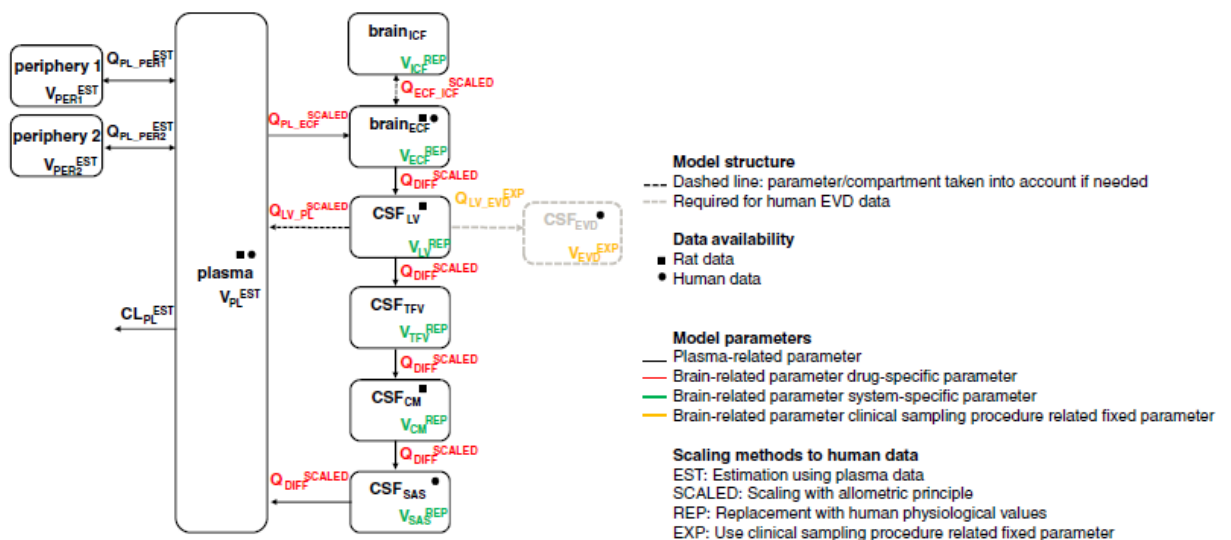


Figure 2.7 A hybrid brain PK model utilised by Yamamoto *et al.* (2016)

The brain PK model consists of plasma, brain<sub>ECF</sub>: brain extracellular fluid compartment; brain<sub>ICF</sub>: brain intracellular fluid compartment; CSF<sub>LV</sub>: compartment of cerebrospinal fluid in lateral ventricle; CSF<sub>TFV</sub>: Compartment of cerebrospinal fluid in third and fourth ventricle; CSF<sub>CM</sub>: compartment of cerebrospinal fluid in cisterna magna and CSF<sub>SAS</sub>: compartment of

cerebrospinal fluid in subarachnoid space, which consists of 4 different categories parameters (colours). The scaling method for each parameter is indicated with colour coding. Reproduced from Yamamoto *et al.* (2016) (239).

The need for quantifying regional brain temporal concentrations is integral to expand existing CNS PBPK modelling approaches, particularly for those drugs that are reported to be unevenly distributed within the brain (240, 241).

The aim of this chapter was to therefore develop a PBPK model of the rat CNS which considers the whole brain ECF in addition to two regional compartments, namely the frontal cortex and hippocampus, to predict regional brain pharmacokinetics of phenytoin (240) and carbamazepine (242). Further, the model was expanded to predict human regional brain pharmacokinetics of morphine. Key objectives of this study are to quantify and predict the extent of drug delivery to the brain and wider CNS across three key drug delivery/barrier sites namely; (i) the BBB; (ii) the hippocampus and (iii) the frontal cortex using phenytoin, carbamazepine and morphine as case studies.

## **2.2 METHODS**

A three-stage workflow methodology was applied to model development. Step 1 focussed on the validation of a whole-body PBPK model incorporating a previously published CNS PBPK model (64), for the prediction of  $K_{p_{uu,brain}}$  for 10 passively transported compound. Step 2 adapted this CNS PBPK model to include two regional brain compartments, namely frontal cortex, and hippocampus and validated these against two reported studies of phenytoin (240) and carbamazepine (242) regional brain ECF temporal concentration from rodent microdialysis studies. Subsequently, Step 3 extrapolated the regional brain PBPK model to humans for the prediction of morphine pharmacokinetics based upon reports of human brain microdialysis of morphine (243, 244).

### 2.2.1 Step 1: a whole-body physiologically based pharmacokinetic (PBPK) CNS model

A whole-body PBPK model was developed in MATLAB 9.1 (The MathWorks, Inc., Natick, Massachusetts, United States) (245). The model incorporated the following compartments: lung, heart, brain, muscle, adipose, skin, spleen, liver, pancreas, gut, stomach, bone, kidney, arterial blood, and venous blood. All tissue compartments were modelled as well-stirred (Figure 2.8).

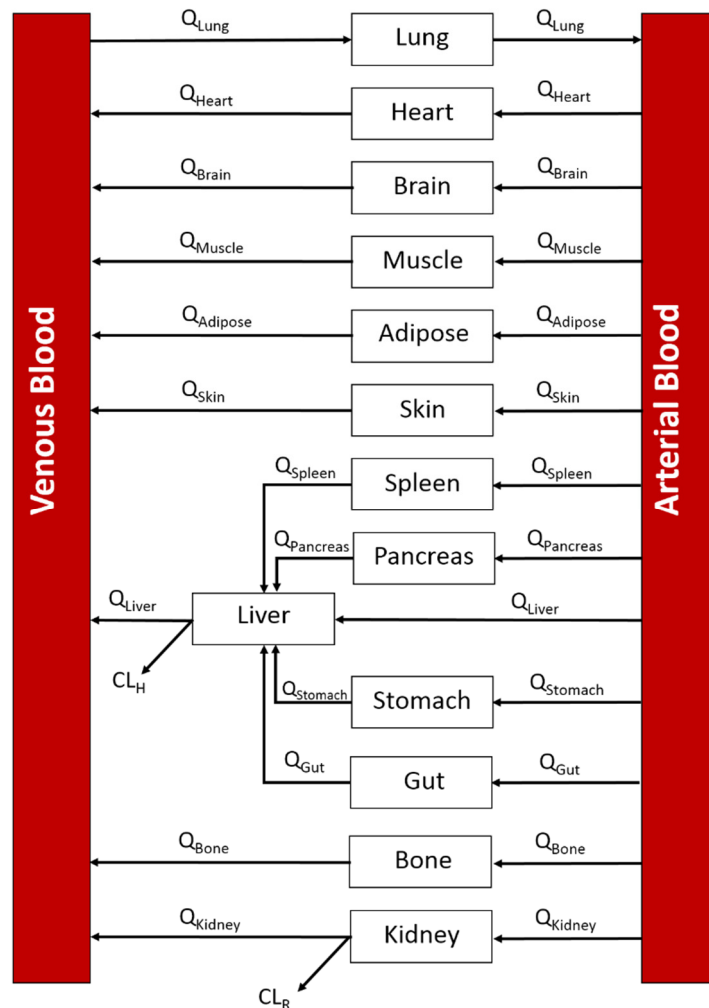


**Figure 2.8** A generic whole-body PBPK model.

Arrows indicated direction of blood flow.  $Q$ : blood flow;  $CL_H$ : hepatic clearance;  $CL_R$ : renal clearance.

Ordinary differential equations were used to describe the whole-body PBPK model with all compartments, except CNS tissues (Figure 2.9), assumed to be well-stirred (equation 2.6-2.7).

*Well-stirred tissues:*

$$\frac{dC_T}{dt} = \left[ \frac{1}{V_T} \times Q_T \times C_{AR} \right] - \left[ \frac{1}{V_T} \times Q_T \times \left( \frac{C_T}{f_{up} \times K_p} \times R_b \right) \right] \quad (2.6)$$

where  $C_T$  is the drug concentration of the respective tissues,  $t$  is for time,  $Q_T$  is the blood flow rate of the tissue,  $C_{AR}$  is the arterial drug input,  $V_T$  is the volume of the respective tissue compartment,  $f_{up}$  is the fraction unbound of drug in plasma,  $K_p$  is the tissue-to-plasma partition coefficient, and  $R_b$  is the blood-to-plasma ratio of the drug.

*Brain:*

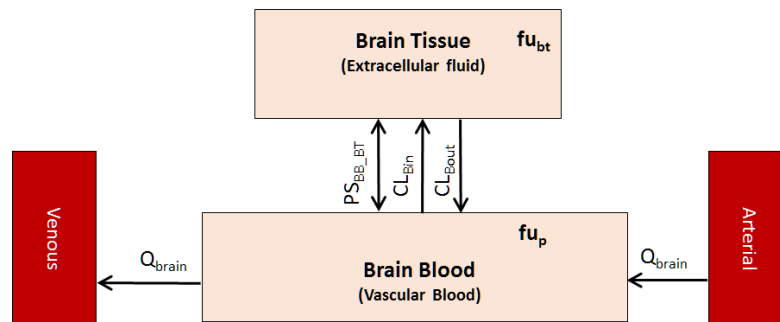


**Figure 2.9 CNS PBPK brain model.**

Q: blood flow; PS: permeability surface-area; BB: intravascular blood; BT: brain tissue; fu: drug fraction unbound

$$\frac{dC_{bb}}{dt} = Q_{brain}(C_{arterial} - C_{bb}) + (PS_{BB}C_{bt}fu_b - PS_{BB}C_{bb}fu_p) \quad (2.7)$$

where  $C_{bb}$  is the drug concentration in the brain blood (brain vascular blood),  $t$  is for time,  $Q_{brain}$  is the blood flow rate to the brain,  $C_{arterial}$  is the arterial drug input,  $fu_p$  is the fraction unbound of drug in plasma and brain ( $fu_p$ ),  $PS$  is the bidirectional passive permeability-surface area product of BBB and  $CL_{Bin}$ , and  $CL_{Bout}$  are the active clearance into and out of the brain, respectively.

Drug removal from eliminating organs (liver and kidney) was described by either a hepatic clearance ( $CL_H$ ) or renal clearance ( $CL_R$ ) term. Hepatic clearance was derived from either *in vitro* intrinsic metabolic clearance ( $CL_{int, in vitro}$ ) or *in vivo* human blood or plasma clearance ( $CL_b$  or  $CL_p$ ). Renal clearance was calculated using a glomerular filtration rate (GFR) correction approach (83).

Intrinsic clearance was scaled to an  $CL_H$ , through the use of microsomal recovery (microsomal protein content: 45 mg protein/g liver) or hepatocellularity ( $130 \times 10^6$  cells/g liver) and assuming a rat liver weight of 40 g/kg body weight (74, 76, 77), before being scaled using a well-stirred liver model (equation 2.8):

$$CL_H = \frac{fu_p \times CL_{int, in vivo} \times Q_L}{Q_L + fu_p \times CL_{int, in vivo} / R_b} \quad (2.8)$$

Tissue volumes and blood flow rates were obtained from published literature (45, 137) (Table 2.1).

**Table 2.1 System-related parameters used for the rat whole-body PBPK model.**

<b>Tissue</b>	<b>Perfusion</b>		<b>Volume</b>	
	<b>Rat</b> (mL/min)	<b>Human</b> (mL/min)	<b>Rat</b> (mL)	<b>Human</b> (mL)
<b>Adipose</b>	4.72	277.5	19.03	10,725
<b>Bone</b>	8.08	270	10.37	9300
<b>Brain</b>	1.12	750	1.43	1552.5
<b>Gut</b>	12	975	6.75	1770
<b>Heart</b>	3.2	160.5	0.825	285
<b>Kidney</b>	11.6	1177.5	1.825	330
<b>Liver</b>	20	1575	10.3	1807.5
<b>Lungs</b>	80	5325	1.25	1252.5
<b>Muscle</b>	18.96	802.5	101	32175
<b>Pancreas</b>	1	142.5	1.3	90
<b>Skin</b>	4.08	322.5	47.5	8325
<b>Spleen</b>	0.88	82.5	0.5	202.5
<b>Arterial blood</b>	-	-	6.8	1927.5
<b>Venous blood</b>	-	-	13.6	3855

Ten passively transported compounds (benzylpenicillin, buspirone, caffeine, carbamazepine, diazepam, midazolam, phenytoin, sertraline, thiopental, and zolpidem) with reported unbound brain: unbound plasma partition coefficient ( $K_{p_{uu,brain}}$ ) were selected to validate the structure of the PBPK model.

Unless otherwise stated, all data contained within the tables below are applied to the rat CNS PBPK model (Table 2.2-2.6).

**Table 2.2 *In vitro* permeability data**

	<b>Parental cells <sup>a</sup></b>	
	<b>P<sub>app</sub></b>	
	<b>cm/s (x10<sup>-6</sup>)</b>	
	<b>AB</b>	<b>BA</b>
Benzylpenicillin	4.35	3.17
Buspirone	34.25	33.6
Caffeine	27.0	29.7
Carbamazepine	32.1	34.5
Diazepam	37.3	36.8
Midazolam	34.8	35.5
Phenytoin	20.94	31.7
Sertraline	2.27	1.61
Thiopental	31.2	30.6
Zolpidem	35.6	35.4

<sup>a</sup> Data obtained from Kalvas *et al.* (2007) (246) and Uchida *et al.* (2011) (247).

**Table 2.3 Model predicted versus literature reported in situ permeabilities**

	<b>Permeability Clearance</b>		<b><i>In Situ</i> Permeability</b>
	<b>mL/h</b>		<b>mL/h</b>
	<b>PS<sub>BB_BT</sub></b>	<b>PS<sub>BT_BB</sub></b>	
Benzylpenicillin	4.3	3	0.97 <sup>(248)</sup>
Buspirone	33.3	32.6	
Caffeine	26.3	28.2	95 ± 33.7 <sup>(249-252)</sup>
Carbamazepine	33.6	33.5	116 <sup>(253)</sup>
Diazepam	36.3	35.8	351 ± 254 <sup>(249, 253, 254)</sup>
Midazolam	33.9	34.5	459 <sup>(253)</sup>
Phenytoin	25.4	30.8	36.7 ± 21 <sup>(252, 253, 255)</sup>
Sertraline	2.2	1.6	129 <sup>(256)</sup>
Thiopental	30.4	29.8	
Zolpidem	34.7	34	

**Table 2.4 Physicochemical parameters used to calculate partition coefficients.**

Physicochemical parameters <sup>a</sup>		
	pKa	LogP
Benzylpenicillin	3.55 <sup>b</sup>	2.74 <sup>c</sup>
Buspirone	7.62	1.95 <sup>d</sup>
Caffeine	14	0.92 <sup>e</sup>
Carbamazepine	15.96	2.1
Diazepam	3.4 <sup>c</sup>	2.82 <sup>f</sup>
Midazolam	6.2	3.89
Phenytoin	8.3 <sup>g</sup>	2.5
Sertraline	9.16 <sup>h</sup>	5.1
Thiopental	7.55 <sup>f</sup>	2.85 <sup>b</sup>
Zolpidem	6.2	1.2

All partition coefficients were subsequently calculated using Rodgers and Rowlands mechanistic approaches (72, 257). Further explanations of these approaches have been explained in chapter 1 (section 1.4.2.2) and Appendix A.

<sup>a</sup>. Unless otherwise stated, calculated using ChemAxon

<sup>b</sup>. Hansch *et al.* (1995) (258)

<sup>c</sup>. Merck Index (2001) (259)

<sup>d</sup>. Ullrich and Rumrich (1992) (260)

<sup>e</sup>. Martin *et al.* (1969) (261)

<sup>f</sup>. Sangster (1994) (262)

<sup>g</sup>. McLure *et al.* (2000) (263)

<sup>h</sup>. Deak *et al.* (2006) (264)

**Table 2.5 Protein binding and metabolic clearance**

	Protein Binding <sup>a</sup>			Metabolic Clearance
	Plasma	Brain	CSF	Rat <sup>b</sup>
	<b>f<sub>u</sub>plasma</b>	<b>f<sub>u</sub>brain</b>	<b>f<sub>u</sub>CSF</b>	<b>CL<sub>int</sub>, in vivo</b>
				mL/min/kg
Benzypenicillin	0.649	2.26	0.998	na
Buspirone	0.45	0.137	0.996	95.34
Caffeine	0.917	0.697	1	0.70
Carbamazepine	0.385	0.17	0.995	0.37
Diazepam	0.211	0.0426	0.989	0.88
Midazolam	0.045	0.0431	0.94	75.66
Phenytoin	0.302	0.0967	0.993	0.56
Sertraline	0.0347	0.00038	0.923	158.01 <sup>c</sup>
Thiopental	0.202	0.244	0.988	na
Zolpidem	0.267	0.265	0.992	7.47

<sup>a</sup>. Taken from Kodaira *et al.* (2011) (265).

<sup>b</sup>. Unless otherwise indicated, intrinsic *in-vivo* clearance was calculated based on a well-stirred liver model assuming average hepatic blood flow ( $Q_H$ , 55 mL/min/kg). Blood clearance and unbound fraction in blood were determined using the blood:plasma ratio ( $R_b$ ) or by assuming a value of 1 for basic and neutral drugs and 0.55 for acidic drugs.

<sup>c</sup>. Calculated from Ronfield *et al.* (1997) (266)

**Table 2.6 Renal Clearance**

<b>Compound</b>	<b>Rat</b>
	$CL_R$ ml/min/kg
Benzylpenicillin	10.22 <sup>a</sup>
Buspirone	na
Caffeine	0.021 <sup>b</sup>
Carbamazepine	na
Diazepam	na
Midazolam	na
Phenytoin	na
Sertraline	na
Thiopental	na
Zolpidem	na

Renal clearance in rats ( $CL_R$ ) was calculated based on glomerular filtration rate (GFR) ratio approach as described by Lin (1998) (267)

<sup>a</sup>. Taken from Scavone *et al.* (1989 (268), 1997 (269)) and Thompson *et al.* (1996) (270)

<sup>b</sup>. Taken from Birkett and Miners (1991) (271)

This approach required prediction of both plasma and brain concentration-time profiles to calculate the  $Kp_{\text{brain}}$  (brain-to-plasma partition coefficient) (equation 2.9) and more specifically when corrected for the unbound fraction,  $Kp_{\text{uu,brain}}$  (equation 2.10):

$$Kp_{\text{brain}} = \frac{C_{\text{brain}}}{C_{\text{plasma}}} \quad (2.9)$$

$$Kp_{\text{uu,brain}} = \frac{\int_0^{\infty} C_{\text{u,brain}} \times dt}{\int_0^{\infty} C_{\text{u,plasma}} \times dt} = \frac{AUC_{\text{u,brain}}}{AUC_{\text{u,plasma}}} \quad (2.10)$$

The brain was modelled with a perfusion limited compartment (Figure 2.10). Absorption (permeability clearances) from the BBB, protein binding (plasma, brain tissue and CSF), metabolic clearance and predicted tissue partition coefficients ( $Kp_i$ ) were previously collated by our group (64) and implemented within the model as described by equation 2.7. In this approach, *in vitro* permeability was scaled to an *in vivo* permeability through correction for the brain microvascular endothelial surface area (150 cm<sup>2</sup>.g brain<sup>-1</sup> for rats (272) or 157 cm<sup>2</sup>.g brain<sup>-1</sup> (273) for humans) and was parameterised into the appropriate unidirectional PS term (equation 2.11 and 2.12):

$$PS_{\text{blood-to-brain direction}} = P_{\text{appAB}} \times \text{Brain weight} \times \text{Surface Area} \times \text{CF} \quad (2.11)$$

$$PS_{\text{brain-to-blood direction}} = P_{\text{appBA}} \times \text{Brain weight} \times \text{Surface Area} \times \text{CF} \quad (2.12)$$

where brain weight was assumed to be 1.8 g in rats, 0.36 g in mice and 1500g in humans (274-276).

The correction factors (CF) terms relate to an *in vitro*-to-*in vivo* extrapolation factor which corrects for the absent physiologically conditions inherent in the determination of the *in vitro* permeability (229, 230). It is also important to note that for actively transported compounds, CF can be replaced by a relative expression factor (REF) which accounts for the differences in transporter abundances from the *in vitro* system to the *in vivo* species being studied permeability (229, 230). CF was assumed as being '1' in the absence of any parameter estimation approaches. When only a single  $P_{\text{app}}$  was reported in the literature, the resultant predicted PS was assumed bidirectional. Further, for active efflux compounds, the  $PS_{\text{blood-to-brain}}$  was assumed to be bidirectional and the active efflux component applied through correction of the  $PS_{\text{brain-to-blood}}$  of the efflux-ratio of the substrate (64).

All compounds were simulated using IV-bolus doses.

The validity of individual compounds was assessed using a fold-error (FE) method whereby whenever the observed  $K_{p_{uu,brain}}$  values were determined to be more than the predicted  $K_{p_{uu,brain}}$  values, therefore,

$$FE = \frac{K_{p_{uu,brain}Observed}}{K_{p_{uu,brain}Predicted}} \quad (2.13)$$

If however, the predicted  $K_{p_{uu,brain}}$  values were more than the observed  $K_{p_{uu,brain}}$  values, therefore,

$$FE = \frac{K_{p_{uu,brain}Predicted}}{K_{p_{uu,brain}Observed}} \quad (2.14)$$

### 2.2.2 Step 2: development of a rat regional brain PBPK sub-model

A study by Walker *et al.* (1996) (240) reported regional brain concentration of phenytoin in distinct brain regions of the rat, namely the hippocampus and frontal cortex. A further study by Van Belle *et al.* (1995) (242) also reported carbamazepine regional brain concentrations in the hippocampus. These studies were used to validate the regional brain PBPK sub-model. Compound-specific parameters for phenytoin and carbamazepine, along with permeability clearances across the hippocampus, frontal cortex and the rest of the brain tissues were obtained from *in-vitro* permeability data previously collated (64).

Model development adapted a previously reported CNS PBPK model (64) to include a hippocampus and frontal cortex compartment (Figure 2.10) and was applied to the whole-body PBPK model with systems parameters detailed in Table 2.1.

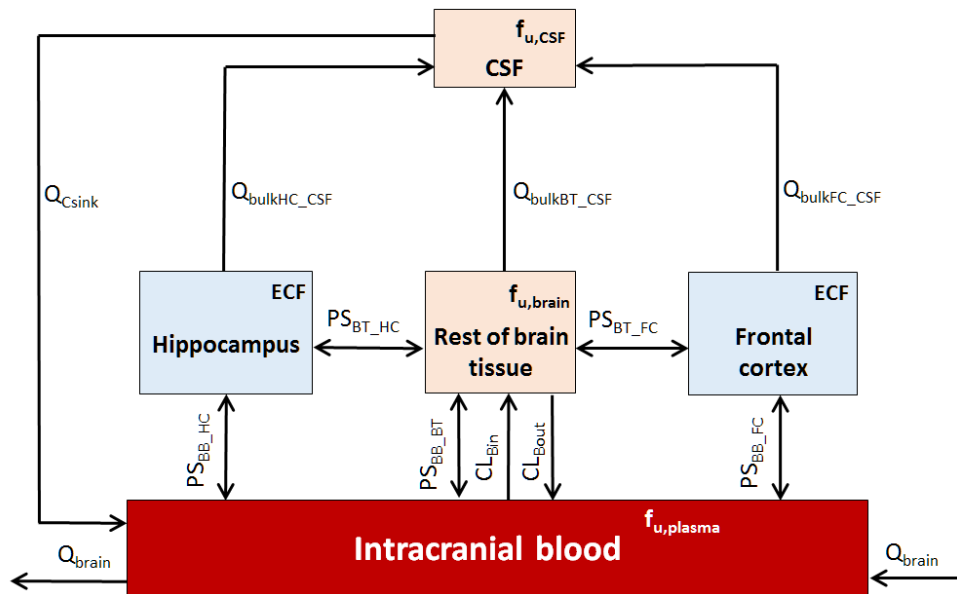


**Figure 2.10 5-compartment rat CNS PBPK brain model.**

Q: blood flow; PS: permeability surface-area; BB: intracranial blood; HC: hippocampus; FC: frontal cortex; C and CSF: cerebrospinal fluid; BT: brain tissue;  $f_u$ : drug fraction unbound.

In the development of this model, the following assumptions are made:

1. The CNS is represented by five compartments, namely CSF, intracranial blood, rest of brain tissue, frontal cortex and hippocampus;
2. All compartments are well-stirred with permeability barriers between the intracranial blood and brain;
3. There is no rate-limiting diffusion barrier between the ECF and CSF, and that drug equilibration between these two compartments is rapid (233);
4. Only unbound drug, governed by unbound fraction in plasma ( $f_{up}$ ), brain tissue ( $f_{ub}$ ) or CSF ( $f_{uCSF}$ ) was considered capable of crossing permeability barriers
5. In the absence of published regional  $f_{ub}$ , unbound brain fraction was assumed equivalent for all brain regions (i.e., hippocampus, rest of brain and frontal cortex) (277).
6. Within the extracellular space of the brain, fluids move either by diffusion or by bulk flow ( $Q_{bulk}$ ) (278);

7. Where absent from literature, hippocampus, and frontal cortex volumes scaled from mice to rats based on brain weight ratio-scalars (64, 275, 276, 279);
8. Due to the absence of regional brain *in-vitro* or *in-vivo* permeability data, the bi-directional passive transport (*PS*) term was assumed scaled based upon the regional tissue weight (assuming density =1) rather than whole brain mass.
9. The temporal concentration profile of the drug in the regional brain ECF would mimic the biophase sampled during microdialysis studies (280).
10. Since the liver was considered as the only site of clearance for phenytoin based on literature (281), the prediction for unbound renal clearance ( $CL_R$ ) was excluded from the simulation.
11. Active transporter from brain tissues (Efflux:  $CL_{Bout}$ ; Influx:  $CL_{Bin}$ ) can be determined as described in our previous CNS PBPK model (64).

The CNS PBPK model equations are detailed in equations 2.15-2.18.

*Intercranial blood ('brain blood'):*

$$\begin{aligned} \frac{dC_{bb}}{dt} = & Q_{brain}(C_{art} - C_{bb}) + (PS_{FC\_BB}C_{fc}fu_{fc} - PS_{BB\_FC}C_{bb}fu_p) + (PS_{BT\_BB}C_{bt}fu_{bt} - \\ & PS_{BB\_BT}C_{bb}fu_p) + CL_{Bout}C_{bt}fu_{bt} - CL_{Bin}C_{bb}fu_p + (PS_{HC\_BB}C_{hc}fu_{hc} - \\ & PS_{BB\_HC}C_{bb}fu_p) + Q_{CSink}C_{csf}fu_{csf} \end{aligned} \quad (2.15)$$

where the subscripts *art*, *bb*, *bt*, *csf*, *hc*, *fc*, *p*, and *Csink* represent arterial blood, brain blood, brain tissue, cerebral spinal fluid, hippocampus, frontal cortex, plasma and CSF absorption, respectively; *Q* is blood or CSF flow; *CL* is transporter clearance, respectively; *PS* is the passive permeability-surface area product of BBB, BCSFB, blood-brain to hippocampus (and *vice versa*), and blood-brain to frontal cortex (and *vice versa*), respectively; *fu* is fraction unbound.

*Brain tissue (rest of brain tissue):*

$$\begin{aligned} \frac{dC_{bt}}{dt} = & (PS_{BB\_BT}C_{bb}f_{u_p} - PS_{BT\_BB}C_{bt}f_{u_{bt}}) + CL_{Bin}C_{bb}f_{u_p} - CL_{Bout}C_{bt}f_{u_{bt}} + \\ & (PS_{FC\_BT}C_{fc}f_{u_{fc}} - PS_{BT\_FC}C_{bt}f_{u_{bt}}) - Q_{bulkBT\_CSF}C_{bt}f_{u_{bt}} + (PS_{HC\_BT}C_{hc}f_{u_{hc}} - \\ & PS_{BT\_HC}C_{bt}f_{u_{bt}}) \end{aligned} \quad (2.16)$$

where  $Q_{bulkBT\_CSF}$  is the bulk flow from the brain tissue to the CSF.

*Frontal cortex:*

$$\begin{aligned} \frac{dC_{fc}}{dt} = & (PS_{BB\_FC}C_{bb}f_{u_p} - PS_{FC\_BB}C_{fc}f_{u_{fc}}) - Q_{bulkFC\_CSF}C_{fc}f_{u_{fc}} + (PS_{BT\_FC}C_{bt}f_{u_{bt}} - \\ & PS_{FC\_BT}C_{fc}f_{u_{fc}}) \end{aligned} \quad (2.17)$$

where  $Q_{bulkFC\_CSF}$  is the bulk flow from the frontal cortex to the CSF.

*Hippocampus:*

$$\begin{aligned} \frac{dC_{hc}}{dt} = & (PS_{HC\_BT}C_{bb}f_{u_p} - PS_{BT\_HC}C_{hc}f_{u_{hc}}) - Q_{bulkHC\_CSF}C_{hc}f_{u_{hc}} + (PS_{BB\_HC}C_{bb}f_{u_p} - \\ & PS_{HC\_BB}C_{hc}f_{u_{hc}}) \end{aligned} \quad (2.18)$$

where  $Q_{bulkHC\_CSF}$  is the bulk flow from the hippocampus to the CSF.

*CSF:*

$$\begin{aligned} \frac{dC_{csf}}{dt} = & Q_{CSink}C_{csf}f_{u_{csf}} + Q_{bulkBT\_CSF}C_{bt}f_{u_{bt}} + Q_{bulkFC\_CSF}C_{fc}f_{u_{fc}} - Q_{CSink}C_{csf}f_{u_{csf}} \end{aligned} \quad (2.19)$$

For the rat brain PBPk model, the tissue volumes, and blood flow rates were obtained from published literature (Table 2.1). Subsequently, the 5-compartment brain model was applied to predict plasma, rest of brain, hippocampus and frontal cortex concentration profiles following an intraperitoneal dose of 50 mg/kg of phenytoin (240) or a 10 mg IV infusion (10 minutes) of carbamazepine.

In order to account for the uncertainty in the ECF volumes of regional brain compartment, Monte Carlo simulations were used to incorporate a 30% CV (log-normal distributed) on the

fixed estimates of ECF compartment volumes (simultaneous applied and simulated to the rest of brain, hippocampus and frontal cortex) resulting in at least 3000-runs per compound (1000-per compartment). This was applied using simulations for both rat (Step 2) and human (Step 3) models. The resultant 5<sup>th</sup> and 95<sup>th</sup> percentiles were graphically assessed.

To assess the impact of PS parameter uncertainty on model predictions, a sensitivity analysis was conducted to assess the impact of variation in  $PS_{HC\_BT}$  and  $PS_{BB\_HC}$  and  $PS_{FC\_BT}$  and  $PS_{BB\_FC}$ , on the hippocampus and frontal cortex  $C_{max}$  over a PS range of 0.01 to 100 mL/min using phenytoin as a model compound. Three-dimensional mesh plots were used to assess this relationship graphically.

### **2.2.3 Step 3: development of a human regional brain PBPK sub-model**

To explore the possibility of utilising the regional brain PBPK model to predict human brain pharmacokinetics, human CNS physiological parameters were used to develop a human regional CNS PBPK model (Table 2.7) based upon the regional brain model described in section 2.2.2. Despite limited human brain concentration data being reported in the literature, two studies were chosen which reported morphine brain concentrations in patients who suffered from traumatic brain injury, acquired using microdialysis cerebral catheter insertion in ‘better’ or ‘worse’ brain tissues, as determined by computed tomography scanning (243, 244). Systems parameters for the human CNS PBPK model are detailed in Table 2.7, and morphine-specific parameters are detailed in Table 2.8.

**Table 2.7 System-related parameters used for the brain PBPK model**

	Rat	Human
<b>Flow Rates <sup>a</sup></b>	<b>Q (mL/min)</b>	
Rest of brain tissue to CSF (bulk flow)	0.00024	0.285
Hippocampus to CSF (bulk flow)	0.00002	0.00114
Frontal cortex to CSF (bulk flow)	0.00005	0.0566
CSF production rate	0.0037 <sup>b</sup>	0.35 <sup>c</sup>
CSF absorption ( $Q_{C_{sink}}$ ) <sup>d</sup>	0.0037	0.35
<b>Volume</b>	<b>V (mL)</b>	
Intercranial blood <sup>e</sup>	0.025	75
Rest of brain tissue <sup>f</sup>	1.222	1211
* Rest of brain tissue ECF <sup>e</sup>	0.243	267
Hippocampus	0.093 <sup>g</sup>	5.68 <sup>h</sup>
* Hippocampus ECF <sup>e</sup>	0.019	1.07
Frontal cortex	0.233 <sup>i</sup>	283 <sup>j</sup>
* Frontal cortex ECF <sup>e</sup>	0.038	53.2
CSF	0.25 <sup>k</sup>	160 <sup>l</sup>

\* Monte Carlo simulations were applied to address uncertainty in true parameter value. A 30% CV was applied as the boundary conditions and predictions conducted with the all parameters identified simultaneous using a log-normal distribution with at least 3000 iterations per compound. <sup>a</sup> Regional brain ISF bulk flow was assumed to be 0.2  $\mu$ L/min.g brain (186) and assumed to be species independent; <sup>b</sup> Taken from Harnish *et al.* (1988) (282); <sup>c</sup> Taken from Brinker *et al.* (2014) (283); <sup>d</sup> Assuming that the rate of CSF absorption is the same with CSF production rate (284); <sup>e</sup> Calculated by assuming fractional volume of brain intravascular fluid is 0.014 and fractional volume of brain interstitial space 0.188 (285); <sup>f</sup> Assumes average brain weight of 1.8 g in rats, 0.36 g in mice and 1500g in humans (274-276); <sup>g</sup> Taken from Lee *et al.* (2009) (286); <sup>h</sup> Taken as mean of total hippocampal volume (right and left) (287); <sup>i</sup> Scaled based on a mean mouse frontal cortex volume of 0.0467 mL (288) and a scalar of 5 (ratio of rat brain weight:mouse brain weight) or 4166 (ratio of human brain weight:mouse brain weight); <sup>j</sup> Taken as mean of range reported values from Semendeferi *et al.* (2002) (289); <sup>k</sup> Taken from Bass and Lundbord (1973) (290); <sup>l</sup> Taken from Sakka *et al.* (2011) (291).

**Table 2.8 Physicochemical parameters for the human regional brain model**

	<i>In-vitro</i> permeability (cm/s $\times 10^{-6}$ )		Permeability clearance (mL/h) <sup>b</sup>		pKa	LogP	fu <sub>plasma</sub>	fu <sub>brain</sub>	fu <sub>CSF</sub>	Rb	CL <sub>int,in-vivo</sub>	CL <sub>R</sub>
	Papp <sub>AB</sub>	Papp <sub>BA</sub>	PS <sub>BB_BT</sub>	PS <sub>BT_BB</sub>								
Carbamazepine	-	-	29818	33818	-	-	-	-	-	-	0.4	na
Phenytoin	-	-	22545	27418	-	-	-	-	-	-	0.47	na
Morphine	1.07 <sup>a</sup>	1.06 <sup>a</sup>	924	926	8.9 <sup>c</sup>	0.89 <sup>d</sup>	0.74 <sup>e</sup>	0.45 <sup>f</sup>	1 <sup>g</sup>	1.02 <sup>f</sup>	18	na

<sup>a</sup> Obtained from Dale *et al.* (2006) (292)

<sup>b</sup> PS was calculated as described in Section 2.2.1. PS was subsequently applied to all regional brain compartments through correction for regional tissue weight (Refer Section 2.2.2 and assumption 8 above)

<sup>c</sup> obtained from Roy *et al.* (1989) (293)

<sup>d</sup> obtained from Illum *et al.* (2002) (294)

<sup>e</sup> obtained from Olsen *et al.* (1975) (295)

<sup>f</sup> obtained from Ball *et al.* (2012) (230)

<sup>g</sup> assumed to be 1

#### 2.2.4 Data and statistical analysis

The accuracy and success of the prediction were assessed by the root mean squared error (*rmse*) (Equation (2.20), where N refers to the number of observations) and the average-fold error (*afe*) (Equation (2.21)) which determine whether the prediction were over- and under-predicted. An  $afe \leq 2$  was considered a successful prediction (137, 138):

$$mse = \frac{1}{N} \sum (\text{Prediction} - \text{Observed})^2, rmse = \sqrt{mse} \quad (2.20)$$

$$afe = 10^{\left| \frac{\sum \log \frac{\text{Predicted}}{\text{Observed}}}{N} \right|} \quad (2.21)$$

### 2.3 RESULTS

#### 2.3.1 Step 1: Validation of the PBPK Model

To develop a broader regional CNS PBPK model, this step focussed upon the development of a base PBPK model consisting of a whole-body PBPK model incorporating a simplistic 1-compartment model of the brain. Predictions of brain temporal concentration profiles were surmised using the unbound brain: plasma ratio ( $K_{p_{uu,brain}}$ ), which is widely used to assess brain drug partitioning. Validation of the whole-body physiologically-based pharmacokinetic (WB-PBPK) model examined the ability of the model to predict  $K_{p_{uu,brain}}$  in rats for 10 compounds demonstrating passive absorption across the BBB which were previously used in PBPK modelling by our group (64). The WB-PBPK model was capable of predicting  $K_{p_{uu,brain}}$  to within 5-fold of the reported  $K_{p_{uu,brain}}$  for all compounds except benzylpenicillin, which was 5.34-fold over predicted (Figure 2.11).

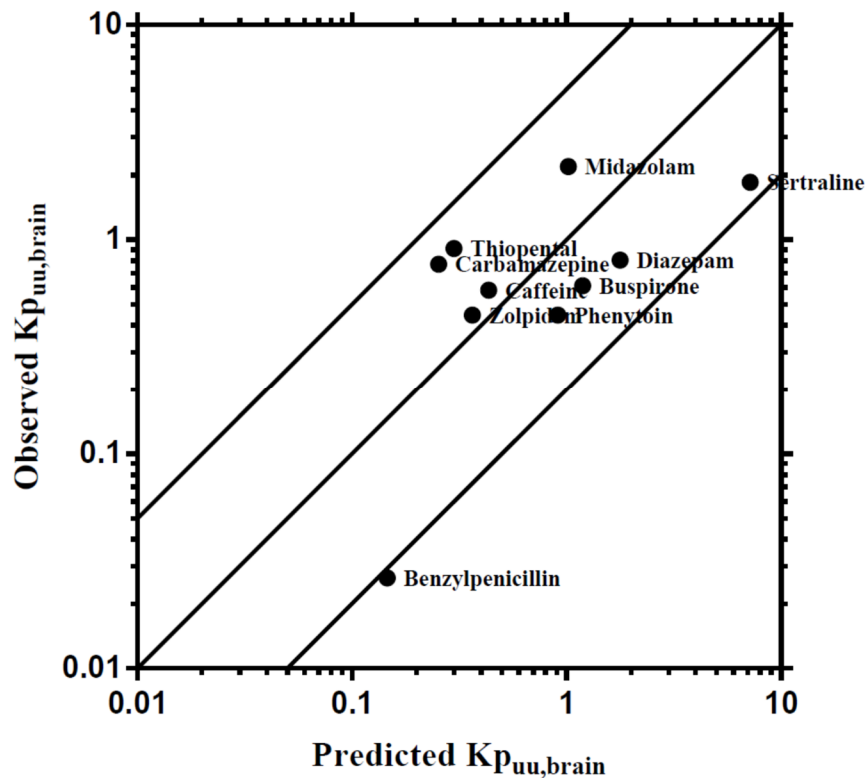


**Figure 2.11 Comparisons of predicted and reported  $K_{p_{uu,brain}}$  in rat.**

Solid bold mid-line represents the line of unity, and solid outer-lines represent 5-fold prediction error.

### 2.3.2 Step 2: development of a rat regional brain PBPK sub-model

#### 2.3.2.1 Case 1: Phenytoin

The base PBPK model described in Step 1 was adapted to replace the 1-compartment brain model with a 5-compartment regional brain model. This model was then used to predict phenytoin plasma and regional brain concentrations.

Predictions of phenytoin plasma concentration profiles were subsequently simulated and found to be within the range of observed profiles (Figure 2.12), with a predicted  $C_{max}$  ( $61.79 \mu\text{mol/L}$ ) similar to that reported by Walker *et al.* (1996) (240),  $61.69 \pm 4.7 \mu\text{mol/L}$ . Furthermore, a similar  $t_{max}$  was predicted compared to that reported by Walker *et al.* (240), approximately 20 mins (Figure 2.12).

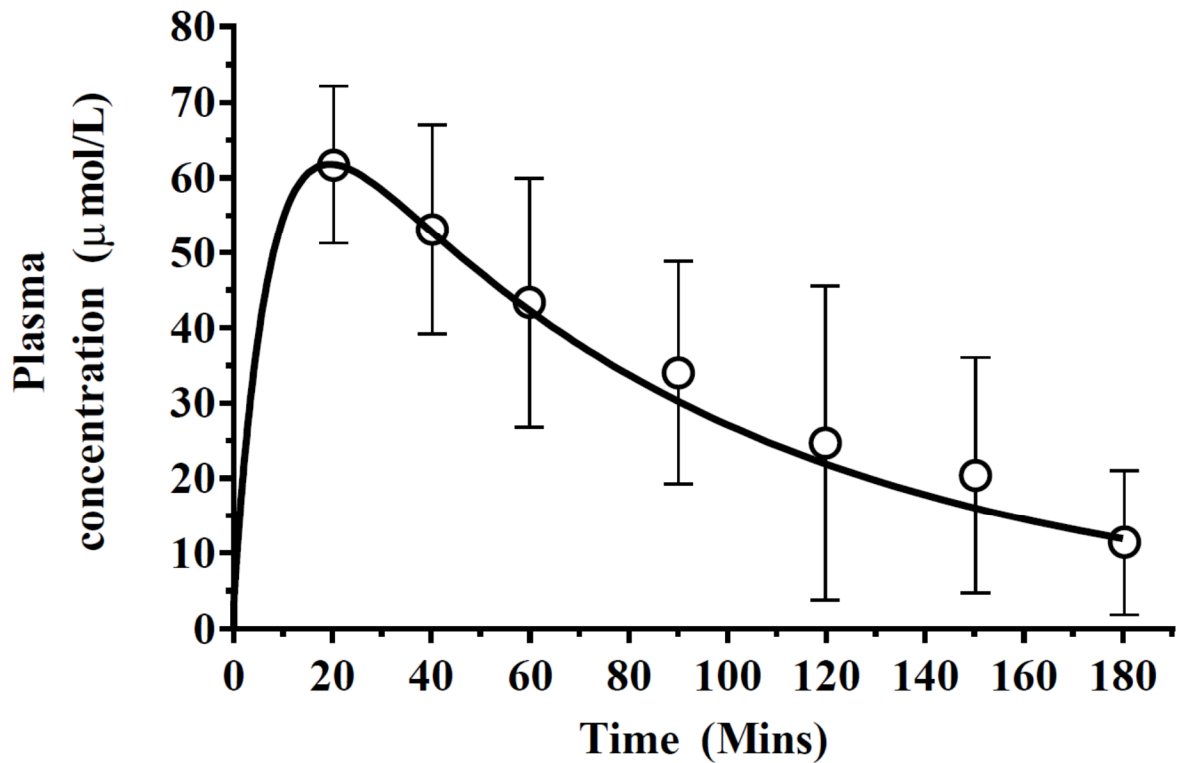


**Figure 2.12 Simulated mean phenytoin plasma concentration-time profiles.**

A 50 mg/kg phenytoin dose was simulated (solid line) with literature reported data represented by open circles with error bars representing standard deviations.

Prediction of regional brain concentrations was accomplished through application of the 5-compartment brain model, which incorporated distinct hippocampus and frontal cortex compartments. When accounting for uncertainty in model parameter predictions, model predictions were compared to those reported using microdialysis sampling in the hippocampus and frontal cortex, as reported by Walker *et al.* (1996) (240) and were generally in agreement in observed profiles in each brain region (Figure 2.13).

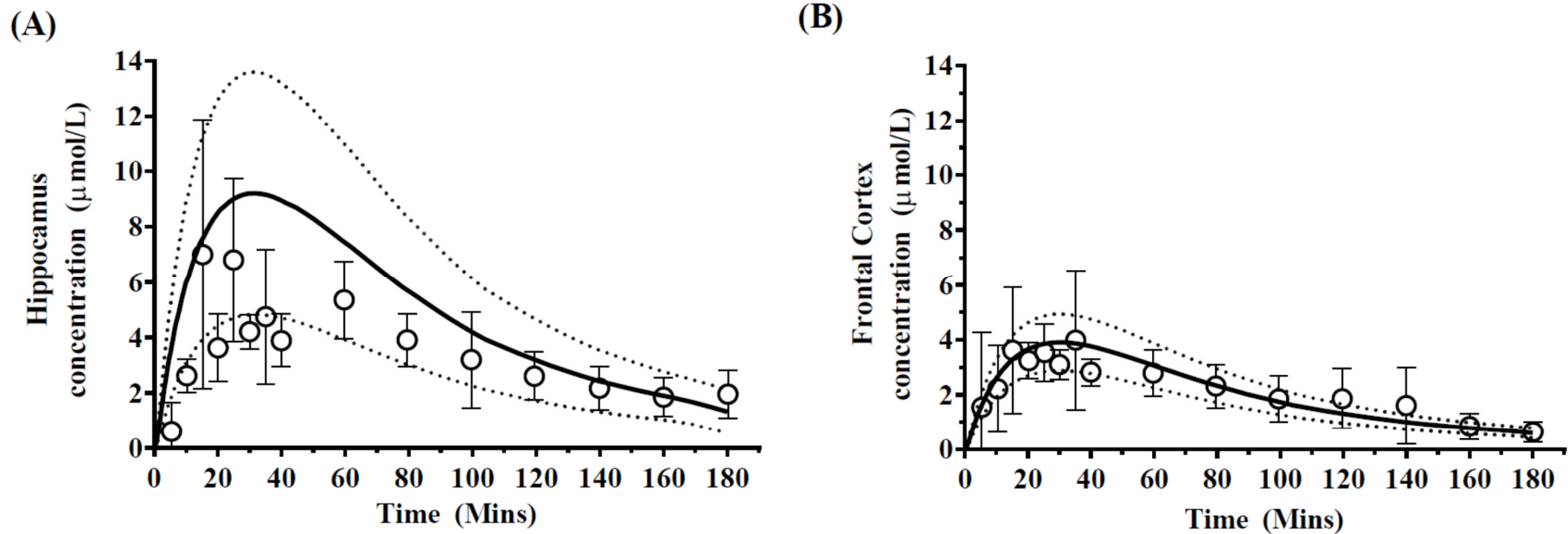


**Figure 2.13 Simulated mean phenytoin hippocampus and frontal cortex concentration-time profiles.**

Simulated mean values of phenytoin-time profiles in (A) hippocampus and (B) frontal cortex after a 50 mg/kg dose of phenytoin. Open circles and errors bars represent literature reported mean and  $\pm$  SD in 5 rats. Solid black line represents model prediction mean profiles and dashed lines indicated 95<sup>th</sup> and 5<sup>th</sup> percentiles.

**Table 2.9 Summary of predicted and observed pharmacokinetic parameters of phenytoin in plasma, hippocampus and frontal cortex in rats.**

	Plasma		Hippocampus		Frontal cortex	
	$C_{max}$	AUC	$C_{max}$	AUC	$C_{max}$	AUC
	( $\mu\text{mol/L}$ )	( $\mu\text{mol/L}\cdot\text{min}$ )	( $\mu\text{mol/L}$ )	( $\mu\text{mol/L}\cdot\text{min}$ )	( $\mu\text{mol/L}$ )	( $\mu\text{mol/L}\cdot\text{min}$ )
<b>Predicted</b>	61.79	5891.97	8.62 $\pm$ 3.42	718.29 $\pm$ 18.31	3.87 $\pm$ 0.24	340.47 $\pm$ 11.53
<b>Observed</b>	61.69 $\pm$ 4.7	5924.55 $\pm$ 340.4	7.00 $\pm$ 2.2	594.74 $\pm$ 21.2	3.98 $\pm$ 1.1	370.97 $\pm$ 17.1

AUC is calculated as  $\text{AUC}_{(0-\text{last})}$ ; Data represent mean  $\pm$  SEM

Model-predicted  $C_{max}$  and AUC were within 2-fold of that reported (240) (Table 2.9). Predictions of hippocampus  $t_{max}$ , approximately 20 minutes, were slightly over-predicted compared to the observed  $t_{max}$  of 15 mins. For the frontal cortex mean concentration,  $C_{max}$  was predicted at  $3.87 \pm 0.24 \mu\text{mol/L}$  and was consistent with the published literature  $C_{max}$  of  $3.98 \pm 1.1 \mu\text{mol/L}$  (Figure 2.13B). In both cases, the *afe* and *rmse* of 0.92 and 0.40 respectively, were indicative of a good model prediction. Furthermore, predictions of the regional  $K_{p_{uu,brain}}$  for the hippocampus (0.12) and frontal cortex (0.057) were within 2-fold of the reported regional  $K_{p_{uu,brain}}$  of 0.11 for hippocampus and 0.08 for frontal cortex.

### 2.3.2.2 Case 2: Carbamazepine

Predictions of carbamazepine plasma concentration profiles were found to be within the range of observed data (Figure 2.14A), with a predicted  $C_{max}$  (1.81 nmol/mL) similar to that reported by Van Belle *et al.* (1995) (242),  $2.14 \pm 0.27 \text{ nmol/mL}$  (Table 2.10). Furthermore, a similar  $t_{max}$  was predicted, 39 mins, compared to the reported  $t_{max}$  (242) of approximately  $44 \pm 9 \text{ mins}$  (Table 2.10).

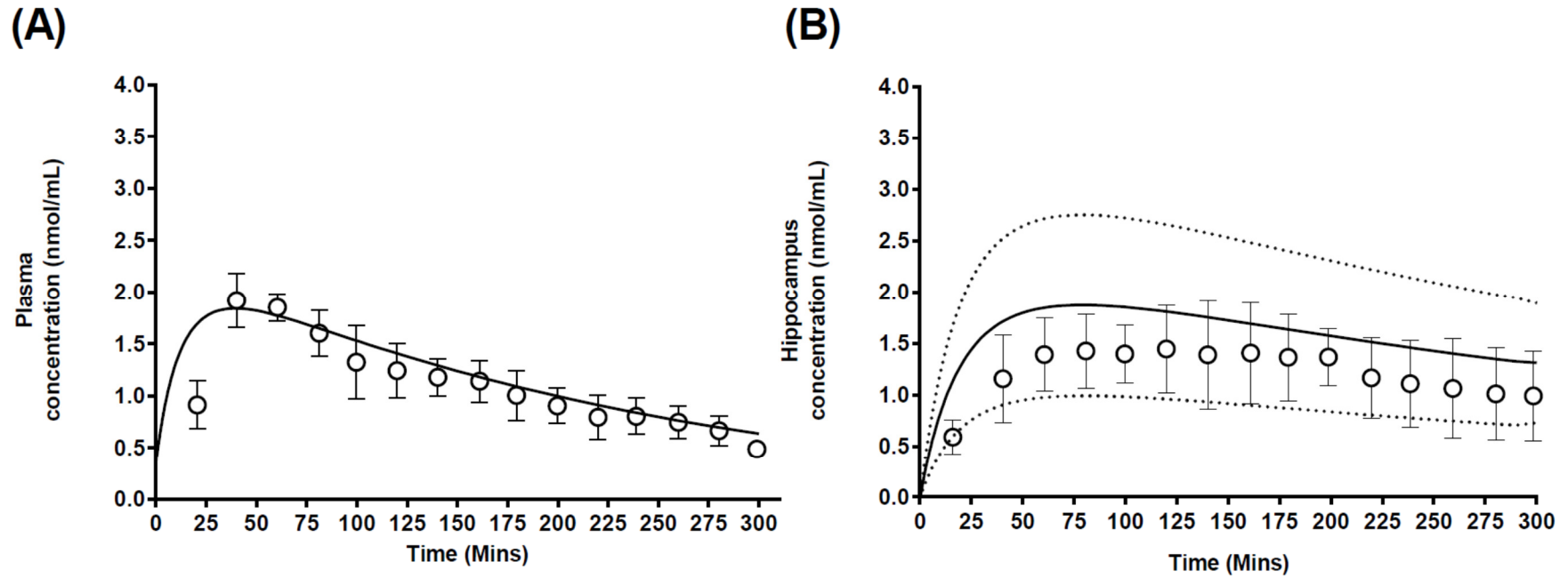


**Figure 2.14 Simulated mean carbamazepine plasma and hippocampus concentration-time profiles.**

Simulated mean values of carbamazepine-time profiles in (A) plasma and (B) hippocampus after a 2.5 mg/kg carbamazepine dose. Open circles and errors bars represent literature reported mean and  $\pm$  SD. Solid black line represents model prediction mean profiles and dashed lines indicated 95<sup>th</sup> and 5<sup>th</sup> percentiles.

Van Belle *et al.* (1995) (242) reported carbamazepine hippocampus pharmacokinetics following a single dose to rats and this was used as a basis to validate the regional brain PBPK model further. The model predicted plasma (Figure 2.14A) and hippocampus (Figure 2.14B)  $C_{max}$  and AUC to within 2-fold of the reported values (Table 2.10). Furthermore, predicted regional  $K_{puu,brain}$  were within 2-fold of the reported  $K_{puu,brain}$  (reconstructed from the AUC ratios) (242), 0.79 and 1.02 respectively.

**Table 2.10 Summary of predicted and observed pharmacokinetic parameters of carbamazepine in plasma and hippocampus brain regions in rats.**

	Plasma		Hippocampus	
	$C_{max}$ (nmol/mL)	AUC <sup>a</sup> (nmol/mL.min)	$C_{max}$ (nmol/mL)	AUC (nmol/mL.min)
<b>Predicted</b>	1.81	367.9	1.87 ± 0.81	470.2 ± 181.2
<b>Observed</b>	1.91 ± 0.25	333 ± 58	1.45 ± 0.41	340 ± 102

<sup>a</sup> AUC<sub>(0-last)</sub>

Data represent mean ± SD

### 2.3.2.3 Model Sensitivity Analysis

To assess the impact of parameter uncertainty on model predictions, a sensitivity analysis assessed the impact of variation in  $PS_{HC\_BT}$ ,  $PS_{BB\_HC}$ ,  $PS_{FC\_BT}$  and  $PS_{BB\_FC}$  on phenytoin (as a model compound) hippocampus and frontal cortex  $C_{max}$  over a PS range of 0.01 to 100 mL/min (Figure 2.15). Model predictions were generally sensitive to changes in both drug flux into each compartment ( $PS_{BBB\_HC}$  or  $PS_{BBB\_FC}$ ) and out of each compartment ( $PS_{HC\_BT}$  or  $PS_{FC\_BT}$ ). Irrespective of changes in hippocampus PS over the range simulated, predicted  $C_{max}$  spanned 3.7 to 8  $\mu$ M. Furthermore, variations in frontal cortex PS resulted in a predicted  $C_{max}$  spanned 2.3 to 3.9  $\mu$ M. Assuming regional differences in the HC and FC compared to the rest of the brain, where flux across the regional BBB located at the ‘rest of brain’ was ten-fold greater than that of the HC or FC, limited sensitivity was simulated across any change in  $PS_{BBB\_HC}$ ,  $PS_{BBB\_FC}$ ,  $PS_{HC\_BT}$  or  $PS_{FC\_BT}$ .

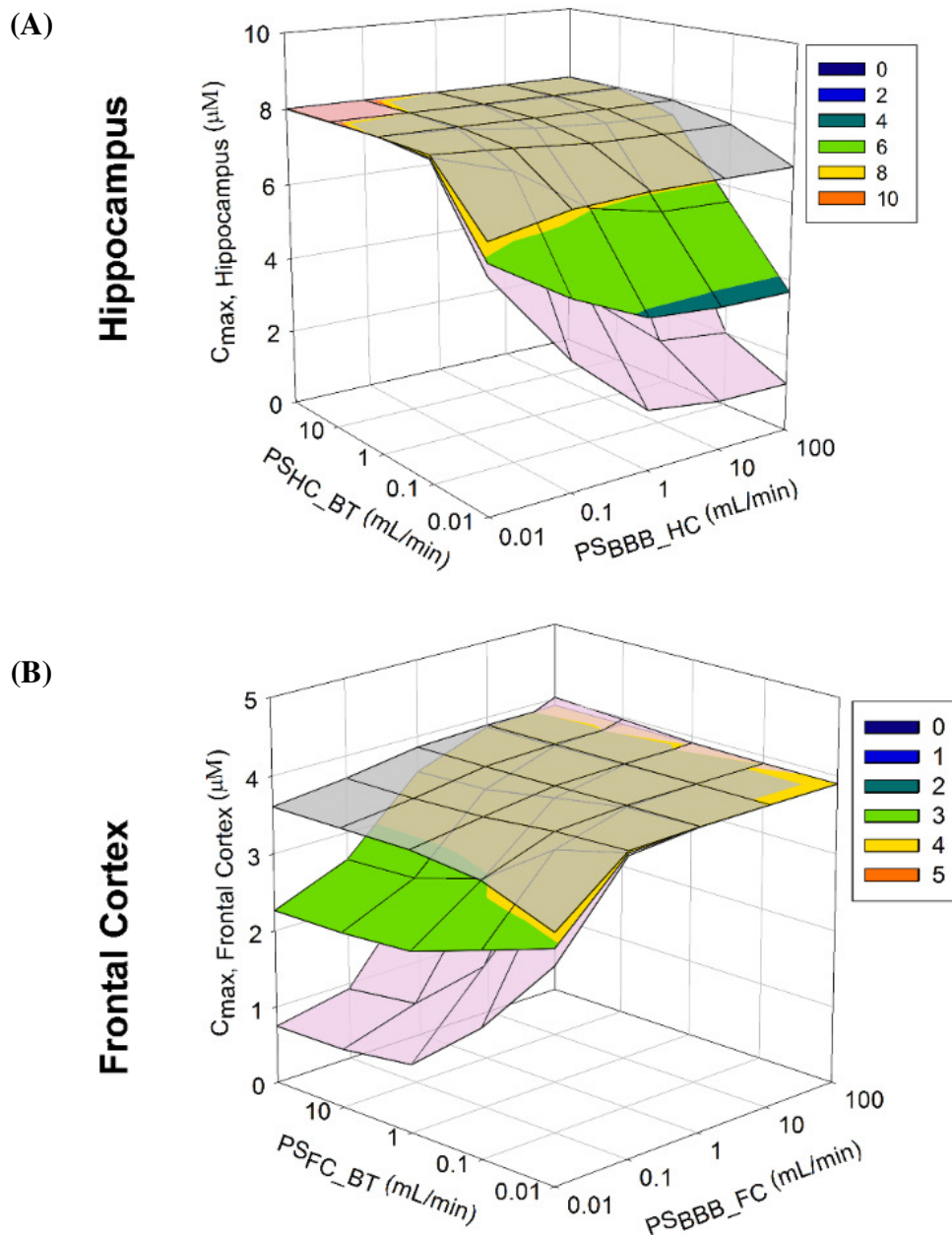


**Figure 2.15 Model sensitivity analysis of brain PS on  $C_{max}$ .**

Sensitivity analysis of the impact of variation in PS on the hippocampus (A) or frontal cortex (B) phenytoin  $C_{max}$ . Grey mesh indicates profiles where  $PS_{BBB\_BT}$  is 10-fold lower and pink mesh indicates profiles where  $PS_{BBB\_BT}$  is 10-fold higher than that presented in the associated multi-colours mesh plots. PS: permeability surface area product; HC\_BT (hippocampus and brain tissue); BBB\_HC (cerebral microvasculature [blood brain barrier] and hippocampus); FC\_BT (frontal cortex and brain tissue) and BBB\_FC (cerebral microvasculature [blood brain barrier] and frontal cortex).

### **2.3.3 Step 3: development of a human regional brain PBPK sub-model**

In an attempt to predict regional brain concentrations in humans, we utilised data reporting morphine brain concentrations in patients who suffered from traumatic brain injury using microdialysis cerebral catheter insertion in ‘better’ or ‘worse’ brain tissues (‘less extensive’ or ‘more extensive’ tissue damage), as determined by computed tomography scanning (243, 244).

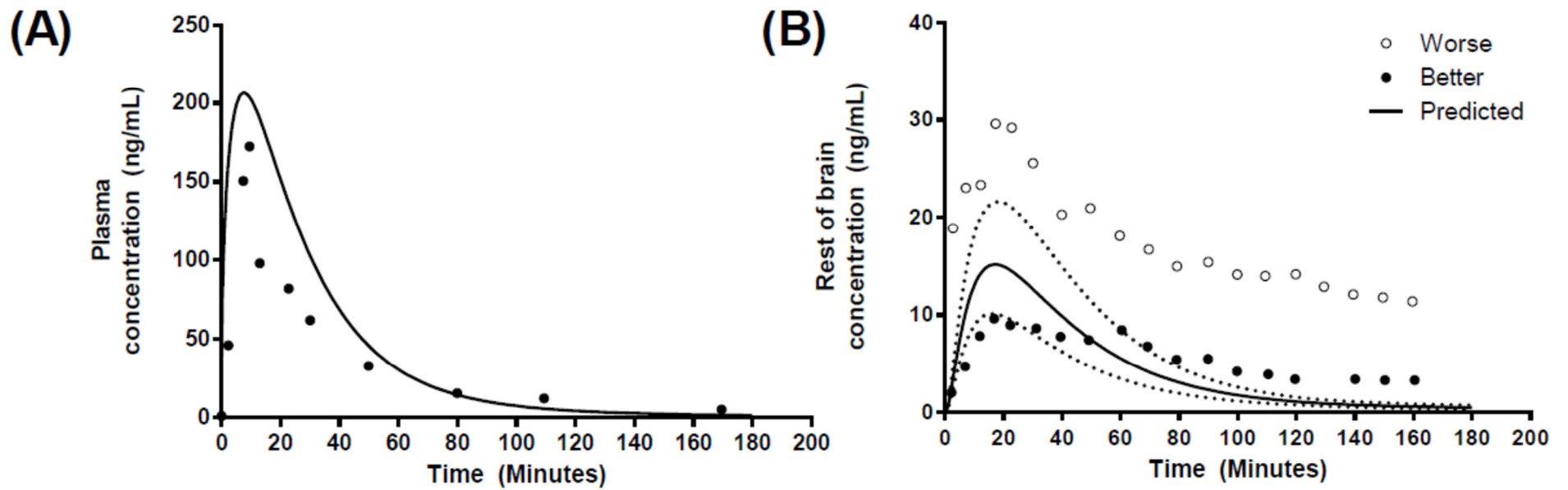


**Figure 2.16. Simulated human morphine concentration-time profiles.** Predicted concentration-time profiles for (A) plasma, (B) rest of brain, (C) hippocampus and (D) frontal cortex, following a 10 mg IV-infusion over 10 minutes. Circles represent literature reported values. Solid black line represents model prediction mean profiles and dashed lines indicated 5<sup>th</sup> and 95<sup>th</sup> percentiles. ‘Better’ and ‘worse’ (‘less extensive’ and ‘more extensive’ tissue damage) regional brain morphine concentrations are highlighted by solid or open circles in (B).

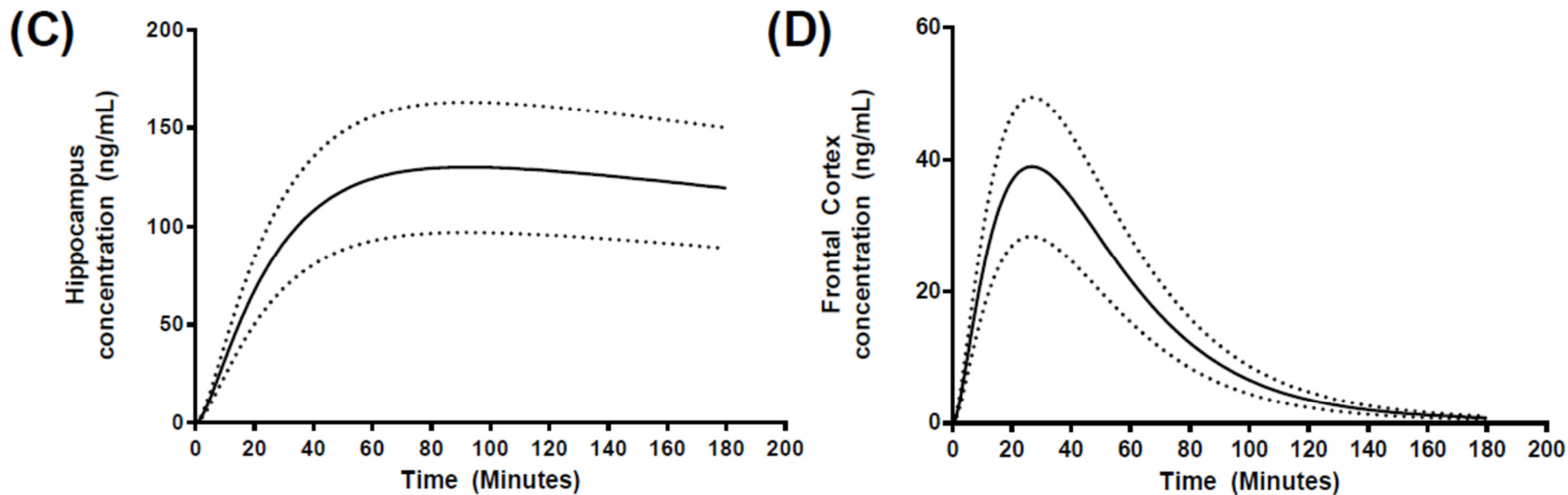


**Figure 2.16 (cont). Simulated human morphine concentration-time profiles.**

Predicted concentration-time profiles for (A) plasma, (B) rest of brain, (C) hippocampus and (D) frontal cortex, following a 10 mg IV-infusion over 10 minutes. Circles represent literature reported values. Solid black line represents model prediction mean profiles and dashed lines indicated 5<sup>th</sup> and 9<sup>th</sup> percentiles. ‘Better’ and ‘worse’ regional brain morphine concentrations are highlighted by solid or open circles in (B).

The plasma concentration-time profile was well predicted (Figure 2.16A) with  $C_{\max}$ ,  $t_{\max}$  and AUC all within 2-fold of the reported values (Table 2.11). In the absence of human hippocampus or frontal cortex temporal concentration profiles, we compared the reported profiles for ‘better’ and ‘worse’ brain morphine temporal concentration profiles to those generated within the ‘rest of brain’ compartment within the regional brain PBPK model (Figure 2.16B). The model predicted a rest of brain (ROB)  $C_{\max}$  of  $14.5 \pm 4.21$  ng/mL, which was within the range reported for both ‘better’ and ‘worse’ brain tissue (‘less extensive’ and ‘more extensive’ tissue damage), in addition to calculated AUC beings within 2-fold of those reported (Table 2.11). However,  $t_{\max}$  was 2.5-fold underpredicted. For regional brain compartments, the hippocampus exhibited a slow transfer of morphine leading to a  $t_{\max}$  of 79.6 minutes and  $C_{\max}$  of  $124.4 \pm 41.2$  ng/mL, whilst the frontal cortex  $t_{\max}$  was shorter (26.5 min) with a  $C_{\max}$  of  $38.91 \pm 15.78$  ng/mL (Figure 2.16C and D).

**Table 2.11 Summary of predicted and observed pharmacokinetic parameters of morphine in plasma and regional brain compartments in humans.**

Compartment		$C_{\max}$ (ng/mL)	AUC (ng/mL.min)	$t_{\max}$ (min)
Plasma	Predicted	208.2	5363	7.2
	Observed	178	$7513 \pm 124$	9.8
Better Brain	Observed	10.1	941.7	$31.4 \pm 17.1$
Worse Brain	Observed	29.8	2732	$17.8 \pm 2.3$
Rest of brain	Predicted	$14.5 \pm 4.21$	$815 \pm 93$	18.1
Hippocampus	Predicted	$124.4 \pm 41.2$	$19971 \pm 3791$	79.6
Frontal Cortex	Predicted	$38.9 \pm 15.7$	$2444 \pm 153$	26.5

Data represent mean  $\pm$  SD

## 2.4 DISCUSSION

Central nervous system (CNS) disorders affect millions of people worldwide despite the availability of a wide range of established treatments (181). The primary challenge to CNS drug delivery is the penetration of the blood-brain barrier in order to attain a sufficiently high enough biophase concentration for a clinical effect. Given the lengthy discovery and development times associated with CNS drug development, the application of mechanistic pharmacokinetic modelling has emerged to bridge the gaps between *in vivo* and *in vitro* approaches to expedite extrapolation of the pharmacokinetics of drug compounds and to aid in the selection of appropriate doses for clinical studies (257, 296).

The primary aim of this research was to employ mechanistic pharmacokinetic modelling approaches to develop models capable of conducting robust *in vitro*-to-*in vivo* correlation and thus allow interspecies extrapolations (rodent-to-human). Such approaches are based around a mechanistic set of physiological ('systems') parameters describing the physiology of the model system (e.g. rodents or humans) and *in vitro* derived or estimated drug ('compound') parameters.

Such extrapolations will enable the quantification and prediction of the extent of drug delivery to the brain and wider CNS across drug barrier sites, namely, the BBB and the regional brain area. These mechanistic platforms are in line with a replacement, reduction and refinement concept that is integrated into the drug discovery framework (297). The aim of this study was therefore to develop a PBPK model of the rat CNS which was capable of predicting to predict regional brain pharmacokinetics (frontal cortex and hippocampus) of phenytoin and carbamazepine in rats, in addition to the prediction of human regional brain pharmacokinetics or morphine.

### 2.4.1 Validation of the PBPK Model

To develop an accurate brain PBPK model that can predict human drug concentrations from a limited set of routinely available pre-clinical and *in vitro* drug-specific parameters, a robust validation process is essential to determine the prediction accuracy and precision. A rat CNS

PBPK model developed by Ball *et al.* (2012) (230) was selected to confirm successful base model development. Initial validation was conducted by comparing the  $K_{p_{uu,brain}}$  values between the predicted and published data for passively transported compounds, namely benzylpenicillin, buspirone, caffeine, carbamazepine, diazepam, midazolam, phenytoin, sertraline, thiopental, and zolpidem (64). Model predictions were all within 5-fold of the observed  $K_{p_{uu,brain}}$ , with prediction of  $K_{p_{uu,brain}}$  for benzylpenicillin being 5.5-fold over predicted (Figure 2.11). This over-prediction found in benzylpenicillin may be a result of the involvement of unclarified molecular active transport mechanism through the BBB as reported by Suzuki *et al.* (248, 298) where the rapid CNS elimination was not captured during the simulation.

As the description of the brain compartment using a simplistic permeability limited compartment is not physiologically relevant, it would be expected that model predictions of temporal brain concentrations would, therefore, be less accurate and this would account for the large error range simulated. This basic CNS PBPK model was subsequently adapted and built upon in Step 2 to propose a regional brain CNS PBPK model which was more mechanistically derived.

#### **2.4.2 Prediction of regional brain concentrations in rats**

In order to expand upon this previously developed model, we adapted the basic CNS PBPK model to include two further tissue compartments, namely the frontal cortex and hippocampus. In this process, we identified two candidate compounds to validate our adapted model against, phenytoin and carbamazepine. Both compounds have been administered to rats and region-specific brain microdialysis conducted to assess the CNS pharmacokinetics. Frontal cortex and hippocampus phenytoin concentrations had been previously reported by Walker *et al.* (1996) (240), with Van Belle *et al.* (1995) (242) also reporting carbamazepine regional brain concentration in the hippocampus. The PBPK model developed incorporated an *in situ* permeability surface area (PS) previously reported in rodents to drive diffusion from the plasma circulation into the CNS. The resultant predictions of plasma and regional concentrations were within the range of concentrations reported for both compounds (Figures 2.12-2.14) with the majority of model predicted pharmacokinetic parameters within 2-fold of that observed (Table 2.9-2.10).

### 2.4.2.1 Model sensitivity analysis

Monte-Carlo based model sensitivity analysis was first addressed by assessing the uncertainty in our calculation of regional brain compartments PS on predictions of regional brain concentrations. The rationale for focussing on regional brain PS when conducting the sensitivity analysis is to identify key parameters that have the greatest influence on model outputs in terms of variability, hence, increasing the model accuracy. Model predictions were sensitive to changes in both drug flux into each compartment ( $PS_{BBB_{HC}}$  or  $PS_{BBB_{FC}}$ ) and out of each compartment ( $PS_{HC_{BT}}$  or  $PS_{FC_{BT}}$ ), however irrespective of any changes in either hippocampus or frontal cortex PS, the resultant impact on the compartment  $C_{max}$  was minimal. Therefore, assuming the permeation of drug across the brain microvascular is uniform (i.e. no regional differences), variations in the inter-regional brain permeability ( $PS_{HC_{BT}}$  or  $PS_{FC_{BT}}$ ) of the drug would play a minimal role in influencing regional brain  $C_{max}$ . Furthermore, assuming that the regional brain penetration of drug was non-uniform across the brain, a 10-fold lower or 10-fold higher shift in  $PS_{BBB_{BT}}$  would significantly increase (10-fold lower) or reduce (10-fold higher) overall regional brain  $C_{max}$  (Figure 2.15).

### 2.4.3 Prediction of regional brain concentrations in humans

The prediction of human CNS pharmacokinetics, from preclinical data, would provide an invaluable approach to assessing the usefulness of candidate molecules progressing through drug development stages.

Human brain pharmacokinetics data is extremely sparse in the literature, however a study was identified which applied microdialysis to quantify morphine pharmacokinetics in human brain tissue and where a relatively rich brain pharmacokinetic profile was available. This data was available for 'brain tissue', and we assumed this was equivalent to the 'rest of brain' compartment within our 5-compartment brain model. The resultant model predictions resulted in a reasonable prediction of the shape of the concentration profiles along with a good estimate of the  $C_{max}$  and AUC, the former of which was predicted within the 'range' of 'better' and 'worse'  $C_{max}$  reported in the observed data sets (Figure 2.16). However, the prediction of the terminal elimination phase was poorer than expected, although the reported data only illustrated

data points for two representative patients, the distribution of resultant morphine concentrations at each time point was not reported, hence we were unable to ascertain the intra-individual variability.

As a first principles approach, we have been able to capture the pharmacokinetics of morphine in human brain tissue and the validated ‘rest of brain’ compartment. Assuming PS is scaled from *in-vitro*  $P_{app}$  based on correction for surface area ( $\text{cm}^2/\text{g}$  tissue), the PS would be ‘corrected’ for overall surface area based on the gross tissue weight. Furthermore, the small regional mass of the hippocampus would result in a highly localised concentration of morphine, which would slowly diffuse out of the brain tissue as a result of the smaller surface area. Similarly, regional differences in both morphine (299) and biperiden have been reported in rat brains (300).

Further, although this model did not consider active transport substrates, it would be possible to model the active transport of, for example, P-glycoprotein substrates. This is made possible by the availability of absolute protein abundance data for a range of transporter proteins at brain barriers as a result of the application of quantitative proteomics (301, 302). Further, we have previously demonstrated the application of this approach to the prediction of  $K_{p_{uubrain}}$  (for whole brain) for 11 active transporter substrates using a similar CNS PBPK (64), where an active transport permeability surface area (PS) can be determined by the use of a corrected efflux ratio (to account for the differentiation between purely active and purely passive transport) (303, 304) in addition to accounting for the abundance of the transporter protein (64).

Finally, the key to driving regional brain drug concentration predictions would be accounting for any potential regional differences in non-specific brain tissue binding (i.e. a brain regional specific  $f_{u_{bt}}$ ). In the absence of any reported regional brain  $f_{u_{bt}}$  data, we assumed  $f_{u_{bt}}$  was uniform across all brain regions. Any regional differences in grey/white matter phospholipid /lipid content may result in localised differences in  $f_{u_{bt}}$ . Indeed, it has been reported that differences in lipid content do exist when comparing white and grey matter regions (305-308). Given these potential regional differences in brain composition, the application of techniques such as equilibrium dialysis should be encouraged to further investigate and determine  $f_{u_{bt}}$  for specific brain regions to provide more appropriate input data in the model.

## 2.5 CONCLUSIONS

With an ageing population, elevated fertility rates and a progressive increase in life expectancy, the number of older adults will increase the demands on both the public health system and on medical and social services. This is particularly true for chronic neurological disorders such as Alzheimer's disease and Parkinson's disease, which affect older adults and contribute to disability and increased health care costs. This situation is made worse as a result of the time that was required to bring a new medicine to market, as well as the high cost.

Recent advances in biotechnology and pharmaceutical sciences have significantly expanded the number of drugs that are being developed for the treatment of CNS disorders. However, drugs identified through novel discovery techniques often do not consider the pharmacokinetic and pharmaceutical properties of the drug candidates. The reasons for the under-developed CNS drug market is the lack of efficient delivery strategies that exist to enable drugs to overcome the BBB and BCSFB and poor knowledge of the relationships between molecular properties and pharmacokinetic parameters and how these should be optimised to enhance CNS drug delivery (225, 309).

With high attrition rates for CNS drug development, there are now major health and regulatory initiatives to improve the potential bio-distribution and clinical efficacy of new chemical or pharmaceutical agents within central nervous system (CNS) drug development strategies. Quantitative techniques, such as PBPK modelling and systems biology are common solutions to the problem of increasing attrition rates within the pharmaceutical industry. Empirical and mechanistic, 'top-down' pharmacokinetic models, are routinely used in quantitative decision making and are easy and simple to develop and use, portable, and good at extrapolating across different doses and subpopulations.

During preclinical and clinical development, these models are routinely used to maximise the information obtained from *in vivo* and *in vitro* experiments, while minimising resource utilisation. In an attempt to explore the drug disposition across the CNS, a regional brain PBPK model was developed for rats and extended to human to model human regional brain pharmacokinetics of morphine. While the limiting factor in the application of this model to human CNS pharmacokinetics is the paucity in human brain (whole) or regional brain drug concentrations, with the greater application of cranial microdialysis, it would be possible to

further refine the proposed model for application in regional brain concentration. Nonetheless, the research has successfully proposed a simplified first-principle approach to the development of a regional brain CNS PBPK model as well as addresses our first aim of the thesis which is to assess hippocampus and frontal cortex drug pharmacokinetics in rodents and humans.

## **CHAPTER 3**

# **Utility of PBPK modelling in dose optimisation for complex drug-drug interactions in HIV- and malaria-infected children**

### **Disclaimer**

Elements of this chapter have been published as follows:

Zakaria, Z. and R. K. Badhan. The impact of CYP2B6 polymorphisms on the interactions of efavirenz with lumefantrine: Implications for paediatric antimalarial therapy.

*European Journal of Pharmaceutical Sciences*. 2018; 119: 90–101

DOI: 10.1016/j.ejps.2018.04.012

## 3.1 INTRODUCTION

### 3.1.1 Background

Malaria represents a considerable healthcare burden, with the World Health Organization (WHO) attributing an estimated 212 million malaria cases and 429 000 malaria-related deaths in 2015. Out of those malaria cases and deaths, 92% are from the African regions and predominantly occur in children aged under 5 years (310). Consequently, areas with high rates of malaria also carry a high incidence of HIV (human immunodeficiency virus)/AIDS (acquired immune deficiency syndrome). Despite a decrease in new HIV infections in children and adults from 2005 onwards, the majority of HIV infections still occur in African regions, making it the number one cause of mortality in that region (311, 312).

### 3.1.2 Malaria

*Plasmodium* parasites have been determined as the main carrier leading to malaria in their hosts. These parasites are spread exclusively by infected female *Anopheles* mosquitoes that act as malaria vectors which bite mainly between dusk and dawn. In humans, five *Plasmodium* species are known to cause malaria, namely *Plasmodium falciparum*, *Plasmodium vivax*, *Plasmodium ovale*, *Plasmodium malariae* and *Plasmodium knowlesi* (313). The majority of cases of malaria are caused by either *P. falciparum* or *P. vivax*, with the former being more common and highly prevalent in in Sub-Saharan Africa (314, 315). In regions such as Asia and Latin America, *P. vivax* is the most common infection as compared to *P. falciparum* due to *P. vivax* resistance to colder climates, higher altitudes and lower temperatures (310).

*Plasmodium* parasites are introduced to human from the infected *Anopheles* mosquitoes' saliva into the human blood. These parasites (sporozoites) invade liver hepatocytes, expand and mature to produce thousands of merozoites before subsequently leaving and reproducing within red blood cells. The invasion and multiplication of the asexual parasites (merozoites) in the red blood cells are the point where the disease occurs (316). All *Plasmodium* species have a similar life cycle (Figure 3.1), however, *Plasmodium falciparum* has the highest rate of parasitaemia due to its ability to invade all red blood cells because of its higher flexibility in the receptor pathways. This characteristic is what makes *Plasmodium falciparum* most deadly as it can

develop adhesive proteins that can stick to the walls (endothelium) of the blood vessels which can prevent the infected red blood cells from being destroyed in the spleen (317, 318).

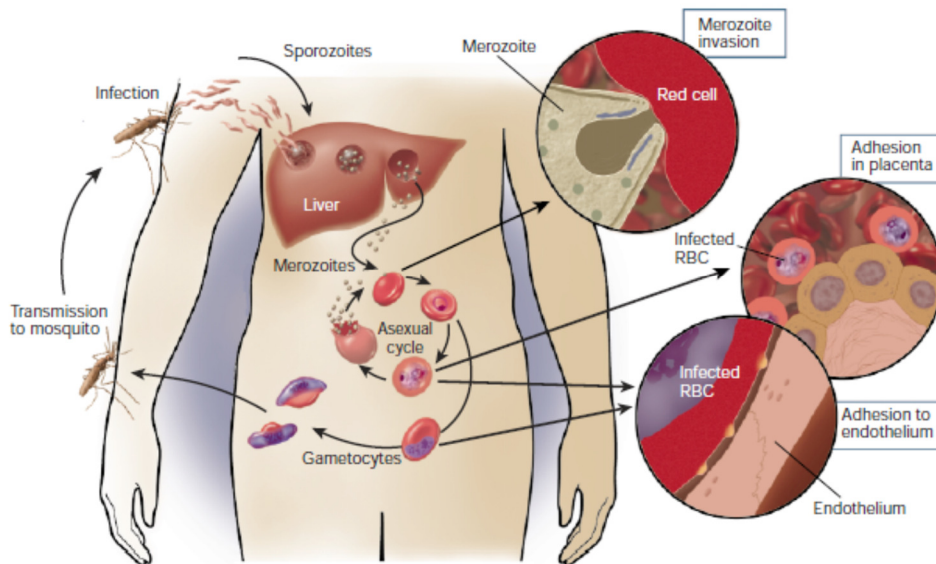


**Figure 3.1** Life cycle of the *plasmodium* species.

Reproduced from Miller *et al.* (2002) (316).

Malaria usually manifests itself in the form of acute febrile illness. Symptoms such as fever, chills, headache, and vomiting usually occur between 10 to 15 days after the infective mosquito bites. These symptoms might be mild and often quite difficult to be recognized as malaria (319). Due to these difficulties, the symptoms might progress to severe illnesses such as the development of respiratory distress which often can lead to death if it is not treated within 24 hours especially those that have been infected with *P. falciparum* (320). Children are most susceptible to these risks whenever they develop severe malaria as the symptoms can manifest to severe anaemia, respiratory distress, and cerebral malaria. As for adults, failure to treat *P. falciparum* infection within 24 hours also could lead to severe multi-organ infection which is often difficult to be treated (321).

According to the WHO, malaria is classified into either 'severe' or 'uncomplicated' (310, 321). The classification of 'severe' occurs when the following symptoms are presented in patients: hyperparasitaemia, jaundice, renal impairment, pulmonary oedema, severe malarial anaemia,

acidosis, hypoglycaemia, multiple convulsion, significant bleeding, multiple convulsion and impaired consciousness.

Treatment for malaria usually depends on the severity and type of the disease. Typically, antimalarial medications are given in the form of oral doses for uncomplicated malaria or intravenous doses for severe malaria. Therapeutic objectives for uncomplicated malaria are to prevent progression to severe malaria and to cure the infections as rapidly as possible. With these objectives in mind, administration of drugs are usually in the form of antimalarial combination therapy (ACT), combining rapidly acting but short half-life artemisinin derivatives (e.g. artemether, artesunate, artemotil, artelinic acid and dihydroartemisinin) with longer acting and long half-life (slowly eliminated) partner drugs (e.g. lumefantrine, mefloquine, amodiaquine, sulfadoxine/pyrimethamine and piperazine) to minimise resistance to any single drug components (310, 322, 323).

The artemisinin derivatives act by reducing parasite numbers rapidly up to a factor of 10,000 in each 48 hours asexual cycle of the malaria parasites. The partner drugs, which possess a longer half-life, act by clearing the remaining parasites thus protects against resistance towards the rapid-acting artemisinin derivatives (324). The ACT recommended by the WHO for treatment of uncomplicated malaria are: 1. artemether plus lumefantrine; 2. artesunate plus mefloquine; 3. artesunate plus amodiaquine; 4. artesunate plus sulfadoxine-pyrimethamine and 5. dihydroartemisinin plus piperazine.

As for severe malaria, which typically occurs due to exacerbation of *P. falciparum* infection, parenteral form of artesunate is often used for children and adult (325). In a case of cerebral malaria in children, another systematic review also suggests intravenous artemisinin derivatives or quinine in combination with supportive care in the critical care unit for better management of complications such as seizures and high fever (310, 311, 321, 326).

### **3.1.3 Human Immunodeficiency Virus (HIV)**

The human immunodeficiency virus (HIV) is a type of retrovirus that can instigate HIV infection and with due time, can develop acquired immunodeficiency syndrome (AIDS) (327). HIV infects the human immune system, specifically the CD4+ helper T cells, dendritic cells and macrophages, hence, weakens the defence system against opportunistic infections (328). Depending on the individual, HIV infection can develop to AIDS in 2 to 15 years without

treatment (312). AIDS manifests itself in the form of development of certain cancers (Kaposi's sarcoma and lymphomas), infections (severe bacterial and fungi infections) and another type of severe clinical manifestations such as cryptococcal meningitis and tuberculosis (329).

The mechanisms in which HIV infect include termination of infected CD4+ T cells by CD8 cytotoxic lymphocytes, direct viral elimination of infected cells, apoptosis of uninfected bystander cell and pyroptosis of abortively infected T cells (330-332). These mechanisms eventually lead to the low levels of CD4+ T cells, hence increase the susceptibility of the body to the opportunistic infections. HIV has some unique characteristics as compared to other viruses in terms of its genetic variability due to its fast replication process (Figure 3.2) and high mutation rate (333-335). There are two types of HIV according to its characterisation: HIV-1 and HIV-2. Initially, HIV-1 is the name that has been given when it was first discovered, and this type of virus has more infective and virulent characteristics as compared to HIV-2 (336). Majority of HIV infection is also originated from HIV-1 type as opposed to HIV-2 which is mainly restricted to West African region (337).

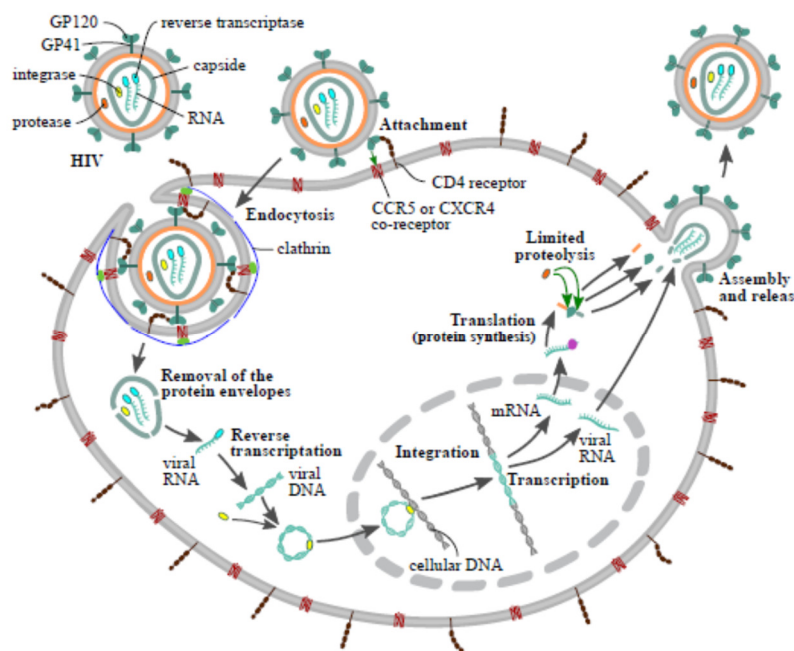


**Figure 3.2 HIV replication cycle.**

Reproduced from Jmarchn *et al.* (2017) (338).

HIV can be transmitted by sexual contacts, mother to child during breastfeeding and pregnancy and through exposure to infected tissues or body fluids (339). There is also a possibility that a patient can be infected with several strains of HIV and this condition is termed as HIV superinfection (340).

Unfortunately, to date, there is still no cure for HIV or AIDS (339). The only alternative towards a cure is to slow the progression of the disease by administering highly active antiretroviral therapy (HAART) (341). This treatment also provides a form of prevention and treatment towards the opportunistic infections that usually occur in AIDS patients. Typically, adults patients will be given a 'cocktail' of HAART combinations as an initial treatment which includes a non-nucleoside reverse transcriptase inhibitor (NNRTI) combined with two nucleoside analogue reverse transcriptase inhibitors (NRTIs) (339). NNRTI drugs include efavirenz (EFV), etravirine (ETV) and nevirapine (NVP) whereas for NRTIs, the drugs include abacavir (ABC), didanosine (ddI), emtricitabine (FTC), lamivudine (3TC), stavudine (d4T) and zidovudine (AZT). For children younger than 3 years of age, a proteases inhibitors (PIs) such as lopinavir/ritonavir (LPV/r)-based regimen should be used as first-line treatment regardless of NNRTI exposure. As for children 3 years of age and older, EFV is the preferred NNRTI for first-line treatment while NVP can be given as an alternative (339).

#### **3.1.4 Malaria and HIV co-infection**

In theory, mortality and morbidity attributed to malaria could potentially increase due to HIV infection. Through immunosuppression, HIV infection could increase susceptibility to malaria, hence, increases the disease clinical and severity occurrences. Also, immunosuppressed patients are more likely to become infected with malaria (in endemic regions) that may lead to delayed parasitaemia clearances, and consequently, higher parasite density and these patients may contribute to the increase of parasite transmission and biomass to the endemic region, especially in the sub-Saharan population (342). Even though malaria has been found not to be the most frequent cause of death in HIV patients, it was found to be the third cause HIV-related morbidity in Africa, akin to tuberculosis (343, 344). Furthermore, pharmacological interactions between antimalarial and HIV drugs could potentially affect the efficacy of antimalarial treatment due

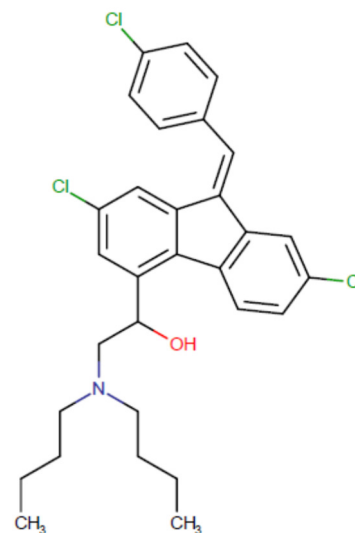
to underexposure and subsequently leads to high recrudescence rate. In contrast, overexposure to the drugs could also lead to toxicity (345).

Lumefantrine, often combined with artemether, is one of the most widely used antimalarials in sub-Saharan Africa, and many countries adopted it as first-line therapy for uncomplicated *falciparum malaria*, including children with HIV co-infection (346). In terms of pharmacokinetics, lumefantrine has similar properties as halofantrine (347), with a large apparent volume of distribution as well as approximately 4 to 5 days of terminal elimination half-life for malaria (348). The bioavailability of oral lumefantrine is very dependent on food and usually reduced effectiveness in acute malaria treatment. However, the cure rate is markedly improved upon recovery (349). Typical treatment regimens for lumefantrine in children include a 3-day six-dose regimen which is stratified based on body weight: 5-15 kg 1 tablet per dose; 15-25 kg 2 tablets per dose; 25-35 kg 3 tablets per dose and >35 kg 4 tablets per dose (311). Lumefantrine is predominantly metabolised by *CYP3A4*. The overall basis of lumefantrine clinical efficacy is the area under the curve, with day 7 concentration ( $C_{d7}$ ) of 280 ng/mL considered to be the primary marker for successful therapy under dosing with standard 3-day dosing regimen (349, 350). Table 3.1 summarises lumefantrine pharmacokinetics and its structure.

Efavirenz is a non-nucleoside reverse transcriptase inhibitor (NNRTI) and is predominantly metabolised by *CYP2B6* (351) and is an inducer of *CYP3A4* (352, 353). It is a standard first-line treatment in paediatrics or pregnancy population groups (339) (354). Efavirenz has a linear pharmacokinetics behaviour, and steady-state plasma concentration was reached within 7 days (355). Similar to lumefantrine, food also has a substantial effect towards efavirenz absorption whereby it could increase to more than 50% when given with a high-fat meal, after a single dose of 1,200 mg (356). Although lumefantrine therapy has a long therapeutic window (357), patients who are exposed to *CYP3A4* inducers, such as efavirenz, may demonstrate reduced lumefantrine exposure which can lead to increase recrudescence rates and therapeutic failure (358). Table 3.2 summarises efavirenz pharmacokinetics and its structure.

**Table 3.1 Summary of lumefantrine pharmacokinetics**

PHARMACOKINETICS	STRUCTURE
<p><b>Absorption and Distribution</b></p>	<ul style="list-style-type: none"> <li>Absorption of lumefantrine, a highly lipophilic compound, starts after a lag-time of up to 2 hours, with peak plasma concentrations about 6 to 8 hours after administration (359).</li> <li>Lumefantrine is highly bound to human serum proteins <i>in vitro</i> (99.7%) (360).</li> <li>Protein binding to human plasma proteins is linear (361).</li> </ul>
<p><b>Metabolism</b></p>	<ul style="list-style-type: none"> <li>Lumefantrine was metabolized mainly by CYP3A4 to desbutyl-lumefantrine (361).</li> <li>The systemic exposure to the metabolite desbutyl-lumefantrine was less than 1 % of the exposure to the parent compound (361).</li> <li><i>In vitro</i>, lumefantrine significantly inhibits the activity of CYP2D6 at therapeutic plasma concentrations (361, 362).</li> </ul>
<p><b>Elimination</b></p>	<ul style="list-style-type: none"> <li>Lumefantrine is eliminated slowly, with a terminal half-life of 3-6 days in healthy volunteers and in patients with <i>falciparum</i> malaria (361).</li> </ul>
<p><b>Renal dysfunction</b></p>	<ul style="list-style-type: none"> <li>Not established</li> </ul>
<p><b>Elderly</b></p>	<ul style="list-style-type: none"> <li>Not established</li> </ul>
<p><b>Chronic liver disease</b></p>	<ul style="list-style-type: none"> <li>Not established</li> </ul>
<p><b>Children aged 3 years and over</b></p>	<ul style="list-style-type: none"> <li>Similar in children to adults after correction for body size (361).</li> </ul>

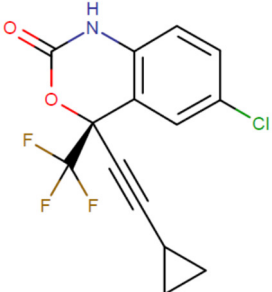


**Formula:** C<sub>30</sub>H<sub>32</sub>Cl<sub>3</sub>NO

**Molar mass:** 528.94 g/mol

**Chemical name:** 2-Dibutylamino-1-[2,7-dichloro-9-(4-chloro-benzylidene)-9H-fluoren-4-yl]-ethanol

**Table 3.2 Summary of efavirenz pharmacokinetics**

PHARMACOKINETICS	STRUCTURE
<b>Absorption and Distribution</b>	
<ul style="list-style-type: none"> <li>• Linear pharmacokinetic behaviour (356)</li> <li>• Steady-state plasma concentrations were reached in 7 days (363).</li> <li>• The rate of absorption was not rapid based on the <math>T_{max}</math> values (356).</li> <li>• Low water solubility of efavirenz probably led to a slow dissolution rate in the gastrointestinal tract and the relatively long time to peak concentrations might be a function of the dissolution rate (363).</li> <li>• The absolute bioavailability of efavirenz has not been determined due to the lack of an adequate intravenous formulation (356).</li> <li>• Highly bound to plasma proteins, primarily to serum albumin, with a mean free fraction of 0.58 % in rat, 0.57 % in rhesus monkey and 0.25-0.5 % in human plasma (363).</li> <li>• <b>Intestinal absorption (364):</b> <ul style="list-style-type: none"> <li>○ Efavirenz was capable of inducing hepatic CYP3A4 activity.</li> <li>○ Efavirenz itself is predominantly metabolized by UGT2B7.</li> <li>○ Efavirenz inhibit intestinal ABCB1, ABCC2 and UGT1A1</li> <li>○ Efavirenz is rapidly absorbed from the upper intestine (<math>T_{max}</math> 2-3h) and does not undergo significant biliary secretion</li> <li>○ Efavirenz undergoes extensive oxidative metabolism by CYP2B6 and CYP3A4 and conjugation via UGT2B7.</li> </ul> </li> </ul>	<p><b>Formula:</b> C<sub>14</sub>H<sub>9</sub>ClF<sub>3</sub>NO<sub>2</sub></p> <p><b>Molar mass:</b> 315.675 g/mol</p> <p><b>Chemical name:</b> (S)-6-chloro-4-(Cyclopropylethynyl)-1,4-dihydro-4-(trifluoromethyl)-2H-3,1-benzoxazin-2-one</p>
<b>Metabolism</b>	<ul style="list-style-type: none"> <li>• Metabolised by the cytochrome P450, especially CYP 2B6 and to a lesser extent CYP3A4 to oxidative inactive metabolites (363)</li> <li>• Induce both CYP2B6 and CYP3A4 and therefore to induce its own metabolism (356).</li> <li>• Inhibitor of CYP2C9, 2C19, and 3A4 and therefore pharmacokinetic interactions of clinical relevance could be expected (363).</li> <li>• The AUCs were approximately 8-10% lower following 20 days of dosing as compared to AUCs after 10 days of dosing (363).</li> </ul>
<b>Elimination</b>	<ul style="list-style-type: none"> <li>• Single oral dose was estimated to be 4.3 l/h in the population analysis consisting of healthy</li> </ul>

	<p>volunteer's data and increased to 11 l/h after multiple dosing (356).</p> <ul style="list-style-type: none"> <li>• Long elimination half-life (<math>t_{1/2}</math>) - (40 to 55 hours) (363)</li> <li>• The elimination pathway for efavirenz was mainly through the faeces (363).</li> </ul>
<b>Renal dysfunction</b>	<ul style="list-style-type: none"> <li>• Not established</li> </ul>
<b>Elderly</b>	<ul style="list-style-type: none"> <li>• Not established</li> </ul>
<b>Chronic liver disease</b>	<ul style="list-style-type: none"> <li>• Reduction in efavirenz <math>C_{max}</math> (356)</li> <li>• Increase in the unbound fraction (356)</li> </ul>
<b>Children aged 3 years and over</b>	<ul style="list-style-type: none"> <li>• Similar in children to adults after correction for body size (363).</li> </ul>

### 3.1.5 Genetic polymorphisms

The human chromosomes consist of approximately 500 million base pairs (bp) of DNA that in turns consist of thousands of genes (365). A gene can be defined as a region of DNA that has a function (Figure 3.3). These genes formed various DNA sequences called genotypes which determines specific characteristics (phenotypes) of an individual (366).

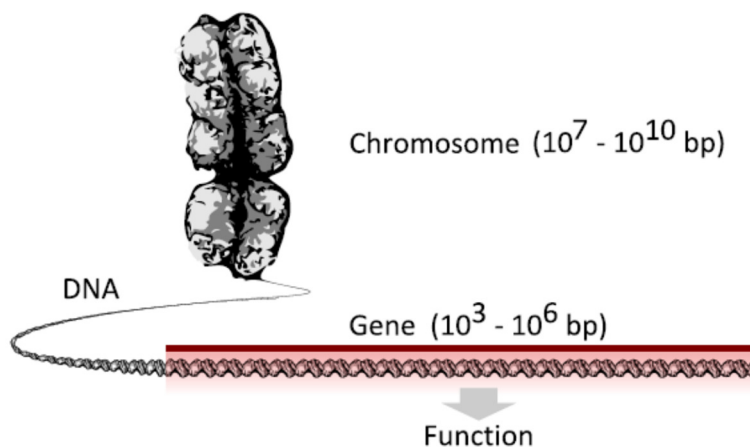


**Figure 3.3 Structure of chromosome, DNA, and gene.**

Reproduced from Shafee *et al.* (2015) (367).

Genetic polymorphisms occur when more than one allele (variant) occupies a gene locus (fixed position on a chromosome) within a population which could underlie differences in health conditions (63). Various types of genetic polymorphism exist and include single nucleotide

polymorphisms (SNPs), small-scale insertions/deletions, polymorphic repetitive elements and microsatellite variation (63).

The most commonest type of polymorphism are SNPs, which occur whenever there are single nucleotide changes in a particular location in the genome, specifically, the replacement of the nucleotide adenine (A), thymine (T), cytosine (C), or guanine (G) in a part of the DNA. These changes lead to two alleles of DNA fragments in different individuals which are defined as SNPs (Figure 3.4). These genetic changes alter the genes that code for proteins and enzymes, which in turn may alter their functional ability. For SNPs occurring on genes encoding for CYP enzymes, the results could be no alteration in function or increased or reduced function of the enzyme, which in turn leads to altered metabolic capacity. This variation in the DNA sequences can affect how a human reacts to certain types of medications, i.e., whether they are extensive metabolisers, poor metabolisers or ultra-rapid metabolisers, develop diseases and respond to other types of xenobiotics.

Drug response often varies between individuals, and about 15% to 30% of this variability is often a result of genetic polymorphisms (368). Within this range, Cytochrome P450 (CYP450) enzymes constitute about 80% of phase 1 drug metabolism and about 65% to 70% of drug clearance (369, 370). Also, the highly polymorphic states of the CYPs enzymes have been the primary cause for the increased risk of adverse drug reactions caused by the drugs (371). These CYP enzymes harbour a significant constituent of single nucleotide polymorphisms (SNP) which are primarily based on the lack of endogenous functions within the gene itself. In terms of clinical practicality, pharmacogenetics testing is currently limited to validation and qualification on phenotyping sequences of the observed genetic variation patterns (372). This testing eventually resulted in an accessible and standardised CYP allele nomenclature system which is designated by 'star (\*) alleles' and is reviewed and regularly updated through a community website (373).

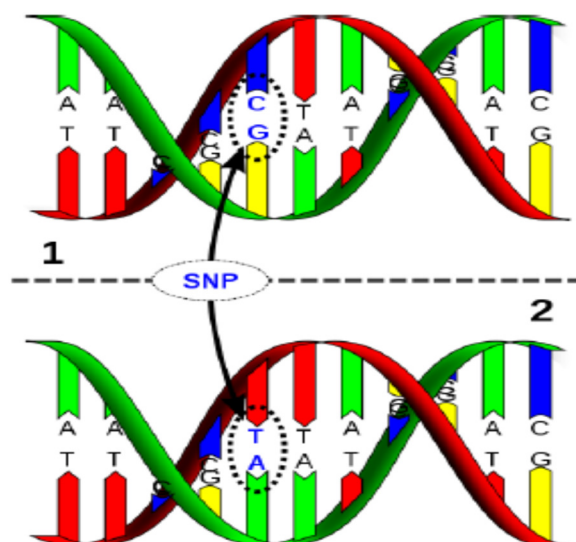


**Figure 3.4 SNP schematic illustrating changes of a nucleotide at a single base-pair location on DNA.**

Reproduced from Eccles *et al.* (2014) (374).

### 3.1.6 *CYP2B6* polymorphisms

*CYP2B6* plays an essential role regarding biotransformation of several essential drugs such as antimalarials and antiretrovirals (375). *CYP2B6* belongs to a family of enzymes that catalyse the biotransformation of drugs called cytochrome P450 (*CYP450*) and thought to consists of less than 1% to the total CYP abundance in the liver. However, recent studies have established that this enzyme contributes between 2 to 10% of total hepatic CYP content (376).

Nevertheless, several important *CYP2B6* SNPs have been identified to have profound effects on drug metabolism and efficacy of drug therapy and in some extents, up to 50% higher frequencies in certain population (377, 378). *CYP2B6* is highly polymorphic with at least 37 distinct star-alleles (379) with the \*1/\*1 carriers considered as wild-type carrier. To date, there are over 100 identified SNPs for *CYP2B6* have been documented which revealed a variety of phenotypic outcomes (376). Amongst the prominent type of *CYP2B6* SNP alleles are *CYP2B6*\*2, *CYP2B6*\*3, *CYP2B6*\*4, *CYP2B6*\*5, *CYP2B6*\*6, and *CYP2B6*\*7 of which the *CYP2B6*\*6 was discovered in about 15 - 40% in Asians and more than 50% in African-Americans population (380-382). The most common variant alleles result in two amino acid changes, Q172H and K262R, and is termed *CYP2B6*\*6, and which has been reported to lead to

a 65% reduction protein expression and 50% reduction in mean enzyme activity in the homozygous state (380).

### 3.1.7 Efavirenz and CYP2B6 polymorphisms

Pharmacogenetic studies have provided valuable information towards the prevalence of efavirenz pharmacokinetic variability between patients (383). The safety, efficacy and adherence to treatment for HIV patients that have been administered efavirenz were often compromised whenever efavirenz is given concomitantly with other medication such as antimalarials or other antiretrovirals and these effects are difficult to predict due to its variability (383). Further, efavirenz induces its own metabolism and results in reduced plasma exposure, a phenomena which can confound treatment management since it has also influenced by patients genotype and the presence of CYP2B6 SNPS (384, 385). This fact is fundamental to the pharmacokinetics of efavirenz and also its ability to illicit a drug-drug interaction (e.g. with antimalarial agents) as efavirenz can induce CYP3A4, a CYP isozyme through which many antimalarial are metabolised. Further, the extent to which this DDI occurs is therefore highly dependant upon the phenotype prevalence within a population group.

Ward *et al.* (2003) (386) suggested that *CYP2B6* polymorphisms are clinically significant for efavirenz treatment. Further, it was discovered that a significant reduction in efavirenz clearance in African patients, resulting in enhanced efavirenz plasma concentration, was attributed to CYP2B6 SNPs which were unique to the African population groups studied (386). Therefore, it is highly likely that the sub-Saharan paediatric population, when predisposed to both HIV and malaria, may have a significantly higher risk of antimalarial treatment failure due to drug-drug interactions mediated by efavirenz. Although *CYP2B6* contributes towards between 2-10 % of total CYP content (376), the impact of the \*6/\*6 genotype (poor metaboliser phenotype) can often result in a 2-3-fold higher efavirenz plasma concentration (378, 387-389), and hence a greater ability of efavirenz to induce *CYP3A4* (353, 390, 391) and thereby enhances the potential for a efavirenz-lumefantrine DDI.

Importantly, the \*6/\*6 polymorphism is more frequent in African population groups than Caucasian population groups (46.9% vs. 25.5%, respectively) (375, 392), and this places considerable risk-burden on this geographic population group. However, the impact of *CYP2B6* polymorphisms in antiretroviral-antimalarial mediated DDIs in African paediatric

populations is lacking, and warrants investigation as it may contribute to significantly increased the risk of recrudescence especially in highly endemic regions and the potential resistance towards these antimalarial treatments (310, 393-395). This is further confounded by the risk of placental transfer of HIV (396) and malaria (397), and the lack of naturally acquired immunity towards children, often puts paediatric population groups at significant risk of succumbing to either infection or being exposed to complex DDIs (398).

Due to the complexity and ethical issues of recruitment of paediatrics into complex DDI studies in HIV-infected malaria subjects, PBPK modelling can be used to explore the potential risk of DDIs in adults (399-401) and paediatric populations (402-405). The benefit of this approach is both the ability to model population variability in physiology (84, 401, 405-407), but to also specifically develop a modelling approach that is tailored towards a specific geographical population group of interest rather than a standard healthy (Caucasian) adult male.

In contrast to *in vivo* and *in vitro* assessments, generating population-based PBPK models to predict human pharmacokinetics and potential risk of DDIs in the paediatric population is particularly challenging. However, during the past decade, research has been ongoing to explore this area in-depth in the sub-Saharan paediatric population, *albeit* many authors observing pharmacokinetic profiles of efavirenz and lumefantrine separately (23, 408-411). In 2013, Xu *et al.* established a clinical link between CYP2B6 metabolic status and efavirenz clearance through the development of a PBPK (412). This research provides a rationale and basis for the current study in providing a method and preliminary data for the paediatric population.

Additional studies have been undertaken to explore the pharmacokinetics of lumefantrine and efavirenz in a sub-Saharan paediatric population with the most recent study conducted in 2016 by Parikh *et al.* (408). The author has successfully shown that efavirenz exposure leads to a reduction of lumefantrine plasma concentration up to 2.1-fold. However, this study does not consider the impact of *CYP2B6* polymorphism within the paediatric population.

Therefore, our primary goal is to bridge this gap by not only providing a robust DDI profile of lumefantrine-efavirenz by accounting *CYP2B6* polymorphism into the metabolic clearance profile of efavirenz but also provide a dose evaluation prediction for lumefantrine to overcome the issue of treatment failure and recrudescence specifically in this co-infected paediatric population. The objectives of the present study were 2-fold: (i) to predict efavirenz pharmacokinetics in African population groups (adults and paediatrics) and (ii) to assess the

impact of efavirenz in the attenuation of lumefantrine pharmacokinetics through a CYP3A4 induction effect. In all cases, it was important also to address the impact of the *\*6/\*6 CYP2B6* phenotype on efavirenz pharmacokinetics and the effect of this on efavirenz and thus its ability to alter lumefantrine pharmacokinetics.

## **3.2 METHODS**

### **3.2.1 Compounds selection and development**

Input parameters for use in the development of lumefantrine and efavirenz compound files are detailed in Table 3.3. These parameters derived from previously validated publications, with lumefantrine, develop by Olafuyi *et al.* (2017) (8) and efavirenz developed and pre-validated by Simcyp (413).

**Table 3.3 Compound-specific parameters for lumefantrine and efavirenz**

Parameters	Lumefantrine	Efavirenz
<b>Compound type</b>	Diprotic base	Monoprotic acid
<b>Molecular weight (g/mol)</b>	528.94 <sup>1</sup>	315.68 <sup>8</sup>
<b>Log P</b>	8.70 <sup>1,2</sup>	4.02 <sup>8</sup>
<b>fu</b>	0.003 <sup>1,3</sup>	0.029 <sup>8</sup>
<b>pKa 1</b>	14.10 <sup>1</sup>	10.20 <sup>8</sup>
<b>pKa 2</b>	9.80 <sup>1</sup>	-
<b>B/P</b>	0.80 <sup>1,4</sup>	0.74 <sup>8</sup>
<b>Vss (L/kg)</b>	0.70 <sup>1</sup>	14.26 <sup>8</sup>
<b>Pe<sub>eff</sub> (10<sup>-4</sup> cm/s)</b>	0.97 <sup>1</sup>	5.68 <sup>8</sup>
<b>K<sub>p</sub> scalar</b>	0.50 <sup>7</sup>	1 <sup>8</sup>
<b>Solubility (mg/mL)</b>	0.002 <sup>1,5</sup>	-
<b>CL<sub>po</sub> (L/min)</b>	0.25 <sup>1,6</sup>	20 <sup>8</sup>
<b>CL<sub>int3A4</sub> (μL/min/pmol)</b>	4.60 <sup>7</sup>	0.0094 <sup>8</sup>
<b>CL<sub>int2B6</sub> (μL/min/pmol)</b>	-	1.35 <sup>8</sup>
<b>CYP3A4 Ind<sub>max</sub> (fold)</b>	-	3 <sup>8</sup>
<b>CYP3A4 Ind<sub>C50</sub> (μM)</b>	-	3.8 <sup>8</sup>
<b>CYP2B6 Ind<sub>max</sub> (fold)</b>	-	6.2 <sup>8</sup>
<b>CYP2B6 Ind<sub>C50</sub> (μM)</b>	-	1.2 <sup>8</sup>
<b>Absorption model</b>	1st order	1st order
<b>Distribution model</b>	Full	Full

Log P: octanol:buffer partition coefficient, fu: fraction unbound in plasma, pKa: acid dissociation constant, B/P: blood-to-plasma ratio, Vss: volume of distribution at steady-state, Pe<sub>eff</sub>: human effective permeability, K<sub>p</sub>: tissue partition coefficient, K<sub>p</sub> scalar: scalar to predicted K<sub>p</sub> values, CL<sub>po</sub>: clearance of drug after oral administration, CL<sub>int3A4</sub>: *in vitro* intrinsic metabolic clearance of *CYP3A4*, CL<sub>int2B6</sub>: *in vitro* intrinsic metabolic clearance of *CYP2B6*, Ind<sub>max</sub>: calibrated maximal fold induction over vehicle (1= no induction), *CYP3A4* Ind<sub>C50</sub>: calibrated inducer concentration that supports half maximal induction, 1<sup>st</sup> order absorption model: simplest absorption model within the simulator which treats the gut as a single compartment associated with a single first order absorption rate constant (k<sub>a</sub>) and f<sub>a</sub>, full distribution model: the full PBPK distribution model makes use of a number of time-based

differential equations in order to simulate the concentrations in various organ compartments. Inter-individual variability is introduced through tissue volume prediction taking account of age, sex, weight and height.

<sup>1</sup>Olafuyi, O., *et al.* (2017) (8), <sup>2</sup>Huang *et al.* (2012) (414), <sup>3</sup>Colussi, D., *et al.* (1999) (415), <sup>4</sup>Zaloumis *et al.* (2012) (416), <sup>5</sup>Kotila *et al.* (2013) (417), <sup>6</sup>Ezzet *et al.* (1998) (348), <sup>7</sup>Parameter estimated, <sup>8</sup>Simcyp® default values.

### 3.2.2 Model development

Population-based PBPK modelling was conducted using the virtual clinical trials simulator Simcyp (Simcyp Ltd., a Certara company, Sheffield, UK, Version 16). For all simulations, doses for both lumefantrine and efavirenz were employed according to standard weight-based dosing regimens (361, 363) (Table 3.4), unless stated otherwise. Further, for all lumefantrine simulations, dosing occurred under fed-conditions unless otherwise indicated.

**Table 3.4 Weight-based dosing regimens for lumefantrine and efavirenz**

Body weight	Tablets per dose	Total mg per dose
		Lumefantrine
5 to < 15 kg	1	120
15 to < 25 kg	2	240
25 to < 35 kg	3	360
		Efavirenz
10 to < 15 kg	-	200
15 to < 20 kg	-	250
20 to < 25 kg	-	300
25 to < 35 kg	-	350

#### 3.2.2.1 Model development workflow

A five-stage stepwise approach was implemented for model development, validation and model refinement (Figure 3.5). Unless otherwise stated, efavirenz was dosed for 20 days prior to initiation of a DDI (and throughout the study). Lumefantrine was dosed at over 3 days at 0, 8, 24, 36, 48 and 60 hours. Clinical data from nine published studies were utilised throughout the model development and validation phases (Table 3.5) to demonstrate that the model could reasonably predict drug exposure in adult and paediatric populations.

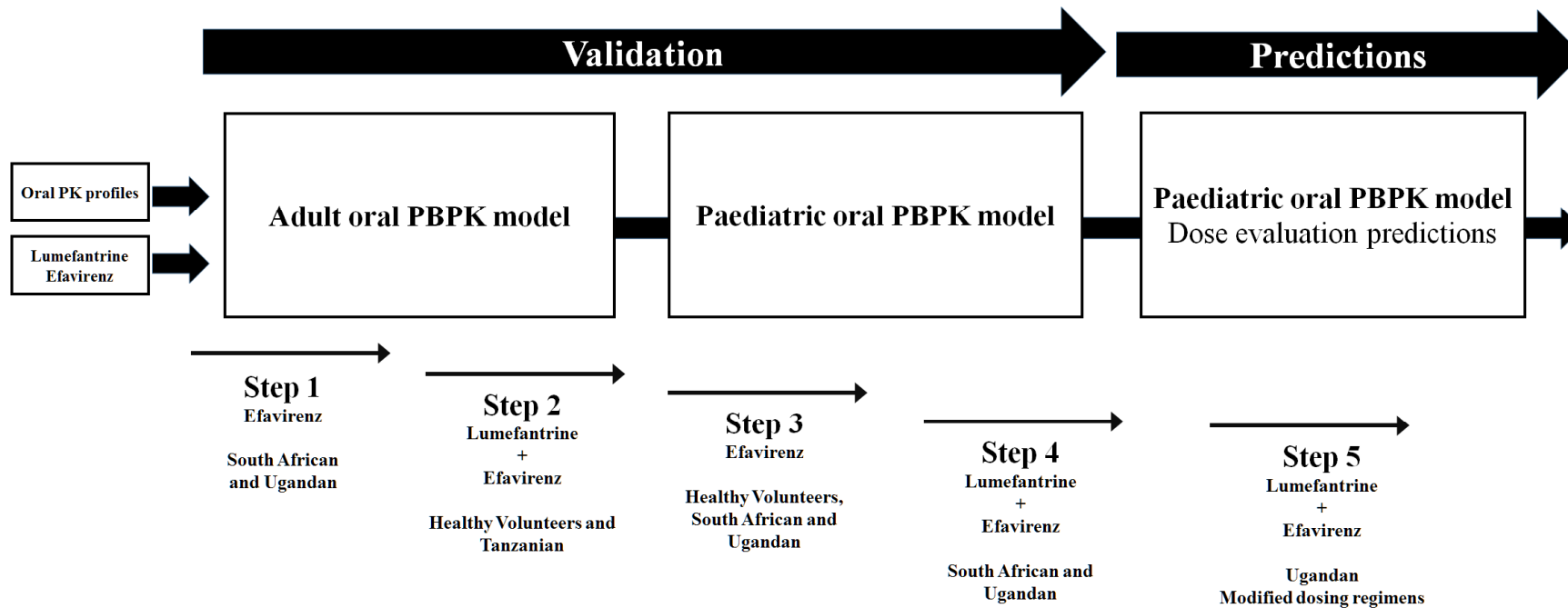


**Figure 3.5 Model development strategy.**

PK: pharmacokinetics, PBPK: physiologically based pharmacokinetic modelling.

**Table 3.5 List of published papers utilised for validation purposes**

<b>STEP 1 – Adult Oral PBPK Model</b>	<b>Population groups</b>	<b>Reference</b>
Efavirenz (EM/PM genotyping data available)	<ul style="list-style-type: none"> <li>• Healthy volunteers</li> <li>• Ugandan and South African population</li> </ul>	<ul style="list-style-type: none"> <li>• Xu et al. (2013) (418)</li> <li>• Mukonzo <i>et al.</i> (2013) (419)</li> </ul>
<b>STEP 2 – Adult Oral DDI PBPK Model</b>	<b>Population groups</b>	<b>Validation</b>
Lumefantrine + Efavirenz (Inducer) (EM/PM genotyping data available)	<ul style="list-style-type: none"> <li>• Healthy volunteers</li> <li>• South African as surrogate for Tanzanian populations</li> </ul>	<ul style="list-style-type: none"> <li>• Huang <i>et al.</i> (2012) (414)</li> <li>• Maganda <i>et al.</i> (2015) (420) (EM/PM genotyping data available)</li> </ul>
<b>STEP 3 – Paediatric Oral PBPK Model (Ugandan)</b>	<b>Population groups</b>	<b>Validation</b>
Lumefantrine	Custom designed (virtual twins) Ugandan paediatric population	Parikh <i>et al.</i> (2016) (408)
Efavirenz	Custom designed Ugandan paediatric population	<ul style="list-style-type: none"> <li>• Parikh <i>et al.</i> (2016) (408)</li> <li>• Fillekes <i>et al.</i> (2011) (409)</li> <li>• Luo <i>et al.</i> (2016) (23)</li> <li>• Pressiat <i>et al.</i> (2017) (410)</li> <li>• Viljoen <i>et al.</i> (2011) (411) (EM/PM genotyping data available)</li> </ul>
<b>STEP 4 – Paediatric Oral DDI PBPK Model (Ugandan)</b>	<b>Population groups</b>	<b>Validation</b>
Lumefantrine + Efavirenz (Inducer) (EM/PM genotyping data available)	Custom designed Ugandan paediatric population	<ul style="list-style-type: none"> <li>• Parikh <i>et al.</i> (2016) (408)</li> </ul>
<b>STEP 5 – Paediatric Dose Evaluation Prediction</b>		<b>Simulation</b>
Simulations were run using the Ugandan population group and stratified across 4 age groups:		
<ul style="list-style-type: none"> <li>• 0.25-1 year-old (120mg LUM/300mg EFV), 1-4 year-old (120mg LUM/400mg EFV),</li> <li>• 4-8 year-old (240mg LUM/500mg EFV) and 8-13 year-old (240mg LUM/600mg EFV)</li> </ul>		

EM: extensive metabolisers, PM: poor metabolisers.

### ***Step 1: Adult simulations with efavirenz***

For all simulations steps involving efavirenz, metabolism was modelled using intrinsic clearance (CL<sub>int</sub>) that were specific to \*1/\*1 and \*6/\*6 alleles, *via* ‘CYP allelics’ kinetics. Subsequently, when simulating either entirely \*1/\*1 (EM) or \*6/\*6 (PM) genotypes, the frequency of *CYP2B6* was set at 1 for either \*1/\*1 or \*6/\*6. For efavirenz, unless otherwise stated, doses were administered to steady state or beyond (at least 20 days) prior to the initiation of lumefantrine dosing.

Step 1 attempted to apply the compound file to model prediction in Healthy Volunteer (Caucasian), South African and Ugandan population groups, which were generally the focus of clinical studies identified.

Clinical studies selected included: (i) A single 600 mg oral dose to healthy adult volunteers with results genotyped for \*1/\*1 and \*6/\*6 (418) and (ii) a 600 mg multi-dose study over 32 weeks in Ugandan adults (421).

The Ugandan population group was developed from reported age-weight relationships for Ugandan males and females (422), and are detailed in Section 3.3.1.1. A similar approach was reported and applied in PBPK modelling by our group (401). In the absence of literature reported abundance of *CYP2B6* in Ugandan subjects, we fixed \*1/\*1 and \*6/\*6 genotype abundances to 6.9 and 2.4 pmol/mg protein, respectively, based upon adaptations found in a South African population group developed by Simcyp as part of the Critical Path to TB Drug Regimens (CPTR) (423) and which is available from population the library repository of Simcyp. The South African population group includes appropriate age-weight-height distributions, CYP expression and blood biochemistry changes compared to standard (Caucasian) Healthy Volunteer population group (424). All simulations replicated the study design reported by the validation clinical studies cited above.

### ***Step 2: Adult simulations with lumefantrine-efavirenz drug-drug interactions***

The validation of the lumefantrine-efavirenz DDI was conducted using two published clinical studies: (i) dosing of 480 mg lumefantrine and 600 mg efavirenz to a healthy volunteer population group (414) where no genotyping was reported and (ii) dosing of 480 mg lumefantrine and 600 mg efavirenz to a Tanzanian population group where genotyping of plasma concentration profiles were reported (425). As a result of similar age-weight

relationships (422), the South African population group was used as a surrogate for a Tanzanian population.

For population groups co-administered with lumefantrine, the blood biochemistry was alerted based on reported changes in malaria population groups (Table 3.6). In malaria population groups, it has been reported that a reduction in albumin (HSA) is commonly detected (426), often coupled with a 3-4 fold increase in alpha-1-acid glycoprotein (AAG) (427). Due to an absence of specific males and females values for the blood biochemistry, these values were assumed to be equivalent for both sexes in the Ugandan population. Furthermore, analysis has shown that there were no significant sex differences in the different haematological parameters in the parasitaemic groups (428).

**Table 3.6 Malaria population biochemistry**

Biochemistry	Caucasian	Ugandan
Haematocrit (%)	M : 43 F : 38	40.08 <sup>(429)</sup>
AAG (g/L)	M : 0.811 F : 0.791	0.7 <sup>(430)</sup>
HSA (g/L)	M : 50.34 F : 49.38	33.5 <sup>(429)</sup>

AAG:  $\alpha$ 1-acidic glycoprotein; HSA: human serum albumin.

<sup>a</sup>Simcyp default values

### ***Step 3: Paediatric simulations with efavirenz***

After successful validation and refinement of efavirenz compound in the adult population, this step focused on the validation of efavirenz and lumefantrine in paediatrics. Similar with the adult population, the paediatric Ugandan population group was developed from reported age-weight relationships for Ugandan males and females (422), and are detailed in Section 3.3.1.2. For the default Simcyp paediatric population groups, the age-weight relationships' equations were specified into two age ranges: (i) 0 to 18 years old and (ii) 18 to 25 years old. These two equations allow not only prediction of pharmacokinetics in neonates, infants and children (431), but also considers the problems associated with scaling adult doses to children (432) under one paediatrics module.

The studies used for validation of efavirenz pharmacokinetics in paediatrics included: (i) weight-based once daily 300 mg dose of oral efavirenz in HIV-infected Ugandan children and simulated using the Ugandan population group with dosing to steady state (409); (ii) weight-based once daily dose of oral efavirenz in HIV-infected children with weight-based stratification of plasma concentration profiles (23) simulated using the Ugandan population group; (iii) a single high dose (25 mg/kg) dosed once daily to 2-3 year old Ugandan children and simulated using the Ugandan population group (410) and (iv) a single oral 300 mg dose administered to 6-7 year old South African subjects and simulated using the South African population group (411) with genotyping of plasma concentration profiles.

#### ***Step 4: Paediatric simulations with lumefantrine-efavirenz drug-drug interactions***

To validate the prediction of a lumefantrine-efavirenz based DDIs in paediatrics, we utilised the only study reporting the lumefantrine plasma concentration-time profile in the absence and presence of efavirenz (408), although this study did not report genotyped pharmacokinetics. Trial simulations were performed using a standard 6-dose regimen of weight-based dosing of lumefantrine administered on day 20 (unless otherwise indicated), with weight-based dosing of efavirenz from day 1 to day 40 in Ugandan children and simulated using the Uganda population group. To account for the impact of genotype on the pharmacokinetics of lumefantrine, our results were stratified for two extreme cases of an entire population of CYP2B6 \*1/\*1 or entirely CYP2B6 \*6/\*6, and this represents the ‘best’ and ‘worst’ clinical scenarios.

#### ***Step 5: Paediatric dose evaluation prediction***

Having validated the lumefantrine-efavirenz DDI in Ugandan paediatric patients, this step simulated the potential impact of dosage regimen alterations on target day-7 ( $C_{d7}$ ) lumefantrine plasma concentrations. Simulations were run using the Ugandan population group and stratified across 4 age groups: 0.25-1-year-old (120mg LUM/300mg EFV), 1-4-year-old (120mg LUM/400mg EFV), 4-8 year-old (240mg LUM/500mg EFV) and 8-13 year-old (240mg LUM/600mg EFV). Further, each simulation included 100 subjects (10 trials with 10 subjects per trial) where the age-weight distribution matched the appropriate dose banding.

### **3.2.3 Predictive performance**

In all of the simulations, a prediction to within 2-fold of the observed data is generally expected as part of the ‘optimal’ predictive performances range even though there is no uniform standard of acceptance to determine this criterion (87, 135, 136). This acceptance criterion was used in our  $C_{max}$  and AUC comparisons with the published clinical data reported. For the efavirenz DDI simulations, since the therapeutic efficacy of lumefantrine is determined by its  $C_{d7}$  of 280 ng/mL (433), a direct analysis of lumefantrine day-7 concentration was set as a cut-off value to determine the impact of a DDI in lumefantrine pharmacokinetics.

### **3.2.4 Data analysis**

The observed data that was used for visual predictive checks when compared with the simulated profiles were extracted using the WebPlotDigitizer v.3.10 (<http://arohatgi.info/WebPlotDigitizer/>). All simulations of plasma concentration-time profiles were presented in 5<sup>th</sup> to 95<sup>th</sup> percentiles and either in mean or median unless otherwise specified.

For all adult simulations, age ranges and subject gender ratios were matched, where possible, to reported clinical studies. Where this information was not cited in clinical studies, a default age range of 20-50 years and gender ratio of 50% was selected.

For simulations employing weight-based dosing, unless otherwise stated, a 100-subject simulation was run in a 10x10 trial (10 subjects per trial with 10 trials) to ensure that reasonable inter-/intra individual variability is captured within the model simulations. However, as simulations are not possible with defined age and weight ranges, pooling and post-processing of output data were conducted to match individuals to the required age-weight boundary conditions for the study.

### 3.3 RESULTS

#### 3.3.1 Characterisation of selected population

##### 3.3.1.1 Age-weight relationship for adult population groups

Based on the age-weight mathematical equations between the default and the customised sub-Saharan (Ugandan) population groups, these relationships can be graphically visualised as detailed in Figure 3.6. In a 10x10 virtual clinical trial to simulate the age-weight distribution in this population, the plots indicated that there were significant differences between the mean weight distribution of Caucasian and Ugandan adult population from age 19 to 65 years old for both male and female groups ( $p < 0.001$  and  $p < 0.0001$ , respectively).

#### *Default Simcyp adult population groups*

*Females:*

$$Height = 161.66 + 0.1319 * age - 0.0027 * age^2 \quad (3.1)$$

$$Body\ weight = e^{(2.7383 + 0.0091 * Height)} \quad (3.2)$$

*Males:*

$$Height = 175.32 + 0.1113 * age - 0.0025 * age^2 \quad (3.3)$$

$$Body\ weight = e^{(2.643 + 0.0099 * Height)} \quad (3.4)$$

### ***Malaria adult population groups***

*Ugandan females:*

$$\text{Body weight} = (4.777 + 2.607 * \text{age} + -0.412 * \text{age}^2 + 0.0181 * \text{age}^3)/(1 + -0.068 * \text{age} + -0.002529 * \text{age}^2 + 0.000257 * \text{age}^3) \quad (3.5)$$

*Ugandan males:*

$$\text{Body weight} = (7.037 + 0.42399 * \text{age}^2 + -0.0032 * \text{age}^4 + 0.000009118 * \text{age}^6)/(1 + 0.00356 * \text{age}^2 + -0.0000459 * \text{age}^4 + 0.00000014335 * \text{age}^6) \quad (3.6)$$

The age-weight distributions follow a descending pattern in both shape and the spread of attained weights as they advance from age 19 years to the end of the age range. For the male population, the Caucasian group had a higher mean weight range at 80.85 kg ± 13.92 kg (19.96 years ± 6.82 years) as compared to the Ugandan group which was at 67.45 kg ± 17.56 kg (41.30 years ± 10.72 years). At the larger age ranges of the distribution, the greatest difference between the Caucasian and the Ugandan male group was at 20 years of age where the Caucasian distributions were approximately 14.8 kg larger (p<0.001). On the other hand, for the female population, the Ugandan group has a higher mean weight range of 70.93 kg ± 21.62 kg (36.01 years ± 11.09 years) when compared with the Caucasian group which was at 68.45 kg ± 14.38 kg (20.19 years ± 7.75 years).

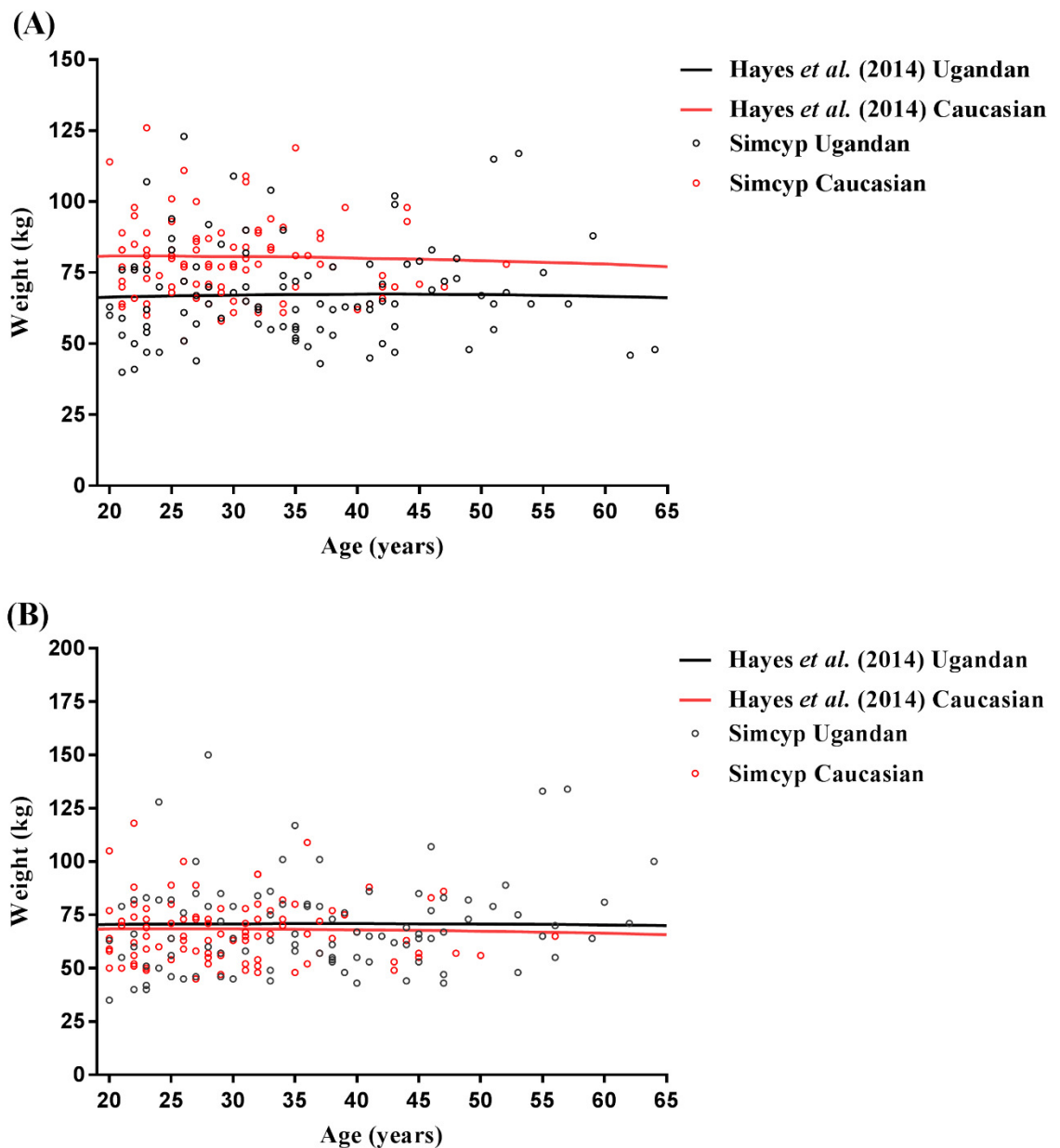


**Figure 3.6 Age-weight relationship comparison between adult Ugandan and Caucasian males (A) and females (B).**

Black open circles indicate the Ugandan and red open circles indicate the Caucasian individual virtual data simulated by Simcyp. Black lines indicate the mean adult Ugandan and red lines indicate the mean adult Caucasian age-weight population group derived from Hayes *et al.* (2014) (434) regression equation.

### 3.3.1.2 Age-weight relationship for paediatric population groups

The mathematical relationships for the age-weight distribution for Caucasian and Ugandan paediatric populations are detailed in Figure 3.7. In a 10x10 virtual clinical trial to simulate the age-weight distribution in this paediatric population, the plots exhibit a similar age-dependant increase in body-weight for males and females across all age range (Figure 3.7).

#### *Default Simcyp paediatric population groups*

*Females:*

0-18 years old,

$$\begin{aligned} \text{Height} = & -0.00000151027 * \text{age}^8 + 0.000121261 * \text{age}^7 - 0.0040023 * \\ & \text{age}^6 + 0.070179 * \text{age}^5 - 0.708233 * \text{age}^4 + 4.1872 * \text{age}^3 - 14.3393 * \\ & \text{age}^2 + 33.84778 * \text{age} + 51.535477 \end{aligned} \quad (3.7)$$

More than 18 years old,

$$\text{Height} = 161.66 + 0.1319 * \text{age} - 0.0027 * \text{age}^2 \quad (3.8)$$

$$\text{Body weight} = 5.454 * (1.0 - e^{(\text{age} * -1.57)}) + e^{((\text{Height} * 0.0224) + (0.019 * \text{age}))} \quad (3.9)$$

*Males:*

0-18 years old,

$$\begin{aligned} \text{Height} = & 0.0000176179 * \text{age}^7 - 0.00119874 * \text{age}^6 + 0.0323848 * \text{age}^5 - \\ & 0.444112 * \text{age}^4 + 3.2946 * \text{age}^3 - 13.2191 * \text{age}^2 + 33.75 * \text{age} + 52.62152 \end{aligned} \quad (3.10)$$

More than 18 years old,

$$\text{Height} = 175.32 + 0.1113 * \text{age} - 0.0025 * \text{age}^2 \quad (3.11)$$

$$\text{Body weight} = 7.826 * (1.0 - e^{(\text{age} * -1.2)}) + e^{((\text{Height} * 0.0209) + (0.023 * \text{age}))} \quad (3.12)$$

### *Malaria paediatric population groups*

*Ugandan females:*

$$\begin{aligned} \text{Body weight} = & (3.9033133 + 0.43769058 * \text{age}^{0.5} + -0.73539741 * \text{age} + \\ & 0.031919235 * \text{age}^{1.5} + 0.019365454 * \text{age}^2) / (1 + -0.70490582 * \text{age}^{0.5} + \\ & 0.18985506 * \text{age} + -0.024825615 * \text{age}^{1.5} + 0.0015213393 * \text{age}^2) \end{aligned} \quad (3.13)$$

*Ugandan males:*

$$\begin{aligned} \text{Body weight} = & (4.2596993 + 6.0143271 * \text{age} + -1.2976996 * \text{age}^2 + 0.15386155 * \\ & \text{age}^3 + -0.0099043391 * \text{age}^4 + 0.0002557705 * \text{age}^5) / (1 + 0.12029078 * \text{age} + \\ & -0.039177947 * \text{age}^2 + 0.003871229 * \text{age}^3 + -0.00019964827 * \text{age}^4 + \\ & 0.0000045231346 * \text{age}^5) \end{aligned} \quad (3.14)$$

For the males, the Caucasian population group had a greater mean weight range at  $69.94 \text{ kg} \pm 26.63 \text{ kg}$  ( $17.99 \text{ years} \pm 6.85 \text{ years}$ ) when compared to the Ugandan group,  $51.72 \text{ kg} \pm 19.10 \text{ kg}$  ( $17.87 \text{ years} \pm 6.85 \text{ years}$ ). Further, for the body weight deviated further from each population as the age increased, culminating in an approximate  $18.22 \text{ kg}$  difference between the two population groups at 18 years ( $p < 0.002$ ). With regards to the female paediatric population groups, Caucasians demonstrated a higher mean weight range at  $60.36 \text{ kg} \pm 21.26 \text{ kg}$  ( $18.25 \text{ years} \pm 6.85 \text{ years}$ ) when compared with the Ugandan population,  $52.65 \text{ kg} \pm 17.13 \text{ kg}$  ( $18.31 \text{ years} \pm 6.85 \text{ years}$ ). The greatest difference in body weight was observed at 18 years of age with a difference of approximately  $7.71 \text{ kg}$  between each population ( $p < 0.08$ ).

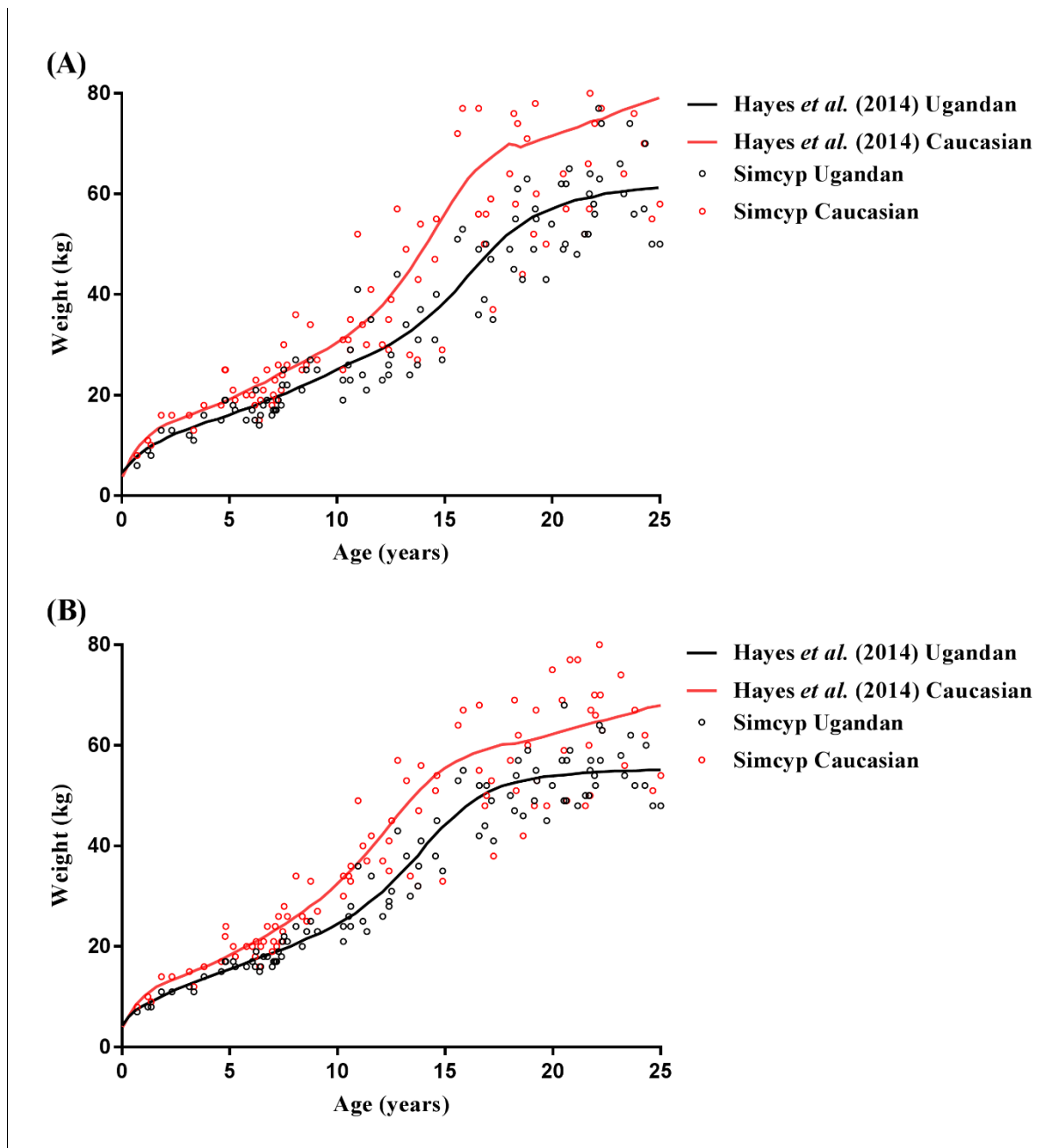


**Figure 3.7 Age-weight relationship comparison between paediatric Ugandan and Caucasian males (A) and females (B).**

Black open circles indicate the paediatric Ugandan and red open circles indicate the paediatric Caucasian individual virtual data simulated by Simcyp. Black lines indicate the mean paediatric Ugandan and red lines indicate the mean paediatric Caucasian age-weight population group derived from Hayes *et al.* (2014) (434) regression equation.

### 3.3.2 Step 1: Adult simulations with efavirenz

In order to predict the impact of efavirenz-mediated DDIs on lumefantrine pharmacokinetics, the capability of the model to predict efavirenz pharmacokinetics alone within a healthy volunteer population was first assessed. Using the efavirenz compound file within the Simcyp library and the Simcyp 'Healthy Volunteer' population group, the predicted population plasma concentration-time profile for a single 600 mg oral dose of efavirenz were within the range of observed reported values for both \*1/\*1 (Figure 3.8A) and \*6/\*6 population groups (Figure 3.8B).

Furthermore, the model predicted  $t_{\max}$ ,  $C_{\max}$  and AUC were within 2-fold of the reported parameters for each genotype (Table 3.7).

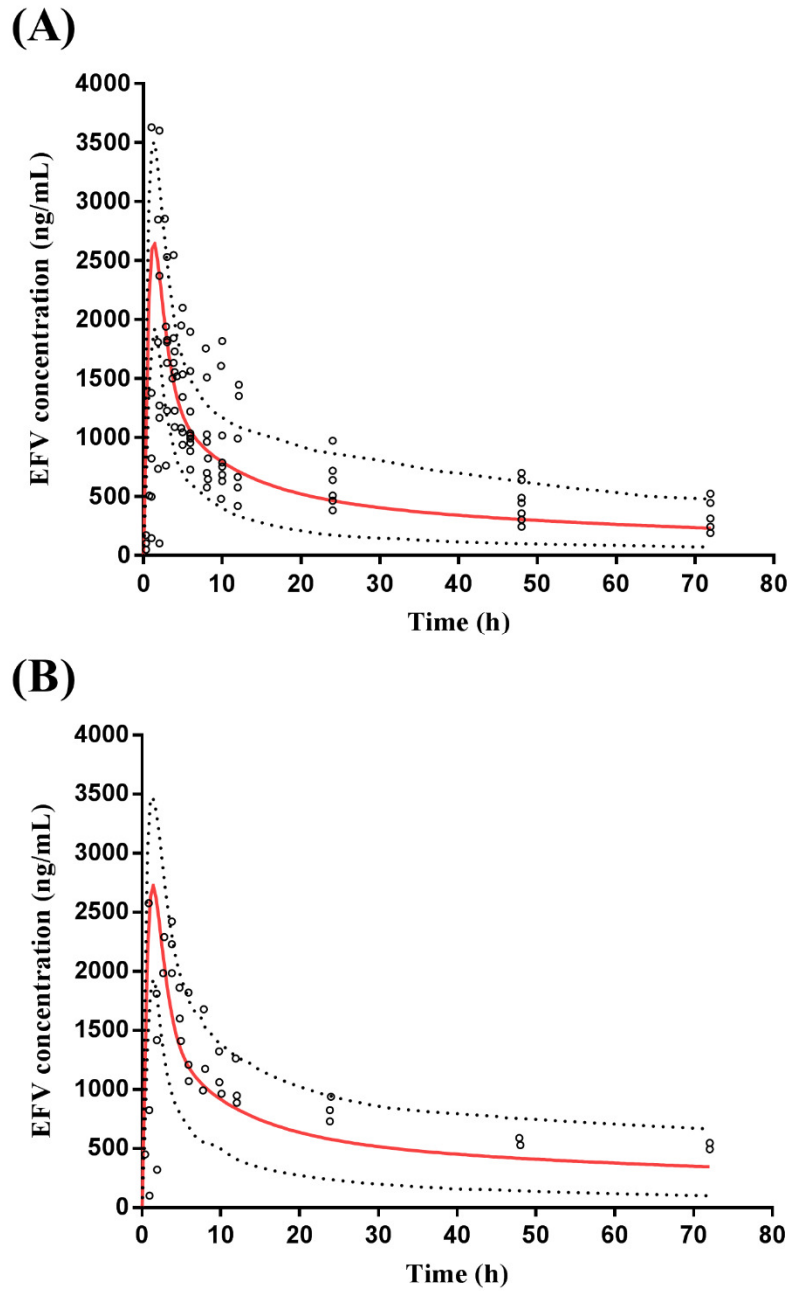


**Figure 3.8 Simulated single dose plasma concentration-time profiles of efavirenz in healthy volunteer adults.**

Simulated efavirenz concentration-time profiles after a single 600 mg oral dose of efavirenz (EFV) in healthy adults to *CYP2B6*\*1/\*1 extensive metabolisers (A), and *CYP2B6*\*6/\*6 poor metabolisers (B) genotypes (n=20). Solid lines represent mean with dotted lines representing 5<sup>th</sup>-95<sup>th</sup> percentile range. Open circles represent observed data points.

**Table 3.7 Summary of predicted and observed pharmacokinetic parameters of efavirenz in adults with *CYP2B6*\*1/\*1 and *CYP2B6*\*6/\*6 genotypes in a Healthy Volunteer population**

	Genotype	Pharmacokinetic parameters		
		$t_{max}$ (h)	$C_{max}$ (ng/ml)	$AUC_{0-inf}$ (ng/mL.h)
Observed	*1/*1	2.3 ± 1.0	2300 ± 700	79800 ± 28400
Predicted	*1/*1	1.5 ± 0.02	2643 ± 53	59126 ± 1520
Observed	*6/*6	2.7 ± 1.5	2400 ± 200	101700 ± 7900
Predicted	*6/*6	1.5 ± 0.02	2727 ± 136	93857 ± 4693

$t_{max}$ : time to reach  $C_{max}$ ,  $C_{max}$ : the maximum concentration recorded,  $AUC_{0-inf}$ : a measure of the exposure to the drug from time zero to infinity. Data represent mean ± SD. Simulations: n=20 with 50 % female and age range of 20-50 years.

Subsequently, to further validate model simulations, the ability to predict efavirenz plasma concentrations following multi-dosing was assessed in each genotype patient group using a Ugandan population group. In both \*1/\*1 (Figure 3.9A) and \*6/\*6 (Figure 3.9B) populations, the predicted concentrations were within the range reported (421), and all within 2-fold of reported concentrations (Table 3.8) (Figure 3.9B).

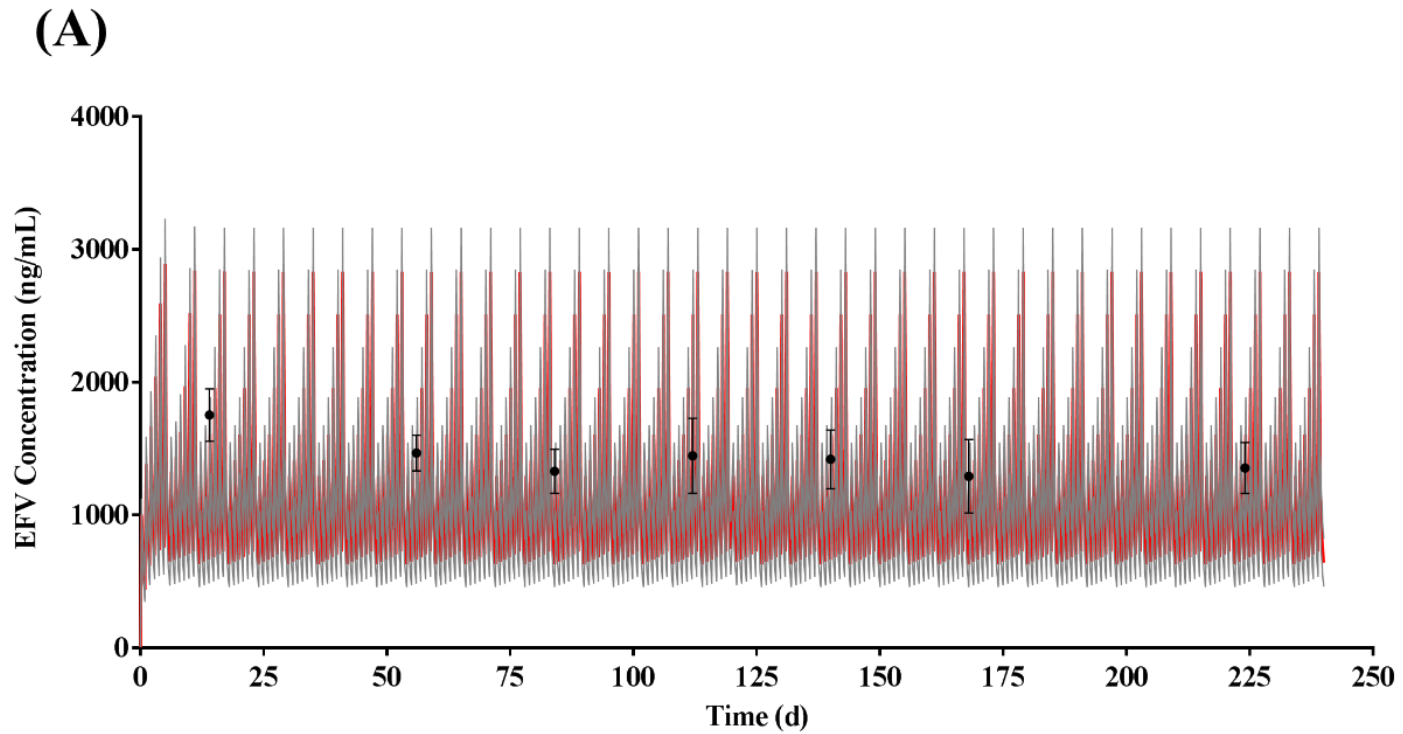


**Figure 3.9 Simulated multidose plasma concentration-time profile of efavirenz in a Ugandan population group**

Simulated efavirenz (EFV) concentration-time profiles after single daily oral doses of 600 mg in adults with *CYP2B6*\*1/\*1 extensive metabolisers (A), and *CYP2B6*\*6/\*6 poor metabolisers (B) genotypes from day 1 to day 224 (n=157). Comparison of mean plasma concentration-time profiles for the two simulated groups. Solid line represents mean. Close circles represent observed mean data point with error bars indicating standard deviation.

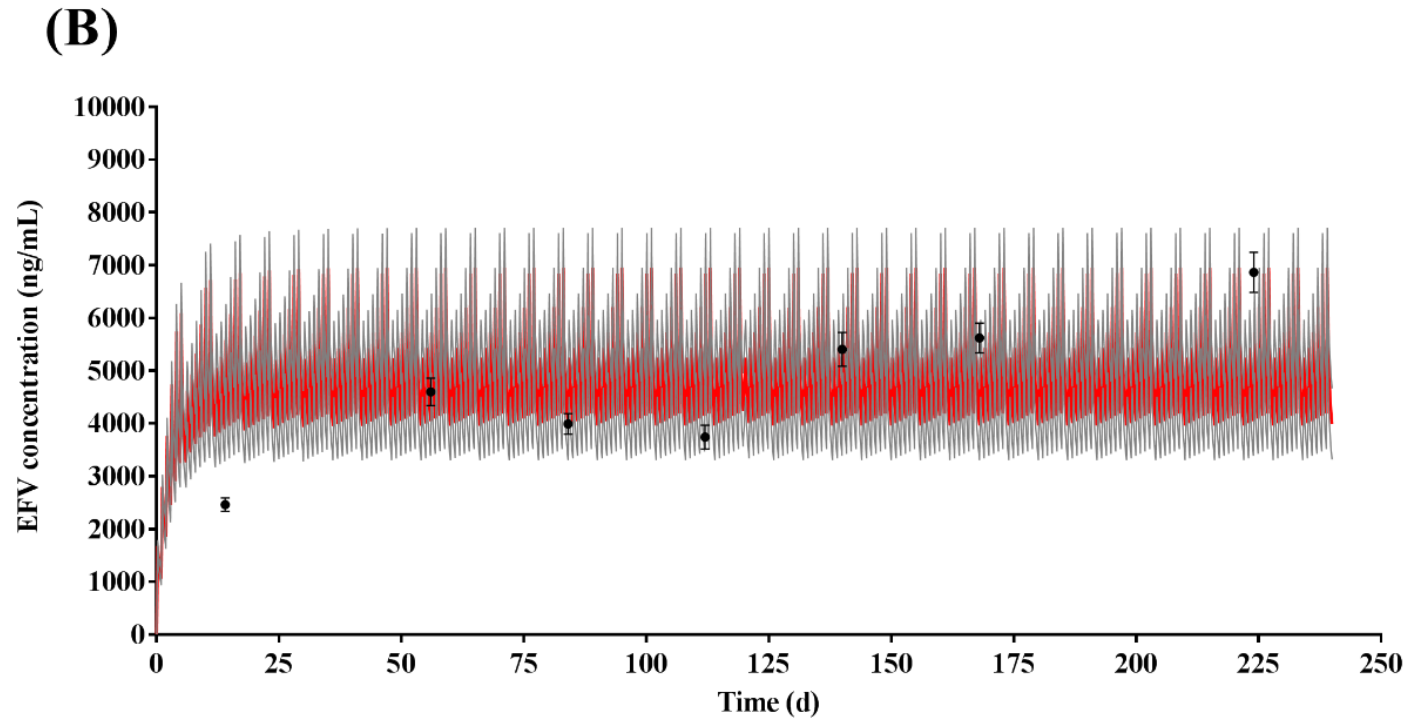


**Figure 3.9 Simulated multidose plasma concentration-time profile of efavirenz in a Ugandan population group**

Simulated efavirenz (EFV) concentration-time profiles after single daily oral doses of 600 mg in adults with *CYP2B6*\*1/\*1 extensive metabolisers (A), and *CYP2B6*\*6/\*6 poor metabolisers (B) genotypes from day 1 to day 224 (n=157). Comparison of mean plasma concentration-time profiles for the two simulated groups. Solid line represents mean. Close circles represent observed mean data point with error bars indicating standard deviation.

**Table 3.8 Summary of predicted and observed efavirenz plasma concentrations in Ugandan adults with *CYP2B6*\*1/\*1 and *CYP2B6*\*6/\*6 genotypes.**

Sampling day		*1/*1	*6/*6
		Concentration (ng/mL)	
Day 14	Observed	1752 ± 197	2462 ± 130
	Predicted	1597 ± 80	3921 ± 196
Day 56	Observed	1466 ± 134	4600 ± 262
	Predicted	1594 ± 80	4074 ± 204
Day 84	Observed	1329 ± 166	3991 ± 194
	Predicted	1284 ± 64	3989 ± 199
Day 112	Observed	1446 ± 283	3741 ± 225
	Predicted	1140 ± 57	4170 ± 209
Day 140	Observed	1420 ± 221	5404 ± 319
	Predicted	1595 ± 80	5698 ± 285
Day 168	Observed	1292 ± 278	5621 ± 284
	Predicted	1284 ± 64	5219 ± 261
Day 224	Observed	1353 ± 198	6861 ± 382
	Predicted	1595 ± 80	5698 ± 285

Data represent mean ± SD. Simulations: n=100 with 38.5 % female and age-range of 20-40 years.

### 3.3.3 Step 2: Adult simulations with lumefantrine-efavirenz drug-drug interactions

To further validate the proposed model, DDIs were simulated between lumefantrine and efavirenz using the Simcyp ‘Healthy Volunteer’ population group. The impact of the predicted DDI on lumefantrine pharmacokinetics was within the range of the observed data reported (414) (Figure 3.10), with  $C_{max}$ ,  $t_{max}$  and AUC predictions within 2-fold of those reported by Huang *et al.* (2012) (414) (Table 3.9). Furthermore, the predicted day 7 lumefantrine concentration ( $C_{d7}$ ) in the presence of efavirenz,  $679 \pm 361$  ng/mL, was within 2-fold of that observed ( $554 \pm 432$  ng/mL) (Table 3.9).

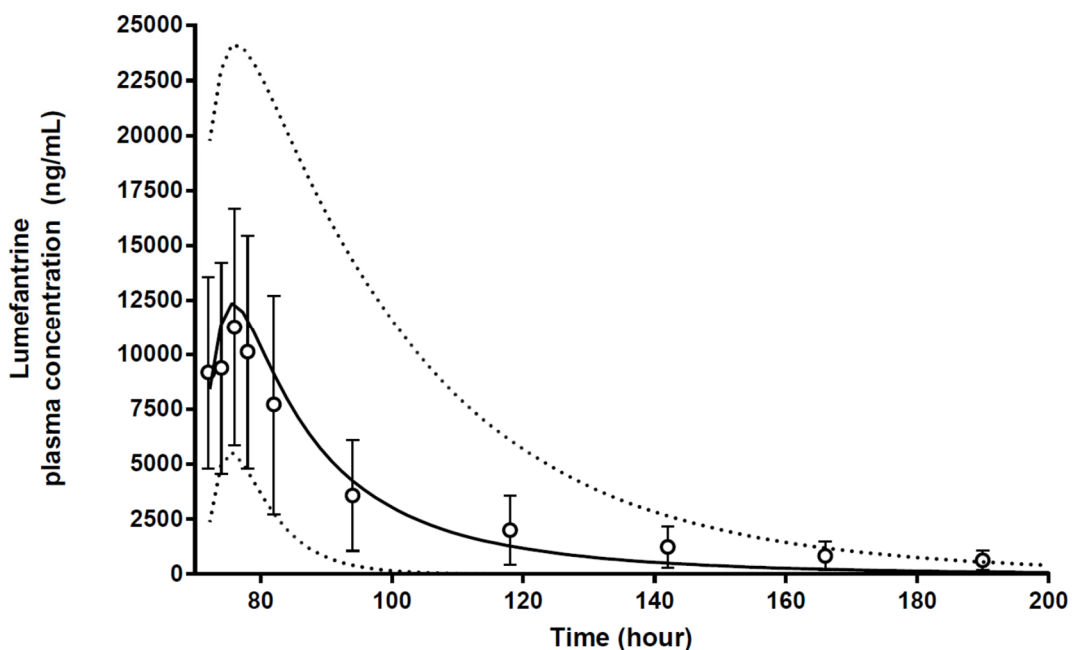


**Figure 3.10 Simulated lumefantrine plasma concentration following co-administration with efavirenz in a healthy volunteer population group**

Lumefantrine was dosed for 6 doses of 480 mg, twice daily for three days commencing on day 12, with efavirenz (600mg once daily) dosed for the entire study duration (25 days) to 12 ‘Healthy Volunteer’ subjects. Solid lines represent predicted mean plasma concentration with dashed lines indicated 5<sup>th</sup> and 95<sup>th</sup> percentiles. Open circles with errors bars indicate observed plasma concentrations and associated standard deviation.

**Table 3.9 Summary of predicted and observed PK parameters of lumefantrine in the absence and presence of efavirenz in healthy adults.**

		<b>C<sub>max</sub></b> (µg/mL)	<b>AUC<sub>last</sub></b> (µg/mL.h)	<b>t<sub>max</sub></b> (h)	<b>C<sub>d7</sub></b> (ng/mL)
- EFV	Predicted	12.39 (8.12-19.2)	276 (320-711)	3.6 (2-5.9)	1162 ± 557
	Observed	11.6 (9.5-17.4)	418 (339-693)	2.0 (2-6)	1020 ± 478
+ EFV	Predicted	12.42 (7.14-18.7)	236 ± (201-617)	4.2 (0.4-5.7)	679 ± 361
	Observed	12.1 (10.6-16.4)	331 ± (270-503)	6.0 (0.5-6)	554 ± 432

t<sub>max</sub>: time to reach C<sub>max</sub>, C<sub>max</sub>: the maximum concentration recorded, AUC<sub>0-last</sub>: a measure of the exposure to the drug from time zero to last measured, C<sub>d7</sub>: day 7 concentration. Data represents mean ± SD. Simulations: n=12 with 16.6 % female and age-range of 24-53 years. EFV: efavirenz.

The model was then extended to assess its application within an African population group. Recent studies reported lumefantrine  $C_{d7}$  in a Tanzanian population group for \*1/\*1 and \*6/\*6 population groups (425, 435). *In lieu* of the development of a Tanzanian population group, a recently developed Simcyp ‘South-African’ population group was used as a surrogate for a Tanzanian population group to predict lumefantrine  $C_{d7}$  in \*1/\*1 and \*6/\*6 population groups (Figure 3.11). In this simulation, we assumed some similarity between the population groups in terms of body weight demographics (422).

Predictions of median lumefantrine  $C_{d7}$  in the absence of efavirenz, for both \*1/\*1 and \*6/\*6, were well predicted and within 2-fold of that reported (425) (Table 3.10). In the presence of efavirenz, the \*1/\*1 predicted median  $C_{d7}$  was within 2-fold of that reported, however for the \*6/\*6 population, although within the overall range of reported values, the predicted median  $C_{d7}$  was within 3-fold of that reported. In the absence of efavirenz, *CYP2B6* genotypes have no significant impact on any pharmacokinetic parameter modelling. However, in the presence of efavirenz, the  $C_{max}$  and  $C_{d7}$  for the \*6/\*6 population were significantly reduced ( $P < 0.01$ ), 17,500 to 9,010 ng/mL and 901 to 201 ng/mL, when compared to the \*1/\*1 population group (Table 3.10).

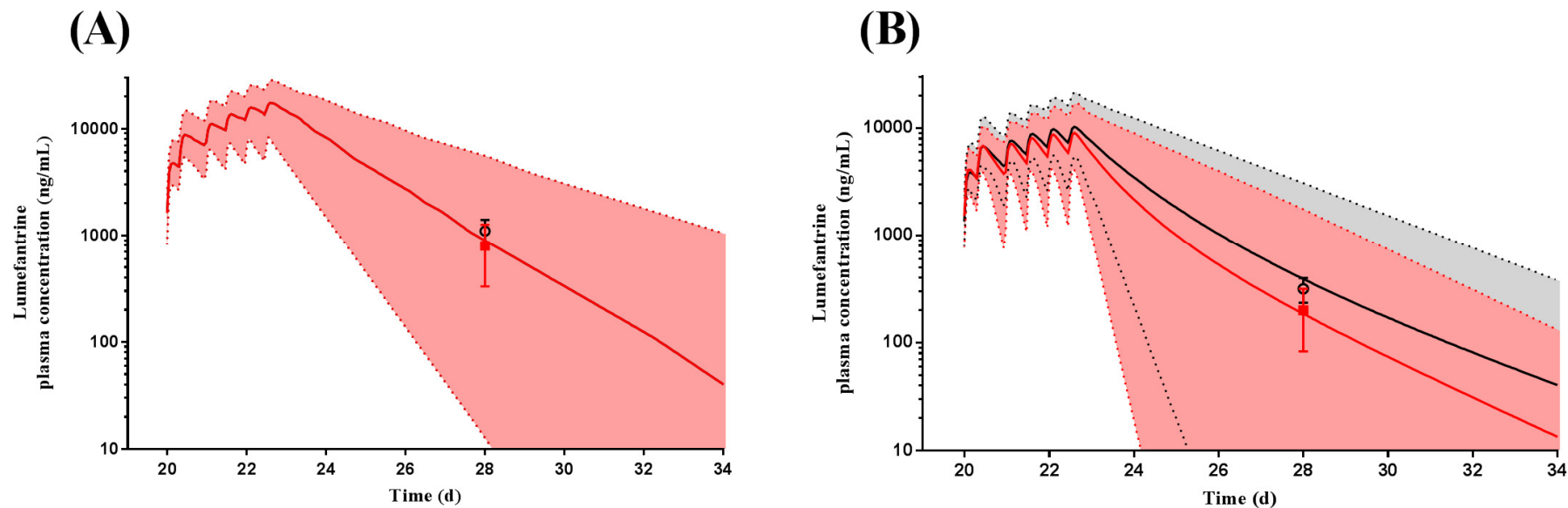


**Figure 3.11 Simulated drug-drug interaction between lumefantrine and efavirenz in a South African population groups.**

Lumefantrine was dosed for 6 doses of 480 mg, twice daily for three days commencing on day 20, in the absence (A) and presence (B) of efavirenz (600mg once daily) dosed for the entire study duration (40 days) to 141 South African healthy adults. \*1/\*1 (EM) and \*6/\*6 (PM) genotype pharmacokinetic profiles are indicated by the red and black colours. Median observed plasma day-7 lumefantrine concentrations (425) represented by the open circles (EM) and closed square (PM) with error bars indicating standard deviation. Solid lines represent predicted mean plasma concentration with dashed lines indicated 5<sup>th</sup> and 95<sup>th</sup> percentiles.

**Table 3.10 Summary of the simulated lumefantrine pharmacokinetics parameters in the absence and presence of efavirenz in South African adults with *CYP2B6*\*1/\*1 and *CYP2B6*\*6/\*6 genotypes.**

Parameters	Lumefantrine alone		Lumefantrine plus Efavirenz	
	*1/*1 Median (Range)	*6/*6 Median (Range)	*1/*1 Median (Range)	*6/*6 Median (Range)
$C_{max}$ (ng/mL)	17500 (8350-28500)	17500 (8350-28500)	12100 (5550-21500)	9010 (4200-16800)
$AUC_{0-inf}$ (ng/mL.d)	60002 (20195-138896)	60002 (20195-138896)	38243 (12171-92638)	25578 (7685-67347)
$t_{max}$ (h)	22.59 (22.54-22.64)	22.59 (22.54-22.64)	22.59 (22.10-22.60)	22.59 (22.05-22.64)
Predicted $C_{d7}$ (ng/mL)	901 (13-4620)	901 (13-4620)	382 (1-1650)	201 (1-1280)
Observed $C_{d7}$ (ng/mL)	1000 (686–1929)	893 (562–1732)	299 (253–384)	226 (173–278)

$C_{max}$ : the maximum concentration recorded,  $AUC_{0-inf}$ : a measure of the exposure to the drug from time zero to infinity,  $C_{d7}$ : day 7 concentration Data represent median (range). Simulations: n=59 with 52.3 % female and age-range of 21-65 years

### **3.3.4 Step 3: Paediatric simulations with efavirenz**

Having established the ability of the proposed model to predict adult lumefantrine-efavirenz DDIs in genotyped African population groups, the model was expanded to assess the impact of such interactions in paediatric population groups.

Simulations were performed in a custom developed Ugandan paediatric population group with validation of efavirenz pharmacokinetics based on WHO weight-based dosing recommendation for children and compared to a report of efavirenz dosing in Ugandan paediatric malaria patients (409) where 41 children were dosed at 300 mg once daily. Based on this dosing approach, predicted efavirenz concentration profiles (Figure 3.12) were within the range reported (409) with the predicted  $C_{max}$  for the population group, 3.59 mg/L (1.65-9.52 mg/L), within 2-fold of that reported 3.62 mg/L (2.86-4.38 mg/L) (Table 3.11).

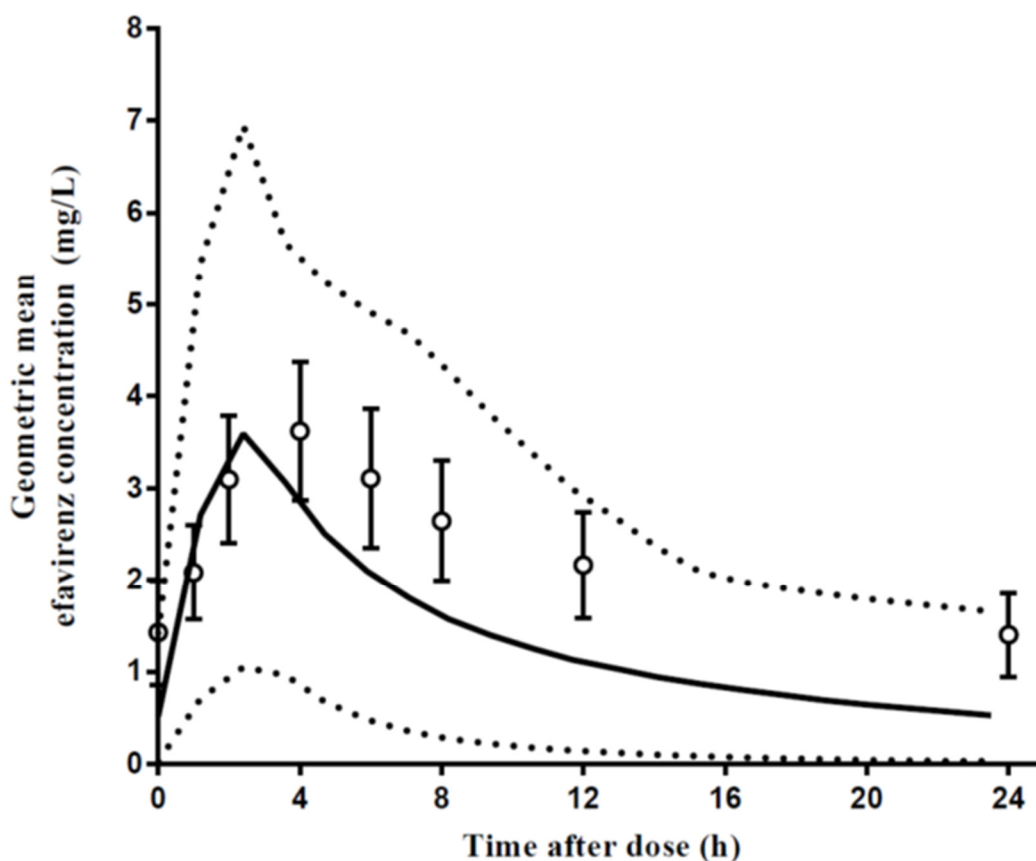


**Figure 3.12 Simulated efavirenz plasma concentration-time profile in a Ugandan paediatric population group.**

Efavirenz was dosed to as a 300 mg daily dose to steady state using the Ugandan paediatric population group. Solid lines represent geometric mean with dotted-lines representing 5<sup>th</sup>-95<sup>th</sup> percentile range. Geometric mean observed plasma concentrations (409) are represented by the open circles, with error bars indicating standard deviation.

**Table 3.11 Summary of predicted and observed efavirenz pharmacokinetics parameters in HIV-infected Ugandan children.**

	$C_{max}$ (mg/L)	$AUC_{0-last}$ (mg/L.h)	$t_{max}$ (h)
Predicted	3.59 (1.65-9.52)	33.52 (11.24-94.43)	2.4 (2.3-2.6)
Observed	3.62 (2.86-4.38)	54.52 (44.53-64.51)	4.0 (3.2-4.8)

$t_{max}$ : time to reach  $C_{max}$ ,  $C_{max}$ : the maximum concentration recorded,  $AUC_{0-last}$ : a measure of the exposure to the drug from time zero to last measured. Data represents mean (range). Simulations: n=41 with 58.5 % female and age-range of 3-12 years.

To further validate the ability of the model to predict efavirenz plasma concentrations in paediatric population groups, predictions were stratified over weight ranges, where efavirenz was dosed based on body weight using the Ugandan population group, and compared with published population-based data (23) for matching weight ranges (Figure 3.13). In all weight groups, the predicted mean plasma concentration profiles were generally well predicted, and the 5<sup>th</sup> and 95<sup>th</sup> prediction percentiles spanned the range of observed population data points for each weight banding.

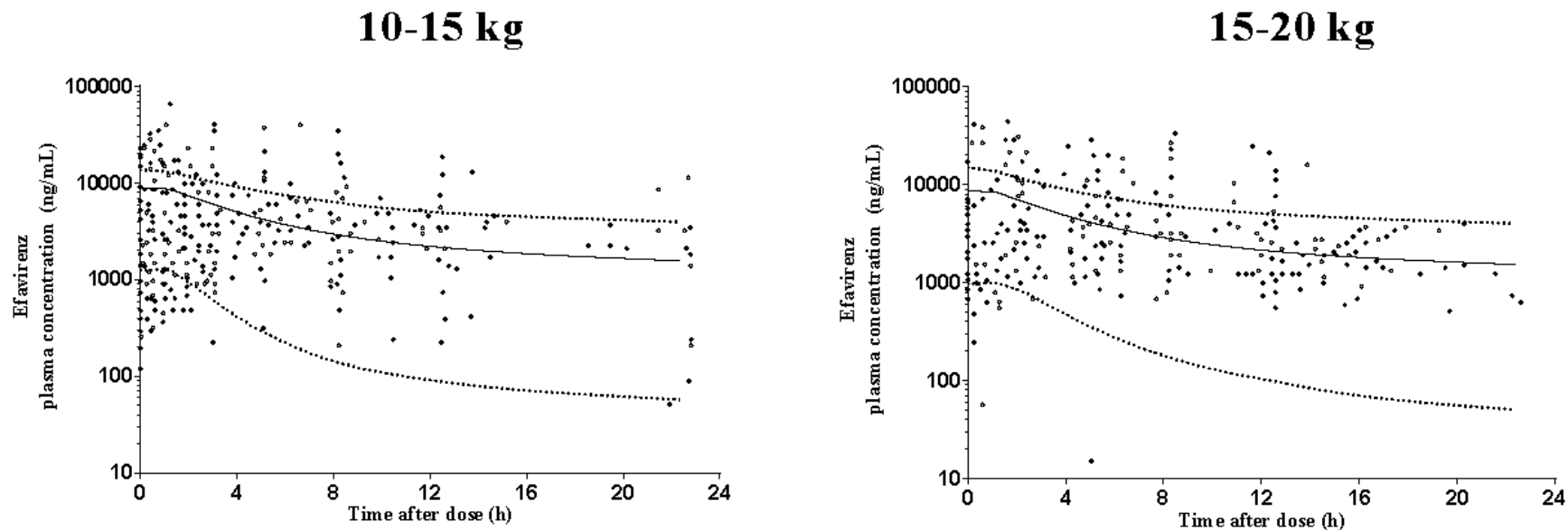


**Figure 3.13A Simulated plasma concentration-time profile of body weight efavirenz dosing in Healthy Volunteers (10-15 kg and 15-20 kg).**

A 10x10 trial was run with efavirenz dosed in a standard body-weight based single daily dose regimen for 30 days. Results are presented stratified based on body-weight bandings each possessing at least 80 virtual trial subjects. Solid lines represent mean predictions with dotted-lines representing 5<sup>th</sup>-95<sup>th</sup> percentile range for the final dose. Open circles represent data for observed study for each body weight banding (23).

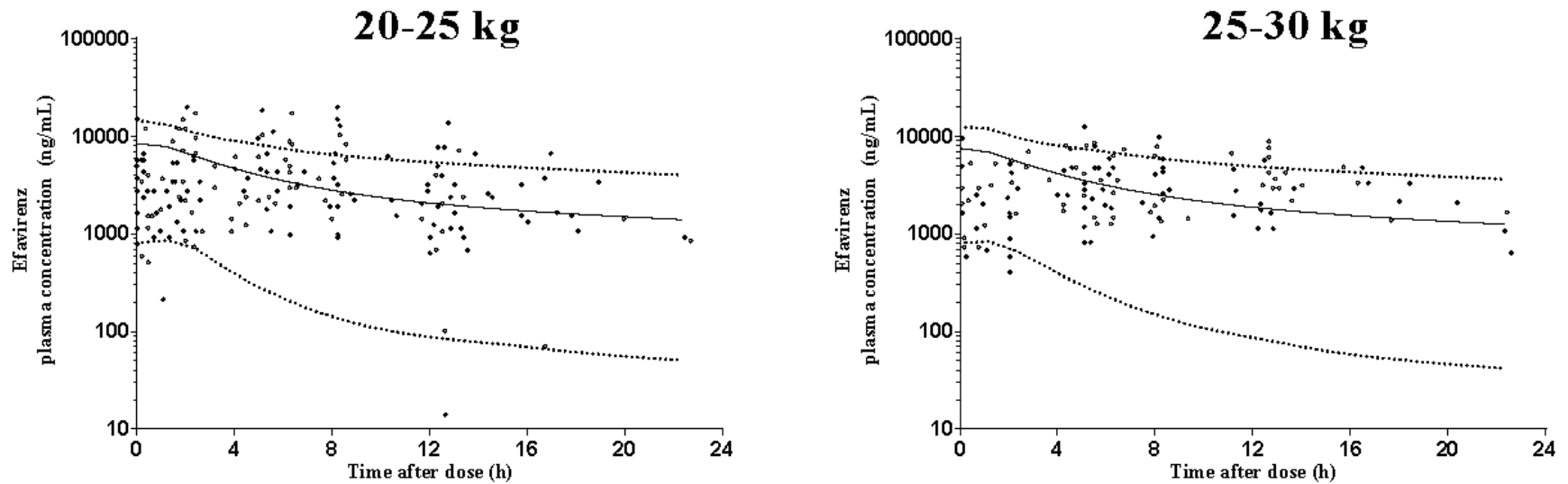


**Figure 3.13B: Simulated plasma concentration-time profile of body weight efavirenz dosing in Healthy Volunteers (20-25kg and 25-30kg)**

A 10x10 trial was run with efavirenz dosed in a standard body-weight based single daily dose regimen for 30 days. Results are presented stratified based on body-weight bandings each possessing at least 80 virtual trial subjects. Solid lines represent mean predictions with dotted-lines representing 5<sup>th</sup>-95<sup>th</sup> percentile range for the final dose. Open circles represent data for observed study for each body weight banding (23).

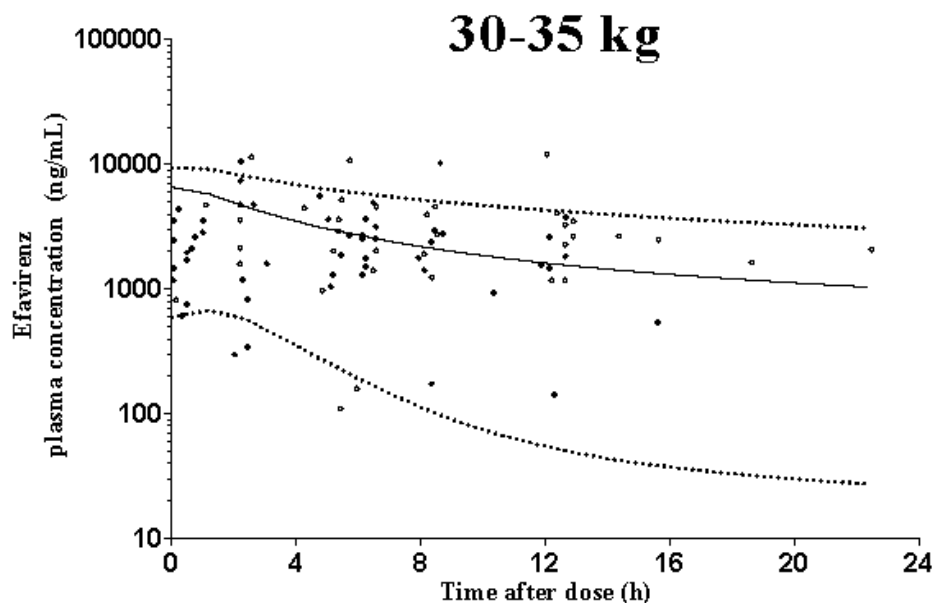


**Figure 3.13C: Simulated plasma concentration-time profile of body weight efavirenz dosing in Healthy Volunteers (30-35 kg)**

A 10x10 trial was run with efavirenz dosed in a standard body-weight based single daily dose regimen for 30 days. Results are presented stratified based on body-weight bandings each possessing at least 80 virtual trial subjects. Solid lines represent mean predictions with dotted-lines representing 5<sup>th</sup>-95<sup>th</sup> percentile range for the final dose. Open circles represent data for observed study for each body weight banding (23).

Further, following a high dose of efavirenz (25mg/kg), dosed once daily to 2-3 year old Ugandan children, simulations of the mean efavirenz plasma concentration profile (Figure 3.14) were in good agreement with data published (410), with prediction of C<sub>12h</sub> and AUC<sub>0-24</sub> within 2-fold of that reported (Table 3.12).

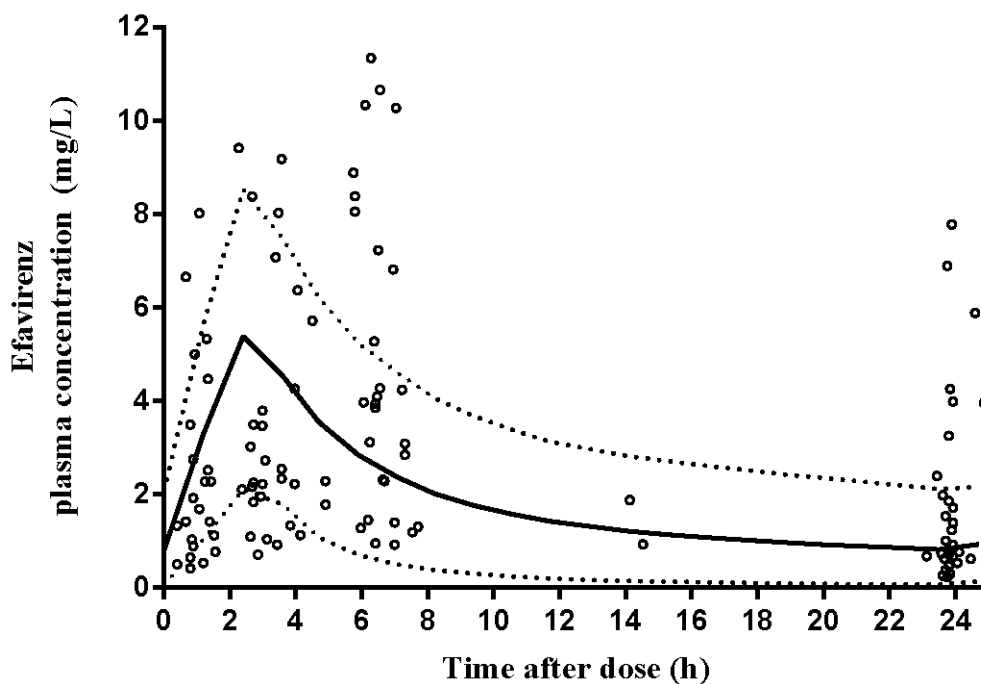


**Figure 3.14 Simulated plasma concentration-time profile of efavirenz dosed at 25 mg/kg to 2-3 years old Ugandan children.**

A dose of 25 mg/kg efavirenz was administered once daily to 2-3 years old Ugandan children (n=53) using the Ugandan Simcyp population group. Solid lines represent mean predictions with dotted-lines representing 5<sup>th</sup>-95<sup>th</sup> percentile range. Open circles represent data for observed study (410) originating from Burkina Faso and Cote d'Ivoire.

**Table 3.12 Summary of predicted pharmacokinetic parameters of efavirenz in Ugandan children.**

	$C_{max}$ mg/L	$C_{12h}$	$AUC_{0-24}$ mg/L.h	$t_{max}$ h
Predicted	5.38 (2.95-8.63)	1.51 (0.23-6.12)	46.85 (35.13-89.33)	2.4 (2.12-2.70)
Observed	-	2.66 (0.95-14.06)	80.44 (46.98-279.16)	-

$t_{max}$ : time to reach  $C_{max}$ ,  $C_{max}$ : maximum plasma concentration,  $AUC_{0-24}$ : area under the curve from time zero to 24 hours,  $C_{d7}$ : day 7 concentration. Data represents median (range).  $C_{12h}$ : concentration 12 hours after dosing

To further validate the ability of the model to predict efavirenz concentrations in *CYP2B6* genotyped paediatric subjects, simulations were performed in a South African paediatric population group where efavirenz was dosed at 300mg to 6-7 years old (Figure 3.15), and where genotyped plasma concentration had been previously published in a South African paediatric population group (411) for 2 hours around the  $C_{12h}$ . Model predictions for both \*1/\*1 and \*6/\*6 were generally in good agreement with that published, with a slight under-prediction for \*1/\*1 subjects. Further, \*6/\*6 demonstrated a significantly higher  $C_{max}$ , 8.27 ng/mL (3.18-17.44 ng/mL), when compared to \*1/\*1, 4.26 ng/mL (1.45-7.98 ng/mL) ( $P < 0.001$ ) (Table 3.13).

**Table 3.13 Summary of predicted pharmacokinetic parameters of efavirenz in South African children.**

Parameters	Efavirenz	
	<i>CYP2B6</i> *1/*1 Mean (Range)	<i>CYP2B6</i> *6/*6 Mean (Range)
$C_{max}$ (µg/mL)	4.26 (1.45-7.98)	8.27 (3.18-17.44)
$AUC_{0-inf}$ (µg/mL.h)	29.96 (8.58-81.23)	108.1 (31.13-298.3)
$t_{max}$ (h)	2.4 (2.1-2.6)	2.4 (2.1-2.6)

$t_{max}$ : time to reach  $C_{max}$ ,  $C_{max}$ : maximum plasma concentration,  $AUC_{0-inf}$ : area under the curve from time zero and extrapolated to infinity. Data represents mean (range).

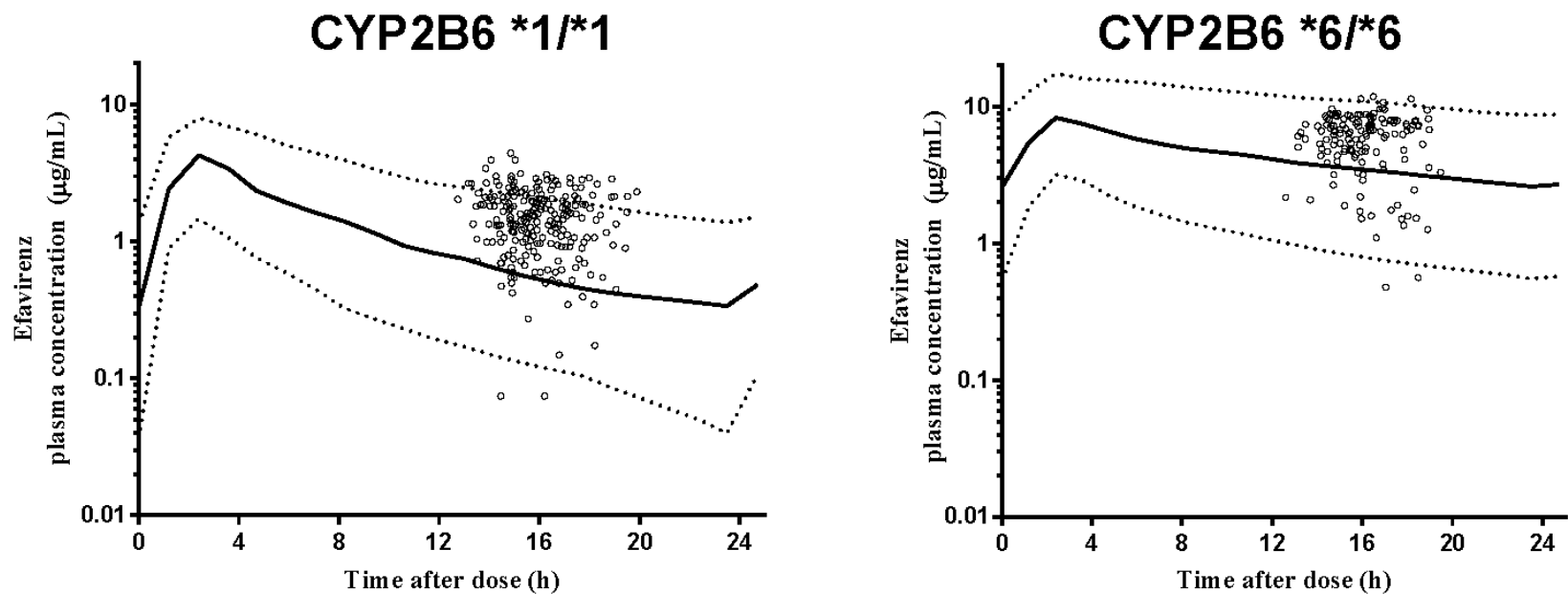


**Figure 3.15 Simulated plasma concentration-time profile of efavirenz in South African children stratified by genotype.**

A dose of 300 mg was administered to 60 children (using the South African population group), aged between 6-7 years and possessing a weight of 20-24.9kg, for 25 days. Simulations were run for genotypes of all subjects being either \*1/\*1 or all \*6/\*6 genotypes. Results are presented for day 20 with solid lines representing median predictions with dotted-lines representing 5<sup>th</sup>-95<sup>th</sup> percentile range. Open circles represent data for observed study (411) from a South African population group.

### 3.3.5 Step 4: Paediatric simulations with lumefantrine-efavirenz drug-drug interactions

Having demonstrated the ability to predict efavirenz concentrations in paediatric subjects, we next attempted to predict lumefantrine-efavirenz based DDIs in African population groups. We utilised the Ugandan paediatric population group, and a report by Parikh *et al.* 2016 (408), to predict lumefantrine concentrations in the presence and absence of efavirenz (Figure 3.16).

Parikh *et al.* (2016) (408) applied weight-based dosing across a wide age range (3.1-8.6 years) with dosing that spanned different weight bands, but did not present plasma concentration profiles genotyped for *CYP2B6*. Results presented in Figure 3.16 are therefore stratified for two extreme cases of an entire population of *CYP2B6* \*1/\*1 or entirely *CYP2B6* \*6/\*6, and this represent the ‘best’ and ‘worst’ clinical scenarios.

When considering the two extreme scenarios, model predictions of the final dose  $C_{max}$  were within 2-fold of that reported (408), and spanned a range of total values (2060-11083 ng/mL) that were similar to the population range reported by Parikh *et al.* (2016) (408) (2611-6673 ng/mL) (Table 3.14). In the absence of efavirenz, the predicted \*1/\*1 and \*6/\*6 lumefantrine profiles are largely overlapping with no significant differences in the last  $C_{max}$  between genotypes (Table 3.14). Further, model prediction of  $C_{d7}$ , (Figure 3.16), were within 2-fold of that reported (408) (Table 3.14) in the absence of efavirenz.

In the presence of efavirenz median last-dose  $C_{max}$  was significantly lower ( $P < 0.01$ ) in the \*6/\*6 group (for both weight bands) (5-15 kg: 1532 ng/mL; 15-25kg: 1979 ng/ml) compared to the \*1/\*1 group (5-15 kg: 2494 ng/mL; 15-25kg: 2994 ng/ml) (Table 3.14). Similarly,  $C_{d7}$  was significantly lower ( $P < 0.01$ ) in the \*6/\*6 group (5-15 kg: 20 ng/mL; 15-25kg: 51 ng/ml) compared to the \*1/\*1 group (5-15 kg: 120 ng/mL; 15-25kg: 221 ng/ml) (Table 3.14).

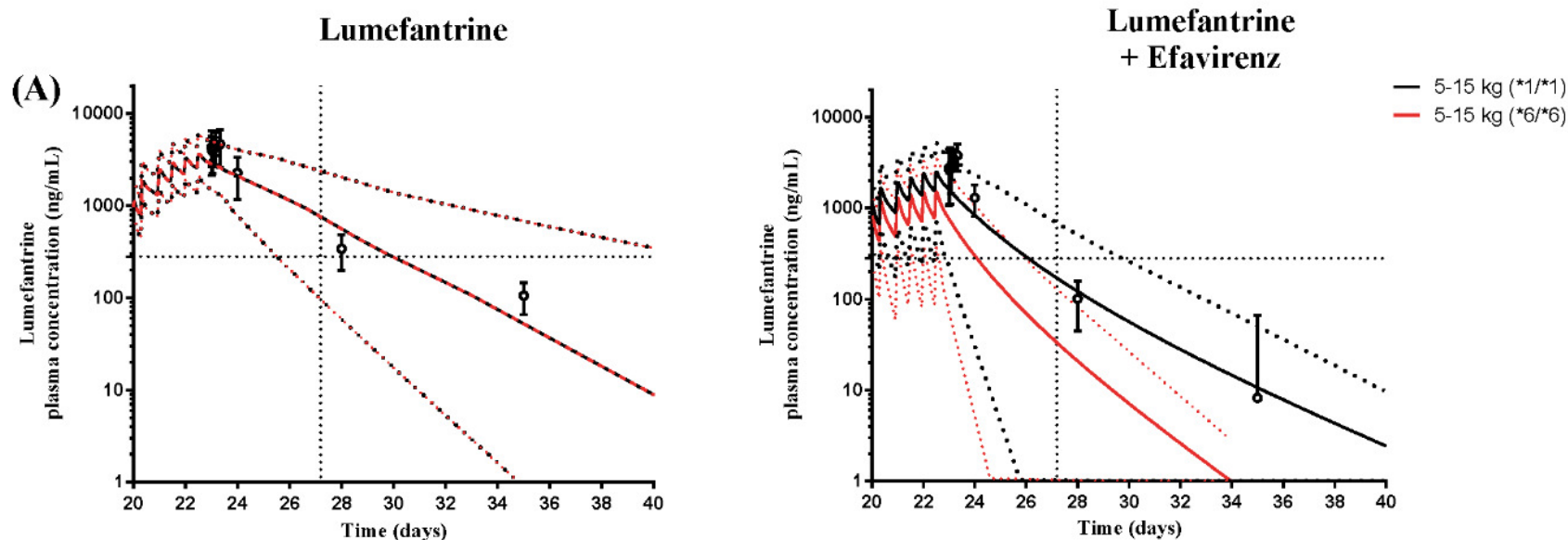


**Figure 3.16A Simulated median plasma concentration-time profile of lumefantrine administered to Ugandan children in the absence and presence of efavirenz (5-15 kg).**

Lumefantrine (LUM) and efavirenz (EFV) were dosed to Ugandan children aged 3-9 years of age using weight-based dosing strategies of (A) 5-15 kg (LUM: 120 mg per dose; EFV: 200 mg per dose) and (B) 15-25 kg (LUM: 240 mg per dose; EFV: 250-300 mg per dose) with simulated profiles for population groups of all *CYP2B6* \*1/\*1 or all *CYP2B6* \*6/\*6. All simulations included 40-50 subjects per dosing band. Open circles and error bars represent mean and standard deviation respectively (408). Dotted-lines represent the 5<sup>th</sup>-95<sup>th</sup> percentile range. Dashed horizontal and vertical lines originated from each axis represent day 7 concentration (280 ng/mL) and simulation day respectively.

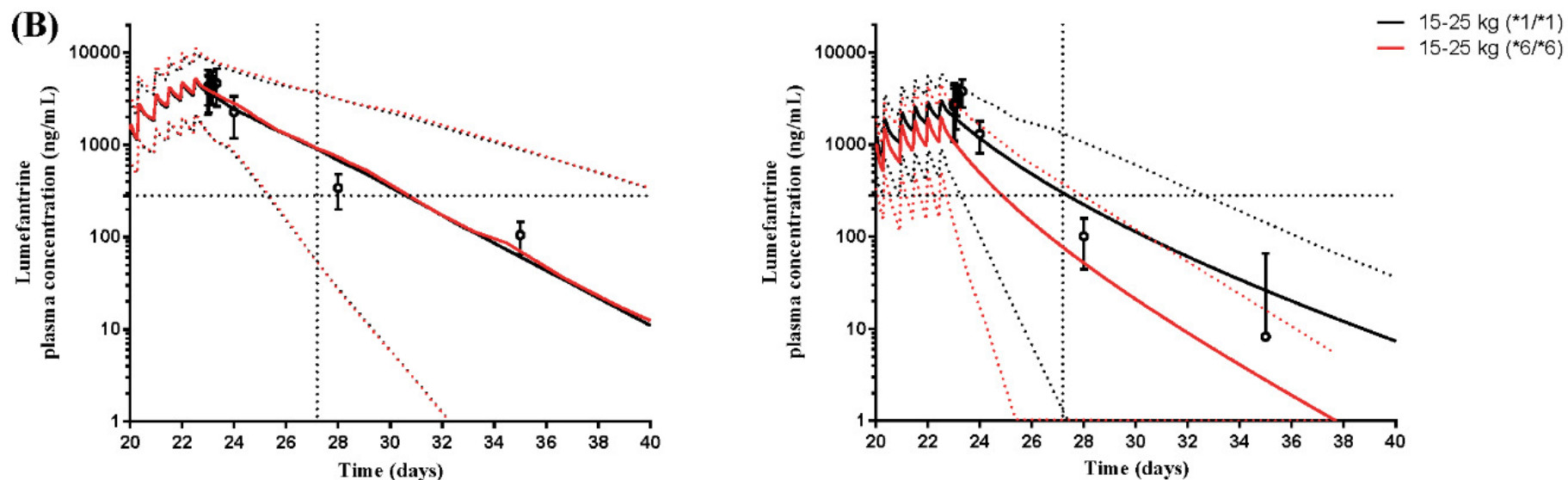


**Figure 3.16B: Simulated median plasma concentration-time profile of lumefantrine administered to Ugandan children in the absence and presence of efavirenz (15-25 kg).**

Lumefantrine (LUM) and efavirenz (EFV) were dosed to Ugandan children aged 3-9 years of age using weight-based dosing strategies of (A) 5-15 kg (LUM: 120 mg per dose; EFV: 200 mg per dose) and (B) 15-25 kg (LUM: 240 mg per dose; EFV: 250-300 mg per dose) with simulated profiles for population groups of all CYP2B6 \*1/\*1 or all CYP2B6 \*6/\*6. All simulations included 40-50 subjects per dosing band. Open circles and error bars represent mean and standard deviation respectively (408). Dotted-lines represent the 5<sup>th</sup>-95<sup>th</sup> percentile range. Dashed horizontal and vertical lines originated from each axis represent day 7 concentration (280 ng/mL) and simulation day respectively.

**Table 3.14 Summary of simulated lumefantrine pharmacokinetic parameters in the absence and presence of efavirenz in children with *CYP2B6* \*1/\*1 and *CYP2B6* \*6/\*6 genotypes.**

			Weight Band	C <sub>max</sub> (ng/mL)	AUC <sub>0-inf</sub> (ng/mL.d)	t <sub>max</sub> (h)	C <sub>d7</sub> (ng/mL)
<b>Lumefantrine</b>	<i>CYP2B6</i> *1/*1	Predicted	5-15 kg	3649 (2093-5857)	15669 (6194-40144)	22.5 (14.1-30.9)	555 (58-2027)
			15-25 kg	5007 (2060-10055)	19855 (5906-60356)	22.5 (14.1-30.9)	675 (27-3115)
	<i>CYP2B6</i> *6/*6	Predicted	5-15 kg	3649 (2093-5857)	15669 (6194-40144)	22.5 (14.1-30.9)	555 (58-2027)
			15-25 kg	5215 (2151-11083)	21083 (6056-64479)	22.5 (14.1-30.9)	672 (22-3105)
	<i>Non-genotyped</i>	Observed	-	4642 (2611-6673)	10547 (5822-15271)	23.3 (19.2-27.1)	340 (199-481)
<b>Lumefantrine + Efavirenz</b>	<i>CYP2B6</i> *1/*1	Predicted	5-15 kg	2494 (702-5193)	7617 (1299-18962)	22.5 (14.1-30.9)	120 (1-508)
			15-25 kg	2994 (893-5933)	10005 (1949-25938)	22.5 (14.1-30.9)	221 (1-1049)
	<i>CYP2B6</i> *6/*6	Predicted	5-15 kg	1532 (383-3420)	3691 (596-9807)	22 (14-30)	20 (1-81)
			15-25 kg	1979 (505-4582)	5146 (912-13743)	22.5 (14.1-30.3)	51 (1-269)
	<i>Non-genotyped</i>	Observed	-	3795 (2543-5047)	6053 (3840-8267)	23.3 (19.2-27.1)	111 (65-157)

Data represents median (range).

### 3.3.6 Step 5: Paediatric dose evaluation prediction

Given the variability in *CYP2B6* polymorphisms across different population groups, it was essential to assess the risks associated with antiretroviral agents, such as efavirenz, attenuating CYP-mediated drug metabolism of antimalarials, where variability in efavirenz plasma concentrations, as a result of poor metabolism, may alter antimalarial concentrations in a highly polymorphic *CYP2B6* population groups. Confounding this is *CYP2B6* ontogeny, where expression is known to be low at < 1 years (10-30% of adult mRNA/protein/activity) and stabilising at approximately 18 years of age (436, 437). Simulations were therefore conducted to predict the impact of efavirenz on lumefantrine plasma concentrations for subjects aged 0.25-13 years of age where weight-based dosing was used, with efavirenz dosed for at least 20 days prior to the initiation of lumefantrine to establish the stable induction of *CYP3A4*.

In the absence of an increase in the treatment duration, significant difference in the percentage of subjects possessing a  $C_{d7}$  above the 280 ng/mL threshold were apparent ( $P < 0.001$ ) between \*1/\*1 and \*6/\*6 alleles for all dosing bands, with 1-11% of \*6/\*6 subjects attaining this threshold (Table 3.15). With an increase in treatment duration of 5- or 7-days (Figure 3.17), an increase in the percentage of subjects attaining the target  $C_{d7}$  was evident (Table 3.15) and most noticeable for the \*6/\*6 population group for the 7-day regimen where 28-57% of subjects attained the target concentrations across all dosing bands (Table 3.15).

Further, extension of the dosing interval from 5-days to 7-days did not alter the half-life within the same genotyped subjects (\*1/\*1 or \*6/\*6). However a significant decrease in the half-life ( $P < 0.001$ ) was noted when comparing the same dosing regimen extension but across the different genotypes. Additionally, when comparing the half-life across increasing dosing-bands, the half-life increased but this was not significant ( $P > 0.05$ ) (Table 3.16).

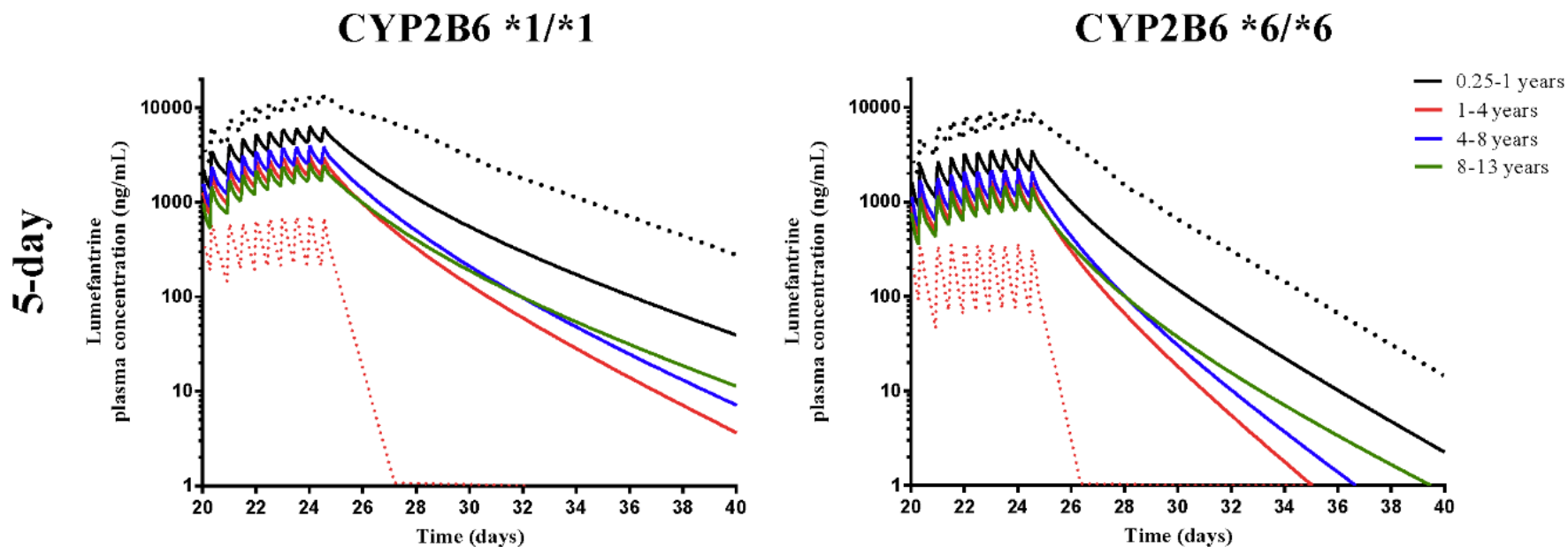


**Figure 3.17A Simulated mean plasma concentration-time profile of lumefantrine administered in a 5-day to Ugandan children.**

Lumefantrine (LUM) and efavirenz (EFV) were dosed to Ugandan children aged 0.25-13 years of age using weight-based dosing strategies (0.25-1 year-old (120mg LUM/300mg EFV), 1-4 year-old (120mg LUM/400mg EFV), 4-8 year-old (240mg LUM/500mg EFV) and 8-13 year-old (240mg LUM/600mg EFV)), with population groups simulating all EFV extensive metabolisers (*CYP2B6* \*1/\*1) or poor metabolisers (*CYP2B6* \*6/\*6). All simulations included 40-50 subjects per dosing band. Upper and lower dashed lines represent the 95<sup>th</sup> percentile for the 0.25-1 years old and 5<sup>th</sup> percentile for the 1-4 years old groups respectively.

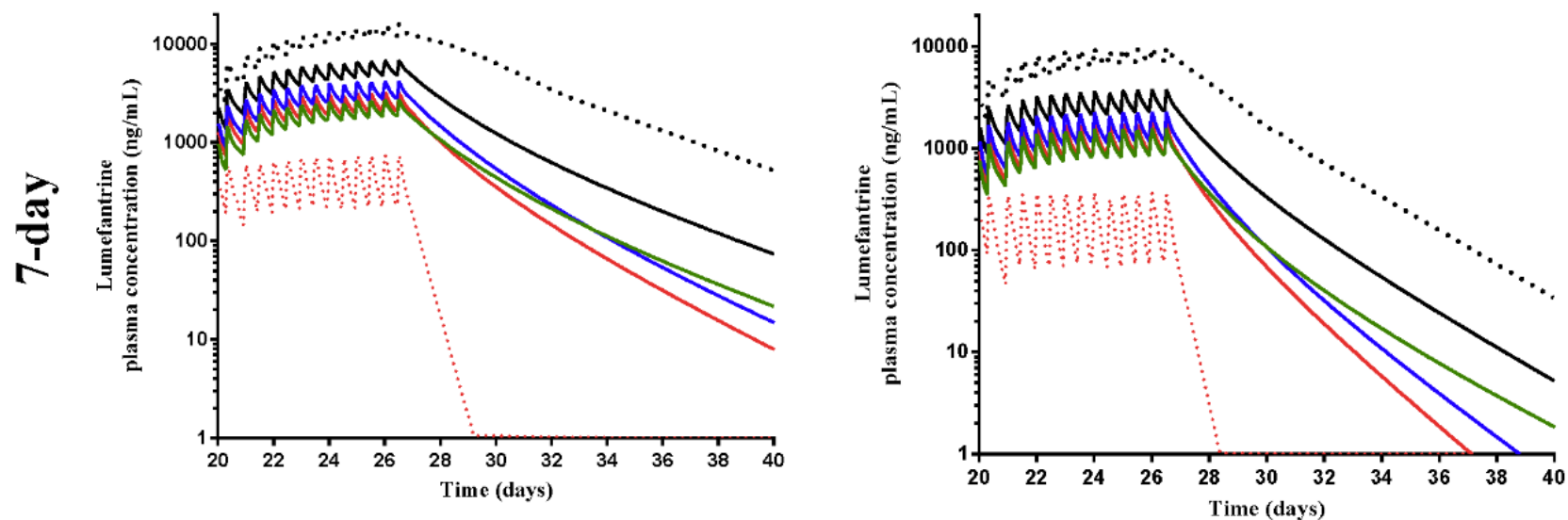


**Figure 3.17B: Simulated mean plasma concentration-time profile of lumefantrine administered in a 7-day regimen to Ugandan children**

Lumefantrine (LUM) and efavirenz (EFV) were dosed to Ugandan children aged 0.25-13 years of age using weight-based dosing strategies (0.25-1 year-old (120mg LUM/300mg EFV), 1-4 year-old (120mg LUM/400mg EFV), 4-8 year-old (240mg LUM/500mg EFV) and 8-13 year-old (240mg LUM/600mg EFV)), with population groups simulating all EFV extensive metabolisers (*CYP2B6* \*1/\*1) or poor metabolisers (*CYP2B6* \*6/\*6). All simulations included 40-50 subjects per dosing band. Upper and lower dashed lines represent the 95<sup>th</sup> percentile for the 0.25-1 years old and 5<sup>th</sup> percentile for the 1-4 years old groups respectively.

**Table 3.15 Summary of the percentage of subjects attaining a lumefantrine C<sub>d7</sub> > 280 ng/mL**

Age-band (years)	Dosing		Lumefantrine ≥ 280 ng/mL <sup>a</sup>					
	Lumefantrine (mg)	Efavirenz (mg)	<i>CYP2B6*1/*1</i>			<i>CYP2B6*6/*6</i>		
			3-day	5-day	7-day	3-day	5-day	7-day
0.25-1	120	300	27	54	82	11	20	57
1-4	120	400	11	29	64	1	5	28
4-8	240	500	18	44	77	4	11	36
8-13	240	600	13	37	72	2	9	35

<sup>a</sup> Percentage of subjects with C<sub>d7</sub> ≥ 280 ng/mL, where a population group of 100 were used for all simulations.  
C<sub>d7</sub>: day-7 lumefantrine plasma concentration.

**Table 3.16 Summary of predicted mean day 7 lumefantrine concentrations during a 5 and 7-day treatment schedule in children stratified for *CYP2B6*\*1/\*1 and *CYP2B6*\*6/\*6 genotypes (n=100).**

Age-band (years)	Weight-band (kg)	Dosing		Mean C <sub>d7</sub> (Range) (ng/mL)				Mean half-life (t <sub>1/2</sub> ) (SD) (h)			
		Lumefantrine (mg)	Efavirenz (mg)	<i>CYP2B6</i> *1/*1		<i>CYP2B6</i> *6/*6		<i>CYP2B6</i> *1/*1		<i>CYP2B6</i> *6/*6	
				5-day	7-day	5-day	7-day	5-day	7-day	5-day	7-day
0.25 - 1	5 - 6.9	120	300	1100 (1-5585)	2800 (45-10345)	306 (1-1497)	1030 (11-4308)	27.18 (8.36)	27.18 (8.36)	19.12 (6.98)	19.12 (6.98)
1 - 4	7 - 13.9	120	400	325 (1-1515)	1013 (17-3327)	65 (1-259)	305 (3-1072)	28.12 (10.68)	28.12 (10.68)	21.03 (7.91)	21.03 (7.91)
4 - 8	14 - 16.9	240	500	496 (1-1735)	1456 (45-4374)	100 (1-380)	438 (7-1568)	29.12 (11.11)	29.12 (11.11)	22.11 (8.51)	22.11 (8.51)
8 - 13	17 - 24.9	240	600	397 (3-1843)	1053 (56-3456)	100 (1-390)	359 (9-1315)	30.62 (12.28)	30.62 (12.28)	24.93 (9.78)	24.93 (9.78)

Half-life was calculated from the final dose. SD: standard deviation.

### 3.4 DISCUSSION

In 2013 it was estimated that 35 million people were living with HIV worldwide with sub-Saharan Africa accounting for 71% of the total global burden, predominantly centred around Southern and Eastern African countries (South Africa > Nigeria > Mozambique > Uganda > Tanzania > Zambia > Zimbabwe > Kenya > Malawi > Ethiopia) (438). Further at least 1 million pregnancies are complicated by the co-infection of malaria and HIV, resulting in a paediatric population group which may be subjected to complex pharmacotherapy (439).

Although HIV infections can directly impact upon malaria through changes in parasitaemia (440), as well as the severity of the disease and mortality rates during pregnancy (441), the use of weight-based dosing strategies and fixed-dosed combination system for both antiretroviral therapies and antimalarial therapies can hinder mitigation of DDIs.

A recent systematic review by Seden *et al.* (2017) (442), assessed the literature reported DDIs between subjects co-administered with HIV and malaria pharmacotherapy. They identified efavirenz as being an important mediator of DDIs, particularly when co-administered with artemisinins (and lumefantrine), leading to reduced antimalarial plasma concentrations and potential recrudescence.

Efavirenz is a non-nucleoside reverse transcriptase inhibitor (NNRTI), being predominantly metabolised by *CYP2B6* and an inducer of *CYP3A4*. These interactions with CYP isozymes can complicate both antiretroviral therapy and antimalarial therapy. Further confounding this, is the fact that *CYP2B6* is highly polymorphic, with the most common variant alleles resulting in two amino acid changes, *Q172H* and *K262R*, and referred to as the \*6/\*6 polymorphism with wild-types as \*1/\*1. The \*6/\*6 polymorphism has been reported to lead to a 65% reduction in protein expression and 50% reduction in mean enzyme activity in the homozygous state (380). Further, although *CYP2B6* contributes towards between 2-10% of total CYP content (376), the \*6/\*6 genotype can result in a 2- or 3-fold higher efavirenz plasma concentrations (378, 387-389), with this genotype being more frequent in African population groups than Caucasian population groups (375, 392). A consequence of this alteration in efavirenz plasma concentration would be a greater ability of efavirenz to induce *CYP3A4* (353, 390, 391).

### 3.4.1 Characterisation of selected populations

The approach used in constructing the age-weight mathematical equations addressed the variability between the Ugandan and Caucasian populations. In the adult population, the higher mean weight range observed in the Caucasian male group (80.85 kg  $\pm$  13.92 kg (19.96 years  $\pm$  6.82 years)) and the Ugandan female population (70.93 kg  $\pm$  21.62 kg (36.01 years  $\pm$  11.09 years)) coincides with the trends observed in the WHO Global Health Observatory Data (Mean BMI in 2016: Caucasians: 27.3 kg/m<sup>2</sup> (male) vs. 27 kg/m<sup>2</sup> (female) ; Ugandan: 29.3 kg/m<sup>2</sup> (female) vs. 25 kg/m<sup>2</sup> (male)) (443).

Trends observed in the paediatric population demonstrated that the Caucasian group had a higher mean weight range (69.94 kg  $\pm$  26.63 kg (17.99 years  $\pm$  6.85 years)) when compared to the Ugandan population, with similar trend reported in the WHO data (Mean BMI in 2016: Caucasians: 19.5 kg/m<sup>2</sup> vs Ugandan: 17.4 kg/m<sup>2</sup>) (443). Factors that could potentially lead to these variabilities include malnutrition, cultural and traditional perception concerning body size, and degree of urbanisation (444). In terms of pharmacokinetics, weight, volume of distribution ( $V_d$ ), clearance (CL), and elimination half-life ( $t_{1/2}$ ) play an important role in determining drug disposition in the human body especially for infants, children or obese patients (445, 446). Since  $V_d$  of a drug depends upon its degree of plasma protein binding, tissue blood flow and physiochemical properties, the design of any treatment regimens should account for any significant differences in the  $V_d$  and CL especially for vulnerable subjects, i.e. infants, children and obese. As an example, the  $t_{1/2}$  of a drug is dependent on both the CL and  $V_d$ . Since both are biologically independent entities, changes in the  $t_{1/2}$  of a drug in obese patients will reflect changes in the CL,  $V_d$ , or both.

Pharmacokinetics assessment of drug therapy in paediatric population groups is often neglected due to ethical complications and the sparse plasma sample collections inherent in such population groups. However, PBPK modelling represents a novel modelling strategy that has gained regulatory acceptance (447) in its applications in the paediatric population and has been used previously to model malaria pharmacokinetic in special population groups such as paediatrics (405) and pregnancy populations (401).

### 3.4.2 Model validation and DDI dose evaluation in paediatric populations

Recently, we demonstrated the ability of rifampicin to alter antimalarial drug concentrations through a CYP3A4-induction process, and thereby reducing  $C_{d7}$  (405). In this present study, we addressed the impact of a similar induction process with the confounding complexity of potential CYP2B6 polymorphisms on the pharmacokinetics of lumefantrine in paediatric population groups. In this study, we adopted a 5-stage modelling approach which spanned efavirenz and efavirenz-lumefantrine DDI model predictions in adults in African and Healthy Volunteer population groups (Steps 1 and 2), followed by efavirenz and efavirenz-lumefantrine DDI model predictions in African and Healthy Volunteers paediatric populations (Steps 3 and 4). This culminated in predictions of potential DDI risks in *CYP2B6* genotyped paediatric population groups with an assessment of the impact of a revised dosing adjustments on  $C_{d7}$  (Step 5).

Although efavirenz is a compound that has been previously developed and validated by researchers associated with Simcyp (413), step 1 attempted to predict efavirenz concentration profiles in a African population groups with altered CYP2B6 abundances (6.9 and 2.4 pmol/mg for \*1/\*1 and \*6/\*6 genotypes), in contrast to those of the default values set by Simcyp within the Healthy Volunteer population group (17 pmol/mg and 6 pmol/mg). This step integrated revised CYP2B6 abundances for EM and PM phenotypes, based on the incorporation of these abundances into a Simcyp developed South African population group, and *in-lieu* of any further published Ugandan CYP2B6 abundances (423, 424).

In adults, successful predictions of efavirenz concentrations were validated against 2 clinical trials in both single (Table 3.7) and multiple dosing (Table 3.8) regimens in Ugandan population groups, with model predictions within 2-fold of the reported  $C_{max}$ , AUC or single day point concentrations from clinical studies for each genotype. Following validation of genotype-specific efavirenz pharmacokinetics, we next attempted to simulate the proposed lumefantrine-efavirenz DDI, whereby efavirenz would induce CYP3A4 expression, resulting in reduced lumefantrine plasma concentrations.

A healthy volunteer population was first utilised to demonstrate successful  $C_{d7}$  predictions, which were within 2-fold of that reported by Huang *et al.* (2012) (414). This was subsequently extended

to simulate the DDI in a South-African population group, as a surrogate for the use of a Tanzanian population group, where the clinical DDI was reported within each CYP2B6 genotype (425, 435). Based on recent age-weight relationships for malaria subjects in Africa, we assumed that the South African population group would demonstrate similar demographics to that of the Tanzanian population (422), and this was further supported by the lack of reported CYP2B6 specific abundance data for EM or PM phenotypes within the Tanzanian population group.

As expected, in the absence of efavirenz,  $C_{d7}$  were well predicted for both genotypes, confirming that in the absence of efavirenz, CYP2B6 \*6/\*6 has no significant effect on lumefantrine pharmacokinetics (358). In the presence of efavirenz, simulations with the \*1/\*1 and \*6/\*6 population groups resulted in predictions for median  $C_{d7}$  to within 2-fold of those reported, albeit with a broader range of values across the simulation study (358, 435), and demonstrated that lumefantrine pharmacokinetics are significantly altered following co-treatment with efavirenz.

Having established a working model for genotype-based DDI predictions in adult, we subsequently assessed the ability to predict efavirenz plasma concentrations within an African paediatric population group, using a custom developed Ugandan paediatric population group and validated against 3 clinical studies employing/reporting weight-based dosing strategies in non-genotyped (23, 409, 410) and genotyped subjects (411). The validation of efavirenz concentrations within an African paediatric population group was important as any changes in efavirenz plasma concentrations, for example as a result of the impact of CYP2B6 genotypes, would be the key function for driving a DDI with lumefantrine, the extent of which would, therefore, be sensitive to change in the availability of efavirenz. For both non-genotyped (Figure 3.12-3.14) and genotype predictions (Figure 3.15), overall 5<sup>th</sup> and 95<sup>th</sup> percentiles of the mean/median predicted profiles were within the range reported in existing published literature and contributed to our efavirenz validation attempts. However, for the high dose administration (25 mg/kg) (Figure 3.14), we were unable to capture the wide variability in the absorption phase reported (410), and this may have been a result of the influence of food on the absorption and bioavailability of efavirenz.

Having established a working model for efavirenz-mediated DDIs in paediatric predictions, we addressed the ability of this model to predict the lumefantrine-efavirenz DDI, and validation was attempted based upon a report of the interaction in Ugandan children across an age range of 3.1-

8.6 years and weight range of 11.4-25.1 kg, using weight-based dosing for both efavirenz and lumefantrine (408) (Figure 3.16). The reported study did not differentiate lumefantrine plasma concentration profiles by genotype, although our simulations were stratified for two extreme cases of an entire population of *CYP2B6* \*1/\*1 or entirely *CYP2B6* \*6/\*6, and this represent the 'best' and 'worst' clinical scenarios. Further, the wider  $C_{d7}$  range simulated in our studies for purely \*1/\*1 populations was outside of the range reported by Parikh *et al.* (2016) (408), however we considered the 'best' and 'worst' clinical scenarios and a proportional 'mixed' genotype population (as potentially sampled by Parikh *et al.* (2016) (408)) would have corrected this disparity.

This study demonstrated a significant difference in median  $C_{d7}$  in the presence and absence of efavirenz and confirmed the capability of efavirenz to initiate this DDI. In our model simulations across all weight bands, we demonstrated a similar significant reduction in  $C_{d7}$ , which was more apparent and resulted in significantly lower ( $P < 0.001$ ) lumefantrine in  $C_{d7}$  in the \*6/\*6 compared to \*1/\*1 population group (Table 3.14).

We previously demonstrated that an increase in lumefantrine treatment duration would significantly increase  $C_{d7}$  under rifampicin-mediated *CYP3A4* induction, and this formed the basis of attempting to address the significantly lower number of \*6/\*6 subjects capable of attaining target  $C_{d7}$  (405). Orally administered lumefantrine is known to display saturated absorption kinetics (448), and therefore increasing the dose of lumefantrine administered within each fixed-dose combination would not be appropriate. Therefore, having established the risk of DDI between efavirenz and lumefantrine (Step 4) the treatment duration was extended to a 5-day or 7-day regimen.

The change in dosing schedule to 7-day regime resulted in a greater number of \*6/\*6 subjects attaining the target  $C_{d7}$ , with 28-57% of subjects (Table 3.15) attaining this across the age bands studied (Figure 3.17). The greatest increase in those attained target  $C_{d7}$  was evident with 1-4 years old (3-day: 1%; 7-day: 28%) (Table 3.15), and this may be accounted for by the maturation of *CYP3A4* which would be the key driver for influencing lumefantrine plasma concentrations. *CYP3A4* ontogeny is known to rapidly increase over this age range (449) to approach adult levels at approximately 6-years onwards.

Determination of the half-life of lumefantrine, typically difficult in paediatrics subjects, given the long-terminal half-life (2-6 days) (450) and the often sparse nature of plasma collections. A recent study by Parikh *et al.* (2016) (408) in Ugandan children (3.1-8.6 years) reported the median half-life of lumefantrine when dosing in the presence of efavirenz, as 23.7 hours. When comparing model predictions of the half-life across all age range simulations (0.25-13 years), our predictions are broadly in line with those of Parikh *et al.* (2016) (408). Further, the extension of the dosing interaction from 5-days to 7-days does not alter the half-life within the same genotype (Table 3.16), suggesting this extension would not alter the elimination clearance of lumefantrine. As expected, the \*6/\*6 subjects demonstrated a significant decrease in half-life of lumefantrine, which would correspond to the increased circulating concentration of efavirenz, thereby handing the DDI and reducing the residency of lumefantrine within the subjects (Table 3.16). However, although CYP2B6 ontogeny may influence circulating efavirenz (436, 437), the impact of this DDI may be less apparent or masked by the rapid changes in CYP3A4 ontogeny across this range, which would directly influence circulating lumefantrine concentrations. Further clinical studies are encouraged to delineate the relative impact of CYP3A4 and CYP2B6 ontogeny on the extent of this DDI.

Given the resource limitations and cost implications of dose extensions, we halted the study at a 7 day dosing regimen and believe further extended dosing would likely not succeed clinically, due to medicine adherence concerns in resource-limited countries (451). While a 5- or 7-day extension may not result in all subjects attaining the target  $C_{d7}$ ; the proposed extension can be considered to be a pragmatic approach, given the complexity of treatment regimens in developing countries. Further, using a standard 3-day regimen Parikh *et al.* (2016) (408) demonstrated that the median lumefantrine  $C_{d7}$  for 3.1-8.6-year-old, 111 ng/mL, was significantly below the target concentration in the presence of efavirenz. Therefore, although there may be some scope for further optimisation, the 5- or 7-day regimen would provide a greater level of subject's attainment appropriate  $C_{d7}$  compared to existing 3-day regimens. Despite the paucity in clinical data investigating altered dosing regimens for efavirenz-mediated DDI with lumefantrine, the relationship between the DDI, resultant reduction in lumefantrine concentration (primarily based around changes in day-7 concentration) and the emergence of recurrent malaria has recently been highlighted in studies by

Parikh *et al.* (2016) (408) and Maganda *et al.* (2014) (452). Finally, a number of groups are now advocating increasing the dosing duration to counteract this interaction (345, 453).

### 3.5 CONCLUSION

Although the rates of malaria infections have decreased globally, persistent complications still exist in 'at-risk' population groups, particularly paediatrics and pregnant women (397, 454). This is further confounded in situations where genetic polymorphisms contribute towards cross-population variability in complex pharmacokinetics situation, such as antiretroviral mediated-DDIs, may increase the risk of parasite resistance and treatment recrudescence.

Exploration of these risks is difficult clinically, however population-based pharmacokinetic modelling provides a practical approach for simulating such complex interactions. This study attempted to explore the application of PBPK modelling to simulate the pharmacokinetics of drugs in special population, specifically, the paediatrics. In addition, we also attempted to address the impact of complex DDIs associated with genotype-specific effects as well as managing these effects via dose optimisation.

This study focussed on predicting the risk of efavirenz-mediated DDIs on lumefantrine pharmacokinetics in African paediatric population groups with consideration of the polymorphic nature of CYP2B6. We demonstrated that an extension of the current artemether-lumefantrine treatment regimen from 3-days to 7-days would counteract the reduction in efavirenz metabolism common with the  $*6/*6$  genotype and hence enhance the attainment of the target day-7 lumefantrine concentration in both  $*1/*1$  and  $*6/*6$  genotype groups, thereby reduce the risk of recrudescence.

## **CHAPTER 4**

# **The application of PBPK modelling to address the impact of inter-ethnic variability on the pharmacokinetics of drugs in Malaysian subjects**

### **Disclaimer**

Elements of this chapter have been published as follows:

Zaril Zakaria, Alan Y.Y. Fong and Raj K. S. Badhan. Clopidogrel pharmacokinetics in Malaysian population groups: the impact of inter-ethnic variability. *Pharmaceuticals*. 2018; 11:74.

DOI: 10.3390/ph11030074

## 4.1 INTRODUCTION

Malaysia is a multi-ethnic society with a population of over 32 million which is comprised of three predominant ethnic groups, namely Malays (50.1%), Chinese (20.8%) and Indians (6.2%) (455). In a recent report by the Malaysian National Centre for Adverse Drug Reaction, 13,789 of adverse drug reactions were reported during the period from 2015 to 2016 (456). Given the mixed ethnicity of Malaysia, the impact of pharmacogenetics between different ethnic groups may contribute significantly to the prevalence of toxicity and ineffective clinical therapy (457-459).

One of the leading cause of mortality in Malaysia is cardiovascular disease (CVD) which accounts for 16 % of all hospital deaths annually (460). Among those deaths, ischaemic heart disease accounts for the majority of all reported cardiovascular mortality, followed by acute myocardial infarction. Further, mortality rates have increased steadily since 1990 despite improvements of the health services (460).

CVDs accounted for approximately 17 million deaths per year and considered to be one of leading causes of death in the world (461). Atherosclerosis encompasses the majority of CVDs and is an underlying disease process in the blood vessels which results in cerebrovascular disease (stroke) and coronary heart disease (heart attack) (461, 462). The pathogenesis of atherosclerosis in the walls of blood vessels is complex and develops over several years. During this process, cholesterol and fatty constituents are deposited surrounding the lumen of the arteries which causes the inner surface of the arteries to become narrow and irregular. These deposits or plaques make it harder for blood to flow through and eventually the plaques rupture and form a thrombosis (blood clot). The location of the blood clots determines the type of disease. Heart attack occurs whereby the blood clots develops in a coronary artery whereas, stroke occurs when there is a blood clot that develops in the brain.

Several risk factors are associated with the promotion of the atherosclerosis process (463), and include: (i) metabolic risk factors such as high cholesterol, obesity, hypertension and diabetes; (ii) behavioural risk factors such as unhealthy diet, tobacco use, alcoholism and physical sedentariness;

and (iii) other risk factors such as genetic disposition, advancing age, stress, depression (464), poverty, excess in homocysteine and gender (men are more likely to develop CVD at an earlier age than women) (465). Of all the three types of risk factors, metabolic and behavioural risk factors play a key role in the attribution of atherosclerosis (461).

Treatments of CVDs are mostly dependent on the type of risk factors the patient has with the aim of relieving symptoms, prevent complications and to reduce the risks of complications from worsening (463). Lifestyle changes such as low-fat and low-sodium diet, exercise, limiting alcohol intake and quitting smoking are generally recommended as an initial treatment for those with metabolic and behavioural risk factors.

Pharmacotherapy approaches varies between risk factors (466-469). Aspirin, a pain reliever, is used extensively to prevent and manage stroke and heart disease. Beta-blockers (acebutolol, propranolol, metoprolol, labetalol) are used to manage hypertension and for the treatment of congestive heart failure. Calcium channel blockers (amlodipine, diltiazem, nifedipine, verapamil) are used to reduce systemic vascular resistance and arterial pressure. Digoxin, a cardiac therapy drug, is used for the treatment of atrial fibrillation. Diuretics (furosemide, spironolactone, hydrochlorothiazide) are used to promotes diuresis, therefore, excreted salt and water through urine which leads to reduction of blood pressure and treat heart disease. Nitrates (isosorbide mononitrate, isosorbide dinitrate) are used to treat angina in patients with coronary artery disease. Warfarin, an anticoagulant, is used to treat thrombosis and also as a stroke prevention therapy. And finally, antiplatelet drugs (clopidogrel, prasugrel, ticlopidine) are used as primary and secondary prevention of cardiovascular disease or thrombotic cerebrovascular.

Clopidogrel is a second generation thienopyridine antiplatelet drug and a prodrug that is metabolised in two pathways: initially by CYP2B6, CYP1A2 and CYP2C19 leading to inactive carboxylic acid derivative (2-oxo-clopidogrel), then by CYP2C19, CYP2C9, CYP2B6 and CYP3A4, leading to its active metabolite (clopi-H4) (470). The active metabolite confers clopidogrel its therapeutic response by inhibition of adenosine diphosphate-induced aggregation, which in turns activate the irreversible binding of the platelet P2Y<sub>12</sub> receptor (471). The contribution of CYP2C19 towards the formation of clopi-H4 has been further confirmed by several

studies (472-474) and is responsible for 45% of the first step and 20% of the second step hepatic biotransformation of clopidogrel (475, 476).

Since CYP2C19 plays an integral element in the metabolism of clopidogrel to its active metabolite, clopi-H4, any disruption or modification in CYP2C19 expression could potentially affect the pharmacokinetic profiles of clopi-H4, hence leading to effects on its therapeutic response (477). Clinically, approximately one fourth of individuals who are treated with clopidogrel exhibit a sub-therapeutic response (478), and this can directly impact upon platelet inhibition, with a loss-of-function genotype reducing platelet inhibition by clopidogrel (479, 480) as a result of reduced clopi-H4 levels (475, 481).

Such genetic polymorphisms in processes governing the pharmacokinetics of drugs (e.g. drug metabolism enzymes), within individuals of a mixed-ethnicity population group, can significantly alter the extent of therapeutic response. Knowledge of genetic polymorphisms within drug metabolism enzymes is sparse within the Malaysian population but some examples have been reported in several studies which have suggested that a higher occurrence of CYP2D6 variants, specifically rs1065852 and rs16947 in Malays, contribute to a higher prevalence of poor metabolisers of debrisoquine, an antihypertensive drug when compared to other East Asian populations (482). Additionally, CYP2C9 polymorphisms were found to exist in Malays and Chinese warfarin-treated subjects which contributed to the variability of the warfarin dose-response relationship in a reported clinical study (483).

More than 50 genetic variants have been identified for CYP2C19 (484). The wild-type *CYP2C19*\*1 allele is related to functional CYP2C19 metabolism, with *CYP2C19*\*2 and \*3 being associated with a loss-of-function (LOF) (485). Gain-of-function (GOF) variants have also been identified and are primarily related to the *CYP2C19*\*17 variant, which results in higher catalytic activity of CYP2C19 (486). Thus, individuals presenting with the homozygote and heterozygote allelic variants \*2/\*2, \*3/\*3, or \*2/\*3 are considered to be representative of a poor metaboliser (PM) phenotypes; those with variants \*1/\*2 or \*1/\*3 (and possibly \*2/\*17 or \*3/\*17) are considered intermediate metaboliser (IM) phenotypes; those with \*1/\*1 are considered wild-type or extensive metaboliser (EM) phenotypes and those with \*17/\*17 or \*1/\*17 are considered

ultra-rapid metabolisers (UM) (487). Significant inter-ethnic differences exist in the prevalence of these allelic frequencies, with the *CYP2C19*\*2 (488) and *CYP2C19*\*3 (489) alleles in the broader Asian populations being significantly higher compared to other racial groups (490, 491). This would suggest that Asian population groups would be more likely to be resistant to clopidogrel therapy. In European population groups, EM phenotypes predominate (~70 %) with approximately 30 % EM and 2 % presenting as PM (492-494). Within the Malaysian population group, Chinese and Malays have broadly similar prevalence of the *\*1/\*1* genotype, 31.6 % and 34.5 % respectively (495), which is significantly lower than that observed within the European population groups (492-494). Further, *\*1/\*17* genotypes were broadly similar (3.5 % and 3.5 % for Chinese and Malays respectively). However, some difference were noted in the prevalence of PM phenotypes, for example, *\*1/\*2* was greater for Chinese (43.9%) compared to Malay (31 %) and *\*1/\*3* was higher for Malay (17.2 % compared to Chinese (3.5 %) (495).

Clinically, LOF genotypes can often result in reduced active metabolite plasma concentrations. For example, in a clinical study by Brandt *et al* (2007) (481), the maximum clopi-H4 plasma concentration ( $C_{max}$ ) for wild-type *CYP2C19* subjects (n = 56) was  $58.4 \pm 9.2$  ng/mL, compared to *CYP2C19*\*2 carriers, for whom the mean  $C_{max}$  was reported to be  $35.3 \pm 4.3$  ng/mL, a 40 % decrease in  $C_{max}$ . Further, pharmacogenetic studies have utilised dose optimisation to counter this reduced clopi-H4  $C_{max}$ , whereby a loading dose of 600 mg followed by a maintenance dose of 150 mg could partially restore clopi-H4 to levels observed with a lower loading dose of 300 mg and the standard 75 mg maintenance dose (472).

The advent of personalised medicine has allowed the clinicians to better respond to the impact of genetic variability on clopidogrel therapy. However such genotyping techniques have met with some contrasting views in relation to their clinic usefulness (496, 497). The impact of anthropometric difference within a diverse patient population group can further confound the understanding of the impact of *CYP2C19* genetic variability within mixed populations, and these factors together may significantly alter the pharmacokinetics of drugs. Examples of these factors may include differences within patient demographics (body weight, age, glomerular filtration rate (GFR)), blood biochemistry (plasma proteins, haematocrit) and drug metabolism enzyme abundances (*CYP* abundance and polymorphism).

Precision medicine allows an individual's unique physiological characteristics to be incorporated into treatment options, whereby treatments are tailored to individual patients based on their individual genetic, biomarker, phenotypic, and psychosocial characteristics (498, 499). To assist in the process of integrating such a diverse range of anthropometric and genetics factors into clinical decision making, the application of pharmacokinetic modelling and simulation has emerged as techniques to better individualise drug therapy. In particular, the field of population-based physiologically based pharmacokinetic (PBPK) modelling has rapidly gained traction by drug regulatory authorities and the wider pharmaceutical industry as a viable means to 'simulate' clinical trials and the pharmacokinetics of drug compounds within virtual population groups representative of individual population groups (159) (169) (160, 161, 170-172). Further, the application of PBPK modelling can allow for the use of population-specific anthropometric variability within virtual subjects, and this was recently demonstrated by our group when considering the optimisation of anti-malarial therapy in sub-Saharan African population groups using PBPK-based virtual clinical trials, where the population groups incorporated anthropometric and biochemical alterations from standard 'healthy volunteer' clinical trials subjects (405, 500).

To our knowledge, we present here the first application of PBPK modelling to develop a Malaysian population group for the specific purpose of understating drug therapy within this mixed-ethnicity population. The study directly addresses this inter-ethnicity variability and provides a research tool that brings together the complexity (at a cellular level) of systems-biology with the easy-of-use applicability of pharmacokinetic modelling to provide a robust predictive platform which can easily be adapted and developed as required within the Malaysian population. The objectives of the present study were 2-fold: (i) to predict clopidogrel pharmacokinetics in the Malay and Malaysian Chinese adult population groups and (ii) to address the impact of the  $*1/*1$ ,  $*2/*2$ ,  $*1/*2$  and  $*1/*17$  genotypes on clopidogrel pharmacokinetics.

## 4.2 METHODS

Population-based PBPK modelling was conducted using the virtual clinical trials simulator Simcyp (Simcyp Ltd., a Certara company, Sheffield, UK, Version 16). Simulations were performed for an exclusively CYP2C19 extensive metaboliser (EM) (*CYP2C19\*1/\*1*), poor metaboliser (PM)

(*CYP2C19\*2/\*2*), intermediate metaboliser (IM) (*CYP2C19\*1/\*2*) and ultrarapid metaboliser (UM) (*CYP2C19\*1/\*17*). For all simulations, dosing occurred under fasted-conditions unless otherwise indicated.

#### **4.2.1 Model development**

A five-stage stepwise approach was implemented for model development, validation and model refinement (Figure 4.1) which is fully described below.

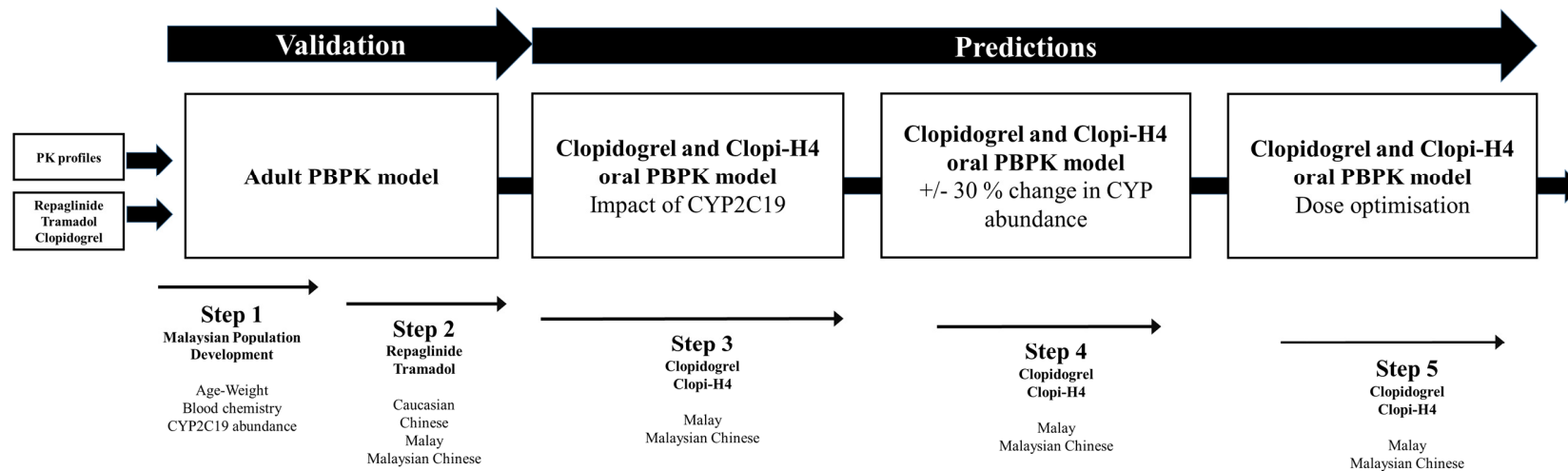


**Figure 4.1 Model development strategy**

A five-stage workflow approach was implemented to study clopidogrel and clopi-H4 pharmacokinetics within Caucasian, Chinese, Malay and Malaysian Chinese population groups.

#### 4.2.1.1 Step 1: Malaysian population development

To develop a Malaysian population group for use in pharmacokinetic modelling, the National Cardiovascular Database (NCVD) Registry (460) was analysed for relevant population-level data. The NCVD register is a Malaysian nation-wide registry consisting of 33,043 anonymised and voluntary patient records for patients undergoing acute coronary syndrome and percutaneous coronary intervention, spanning the years 2006-2015. The NCVD is supported by the Ministry of Health Malaysia and co-sponsored by National Heart Association of Malaysia, with the aim to gather information about cardiovascular diseases in Malaysia. Within this database, relevant physiological parameters were limited to (i) gender; (ii) age; (iii) weight and (iv) ethnicity.

To develop the Malaysian population group the two largest ethnic groups, Malays and Malaysian Chinese, were considered as they constitute 50.1 % and 22.6 % of the total Malaysian population, respectively (455). Appropriate anthropometric age-body weight distributions were generated and used to establish mathematical (polynomial regression) relationships to predict body weight from age, using TableCurve2D (Systat Software, San Jose, CA, USA). The resultant polynomial regression equations were then applied within the population ‘Demographics’ section of Simcyp to create user-defined age-weight relationships for each population. Further, blood chemistry was revised to match reported haematocrit and plasma protein concentrations within the Malay and Chinese population groups, as reported in the literature (Table 4.1).

**Table 4.1 Malay and Malaysian Chinese blood biochemistry**

Biochemistry	Malay	Malaysian Chinese
Haematocrit (%)	M : 43 <sup>b</sup> F : 38 <sup>c</sup>	M : 45.3 F : 40.5
AAG (g/L)	M : 0.65 <sup>a</sup> F : 0.64 <sup>a</sup>	M : 0.65 F : 0.64
HSA (g/L)	M : 47.3 <sup>b</sup> F : 46.3 <sup>b</sup>	M : 50.34 F : 49.38

AAG:  $\alpha$ 1-acidic glycoprotein; HSA: human serum albumin M: male; F: female.  
<sup>a</sup>Simcyp default values; <sup>b</sup>Hamzah *et al.* (2016) (501); <sup>c</sup>Khor *et al.* (2006) (502)

In the absence of literature reported CYP2C19 hepatic abundance in the Malaysian Chinese and Malaysian Malay subjects, the dominant CYP2C19 genotypes, *\*1/\*1* (Extensive metaboliser [EM]), *\*2/\*2* (Poor metaboliser [PM]), *\*1/\*2* (Intermediate metaboliser [IM]) and *\*1/\*17* (Ultrarapid metaboliser [UM]) were allocated a hepatic abundance of 8, 0, 6 and 10 pmol/mg protein respectively, based upon adaptations detailed within in a validated Chinese population group developed by Simcyp, and which is available from population library repository of Simcyp software. These abundances were assumed to be the same for both Malaysian Chinese and Malay population groups.

#### **4.2.1.2 Compound selection**

A search for published clinical studies reporting plasma concentration-time profiles for ethnicity-specific Malaysian patients identified repaglinide, tramadol and clopidogrel as therapeutics drugs where clinical data was available for the population groups of interest. These studies were used for model development and validation. Further, additional clinical studies were identified for Chinese populations for repaglinide and clopidogrel were identified and applied for model development and validation of the Malaysian Chinese population group.

The three compounds of interest had previously been developed and validated by researchers and are available within the Simcyp library compound database, with repaglinide developed and pre-validated by Simcyp (503), tramadol developed and validated by T'jollyn *et al.* (2015) (504) and clopidogrel and its' primary metabolite (2-oxo-clopidogrel) and secondary metabolite (clopi-H4) previously developed and validated by Djebli *et al.* (2015) (477). Physicochemical and pharmacokinetic parameters used in the simulation for repaglinide, tramadol, clopidogrel, 2-oxo-clopidogrel and clopi-H4 (active metabolite) are provided for references in Appendix E.

#### **4.2.1.3 Step 2: Adult simulations with repaglinide and tramadol**

To confirm the validity of the modelling approaches and the appropriateness of the customised Malaysian population groups, validation of repaglinide and tramadol were conducted using five published clinical studies: (i) a single 2 mg oral dose of repaglinide to healthy adult volunteers

(505), (ii) a single 2 mg oral dose of repaglinide on day 1 and subsequently 2 mg multiple doses orally on day 2 to day 9 in healthy young adults (506), (iii) a single 2 mg oral dose of repaglinide dosed to healthy native Han Chinese adult volunteers (507), (iv) a single 4 mg oral dose of repaglinide dosed to healthy adult Malay volunteers (508), and (v) a single dose of 100 mg tramadol given intravenously to adult mixed Malaysian volunteers (509). All simulations replicated the study design reported by the validation clinical studies cited above.

#### **4.2.1.4 Step 3: Prediction of the impact of CYP2C19 polymorphisms on clopidogrel pharmacokinetics**

After successful validation of Simcyp software prediction, this step focused on the validation of clopidogrel and its active metabolite, clopi-H4 in healthy adult volunteers. The metabolism of clopidogrel and its metabolites were modelled using the application of allele-specific intrinsic clearance ( $CL_{int}$ ) for EM, PM, IM and UM phenotypes, as described by Djebli *et al.* (2015) (477). Subsequently, when simulating either entirely EM, PM, IM, and UM phenotypes, the frequency of CYP2C19 genotype was set at 1 for either EM, PM, IM, or UM. The study design used for validation of clopidogrel pharmacokinetics in healthy adult volunteers consisted of a 300 mg loading dose followed by a 75 mg dose orally for 4 days with results phenotyped for EM, PM, IM, and UM for clopidogrel and its active metabolite, clopi-H4 (477). Similar to step 2, all simulations replicated the study design reported in the clinical study cited above.

Subsequently, we next simulated the potential impact of SNPs CYP2C19 on the resultant clopi-H4 target plasma concentration range for patients known to result in a clinical response, namely 0.81 to 13.45 ng/mL (510), within the Malay and Malaysian Chinese population groups. For all simulation, clopi-H4 concentration of below 0.81 ng/mL was used as a cut-off value to depict patients who were unresponsive to clopidogrel treatment. Simulations were performed using the Malay and Malaysian Chinese population groups and stratified across EM, PM, IM, and UM phenotypes. Simulations were performed using a validated clopidogrel compound (18) and using a trial design of 63 adult subjects were administered clopidogrel regimen of a 300-mg loading dose (LD) and a 75-mg/day maintenance dose (MD) for 4 days.

#### **4.2.1.5 Step 4: Sensitivity analysis for CYP2C19 hepatic abundances**

To address the absence of literature reported CYP2C19 hepatic abundances in the Malaysian population, two further scenarios were simulated whereby the mean abundances for the Malay and Malaysian Chinese population were set at 30 % greater/less than that used as default (see Step 1). This allowed for the analysis of the sensitivity of model predictions to changes in abundance to be simulated through assessing the resulting impact on the percentage of subjects attaining clopi-H4 target concentrations.

#### **4.2.1.6 Step 5: Dose optimisation in CYP2C19 poor metabolisers**

This step attempted to predict the potential impact of dosage optimisation in the CYP2C19 PM population, with an aim to recapitulate subjects into the clopi-H4 therapeutic window range. Simulations were run using the Malay and Malaysian Chinese population groups. Further, based on the study by Simon *et al.* (2011) (511) the dosing regimen for clopidogrel was increased to a ‘high-dose’ scenario with a 600 mg loading dose followed by a 4 day regimen of 150 mg daily.

### **4.2.2 Data analysis**

The observed data that was used for visual predictive checks when compared with the simulated profiles were extracted using the WebPlotDigitizer v.3.10 (<http://arohatgi.info/WebPlotDigitizer/>). All simulations of plasma concentration-time profiles were presented in 5<sup>th</sup> to 95<sup>th</sup> percentiles and either in mean or median unless otherwise specified. For all adult simulations, age ranges and subject gender ratios were matched, where possible, to reported clinical studies. Where this information was not cited in clinical studies, a default age range of 20-50 years and gender ratio of 50% was selected. For simulations employing genotypes stratification, unless otherwise stated, a 100-subject simulation was run in a 10x10 trial (10 subjects per trial with 10 trials) per genotypes to ensure that reasonable inter-/intra individual variability is captured within the model simulations.

### **4.2.3 Predictive performance**

In all simulations, a prediction to within 3-fold of the observed data was generally accepted as part of the ‘optimal’ predictive performances range despite there being no uniform standard of

acceptance to determine this criterion (87, 135, 136). This acceptance criterion was used in our  $C_{\max}$  and AUC comparisons with the published clinical data reported. For the clopidogrel simulations, the target clopi-H4 plasma concentration was set at the lowest value of 0.81 ng/mL from the range of 0.81 – 13.45 ng/mL obtained from literature (510) and used to determine the impact of SNPs CYP2C19 on Malay and Malaysian Chinese population pharmacokinetics.

#### **4.2.4 Visual predictive checks**

To further validate model predictions where comparison was made to existing clinical studies, a visual predictive checking (VPC) strategy was adopted. This approach was described at the 2012 FDA Paediatric Advisory Committee (US Food and Drug Administration, 2012) (512). In this approach, to graphically validate the predictability of the model, the 5<sup>th</sup> and 95<sup>th</sup> percentiles (along with mean or median) of predicted concentration-time profiles (generated from Simcyp) were graphically displayed along with the observed data for any validation data sets to ensure predicted data points largely overlapped with those from the observed data sets.

### **4.3 RESULTS**

#### **4.3.1 Step 1: Malaysian population group development**

##### **4.3.1.1 The NCVD database**

The three largest population groups were selected for analysis and identified as Malay, Chinese and Indian, with Malay comprising the largest ethnic group contained within the NCVD (Table 4.2). The mean age, weight and BMI were significantly different between Malay and Malaysian Chinese ( $P < 0.0001$ ) and Malaysian Chinese and Malaysian Indian ( $P < 0.0001$ ), whereas mean height was relatively consistent across all population group (1.63 m) and not statistically significantly different (Table 4.2).

**Table 4.2 Summary demographic data from the NCVD database**

Ethnicity		Age (years)	Height (m)	Weight (kg)	BMI (kg/m <sup>2</sup> )
Malay	Mean	57.75	1.63	69.79	26.19
	N	23114	10250	12193	10170
	SD	11.62	0.08	14.24	4.35
	Median	57.60	1.63	69.50	25.78
	Minimum	20.00	1.30	30.00	14.17
	Maximum	99.50	2.09	179.00	50.00
Malaysian Chinese	Mean	62.89	1.63	67.17	25.11
	N	9929	4111	5259	4086
	SD	12.04	0.08	13.18	3.84
	Median	63.10	1.63	66.00	24.79
	Minimum	20.50	1.30	31.20	14.69
	Maximum	101.90	1.93	178.00	48.07
Malaysian Indian	Mean	57.70	1.63	69.61	25.95
	N	9167	4257	4809	4229
	SD	11.91	0.09	13.91	4.25
	Median	57.30	1.64	69.00	25.52
	Minimum	21.10	1.30	31.50	14.52
	Maximum	100.90	1.97	180.00	48.89

N: total number of recorded metrics; SD: standard deviation.

#### 4.3.1.2 Development of age-weight relationships for Malaysian populations

Polynomial mathematical relationship for gender-specific age-weight relationships for the Malay population group are described in equations 4.1 and 4.2 for 20-65-year-olds:

$$\text{Malay male body weight} = -786.757075 + 105.598305 * \text{age} + 9.79604022 * \text{age}^{1.5} + 0.33871491 * \text{age}^2 + 498.1612119 * \text{age}^{0.5}$$

(4.1)

$$\text{Malay female body weight} = -3348.57622 + 2424.271248 * \text{age}^{0.5} + 676.182360 * \text{age} + 92.98417478 * \text{age}^{1.5} + 6.31405170 * \text{age}^2 + 0.169288237 * \text{age}^{2.5}$$

(4.2)

Visual predictive check (VPC) was performed to confirm a suitable range of age-weight relationships for Malay males (Figure 4.2A) and females (Figure 4.2B), and confirmed model predicted age-weight relationships retained the same distribution across age ranges when compared to the NCVD (Figure 4.2). The model predicted values generally overlapped with the observed NCVD data.

The polynomial mathematical relationship for gender-specific age-weight relationships for the Malaysian Chinese population group is described in equations 4.3 and 4.4 for 20-65-year-olds.

$$\text{Malaysian Chinese male body weight} = (75.50929026 - 3.86906581 * \text{age} + 0.034908233 * \text{age}^2 + 0.001047109 * \text{age}^3) / (1 + 0.04452164 * \text{age} + 0.0000141817 * \text{age}^2 + 0.0000206378 * \text{age}^3)$$

(4.3)

$$\text{Malaysian Chinese female body weight} = 67.51927661 - 0.00194867 * \text{age}^2 + 0.0000000434656 * \text{age}^4$$

(4.4)

VPC were also performed for the Malaysian Chinese male and female populations (Figure 4.3). Similar with the Malay age-weight simulation, the VPC confirmed that the model predicted age-weight relationships retained the same distribution across age ranges when compared to the NCVD (Figure 4.3). The model predicted values generally overlapped with the observed NCVD data.

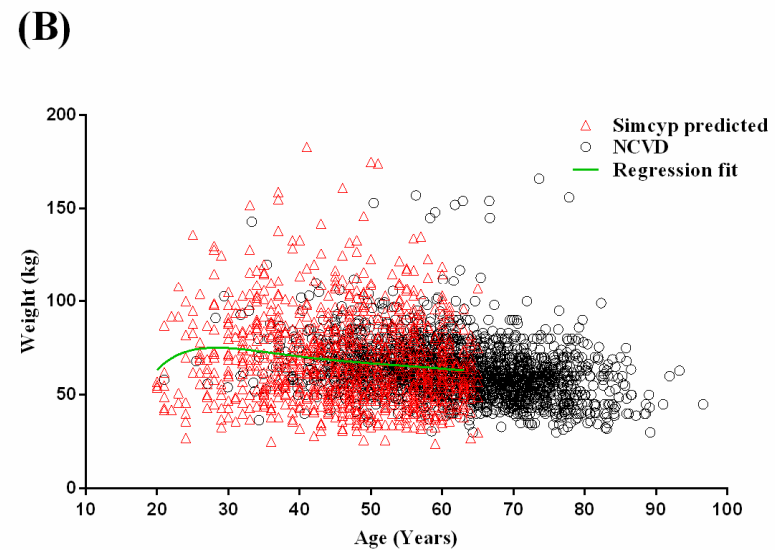
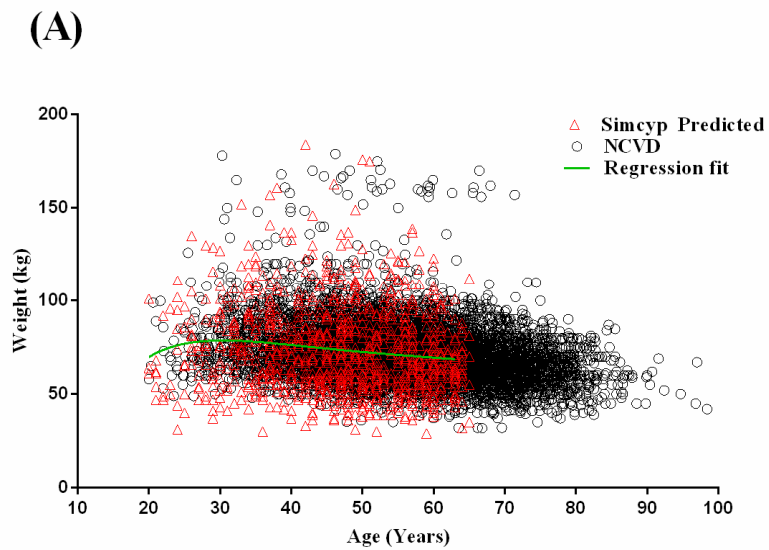
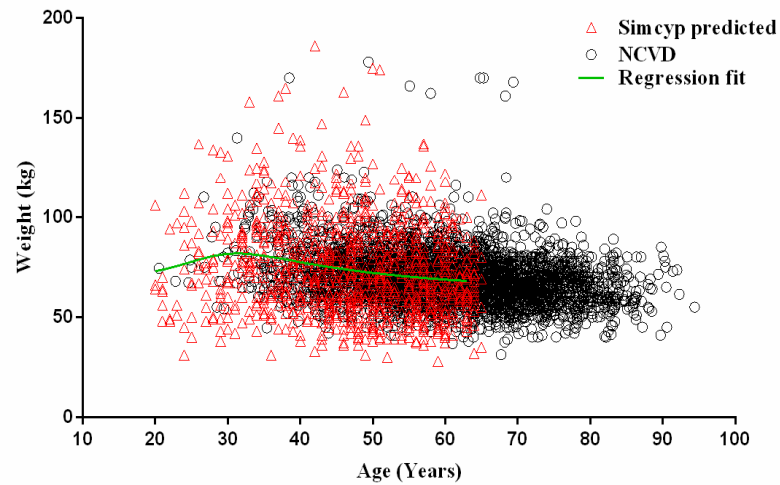


**Figure 4.2 Visual predictive checks on the comparison between predicted and observed (NCVD) age-weight relationship for the Malay male (n=18601) (A) and female (n=4513) (B) populations.**

Red outlined triangles represent the predicted population. Black outlined circles represent the observed population from the NCVD database. Green lines represent the fitted trend-line from the polynomial mathematical relationship.

(A)



(B)

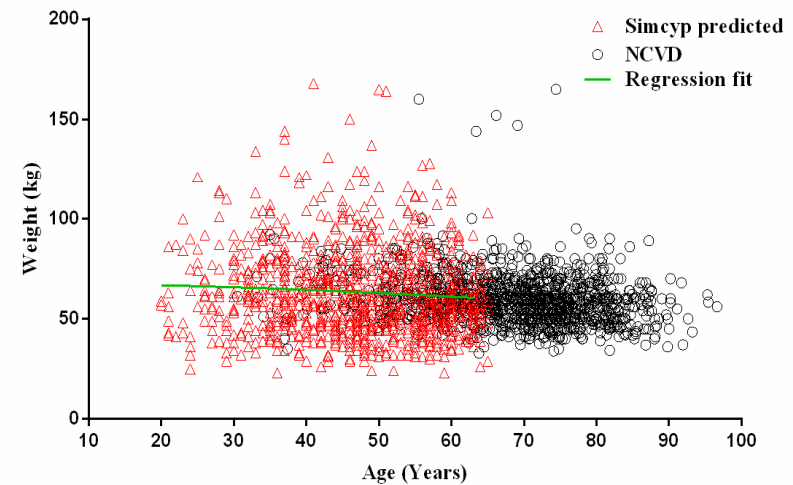


**Figure 4.3 Visual predictive checks on the comparison between predicted and observed (NCVD) age-weight relationship for the Chinese male (n=7445) (A) and female (n=2484) (B) population.**

Red outlined triangles represent the predicted population. Black outlined circles represent the observed population from the NCVD database. Green lines represent the fitted trend-line from the polynomial mathematical relationship.

## 4.3.2 Step 2: Adult simulation with repaglinide and tramadol

### 4.3.2.1 Repaglinide

The repaglinide compound file within the Simcyp library was used in conjunction with the Simcyp ‘Healthy Volunteer’ population group to predict the plasma concentration-time profile for a single 2 mg oral dose of repaglinide in healthy Caucasian subjects. The resultant predictions were within the range of observed reported values (Figure 4.4) with model predicted  $t_{max}$ ,  $C_{max}$  and AUC within 3-fold of the reported parameters (Table 4.3).

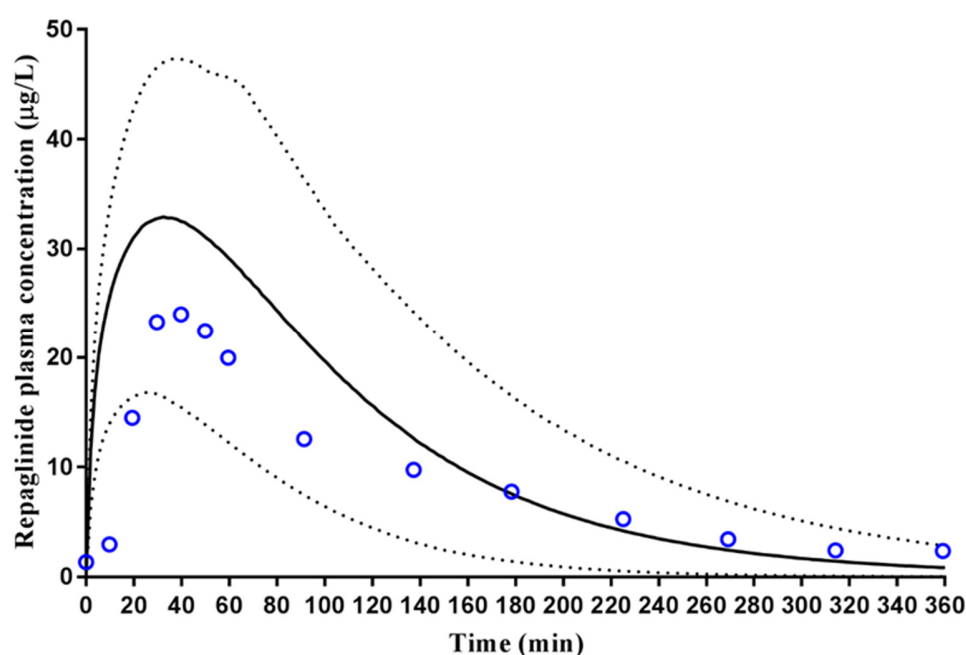


**Figure 4.4 Simulated plasma concentration-time profile of repaglinide in healthy adults.**

A 2 mg oral dose of repaglinide was administered once daily to healthy adult volunteers (n=24). Solid lines represent mean population prediction with dotted-lines representing 5<sup>th</sup> and 95<sup>th</sup> percentile range. Open circles represent data for observed study (Hatorp *et al.* (2002) (505)).

Subsequently, to further validate model simulations, the ability to predict repaglinide plasma concentrations following single and multiple dosing was assessed using a healthy volunteer population group. Predicted plasma concentrations following a single dose (day 1) and multiple

doses (day 9) were within the range reported (506) (Figure 4.5), with model predicted  $t_{max}$ ,  $C_{max}$  and AUC within 3-fold of those reported (506) (Table 4.3).

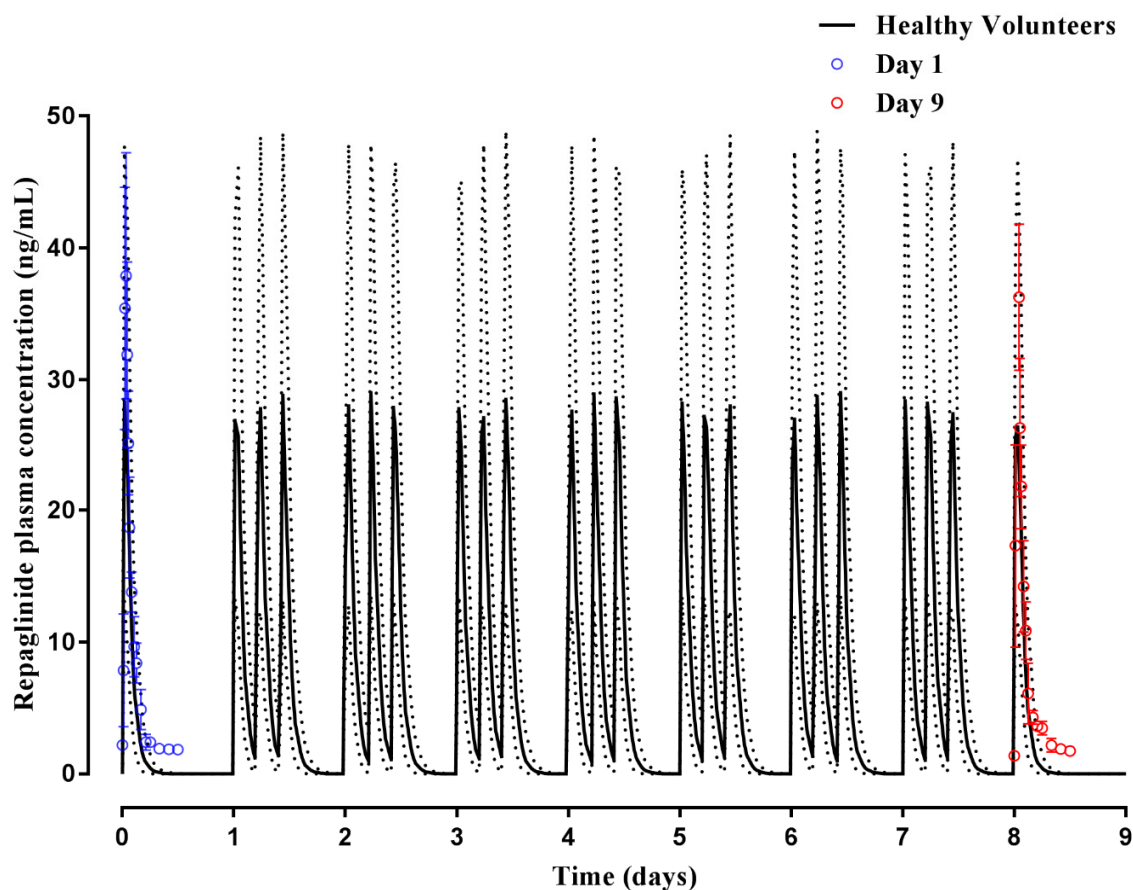


**Figure 4.5 Simulated plasma concentration-time profile of repaglinide following single and multiple oral doses in healthy adults.**

An oral dose of 2 mg repaglinide was administered once daily on day 1, and thereafter daily for 9 days to healthy adult volunteers (n=12) using the healthy volunteers Simcyp population group. Solid lines represent mean predictions with dotted-lines represent the 5<sup>th</sup> and 95<sup>th</sup> percentile range. Open circles represent data for observed study at day 1(single dose) and day 9 (multiple-dosing) (Hatorp *et al.* (1999) (506)).

The model was then extended to assess its application within Malaysian Chinese and Malay population groups. For the Malaysian Chinese population, we utilised the customised Malaysian Chinese population group in the model to predict repaglinide plasma concentrations following a single 2 mg oral dose (Figure 4.6). The predicted repaglinide plasma concentration was within the

range reported with model predicted  $t_{max}$ ,  $C_{max}$  and AUC within 3-fold of those reported (507) (Table 4.3).

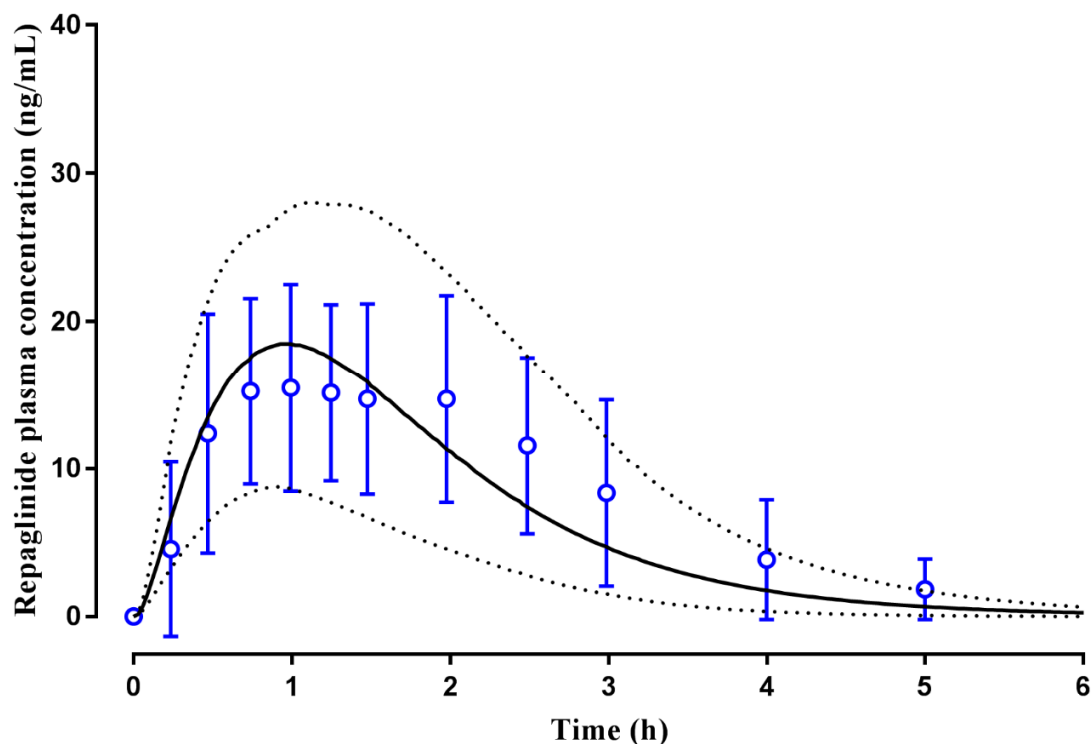


**Figure 4.6 Simulated plasma concentration-time profile of repaglinide in healthy Malaysian Chinese adults.**

A 2 mg oral dose of repaglinide was administered once daily to adult healthy Chinese volunteers (n=22) using the Malaysian Chinese population group. Solid lines represent mean predictions with dotted-lines represent the 5<sup>th</sup> and 95<sup>th</sup> percentile range. Open circles represent data for observed study (Zhai *et al.* (2013) (507)).

For the Malay population group simulation, the model predicted  $C_{max}$  and  $t_{max}$  were within the range reported (Figure 4.7) with AUC and clearance (CL) predictions within 2-fold of that reported (508) (Table 4.3).

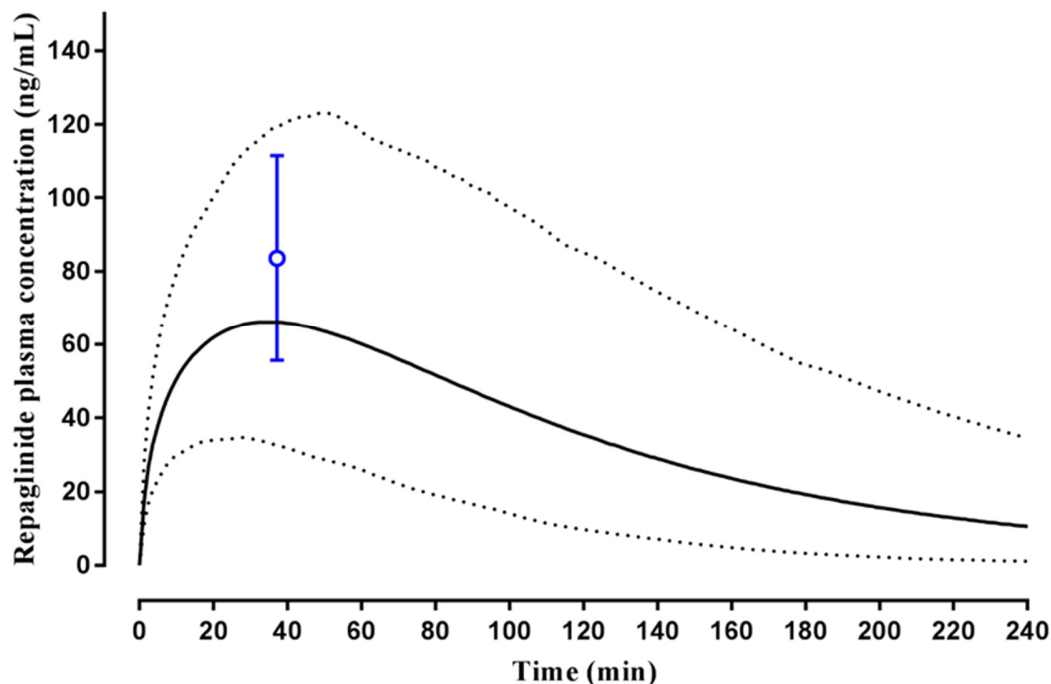


**Figure 4.7 Simulated plasma concentration-time profile of repaglinide in healthy Malay adults.**

A 4 mg oral dose of repaglinide was administered once daily to adult healthy Malay volunteers (n=121) using the custom Malay Simcyp population group. Solid lines represent mean predictions with dotted-lines represent the 5<sup>th</sup> and 95<sup>th</sup> percentile range. Open circle represents data for observed study (Ruzilawati *et al.* (2010) (508)).

#### 4.3.2.2 Tramadol

Tramadol pharmacokinetics have been reported in mixed Malaysian subjects following an IV bolus dose (509). Further, T'jollyn *et al.* (2015) (504) have developed and validated a tramadol compound within Simcyp, and these studies were used as the basis for predicting tramadol pharmacokinetics in the Malay and Malaysian Chinese populations. Following a 100 mg IV-bolus dose of tramadol, simulated plasma concentrations for Malays and Malaysian Chinese were within the range reported by Gan *et al.* (2002) (509) (Figure 4.8) with model predicted CL and AUC within 2-fold of that reported (Table 4.3).

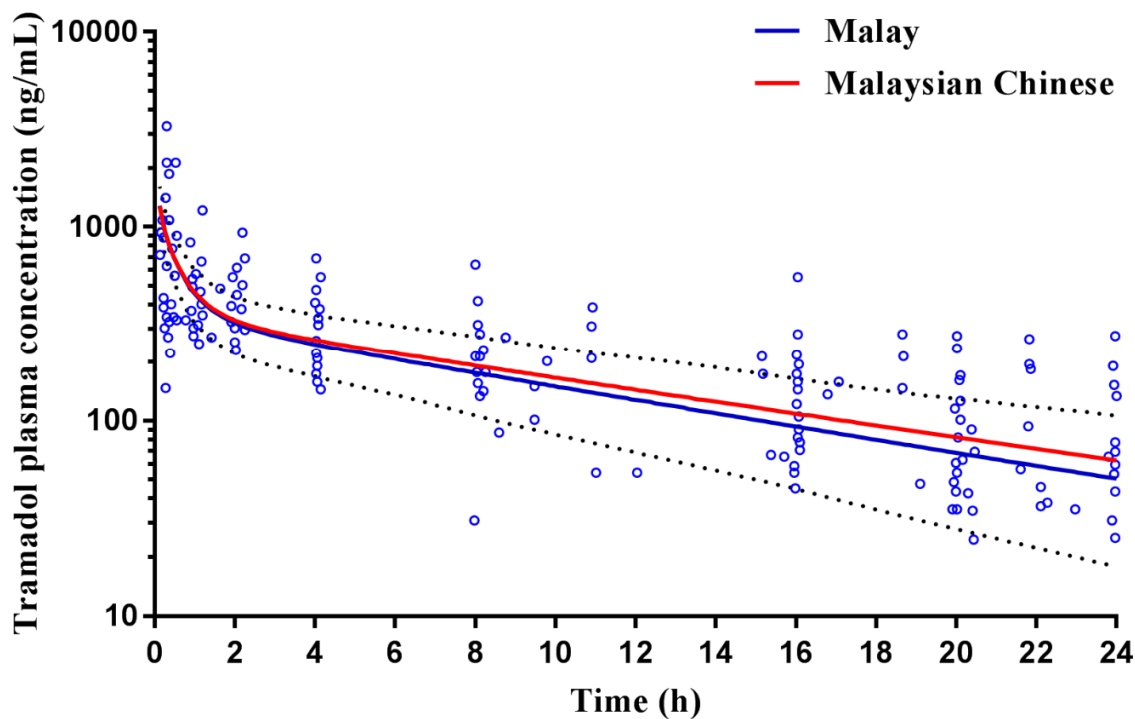


**Figure 4.8 Simulated plasma concentration-time profile of tramadol intravenous bolus dosing in Malay and Malaysian Chinese subjects.**

An IV-bolus dose of 100 mg tramadol was administered to adult healthy mixed Malaysian volunteers (n=100) using the custom Malaysian (Malay and Malaysian Chinese) Simcyp population group. Solid lines represent mean predictions with dotted-lines represent the 5<sup>th</sup> and 95<sup>th</sup> percentile range. Open circles represent data for observed study (Gan *et al.* (2002) (509))

**Table 4.3 Summary of predicted and observed pharmacokinetic parameters of repaglinide and tramadol.**

Compound	Validation	CL (L/h)		C <sub>max</sub> (ng/mL)		t <sub>max</sub> (h)		AUC (ng/mL.h)	
		Observed	Predicted	Observed	Predicted	Observed	Predicted	Observed	Predicted
Repaglinide	Hatorp <i>et al.</i> , 2002 (Healthy volunteers)	-	12.17 (10.03 - 14.77)	26.0 µg/L	32.9 (16.4 - 47.0) µg/L	0.83 (0.31 - 1.35)	0.54 (0.18 - 0.91)	152.4 (62.8 - 242.0) µg/L.h	70.89 (15.51 - 73.82) µg/L.h
	Hatorp <i>et al.</i> , 1999 (Single) (Healthy volunteers)	-	13.9 (10.33 - 18.70)	47.9 (15.9 - 79.9)	26.2 (19.61 - 35.0)	0.8 (0.2 - 1.4)	0.47 (0.31 - 0.60)	69.0 (61.2 - 76.8)	54.87 (21.57 - 106.1)
	Hatorp <i>et al.</i> , 1999 (Multiple) (Healthy volunteers)	-	15.32 (12.24 - 20.57)	58.5 (8.1 - 108.9)	26.39 (11.53 - 46.85)	0.6 (0.5 - 0.7)	0.48 (0.32 - 0.61)	98.1 (84.54 - 111.66)	56.8 (22.59 - 109.1)
	Zhai <i>et al.</i> , 2013 (Chinese) <sup>1</sup>	-	56.66 (21.10 - 146.00) (Malaysian Chinese)	20.0 (14.9 - 25.1)	18.5 (8.79 - 28.0) (Malaysian Chinese)	1.2 (0.5 - 1.9)	0.93 (0.82 - 1.08) (Malaysian Chinese)	46.3 (31.2 - 61.4)	39.51 (16.21 - 74.56) (Malaysian Chinese)
	Ruzilawati <i>et al.</i> , 2010 (Malay)	11.82 (7.86 - 15.78)	10.41 (5.29 - 15.53)	83.56 (55.63 - 111.49)	67.5 (34.4 - 118)	0.62 (0.24 - 1.00)	0.58 (0.20 - 0.96)	340.66 (226.14 - 455.18)	151 (33.61 - 196)
Tramadol	Gan <i>et al.</i> , 2002 <sup>2</sup> (Malaysian)	19.3 (13.1 - 25.5)	19.24 (13.31 - 33.11) (Malay)	-	-	-	-	5078.4	4389 (2915 - 6128) (Malay)
			18.36 (11.73 - 30.19) (Malaysian Chinese)	-	-	-	-	7039.5	4716 (3201 - 6658) (Malaysian Chinese)

Data reported an mean (range). <sup>1</sup> Validation study was reported within a Chinese population group. Simulations were performed within a Malaysian Chinese group for comparison. <sup>2</sup> Validation study was reported within a Malaysian population group without demarking ethnicities. Simulations were performed in Malay and Malaysian Chinese for comparison.

### **4.3.3 Step 3: Prediction of the impact of CYP2C19 polymorphisms on clopidogrel pharmacokinetics in Malaysians**

Having established the ability of the proposed model to predict repaglinide and tramadol compounds in Healthy Volunteers, Malay and Chinese population groups, the model was expanded to assess the impact of the compound of interests, clopidogrel and its active metabolite, clopi-H4 in healthy volunteers population groups phenotyped for EM, PM, IM, and UM.

Simulations were performed in a 'Healthy Volunteers' Simcyp population group and compared to a report of clopidogrel pharmacokinetics in adult healthy volunteers (477) where 63 adult healthy subjects were administered clopidogrel regimen of a 300 mg loading dose (LD) and a 75 mg/day maintenance dose (MD) for 4 days. Based on this dosing approach, predicted clopidogrel concentration profiles (Figure 4.9) were within the range reported for all phenotypes (477) with the predicted  $C_{max}$  and AUC at day 1 and day 5, within the lower and upper limit range of that reported (Table 4.4).

Model predictions for all EM, PM, IM, and UM were generally in good agreement with that published, with a slightly over-prediction at day 1 and day 5 for all phenotypes.

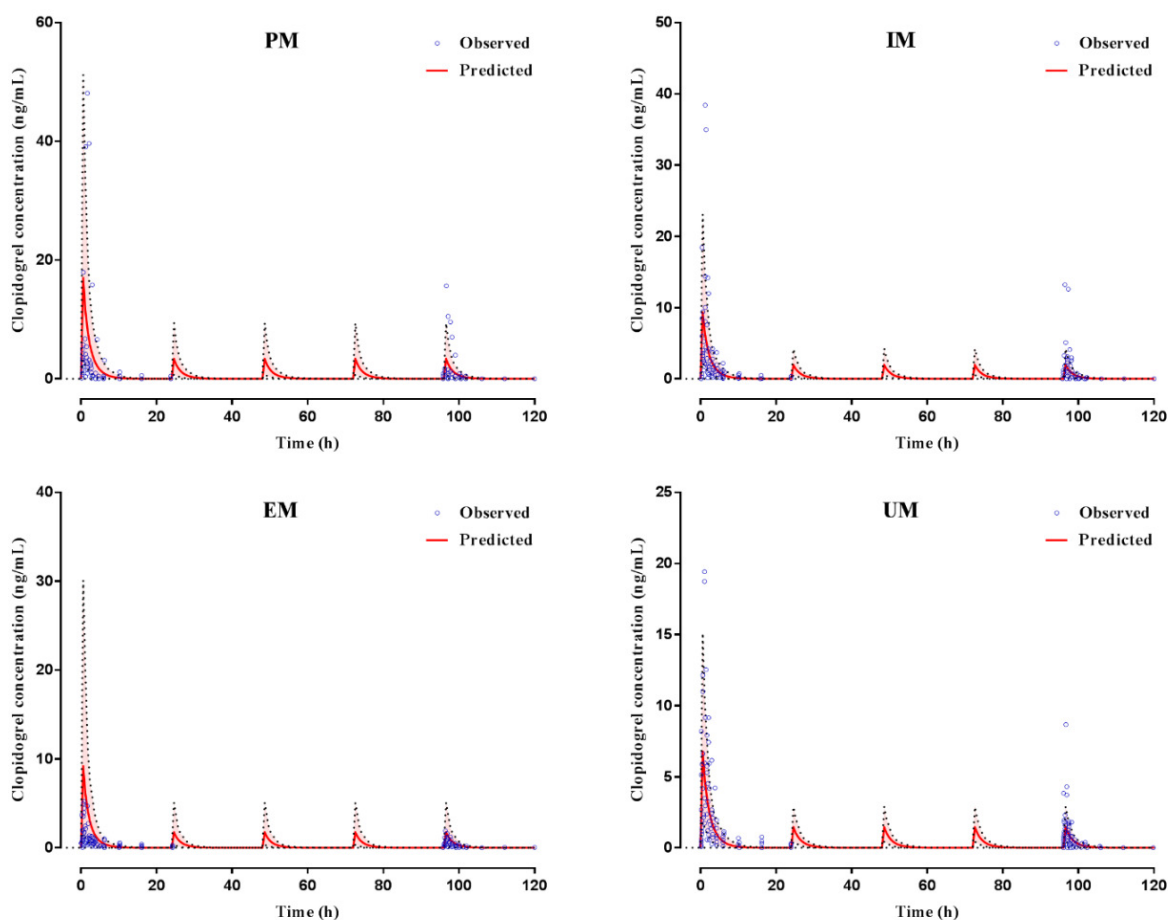


**Figure 4.9 Visual predictive check of clopidogrel in CYP2C19-PM, -IM, -EM and -UM.**

Observed concentrations (blue dots) and mean of predictions (red line) and the ranges of 5<sup>th</sup> and 95<sup>th</sup> percentiles of predictions (pink area) (Djebli *et al.* (2015)) (477). Poor metabolisers (PM); Intermediate metabolisers (IM); Extensive metabolisers (EM); Ultrarapid metabolisers (UM).

Further, for the active metabolite, clopi-H4, simulations of the mean clopi-H4 plasma concentration profile (Figure 4.10) were in good agreement with data published (477), with prediction of  $C_{max}$  and AUC at day 1 and day 5, within 2-fold of that reported (Table 4.4). Model predictions for all EM, PM, IM, and UM were generally in good agreement with that published, with a slightly under prediction at  $C_{max}$  at day 1 and day 5 for CYP2C19 EM and CYP2C19 IM phenotypes.

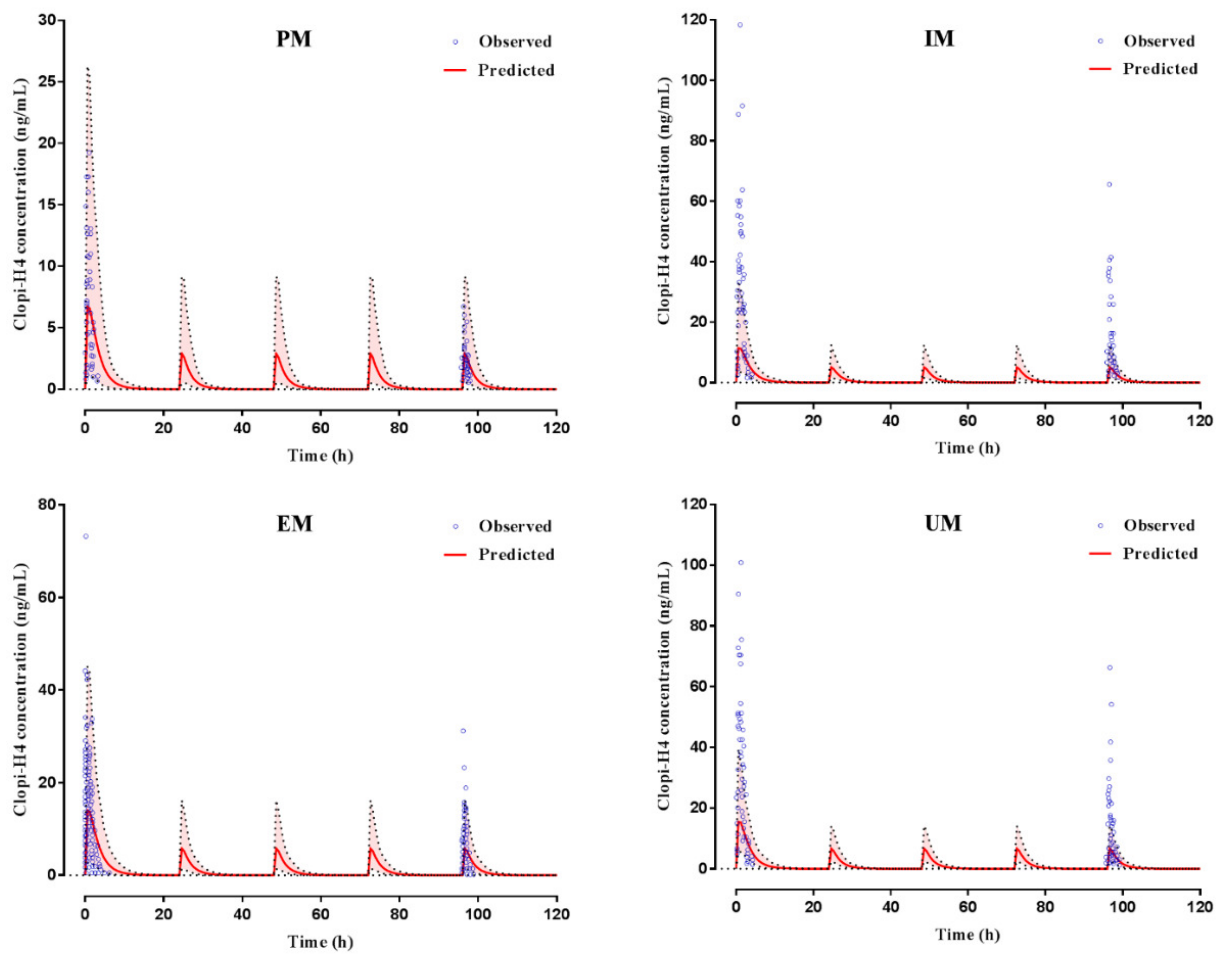


**Figure 4.10 Visual predictive check of clopi-H4 (active metabolite) in CYP2C19-PM, -IM, -EM and -UM.**

Observed concentrations (blue dots) and mean of predictions (red line) and the ranges of 5<sup>th</sup> and 95<sup>th</sup> percentiles of predictions (pink area) (Djebli *et al.* (2015)) (477). Poor metabolisers (PM); Intermediate metabolisers (IM); Extensive metabolisers (EM); Ultrarapid metabolisers (UM).

**Table 4.4 Summary of simulated clopidogrel and clopi-H4 pharmacokinetic parameters at Day 1 (300 mg loading dose) and Day 5 (75 mg last maintenance dose) in Healthy adult Volunteers with *CYP2C19 EM*, *CYP2C19 PM*, *CYP2C19 IM* and *CYP2C19 UM* phenotypes.**

		$C_{max}$ (ng/mL)	$C_{max}$ (ng/mL)	AUC <sub>0-24</sub> (ng/mL.h)	AUC <sub>last</sub> (ng/mL.h)	
		Day 1	Day 5	Day 1	Day 5	
Clopidogrel	<i>CYP2C19 EM</i>	Predicted	8.3 (1.8-43.9)	1.6 (0.4-6.4)	16.2 (3.85-67.61)	3.5 (0.79-11.66)
		Observed	4.5 (2.3-5.2)	1.6 (0.3-1.9)	8.4 (3.19-15.25)	1.4 (0.67-3.83)
	<i>CYP2C19 PM</i>	Predicted	16.2 (3.83-66.88)	3.2 (0.92-11.55)	32.0 (8.04-113.92)	7.1 (1.90-20.78)
		Observed	15.8 (6.6-48.1)	1.2 (0.5-15.7)	8.9 (3.31-73.25)	2.1 (0.83-17.84)
	<i>CYP2C19 IM</i>	Predicted	9.6 (2.6-32.8)	4.4 (1.4-10.8)	19.5 (5.75-53.17)	4.4 (1.39-10.78)
		Observed	4.5 (1.7-38.4)	3.1 (1.1-13.2)	5.1 (1.51-18.66)	1.3 (0.67-4.33)
	<i>CYP2C19 UM</i>	Predicted	7.1 (2.2-20.4)	1.5 (0.5-3.8)	14.8 (4.74-35.77)	3.4 (1.15-7.70)
		Observed	4.2 (1.3-19.4)	2.3 (0.8-8.7)	5.5 (1.71-14.65)	1.2 (0.46-3.23)
Clopi-H4	<i>CYP2C19 EM</i>	Predicted	14.72 (2.9-47.0)	6.0 (1.38-16.3)	39.1 (10.5-147.1)	13.7 (4.24-46.11)
		Observed	31.6 (11.0-52.2)	13.0 (5.67-20.33)	39.8 (15.4-64.2)	11.6 (5.79-17.41)
	<i>CYP2C19 PM</i>	Predicted	7.1 (1.1-30.1)	3.02 (0.54-9.23)	16.7 (4.5-86.6)	5.43 (1.78-29.55)
		Observed	11.2 (7.2-15.2)	3.93 (2.54-5.32)	16.0 (9.8-22.2)	3.23 (1.92-4.54)
	<i>CYP2C19 IM</i>	Predicted	12.1 (3.7-33.7)	5.3 (1.61-12.52)	35.9 (15.0-107.5)	12.0 (5.76-34.01)
		Observed	23.0 (12.1-33.9)	11.6 (6.22-16.98)	33.6 (20.5-46.7)	9.87 (5.45-14.29)
	<i>CYP2C19 UM</i>	Predicted	16.3 (5.97-39.53)	6.9 (2.45-14.21)	50.1 (23.5-127.1)	16.9 (8.20-40.19)
		Observed	24.1 (14.24-33.96)	11.7 (5.95-17.45)	33.9 (11.1-45.0)	10.7 (6.18-15.22)

Data reported as median (range). Simulations: n=63 with 32.5% female and age-range of 20-50 years.

To assess the impact of CYP2C19 polymorphisms on clopidogrel pharmacokinetics, simulations were conducted to predict the impact of CYP2C19 SNPs, in Malay and Malaysian Chinese populations, on the target clopi-H4 plasma concentration,  $C_{max}$  ranging from 0.81 to 13.45 ng/mL (510). For this simulation, the lowest range of 0.81 ng/mL was used as a cut-off value to depict patients who were unresponsive to clopidogrel treatment. In this simulation, a loading dose of 300 mg was administered on day 1 and maintenance dose of 75 mg once daily commenced from day 2 to day 5 and administered to 400 Malay and Malaysian Chinese populations phenotyped with CYP2C19 EM, PM, IM, and UM (40x10 trials, 100 subjects per phenotypes).

Within the Malay population, 3 subjects of EM phenotype did not reach the target concentration, followed by 27 subjects with the PM phenotype, 7 subjects with the IM phenotype and 3 subjects with the UM phenotype (Figure 4.11). In the Malaysian Chinese population, the percentage of subjects who did not reach the target concentration followed a similar pattern to that of the Malay population, with 3 subjects for the EM phenotype, 28 subjects for the PM phenotype, 7 subjects for the IM phenotype and 4 subjects for the UM phenotype (Figure 4.11).

There were no statistically significant differences between Malay and Malaysian Chinese when comparing the peak or trough clopi-H4 concentrations in each phenotype. However, as expected, in both Malay and Malaysian Chinese populations, the PM phenotype resulted in a statistically significant difference in mean clopi-H4  $C_{max}$  when compared to all other phenotypes ( $P < 0.001$ ).

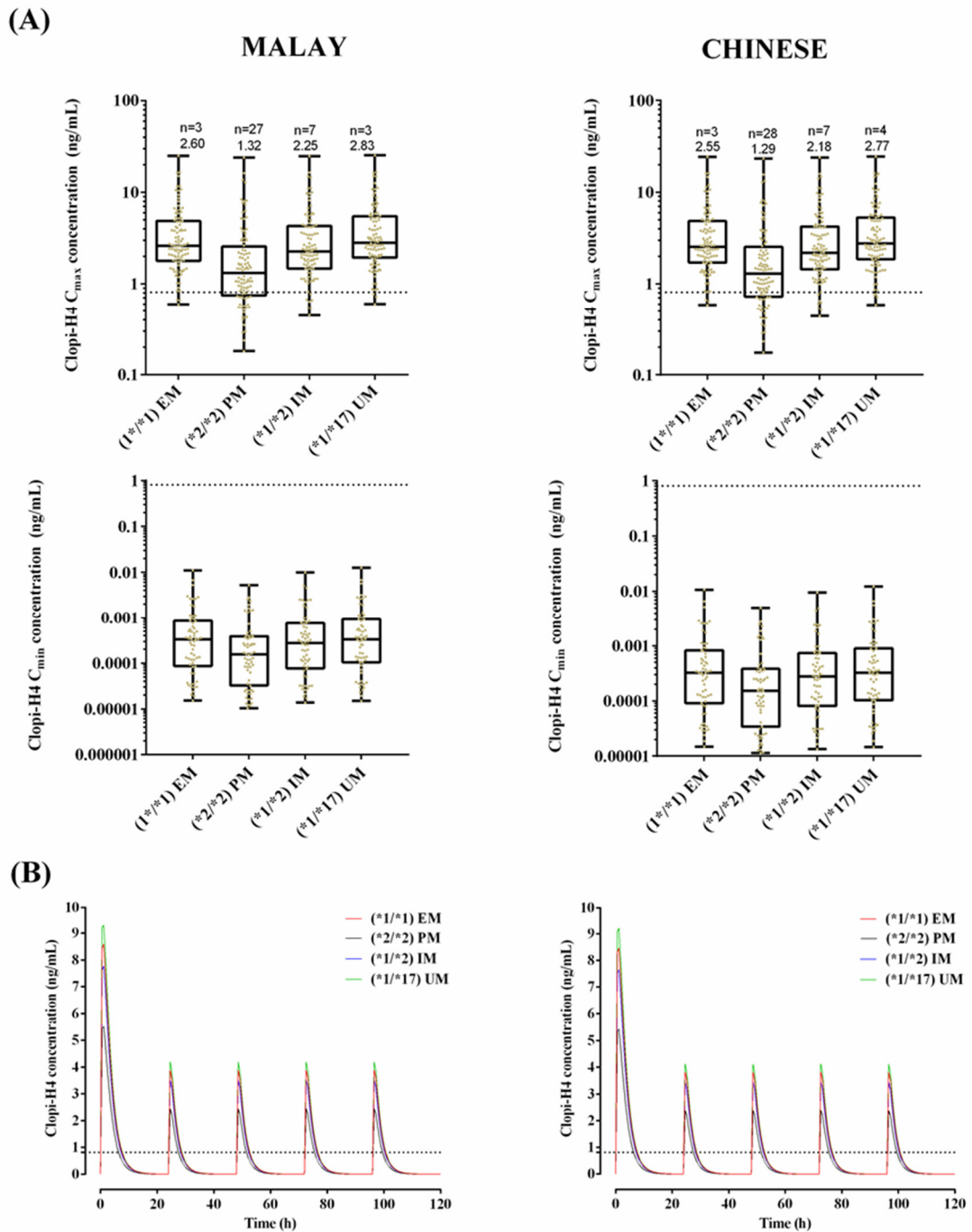


**Figure 4.11 Impact of clopidogrel standard dose regimens on final dose clopi-H4 plasma in Malay and Malaysian Chinese**

$C_{max}$  (upper panels) and  $C_{min}$  (lower panels) in Malay (left panels) and Malaysian Chinese (right panels) subjects, demarked for all EM, PM, IM or UM populations. Box and whisker plots represent maximum, 75<sup>th</sup> percentile, median, 25<sup>th</sup> percentile and minimum clopi-H4  $C_{max}$ . (B) Simulated mean plasma concentration-time profile of clopi-H4 in Malay (left panel) and Malaysian Chinese (right panel) subjects demarked for all EM, PM, IM or UM populations. All subjects (N=100 for each phenotype) received a loading dose of 300 mg on day 1, followed by daily doses of 75 mg for 5 days. Solid plasma concentration lines represent mean predictions. Dashed horizontal line represent the lower therapeutic limit for clopi-H4.

#### **4.3.4 Step 4: Sensitivity analysis for CYP2C19 hepatic abundances**

Considering the lack of literature reported CYP2C19 hepatic abundance data, the sensitivity of model predictions to changes in CYP2C19 hepatic abundance were simulated through simulating the percentage of subjects attaining clopi-H4 target concentrations when the hepatic mean enzyme abundances were increased or decreased by 30 %. In the Malay population, a 30% increase in mean abundances values resulted in 2, 27, 6 and 1 subjects failing to reach the target concentration for the EM, PM, IM and UM phenotypes respectively (Figure 4.12). Further, a 30 % decrease of mean abundances values, resulted in 6, 27, 8 and 6 subjects failing to reach the target concentration for the EM, PM, IM and UM phenotypes respectively (Figure 4.12).

For the Malaysian Chinese population, a 30 % increase in the mean abundances values resulted in 3, 27, 6 and 1 subjects failing to reach the target concentration for the EM, PM, IM and UM phenotypes respectively (Figure 4.13). Further, a 30 % decrease in the mean abundances values resulted in 6, 27, 8 and 6 subjects failing to reach the target concentration for the EM, PM, IM and UM phenotypes respectively (Figure 4.13). There were also no statistically significant interethnic differences between the clopi-H4 peak and trough concentrations for each phenotype.

## MALAY

### Mean Abundances +30%

### Mean Abundances -30%

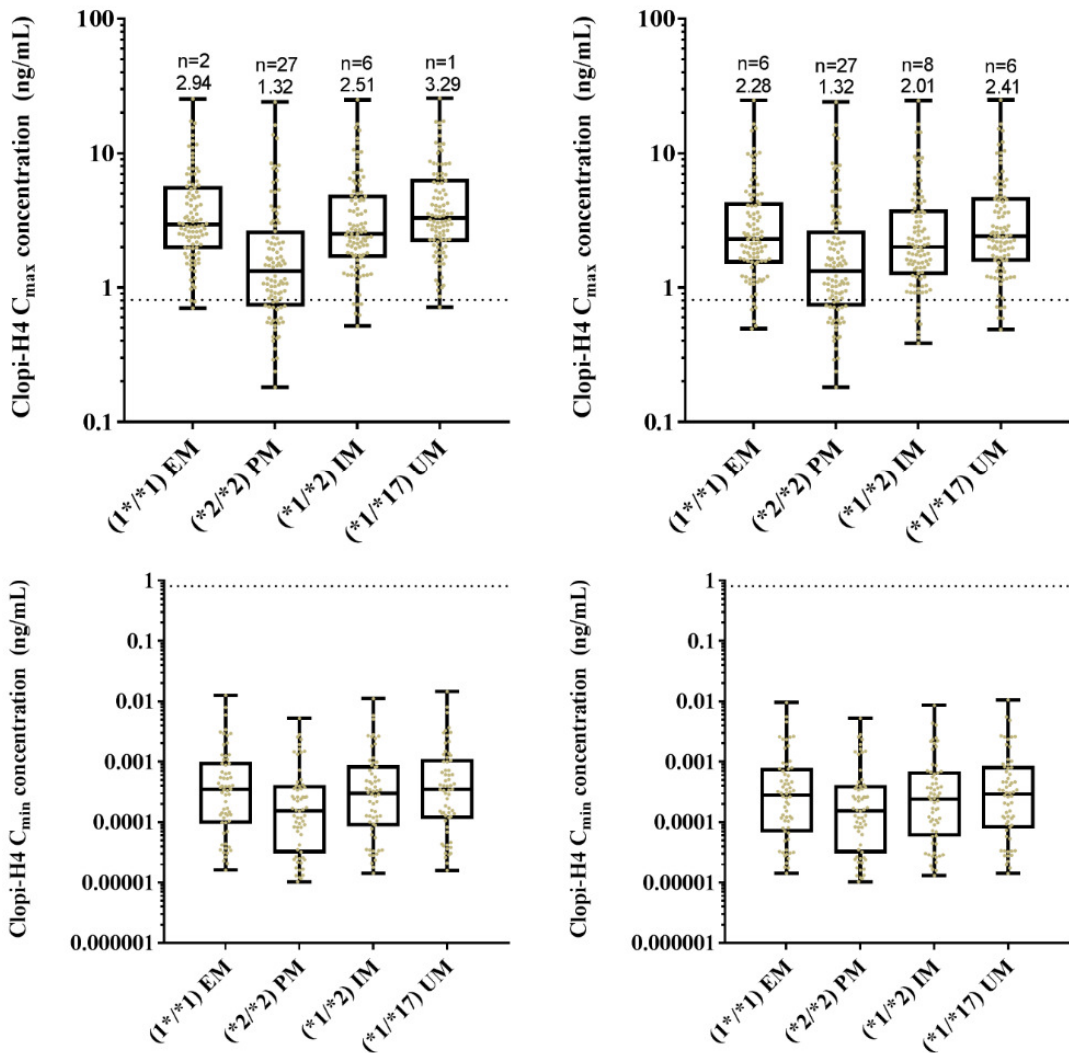


**Figure 4.12 Impact of clopidogrel standard dose regimens on final dose clopi-H4 plasma in Malay subjects**

C<sub>max</sub> (upper panels) and C<sub>min</sub> (lower panels) in Malay subjects under scenarios where mean hepatic CYP2C9 abundance is increased (left panels) or decreased (right panels) by 30%. All subjects are demarked for either all EM, PM, IM or UM populations. Box and whisker plots represent maximum, 75<sup>th</sup> percentile, median, 25<sup>th</sup> percentile and minimum clopi-H4 C<sub>max</sub>. All subjects (N=100 for each phenotype) received a loading dose of 300 mg on day 1, followed by daily doses of 75 mg for 5 days. Dashed horizontal line represent the lower therapeutic limit for clopi-H4.

## CHINESE

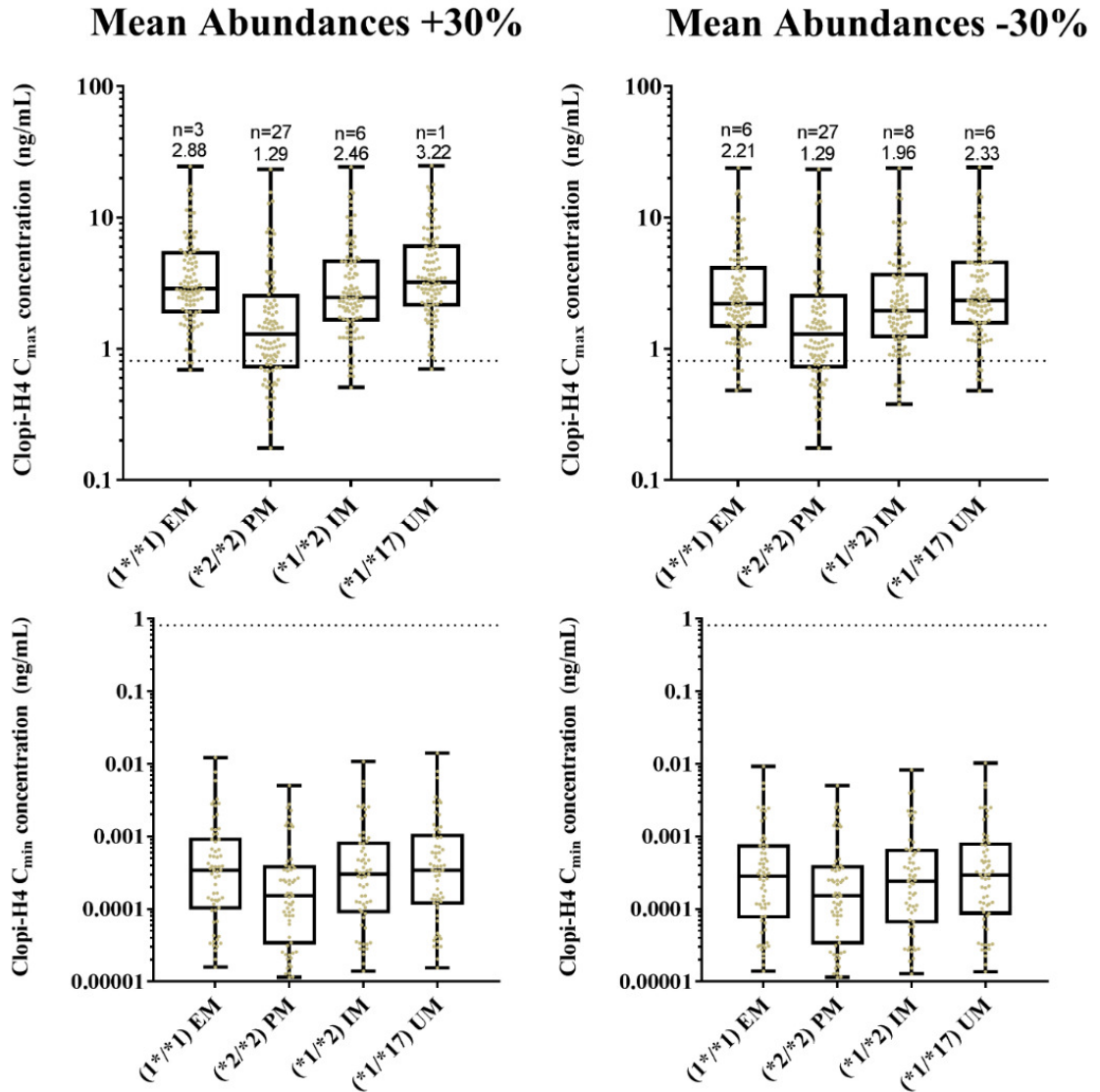


**Figure 4.13 Impact of clopidogrel standard dose regimens on final dose clopi-H4 plasma in Chinese subjects.**

C<sub>max</sub> (upper panels) and C<sub>min</sub> (lower panels) in Chinese subjects under scenarios where mean hepatic CYP2C19 abundance is increased (left panels) or decreased (right panels) by 30 %. All subjects are demarked for either all EM, PM, IM or UM populations. Box and whisker plots represent maximum, 75<sup>th</sup> percentile, median, 25<sup>th</sup> percentile and minimum clopi-H4 C<sub>max</sub>. All subjects (N=100 for each phenotype) received a loading dose of 300 mg on day 1, followed by daily doses of 75 mg for 5 days. Dashed horizontal line represent the lower therapeutic limit for clopi-H4.

#### **4.3.5 Step 5: Dose optimization in CYP2C19 poor metabolisers**

Given the high number of subjects identified with clopi-H4 concentrations below the target threshold (Figure 4.11) in the PM phenotype group, the dosing regimen for clopidogrel was increased to a 'high-dose' scenario with a 600 mg loading dose followed by a 5 day regimen of 150 mg daily (Figure 4.14). For a standard dose 27 % (Malay) and 28 % (Malaysian Chinese) of subjects had a clopi-H4 plasma concentration below the target minimum therapeutic concentration (Figure 4.11), which decrease to 12 % (Malay) and 14 % (Malaysian Chinese) for the high dose regimen (Figure 4.14A). No statistically significant differences were determined between Malay and Malaysian Chinese clopi-H4  $C_{max}$  (Figure 4.14B)

#### **4.4 DISCUSSION**

Cardiovascular disease (CVD) is a leading cause of mortality across the world with recent reports highlighting that approximately 85 % of CVD occurs in low- to middle-income countries (513, 514). A primary cause of this increase is relates to changes in economic development and lifestyle with reduced incidences of infectious disease, all of which has led to a marked improvement in the life expectancy of low- to middle-income countries from 61.7 years in 1980 to 71.8 years in 2015 (513) and the higher incidences of non-communicable disease such as diabetes mellitus, hypertension and dyslipidaemia, which have all contributed to this increase incidence of CVD in low- to middle-income countries.

Within Malaysia, the risks associated with CVD-mediated mortality were known in the 1970s (515), however ischemic heart disease (IHD) was ranked as the 1<sup>st</sup> major cause of death in Malaysia in with 12.9 % of certified cases in 2008, with 4 other CVDs which included arterial diseases (5.6%), diabetes mellitus (3.3%), stroke (1.7%), and hypertension (1.6%), amounting to a total of 48.491 cases in non-medically certified cases of deaths (516). Despite these risk, the Ministry of Healthy (MOH) Malaysia has a proactive stance in relation to CVD and has maintained a long-standing databased of cardiovascular disease in Malaysia, which is utilised to evaluate risk factors and treatment within Malaysia. The National Cardiovascular Database (NCVD) Registry (460) ensure the ongoing systematic collection, analysis and interpretation of cardiovascular disease data essential which is essential and core to planning, implementation and evaluation of clinical and public health services within Malaysia. The NCVD was officially launched in 2006 by Dr Ghani Mohamed Din (Deputy Director General of Health Malaysia)

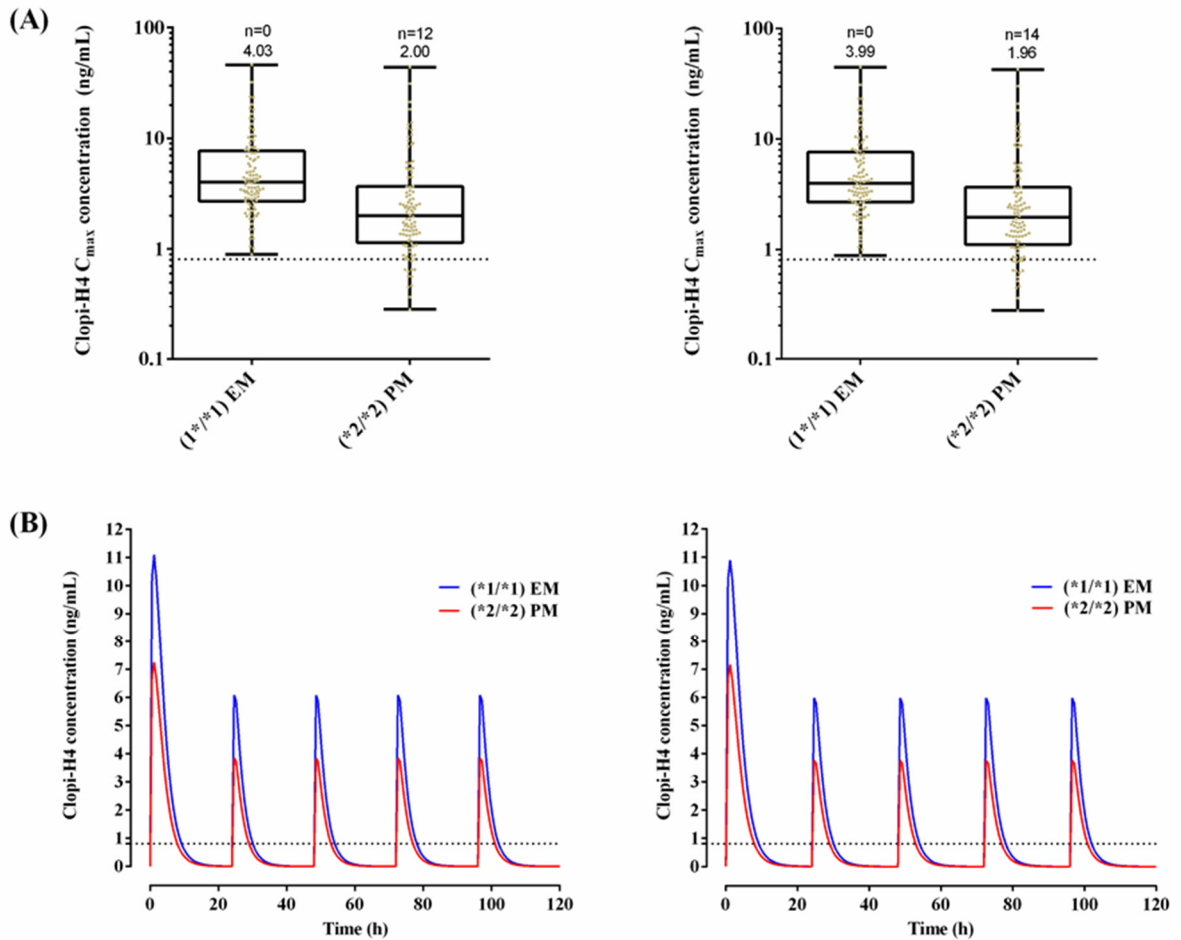


**Figure 4.14 Impact of clopidogrel high dose regimen on clopi-H4 plasma  $C_{max}$  in Malay and Malaysian Chinese subjects.**

(A) Impact of clopidogrel high dose regimen on clopi-H4 plasma  $C_{max}$  in Malay (left panel) and Malaysian Chinese (right panel) subjects. (B) Simulated mean plasma concentration-time profile of clopi-H4 in Malay (left panel) and Malaysian Chinese (right panel) subjects. An oral loading doses of 600 mg was administered on day 1, followed by daily doses of 150 mg for 5 days using the custom Malaysian (Malay and Malaysian Chinese) Simcyp population group (N = 100), with dosing to populations of either all PM or all EM phenotypes. Solid plasma concentration lines represent mean predictions. Dashed horizontal line represent the lower therapeutic limit for clopi-H4. Box and whisker plots represent maximum, 75<sup>th</sup> percentile, median, 25<sup>th</sup> percentile and minimum clopi-H4  $C_{max}$ .

during the 10th Annual Scientific Meeting (ASM) of National Heart Association of Malaysia (NHAM). To date, the NCVD register consists of 33,043 anonymised and voluntary patient records for patients undergoing acute coronary syndrome and percutaneous coronary intervention, spanning the years 2006-2015

Although aspirin remains a primary treatment option for many CVD related disorders due to its cost-effectiveness (517), a key reason for clinicians moving towards a second-line therapy is often hypersensitivity of patients towards aspirin. In Malaysia, clopidogrel is recommended as a second-line therapy for ischemic cardiovascular events and also secondary prevention of ischemic stroke (518, 519). Clopidogrel is an antiplatelet agent, being predominantly metabolised into a prodrug by CYP2C19, CYP2B6, CYP1A2, CYP2C9, and CYP3A4 leading to its active metabolite, clopi-H4. Of all these CYP enzymes, CYP2C19 has been found to be the primary contributor towards the formation of the active metabolite clopi-H4 (472-474). However, CYP2C19 is highly polymorphic (520), with the PM phenotype (\*2/\*2) and UM phenotype (\*1/\*17) known to be of higher prevalence in Asian populations when compared to Caucasians (521, 522). The consequence of administration of clopidogrel to these populations could have a significant impact on its pharmacokinetics and pharmacodynamics.

Considering the multi-ethnic composition of the Malaysian population, inter-ethnic variability may directly contribute to the difference in treatment efficiency for polymorphic-sensitive drugs, such as the antiplatelet drug clopidogrel, in reducing major adverse cardiovascular events (523, 524). Recent studies suggested that there was an association between the CYP2C19 SNPs with antiplatelet activity and ischaemic cardiovascular outcomes (525-530) with up to 12 % of the inter-individual variability of platelet aggregation having been observed in patients and more than 80 % were related to other influences such as environmental, cellular and clinical factors (concomitant diseases, obesity and inflammatory state) (531).

Outside of Southeast Asia, the use of predictive pharmacokinetics modelling to aid in both drug discovery and development along with clinically optimised drug therapy has exponential increased over the past decade and has become routine aspects of all clinical trials phases to both extrapolate dose to optimal therapy in population groups and to also identify covariates which may contribute to the variability in clinical response to drugs (16, 154, 185). However,

within Malaysia, the use of pharmacokinetic modelling to conduct such beneficial model's approaches is lacking.

Recently, we demonstrated the ability of PBPK modelling to optimise dosing of antimalarial drugs in special population groups from sub-Saharan African nations (405, 500, 532), where the unique physiological and anthropometric differences of African subjects (when compared to Caucasians) were incorporated to simulations. We have adapted this approach to now develop, for the first time, an appropriate virtual population group of the Malaysian population group for use in mechanistic pharmacokinetic modelling, with a focus on predicting the impact of CYP2C19 SNPs on clopidogrel and the active metabolite, clopi-H4, pharmacokinetic in the Malay and Malaysian Chinese population group.

We adopted a robust 5-stage modelling approach which incorporated key data from the Malaysian NCVD database to develop virtual population groups, following validation of the modelling approaches using repaglinide and tramadol compounds within healthy volunteers, Chinese and Malay population (Steps 1 and 2), followed by the simulation of clopidogrel and its active metabolite, clopi-H4 in the Malay and Malaysian Chinese population groups (Step 3). Next, the impact of SNPs CYP2C19 on the active metabolite, clopi-H4 in the Malay and Malaysian Chinese population groups were assessed with predictions of potential exposure to the clopidogrel therapy (Step 4). Finally, simulations were conducted to predict the potential impact of dosage optimisation in the CYP2C19 PM population (Step 5).

#### **4.4.1 Step 1: Malaysian population development**

In step 1 we attempted to develop a representative Malaysian population by extracting relevant data such as gender, weight, age and ethnicity from the NCVD database (460), with which to develop the populations. For the Malay, Chinese and Indian population, the mean age, weight and BMI were significantly different between Malay and Chinese ( $P < 0.0001$ ) and Chinese and Indian ( $P < 0.0001$ ), whereas mean height was relatively consistent across all population group at 1.63 m and not statistically significantly different (Table 4.2). Since there was no significant difference between the heights of all the three populations, therefore, the default age-height relationship for the 'Chinese Volunteer' population group within Simcyp was used to represent these populations.

Using the customised age-weight relationships for the two populations, the predicted distribution of body-weight with age for both the Malay (Figure 4.2) and Malaysian Chinese (Figure 4.3) populations were well predicted and in good agreement with individual subject data extracted from the NCVD data over the range of 20 to 65 years of age. This supports the development of appropriate population groups possessing suitable anthropometric age-weight relationship within the Malaysian population. In addition, this step incorporated appropriate blood biochemistry metrics to describe Malay and Malaysian Chinese population groups, something which is critical for driving unbound drug fraction within plasma and essential as clopidogrel, and its metabolites are extensively protein bound (Table 4.1) (533, 534)

#### **4.4.2 Step 2: Adult simulations with repaglinide and tramadol**

Having established a Malaysian virtual population group for use in predictive pharmacokinetic modelling, we subsequently assessed the ability of the customized population groups to predict repaglinide and tramadol plasma concentrations and pharmacokinetics in the Malay (Figure 4.7), Chinese (Figure 4.6) and Caucasian Healthy Volunteers (Figure 4.4 and 4.5) populations. In these simulations, model predictions were successfully predicted to within 2-to-3-fold of the reported  $C_{max}$ ,  $t_{max}$ , CL and AUC (Table 4.3) (507, 508), in addition to recapitulating an appropriate population distribution. It is also to be noted that due to lack of observed values in concentration-time profiles for healthy Malay adults for repaglinide, a full plasma profile comparison could not be conducted, therefore, comparison was only relied on  $C_{max}$  value available on literature (508). Such absence of full observed concentration-time profiles values also leads to the slight under prediction of AUC values (2.3-fold) in repaglinide's validation with Ruzilawati *et al.* (2010) (508) (Table 4.3). There was also a slight under prediction (2.2-fold) of AUC values noted in Hatorp *et al.* (2002) repaglinide's validation which might be due to an absence of observed CL values. Consequently, a model predicted CL values has to be utilised that resulted with this slight under prediction. However, in general, both simulations still performed within an acceptable predictive performance requirement (within 3-fold) (Section 4.2.3).

Subsequently, the customised Malay and Malaysian Chinese population group were further validated against a study whereby an IV bolus dose of tramadol was dosed to Malaysian subjects (509). Model prediction AUC and Clearance were within 2-fold of that reported (Table

4.3) with model predicted plasma concentration-time profiles spanning an appropriate range for the simulated population group when compared to the observed data (Figure 4.8).

#### **4.4.3 Step 3: Prediction of the impact of CYP2C19 polymorphisms on clopidogrel pharmacokinetics in Malaysians**

Having successfully validated the predicting capability of the PBPK model using repaglinide and tramadol compounds within healthy volunteers in Step 1 and Step 2, Malaysian Chinese and Malay populations, the model was expanded to assess its application in the adult simulation with clopidogrel and its active metabolite, clopi-H4 (Figure 4.9 and 4.10). It was integral to assess the risks associated with cardiovascular drugs, such as clopidogrel, due to its pharmacokinetics variability in CYP2C19 polymorphisms within different ethnicity especially in the Asian population, whereby in poor metabolisers, could result in the alteration of clopidogrel plasma concentration, leading to unresponsiveness towards clopidogrel therapy (472).

Having established the robustness of the model in the prediction of numerous compounds with a different mode of administration using the customised population group, we addressed the ability of the model to predict our compound of interest, clopidogrel and its active metabolites, clopi-H4 (Step 3). It is of note that the model was not validated for 2-oxo-clopidogrel due to the absence of plasma concentrations for this metabolite. Validation was attempted based on the report of a clinical study involving clopidogrel and clopi-H4 in four CYP2C19-defined metaboliser (EM, PM, UM and IM) groups (477, 511). For both clopidogrel (Figure 4.9), and clopi-H4 (Figure 4.10), overall 5<sup>th</sup> and 95<sup>th</sup> percentiles of the mean predicted profiles were within the range reported in existing published literature and contributed to our validation attempts. However, for clopidogrel, there was a slight overprediction at day 1 and day 5 for all genotypes when compared with the observed data (477). Similar disparity between the predicted and the same observed data can be seen in a study by Djebli *et al.* (2015) (477) in which he utilised a visual predictive check to confirm a good predictive performance of the PBPK model. This overprediction might be due to the complexity of clopidogrel pharmacokinetics, which involves numerous metabolic pathways including different P450s and esterase of which were difficult to predict using the model. Nevertheless, the model still confirmed a good predictive performance based on the visual predictive check (535-537).

In an attempt to establish the potential impact of CYP2C19 SNPs on clopi-H4 plasma concentration in Malay and Malaysian Chinese populations, we conducted simulations stratified across EM, PM, IM, and UM phenotypes. A statistically significant difference in the clopi-H4  $C_{max}$  was predicted between the EM and PM groups within the Malay and Malaysian Chinese population (Figure 4.11), with clopi-H4  $C_{max}$  decreasing by approximate 50 % in the PM population groups compared to the EM population group in both Malay and Malaysian Chinese (Figure 4.11).

In a study by Simon *et al.* (2011) (538), clopi-H4 plasma concentrations were quantified for each phenotype in European subjects. Following a standard dose (300 mg loading dose followed by 4 days of 75 mg once daily), last dose mean  $C_{max}$  was  $13 \pm 7.33$  ng/mL for EM and  $3.93 \pm 1.93$  ng/mL for PM. In both Malay and Chinese subjects, the median last dose  $C_{max}$  was significantly lower for EM (2.60 ng/mL and 2.55 ng/mL) (Figure 4.11A). However the overall range of prediction  $C_{max}$  were similar to those reported (538). This difference, however, may be attributed to the anthropometric differences between Southeast Asian/Far East Asian population groups and European (Caucasian) populations (539) in addition to differences in the prevalence of each genotype (488-494).

Similar reports for Malaysians subjects are currently lacking. However, in mainland Chinese subjects, clopi-H4  $C_{max}$  for the study duration (i.e. first dose) was reported to be  $18.9$  ng/mL  $\pm$   $11.8$  ng/mL in EM (\*1/\*1) and  $11.8$  ng/mL  $\pm$   $5.1$  ng/mL in PM (\*1/\*2 or \*2/\*2) (540), within 3-fold of the simulated mean  $C_{max}$  for EM ( $8.62$  ng/mL  $\pm$   $11.4$  ng/mL) and PM ( $5.59$  ng/mL  $\pm$   $3.92$  ng/mL) (Figure 4.11B) whilst also being within a similar range of observed concentrations, when taking into account the standard deviations reported for  $C_{max}$  (540).

No significant differences observed in clopi-H4 plasma concentrations between the Malaysian Chinese and Malay populations were noted when comparing in relation to the CYP2C19-genotyped groups (Figure 4.11). This finding is consistent with reports of a similar frequency of CYP2C19 metaboliser groups between the Malay and Malaysian Chinese in a cohort of Malaysian patients taking clopidogrel (495, 541, 542). Thus, although the impact of the CYP2C19 polymorphism on clopidogrel pharmacokinetic may lead to treatment failure in PM within the Malay and Malaysian Chinese population, due to the attenuation of clopi-H4 plasma

concentration, the magnitude of this impact between these populations is largely minimal, with insignificant differences observed between them (Figure 4.11).

#### **4.4.4 Step 4: Sensitivity analysis for CYP2C19 hepatic abundances**

Despite CYP2C19 polymorphisms having been previously characterised for Malaysians, the hepatic abundance of CYP2C19, and how it varies from Caucasian subjects, is currently lacking. Within the context of pharmacokinetic modelling, this is an important quantitative metric, allowing both the prediction of *in-vivo* clearance (from *in-vitro* hepatocyte/microsomal incubations) and, when combined with appropriate phenotype/genotype data, the ability to model the impact of polymorphisms on resultant drug pharmacokinetics. However, for the Chinese population group, hepatic CYP2C19 abundance has been quantified along with phenotype-specific abundances (8, 0, 6 and 10 pmol/mg protein for EM, PM, IM and UM respectively), and these have been incorporated into the Simcyp population database and characterised/validated by Simcyp and other researchers (543) (544).

However, comparisons to other Asian population groups (e.g. Japanese) show variations in the hepatic abundance for EM phenotypes (14 pmol/mg for Caucasians; 9 pmol/mg for Chinese; 1 pmol/mg for Japanese) (544). Given this variation, it was prudent to simulate the impact of variation in CYP2C19 EM and PM phenotype abundance, and this was accomplished through applying a 30 % increase and 30 % decrease of mean abundance values for all CYP2C19-phenotyped groups in the Malay (Figure 4.12) and Chinese population (Figure 4.13).

With a 30 % increase in mean abundances, there was a slight increase in patient's response towards clopidogrel treatment based on the clopi-H4 minimum limit of 0.81 ng/mL, ranging from 10-20 % of the CYP2C19-phenotyped group in both populations. Similarly, with the 30 % decrease of mean abundances, a slight decrease of patient's response can be observed varying between 10-30 % of the CYP2C19-phenotyped group in both populations. Clearly, these observations are not novel, given that clopi-H4 plasma concentrations are related to the functional status of CYP2C19 within Asian populations (545). However, of note was the fact that there was also no significant difference in the clopi-H4  $C_{max}$  between the Malay and Malaysian Chinese population groups in relation to the CYP2C19-phenotyped group with the  $\pm 30$  % mean abundances values (Figure 4.12-4.13), further confirming our earlier findings

#### **4.4.5 Step 5: Dose optimization in CYP2C19 poor metabolisers**

In the final step, given the high percentage of subjects with a clopi-H4  $C_{\max}$  below the minimum therapeutic concentration under standard dosing procedures (300 mg loading dose followed by 75 mg for 4 days), we assessed the impact of a high-dose regimen on clopi-H4  $C_{\max}$ . Under these revised dosing conditions, the percentage of subjects with a clopi-H4  $C_{\max}$  below the minimum therapeutic concentration decreased to 12 % (Malay) and 14 % (Malaysian Chinese) (Figure 4.14). A number of previous clinical studies have considered the high dose versus standard dose clopidogrel treatment regimens, particularly for CYP2C19 PM, and identified no significant clinical concerns, with improved inhibition of platelet aggregation and clinical outcomes (546-549), and our simulation further agreed with these published findings. Thus, a 600 mg loading dose followed by a 150 mg maintenance dose may be appropriate for confirmed CYP2C19 PM Malay and Malaysian Chinese patients, particularly where platelet response is poor.

#### **4.4.6 Study limitations and future directions for clopidogrel use in Malaysia**

It is important to address several limitations of the present study. Firstly, although we were able to develop robust pharmacokinetic models, the limited availability of hepatic CYP2C19 abundance data and phenotype/genotype specific abundance data in Malay or Malaysian Chinese was a primary limitation. We utilised existing data from the Chinese population group, which had been previously validated by Simcyp, as a surrogate for both Malay and Malaysian Chinese. It could be possible that inter-ethnic differences exist between Malay and Malaysian Chinese which may alter the resultant simulations, although no significant differences in clopi-H4  $C_{\max}$  were noted in Step 4 (Section 4.3.4) of our modelling approach. Further, there was a lack of robust genotyped pharmacokinetic data in Malaysian subjects, primarily plasma concentrations-time profiles, which may have aided in model validation of the clopidogrel predictions. However, this has been completed by a prior group in Caucasian subjects (477). Despite this, further investment in research and development infrastructure is required to ensure pharmacokinetic modelling approaches are better integrated into clinical research to optimise study design and better utilise the clinical data obtained to provide evidence-based optimised therapy (550).

## 4.5 CONCLUSIONS

Cardiovascular disease is a leading cause of mortality across regions and is increasingly prevalent in Malaysia, which places the Malaysian healthcare system at ever increasing risks and cost-burden of treatment of patients. Given the unique ethnic diversity of the Malaysian population group, evidence-based approach should account for the individual characteristics of patients rather than focusing on an average patient from a carefully selected patient population. Pharmacokinetic modelling can provide this approach through carefully developed and validated population models which can be applied to study a drug's pharmacokinetics in different geographical regions. This approach was applied to clopidogrel and illustrated the impact of a PM phenotype on reducing clopi-H4  $C_{max}$ , which could be partially recovered using a high-dose strategy (600 mg loading dose followed by 150 mg maintenance dose), which resulted in an approximate 50 % increase in subjects attaining the minimum clopi-H4 plasma concentration for a therapeutic effect. Further, we illustrated limited variation clopi-H4 pharmacokinetics between the two key ethnic groups, Malays and Malaysian Chinese, suggesting inter-ethnic differences within Malaysia may not impact upon clopidogrel therapy.

However, this study has illustrated that Malaysia has the infrastructure to consider pharmacogenetics-based dose recommendations, although the current lack of its application within a pharmacokinetic modelling should be addressed to better aid clinical drug therapy. Further, this study also addresses our final aim to explore further application of PBPK models in the context of CYP2C19 polymorphism on clopidogrel in multi-ethnic populations.

# **CHAPTER 5**

## **Conclusions**

## 5.1 CONCLUSIONS

The overall aim of this work was to illustrate, explore and facilitate the application of mechanistic PBPK modelling towards a diverse range of population based data analysis.

In the first part of this thesis, we develop a region-specific PBPK model to assess the hippocampus and frontal cortex pharmacokinetics using customised coded regional brain pharmacokinetic modelling with MATLAB. We then extrapolated the model to predict human regional brain pharmacokinetics, using morphine as a case study. To develop the model and to assess its ability to predict the human brain pharmacokinetics, a stepwise approach was applied to developing a PBPK model for CNS drug delivery using a mechanistic platform.

Firstly, cellular, biochemical and physiological parameters required to develop system-based models were harvested from the literature and incorporated into a generic whole-body human PBPK model. The model was also populated with relevant pharmacogenetic data. Validation of the WB-PBPK examined the ability of the model to predict  $K_{p_{uu,brain}}$  in rats for 10 compounds demonstrating passive absorption across the BBB which were previously used in previous PBPK modelling. Model predictions were all within 5-fold of the observed  $K_{p_{uu,brain}}$ , except benzylpenicillin compound being 5.5-fold over predicted which may be a result of the involvement of unclarified molecular active transport mechanism through the BBB where the rapid CNS elimination was not captured during the simulation.

Secondly, the PBPK models were established by correlating drug concentration to rodent and human CNS drug pharmacokinetics for a range of compounds, forming a test-data set. Finally, the developed model was validated and qualified by comparing model-predicted CNS profiles with published literature PK data. For this step, we adapted the basic CNS PBPK model to include two further tissue compartments, namely the frontal cortex and hippocampus and using phenytoin and carbamazepine for our model validation. The predictions of plasma and regional concentrations were found to be within the range of concentrations reported for both compounds with the majority of model predicted pharmacokinetic parameters within 2-fold of that observed.

Once developed and qualified, our model successfully predicted human brain region-specific temporal drug concentrations from a limited set of routinely available pre-clinical and *in vitro* drug-specific parameters *albeit* with several *caveats* that need to be addressed for future studies.

To address the feasibility of the model to predict the distribution of drugs within the human brain region-specific area, we utilised data reporting morphine brain concentrations in patients who suffered from traumatic brain injury using microdialysis cerebral catheter insertion in 'better' or 'worse' brain tissues, as determined by computed tomography scanning. The plasma concentration-time profile was well predicted with  $C_{\max}$ ,  $t_{\max}$  and AUC all within 2-fold of the reported values. However, the prediction of the terminal elimination phase was poorer than expected, due to the absence of any reported regional brain  $f_{u_{bt}}$  data. Nonetheless, the research has successfully proposed a simplified first-principle approach to the development of a regional brain CNS PBPK model. This approach has significant implications for assessing drug disposition across the human CNS and provides an opportunity for exploring the relationship between regional brain drug concentration, pharmacodynamics effects, and interspecies extrapolations.

In the second part of this thesis, we developed a population-based PBPK model capable of predicting the impact of efavirenz-mediated DDIs on lumefantrine pharmacokinetics in a Ugandan paediatric population groups with consideration of the polymorphic nature of CYP2B6. The population-based PBPK modelling was conducted using the virtual clinical trials simulator Simcyp, and a five-stage stepwise approach was implemented for model development, validation and model refinement. The model was developed using nine studies looking at lumefantrine and efavirenz pharmacokinetics in adults, young healthy volunteers and Ugandan malaria subjects.

In our model simulations across all weight bands for subjects aged 0.25-13 years of age, we demonstrated a significant reduction in  $C_{d7}$  of lumefantrine when it was dosed with efavirenz, which resulted in significantly lower ( $P < 0.001$ ) lumefantrine in  $C_{d7}$  in the  $*6/*6$  compared to  $*1/*1$  population group. The change in dosing schedule from 3-day standard regimen to 7-day regime resulted in a greater number of  $*6/*6$  subjects attaining the target  $C_{d7}$ , with 28-57% of subjects attaining this across the age bands studied and the highest increase is evident in 1-4 years old (3-day: 1%; 7-day: 28%).

We demonstrated that an extension of the current artemether-lumefantrine treatment regimen from 3-days to 7-days would counteract the reduction in efavirenz metabolism common with the  $*6/*6$  genotype and hence enhance the attainment of the target day-7 lumefantrine

concentration in both  $*1/*1$  and  $*6/*6$  genotype groups, thereby reducing the risk of recrudescence.

The final part of this work focussed on exploring further application of PBPK models for specific population data analyses in the context of CYP2C19 polymorphism on clopidogrel in multi-ethnic populations, with Malaysian population as a case study. The purpose of this population group would be to model the inter-individual variability in serum concentration for drugs. Specifically, clopidogrel, observed within a mixed population group where factors such as patient demographics and genetic polymorphisms would significantly alter the clinical outcome. A Malaysian population group was developed from reported age-weight relationships for Malaysian Chinese, Malays and Indians males and females in the NCVD Registry which consists of 33,043 anonymised and voluntary patients. The model was validated using clinical studies from Malaysian subjects and predicting the impact of inter-ethnic differences in clopidogrel and its active metabolite, clopi-H4 pharmacokinetics in healthy volunteers.

We demonstrated that there was a significant difference with regards to clopidogrel response within a genotyped Malay and Chinese population *albeit* no significant differences can be observed between these populations across CYP2C19 genotyped group. The most significant differences can be observed in a  $CYP2C19*1/*1$  and  $*2/*2$  carriers within the Malay and Chinese population. The ‘what-if’ scenario in which we assumed a variability of  $\pm 30\%$  of mean abundances values for all CYP2C19-phenotyped group in both population also resulted in similar observation, further confirming our findings. In addition, the number of PM individuals with peak clopi-H4 concentrations below minimum therapeutic level was partially recovered using a high-dose strategy (600 mg loading dose followed by 150 mg maintenance dose), which resulted in an approximate 50% increase in subjects attaining the minimum clopi-H4 plasma concentration for a therapeutic effect. In this part of the work, we managed to conclude that population-based PK modelling may provide a cost-effective and practical approach towards providing a preliminary overview of interindividual variability in drug response. These preliminary findings would assist in improving cost-effectiveness and time in conducting clinical trials by minimising exploratory clinical study and concentrating more on confirmatory analyses.

## 5.2 FUTURE WORK

In conclusion, we have demonstrated that PBPK modelling is capable of providing accurate predictions regarding CNS drug disposition and inter-individual variability in specific populations thereby assisting in clinical data interpretation and dose evaluation predictions. However, further work is required around *in vitro* analysis from human tissues and animal models to provide sufficient and quality data for *in vitro-in vivo* extrapolation thereby increasing the accuracy of the PBPK model predictions in non-Caucasian population groups. Furthermore, for a PBPK model to be highly accurate and dependable, a concerted effort is required integrating several disciplines including pharmacy, medicine, physiology, molecular biology, mathematics and pathology to develop a robust and comprehensive platform to predict PK behaviour in populations.

In the Malaysian perspective, PBPK modelling can be a stepping stone that will bridge the gap towards becoming a clinical trials hub within the South East Asian region. Regulatory authorities, academician and health providers can utilise this technology in assessing PK profiles of compounds and its relationship within our multi-racial population, at the same time, able to reduce cost and resources required which are a necessity in a developing country. In the context of regulatory authorities, PBPK modelling could provide a complementary approach towards the evaluation of new drug products especially in areas of predicting DDI, drug formulation, and ethnic-related changes in PK and disposition. Consequently, the acceptance of PBPK modelling approaches as part of evaluation process not only meeting the demand and current trends of pharmaceutical industries but also facilitating accessibility of new drugs to the public. Since PBPK modelling requires a robust biological system data to generate a reliable prediction, regulatory authorities, academician and health providers within Malaysia could collaborate in generating local population system biology data that will be beneficial to address key public health regulatory issues.

## REFERENCES

1. Naci H, Cylus J, Vondoros S, Sato A, Perampaladas K. Raising the bar for market authorisation of new drugs. *BMJ: British Medical Journal (Online)*. 2012;345.
2. Carpenter D. Reputation and power: organizational image and pharmaceutical regulation at the FDA: Princeton University Press; 2014.
3. Knox R. Merck pulls arthritis drug Vioxx from market. *All Things Considered*. 2004;30.
4. Lenzer J. FDA is incapable of protecting US “against another Vioxx”. *BMJ : British Medical Journal*. 2004;329(7477):1253-.
5. Jüni P, Nartey L, Reichenbach S, Sterchi R, Dieppe PA, Egger M. Risk of cardiovascular events and rofecoxib: cumulative meta-analysis. *The lancet*. 2004;364(9450):2021-9.
6. Bhattacharya S. Up to 140,000 heart attacks linked to Vioxx. *New scientist*. 2005;25.
7. De Buck SS, Sinha VK, Fenu LA, Nijsen MJ, Mackie CE, Gilissen RAHJ. Prediction of human pharmacokinetics using physiologically based modeling: A retrospective analysis of 26 clinically tested drugs. *Drug Metabolism and Disposition*. 2007;35(10):1766-80.
8. Olafuyi O, Coleman M, Badhan RKS. Development of a paediatric physiologically based pharmacokinetic model to assess the impact of drug-drug interactions in tuberculosis co-infected malaria subjects: A case study with artemether-lumefantrine and the CYP3A4-inducer rifampicin. *European Journal of Pharmaceutical Sciences*. 2017;106:20-33.
9. Richards D. Drug development and regulation. *Medicine*. 2008;36(7):369-76.
10. DiMasi JA, Hansen RW, Grabowski HG. The price of innovation: new estimates of drug development costs. *Journal of health economics*. 2003;22(2):151-85.
11. Mould DR, Upton RN. Basic Concepts in Population Modeling, Simulation, and Model-Based Drug Development. *CPT: Pharmacometrics & Systems Pharmacology*. 2012;1(9):e6.
12. Organisation for Economic Cooperation and Development. OECD Principles of Good Laboratory Practice 1998 [30 January 2018]. Available from: <http://www.oecd.org/officialdocuments/displaydocumentpdf/?cote=env/mc/chem%2898%2917&doclanguage=en>
13. U.S. Food and Drug Administration. Good Laboratory Practice for non-clinical laboratory studies. 2010 [30 January 2018]. Available from: <http://www.accessdata.fda.gov/scripts/cdrh/cfdocs/cfcfr/CFRSearch.cfm?CFRPart=58>.
14. Aarons L, Karlsson MO, Mentré F, Rombout F, Steimer J-L, van Peer A. Role of modelling and simulation in Phase I drug development. *European journal of pharmaceutical sciences*. 2001;13(2):115-22.
15. McShane LM, Hunsberger S, Adjei AA. Effective incorporation of biomarkers into phase II trials. *Clinical Cancer Research*. 2009;15(6):1898-905.
16. Budha NR, Leabman M, Jin JY, Wada DR, Baruch A, Peng K, et al. Modeling and simulation to support phase 2 dose selection for RG7652, a fully human monoclonal antibody against proprotein convertase subtilisin/kexin type 9. *The AAPS journal*. 2015;17(4):881-90.
17. De Ridder F. Predicting the outcome of phase III trials using phase II data: a case study of clinical trial simulation in late stage drug development. *Basic & clinical pharmacology & toxicology*. 2005;96(3):235-41.
18. Ito K, Houston JB. Prediction of human drug clearance from in vitro and preclinical data using physiologically based and empirical approaches. *Pharmaceutical research*. 2005;22(1):103-12.

19. Gårdmark M, Brynne L, Hammarlund-Udenaes M, Karlsson MO. Interchangeability and Predictive Performance of Empirical Tolerance Models. *Clinical Pharmacokinetics*. 1999;36(2):145-67.
20. Jamei M, Turner D, Yang J, Neuhoff S, Polak S, Rostami-Hodjegan A, et al. Population-Based Mechanistic Prediction of Oral Drug Absorption. *Aaps Journal*. 2009;11(2):225-37.
21. Jones HM, Parrott N, Jorga K, Lave T. A novel strategy for physiologically based predictions of human pharmacokinetics. *Clinical Pharmacokinetics*. 2006;45(5):511-42.
22. Bischoff KB. Physiological pharmacokinetics. *Bulletin of mathematical biology*. 1986;48(3-4):309-22.
23. Luo M, Chapel S, Sevinsky H, Savant I, Cirincione B, Bertz R, et al. Population Pharmacokinetics Analysis To Inform Efavirenz Dosing Recommendations in Pediatric HIV Patients Aged 3 Months to 3 Years. *Antimicrob Agents Chemother*. 2016;60(6):3676-86.
24. Martins IF, Teixeira AL, Pinheiro L, Falcao AO. A Bayesian Approach to in Silico Blood-Brain Barrier Penetration Modeling. *Journal of Chemical Information and Modeling*. 2012;52(6):1686-97.
25. Shargel L, Andrew B, Wu-Pong S. *Applied biopharmaceutics & pharmacokinetics*: McGraw-Hill New York; 2005.
26. Gillespie WR. Noncompartmental versus compartmental modelling in clinical pharmacokinetics. *Clinical pharmacokinetics*. 1991;20(4):253-62.
27. Savic RM, Jonker DM, Kerbusch T, Karlsson MO. Implementation of a transit compartment model for describing drug absorption in pharmacokinetic studies. *Journal of pharmacokinetics and pharmacodynamics*. 2007;34(5):711-26.
28. Benet LZ, Kroetz D, Sheiner L, Hardman J, Limbird L. *Pharmacokinetics: the dynamics of drug absorption, distribution, metabolism, and elimination*. Goodman and Gilman's the pharmacological basis of therapeutics. 1996:3-27.
29. Niazi S. *Textbook of biopharmaceutics and clinical pharmacokinetics*: Appleton-Century-Crofts; 1979.
30. Shargel L, Andrew B, Wu-Pong S. *Applied biopharmaceutics & pharmacokinetics*: McGraw-Hill Medical Publishing Division; 2015.
31. Mueck W, Eriksson BI, Bauer KA, Borris L, Dahl OE, Fisher WD, et al. Population Pharmacokinetics and Pharmacodynamics of Rivaroxaban — an Oral, Direct Factor Xa Inhibitor — in Patients Undergoing Major Orthopaedic Surgery. *Clinical Pharmacokinetics*. 2008;47(3):203-16.
32. Nicolau DP, Freeman CD, Belliveau PP, Nightingale CH, Ross JW, Quintiliani R. Experience with a once-daily aminoglycoside program administered to 2,184 adult patients. *Antimicrobial agents and chemotherapy*. 1995;39(3):650-5.
33. Sawyer BG. *Tietz Fundamentals of Clinical Chemistry and Molecular Diagnostics*: Elsevier; 2015.
34. Pou L, Rosell M, Lopez R, Pascual C. Changes in vancomycin pharmacokinetics during treatment. *Therapeutic drug monitoring*. 1996;18(2):149-53.
35. Rodvold K, Zofuka H, ROTSCHAPER J. Aminoglycoside pharmacokinetic monitoring: an integral part of patient care? 1988.
36. Gabrielsson J, Weiner D. Non-compartmental analysis. *Methods Mol Biol*. 2012;929:377-89.
37. Aarons L. Population pharmacokinetics: theory and practice. *British journal of clinical pharmacology*. 1991;32(6):669-70.

38. Abernethy DR, Azarnoff DL. Pharmacokinetic Investigations in Elderly Patients Clinical and Ethical Considerations. *Clinical pharmacokinetics*. 1990;19(2):89-93.
39. Whiting B, Kelman AW, Grevel J. Population pharmacokinetics theory and clinical application. *Clinical pharmacokinetics*. 1986;11(5):387-401.
40. Graves NM, Ludden TM, Holmes GB, Fuerst RH, Leppik IE. Pharmacokinetics of Felbamate, a Novel Antiepileptic Drug: Application of Mixed-Effect Modeling to Clinical Trials. *Pharmacotherapy: The Journal of Human Pharmacology and Drug Therapy*. 1989;9(6):372-6.
41. Ette EI, Williams PJ. Population pharmacokinetics I: background, concepts, and models. *Annals of Pharmacotherapy*. 2004;38(10):1702-6.
42. Samara E, Granneman R. Role of population pharmacokinetics in drug development. *Clinical pharmacokinetics*. 1997;32(4):294-312.
43. Mahmood I. Pharmacokinetic allometric scaling of antibodies: application to the first-in-human dose estimation. *Journal of pharmaceutical sciences*. 2009;98(10):3850-61.
44. Zhang M, Zhou D, Wang Y, Maier DL, Widzowski DV, Sobotka-Briner CD, et al. Preclinical Pharmacology and Pharmacokinetics of AZD3783, a Selective 5-Hydroxytryptamine 1B Receptor Antagonist. *Journal of Pharmacology and Experimental Therapeutics*. 2011;339(2):567-78.
45. Brown RP, Delp MD, Lindstedt SL, Rhomberg LR, Beliles RP. Physiological parameter values for physiologically based pharmacokinetic models. *Toxicology and Industrial Health*. 1997;13(4):407-84.
46. Espié P, Tytgat D, Sargentini-Maier M-L, Poggesi I, Watelet J-B. Physiologically based pharmacokinetics (PBPK). *Drug Metabolism Reviews*. 2009;41(3):391-407.
47. Zou P, Yu Y, Zheng N, Yang Y, Paholak HJ, Yu LX, et al. Applications of Human Pharmacokinetic Prediction in First-in-Human Dose Estimation. *The AAPS Journal*. 2012;14(2):262-81.
48. Peters SA. Physiologically-based pharmacokinetic (PBPK) modeling and simulations: principles, methods, and applications in the pharmaceutical industry: John Wiley & Sons; 2012.
49. Teorell T. Kinetics of distribution of substances administered to the body, I: the extravascular modes of administration. *Archives internationales de pharmacodynamie et de therapie*. 1937;57:205-25.
50. Teorell T. Kinetics of distribution of substances administered to the body, II: the intravascular modes of administration. *Archives internationales de pharmacodynamie et de therapie*. 1937;57:226-40.
51. Wagner JG. History of pharmacokinetics. *Pharmacology & therapeutics*. 1981;12(3):537-62.
52. Bischoff KB. Applications of a mathematical model for drug distribution in mammals. *Chemical engineering in medicine and biology: Springer*; 1967. p. 417-46.
53. Bellman R, Jacquez JA, Kalaba R. Some mathematical aspects of chemotherapy: I. One-organ models. *The bulletin of mathematical biophysics*. 1960;22(2):181-98.
54. Jiang XL, Zhao P, Barrett JS, Lesko LJ, Schmidt S. Application of physiologically based pharmacokinetic modeling to predict acetaminophen metabolism and pharmacokinetics in children. *CPT: pharmacometrics & systems pharmacology*. 2013;2:e80-e.
55. Johnson TN, Boussery K, Rowland-Yeo K, Tucker GT, Rostami-Hodjegan A. A semi-mechanistic model to predict the effects of liver cirrhosis on drug clearance. *Clinical pharmacokinetics*. 2010;49(3):189-206.

56. Kelly RP, Close SL, Farid NA, Winters KJ, Shen L, Natanegara F, et al. Pharmacokinetics and pharmacodynamics following maintenance doses of prasugrel and clopidogrel in Chinese carriers of CYP2C19 variants. *British journal of clinical pharmacology*. 2012;73(1):93-105.
57. Khalil F, Läer S. Physiologically Based Pharmacokinetic Modeling: Methodology, Applications, and Limitations with a Focus on Its Role in Pediatric Drug Development. *Journal of Biomedicine and Biotechnology*. 2011;2011:907461.
58. Abduljalil K, Furness P, Johnson TN, Rostami-Hodjegan A, Soltani H. Anatomical, physiological and metabolic changes with gestational age during normal pregnancy: a database for parameters required in physiologically based pharmacokinetic modelling. *Clin Pharmacokinet*. 2012;51(6):365-96.
59. Brown RP, Delp MD, Lindstedt SL, Rhomberg LR, Beliles RP. Physiological parameter values for physiologically based pharmacokinetic models. *Toxicology and industrial health*. 1997;13(4):407-84.
60. Price PS, Conolly RB, Chaisson CF, Gross EA, Young JS, Mathis ET, et al. Modeling interindividual variation in physiological factors used in PBPK models of humans. *Critical reviews in toxicology*. 2003;33(5):469-503.
61. Thompson CM, Johns DO, Sonawane B, Barton HA, Hattis D, Tardif R, et al. Database for physiologically based pharmacokinetic (PBPK) modeling: physiological data for healthy and health-impaired elderly. *Journal of toxicology and environmental health Part B, Critical reviews*. 2009;12(1):1-24.
62. Jones H, Rowland-Yeo K. Basic concepts in physiologically based pharmacokinetic modeling in drug discovery and development. *CPT: pharmacometrics & systems pharmacology*. 2013;2(8):1-12.
63. Nestorov I. Whole-body physiologically based pharmacokinetic models. *Expert opinion on drug metabolism & toxicology*. 2007;3(2):235-49.
64. Badhan RKS, Chenel M, Penny JI. Development of a physiologically-based pharmacokinetic model of the rat central nervous system. *Pharmaceutics*. 2014;6(1):97-136.
65. Lennernäs H. Human intestinal permeability. *Journal of pharmaceutical sciences*. 1998;87(4):403-10.
66. Sun D, Lennernas H, Welage LS, Barnett JL, Landowski CP, Foster D, et al. Comparison of human duodenum and Caco-2 gene expression profiles for 12,000 gene sequences tags and correlation with permeability of 26 drugs. *Pharmaceutical research*. 2002;19(10):1400-16.
67. Winiwarter S, Bonham NM, Ax F, Hallberg A, Lennernäs H, Karlén A. Correlation of human jejunal permeability (in vivo) of drugs with experimentally and theoretically derived parameters. A multivariate data analysis approach. *Journal of medicinal chemistry*. 1998;41(25):4939-49.
68. Blakey GE, Nestorov IA, Arundel PA, Aarons LJ, Rowland M. Quantitative structure-pharmacokinetics relationships: I. Development of a whole-body physiologically based model to characterize changes in pharmacokinetics across a homologous series of barbiturates in the rat. *Journal of pharmacokinetics and biopharmaceutics*. 1997;25(3):277-312.
69. Poulin P, Theil FP. A priori prediction of tissue:plasma partition coefficients of drugs to facilitate the use of physiologically-based pharmacokinetic models in drug discovery. *Journal of pharmaceutical sciences*. 2000;89(1):16-35.
70. Rodgers T, Leahy D, Rowland M. Physiologically based pharmacokinetic modeling 1: predicting the tissue distribution of moderate-to-strong bases. *Journal of pharmaceutical sciences*. 2005;94(6):1259-76.

71. Rodgers T, Leahy D, Rowland M. Tissue distribution of basic drugs: accounting for enantiomeric, compound and regional differences amongst beta-blocking drugs in rat. *J Pharm Sci.* 2005;94(6):1237-48.
72. Rodgers T, Rowland M. Physiologically based pharmacokinetic modelling 2: predicting the tissue distribution of acids, very weak bases, neutrals and zwitterions. *Journal of pharmaceutical sciences.* 2006;95(6):1238-57.
73. Carlile DJ, Zomorodi K, Houston JB. Scaling factors to relate drug metabolic clearance in hepatic microsomes, isolated hepatocytes, and the intact liver - Studies with induced livers involving diazepam. *Drug Metabolism and Disposition.* 1997;25(8):903-11.
74. Iwatsubo T, Suzuki H, Shimada N, Chiba K, Ishizaki T, Green CE, et al. Prediction of in vivo hepatic metabolic clearance of YM796 from in vitro data by use of human liver microsomes and recombinant P-450 isozymes. *Journal of Pharmacology and Experimental Therapeutics.* 1997;282(2):909-19.
75. Gomez-Lechon M, Donato M, Lahoz A, Castell J. Cell lines: a tool for in vitro drug metabolism studies. *Current drug metabolism.* 2008;9(1):1-11.
76. Houston JB. UTILITY OF IN-VITRO DRUG-METABOLISM DATA IN PREDICTING IN-VIVO METABOLIC-CLEARANCE. *Biochemical Pharmacology.* 1994;47(9):1469-79.
77. Naritomi Y, Terashita S, Kimura S, Suzuki A, Kagayama A, Sugiyama Y. Prediction of human hepatic clearance from in vivo animal experiments and in vitro metabolic studies with liver microsomes from animals and humans. *Drug Metabolism and Disposition.* 2001;29(10):1316-24.
78. Lipscomb JC, Fisher JW, Confer PD, Byczkowski JZ. In Vitro to In Vivo Extrapolation for Trichloroethylene Metabolism in Humans. *Toxicology and applied pharmacology.* 1998;152(2):376-87.
79. Arias IM. The Liver: Biology and Pathobiology. *Clinical Nutrition Insight.* 1988;14(11):5.
80. De Buck SS, Sinha VK, Fenu LA, Gilissen RA, Mackie CE, Nijsen MJ. The prediction of drug metabolism, tissue distribution, and bioavailability of 50 structurally diverse compounds in rat using mechanism-based absorption, distribution, and metabolism prediction tools. *Drug Metabolism and Disposition.* 2007;35(4):649-59.
81. Graham H, Walker M, Jones O, Yates J, Galetin A, Aarons L. Comparison of in-vivo and in-silico methods used for prediction of tissue: plasma partition coefficients in rat. *Journal of Pharmacy and Pharmacology.* 2012;64(3):383-96.
82. Poulin P, Theil F-P. Development of a novel method for predicting human volume of distribution at steady-state of basic drugs and comparative assessment with existing methods. *Journal of Pharmaceutical Sciences.* 98(12):4941-61.
83. Lin JH. Applications and limitations of interspecies scaling and in vitro extrapolation in pharmacokinetics. *Drug metabolism and disposition.* 1998;26(12):1202-12.
84. Jamei M, Dickinson GL, Rostami-Hodjegan A. A framework for assessing inter-individual variability in pharmacokinetics using virtual human populations and integrating general knowledge of physical chemistry, biology, anatomy, physiology and genetics: a tale of 'bottom-up' vs 'top-down' recognition of covariates. *Drug metabolism and pharmacokinetics.* 2009;24(1):53-75.
85. Rowland M, Balant L, Peck C. Physiologically based pharmacokinetics in drug development and regulatory science: a workshop report (Georgetown University, Washington, DC, May 29-30, 2002). *AAPS PharmSci.* 2004;6(1):56-67.

86. Clewell HJ, Gentry PR, Covington TR, Sarangapani R, Teegarden JG. Evaluation of the potential impact of age- and gender-specific pharmacokinetic differences on tissue dosimetry. *Toxicological sciences : an official journal of the Society of Toxicology*. 2004;79(2):381-93.
87. Edginton AN, Schmitt W, Willmann S. Development and evaluation of a generic physiologically based pharmacokinetic model for children. *Clinical Pharmacokinetics*. 2006;45(10):1013-34.
88. Bois FY. Applications of population approaches in toxicology. *Toxicology Letters*. 2001;120(1):385-94.
89. Sheiner LB. The population approach to pharmacokinetic data analysis: rationale and standard data analysis methods. *Drug metabolism reviews*. 1984;15(1-2):153-71.
90. Lawrence XY, Crison JR, Amidon GL. Compartmental transit and dispersion model analysis of small intestinal transit flow in humans. *International Journal of Pharmaceutics*. 1996;140(1):111-8.
91. Davis SS, Hardy JG, Fara JW. Transit of pharmaceutical dosage forms through the small intestine. *Gut*. 1986;27(8):886-92.
92. Fadda HM, McConnell EL, Short MD, Basit AW. Meal-induced acceleration of tablet transit through the human small intestine. *Pharmaceutical research*. 2009;26(2):356-60.
93. Hilgendorf C, Ahlin G, Seithel A, Artursson P, Ungell A-L, Karlsson J. Expression of thirty-six drug transporter genes in human intestine, liver, kidney, and organotypic cell lines. *Drug Metabolism and Disposition*. 2007;35(8):1333-40.
94. Murakami T, Takano M. Intestinal efflux transporters and drug absorption. *Expert opinion on drug metabolism & toxicology*. 2008;4(7):923-39.
95. Koepsell H, Lips K, Volk C. Polyspecific organic cation transporters: structure, function, physiological roles, and biopharmaceutical implications. *Pharmaceutical research*. 2007;24(7):1227-51.
96. Mouly S, Paine MF. P-glycoprotein increases from proximal to distal regions of human small intestine. *Pharmaceutical research*. 2003;20(10):1595-9.
97. Fallingborg J, Christensen L, Ingeman-Nielsen M, Jacobsen B, Abildgaard K, Rasmussen H. pH-profile and regional transit times of the normal gut measured by a radiotelemetry device. *Alimentary pharmacology & therapeutics*. 1989;3(6):605-14.
98. Fallingborg J. Intraluminal pH of the human gastrointestinal tract. *Danish Medical Bulletin*. 1999;46(3):183-96.
99. Heading RC, Nimmo J, Prescott L, Tothill P. The dependence of paracetamol absorption on the rate of gastric emptying. *British journal of pharmacology*. 1973;47(2):415-21.
100. Oberle RL, Amidon GL. The influence of variable gastric emptying and intestinal transit rates on the plasma level curve of cimetidine; an explanation for the double peak phenomenon. *Journal of pharmacokinetics and biopharmaceutics*. 1987;15(5):529-44.
101. Fleisher D, Li C, Zhou Y, Pao L-H, Karim A. Drug, meal and formulation interactions influencing drug absorption after oral administration. *Clinical pharmacokinetics*. 1999;36(3):233-54.
102. Eichler H-G, Müller M. Drug distribution. *Clinical pharmacokinetics*. 1998;34(2):95-9.
103. Rowland M, Tozer TN. *Clinical pharmacokinetics: concepts and applications*: Lippincott Williams & Wilkins; 1980.
104. Rowland M, Tozer TN. *Clinical pharmacokinetics/pharmacodynamics*: Lippincott Williams and Wilkins Philadelphia; 2005.

105. Grover A, Benet LZ. Effects of drug transporters on volume of distribution. *The AAPS journal*. 2009;11(2):250-61.
106. Ho RH, Kim RB. Transporters and drug therapy: implications for drug disposition and disease. *Clinical Pharmacology & Therapeutics*. 2005;78(3):260-77.
107. Council NR. *Scientific frontiers in developmental toxicology and risk assessment*: National Academies Press; 2000.
108. Thirup P. Haematocrit. *Sports Medicine*. 2003;33(3):231-43.
109. Morse M, Cassels DE, Schlutz FW. Blood volumes of normal children. *American Journal of Physiology--Legacy Content*. 1947;151(2):448-58.
110. Morse M, Cassels DE, Schlutz FW. Available and interstitial fluid volumes of normal children. *American Journal of Physiology--Legacy Content*. 1947;151(2):438-47.
111. Grandison MK, Boudinot FD. Age-related changes in protein binding of drugs. *Clinical Pharmacokinetics*. 2000;38(3):271-90.
112. Woo J. Age-related changes in protein binding of drugs: implications for therapy. *Journal of the Hong Kong geriatrics society*. 1999;9(1).
113. Price PS, Conolly RB, Chaisson CF, Gross EA, Young JS, Mathis ET, et al. Modeling interindividual variation in physiological factors used in PBPK models of humans. *Critical Reviews in Toxicology*. 2003;33(5):469-503.
114. Bjornsson TD, Wagner JA, Donahue SR, Harper D, Karim A, Khouri MS, et al. A review and assessment of potential sources of ethnic differences in drug responsiveness. *The Journal of Clinical Pharmacology*. 2003;43(9):943-67.
115. Dorne J, Walton K, Renwick A. Human variability for metabolic pathways with limited data (CYP2A6, CYP2C9, CYP2E1, ADH, esterases, glycine and sulphate conjugation). *Food and chemical toxicology*. 2004;42(3):397-421.
116. Haber L, Maier A, Gentry P, Clewell H, Dourson M. Genetic polymorphisms in assessing interindividual variability in delivered dose. *Regulatory Toxicology and Pharmacology*. 2002;35(2):177-97.
117. Johnson TN, Rostami-Hodjegan A. Resurgence in the use of physiologically based pharmacokinetic models in pediatric clinical pharmacology: parallel shift in incorporating the knowledge of biological elements and increased applicability to drug development and clinical practice. *Pediatric Anesthesia*. 2011;21(3):291-301.
118. Paine MF, Hart HL, Ludington SS, Haining RL, Rettie AE, Zeldin DC. The human intestinal cytochrome P450 "pie". *Drug metabolism and disposition*. 2006;34(5):880-6.
119. Dvorchik BH, Vesell ES. Pharmacokinetic interpretation of data gathered during therapeutic drug monitoring. *Clinical chemistry*. 1976;22(6):868-78.
120. Tett SE, Kirkpatrick CM, Gross AS, McLachlan AJ. Principles and clinical application of assessing alterations in renal elimination pathways. *Clinical pharmacokinetics*. 2003;42(14):1193-211.
121. Garrett E. Pharmacokinetics and clearances related to renal processes. *International journal of clinical pharmacology and biopharmacy*. 1978;16(4):155-72.
122. Tucker G. Measurement of the renal clearance of drugs. *British journal of clinical pharmacology*. 1981;12(6):761-70.
123. Wang Z-J, Yin OQ, Tomlinson B, Chow MS. OCT2 polymorphisms and in-vivo renal functional consequence: studies with metformin and cimetidine. *Pharmacogenetics and genomics*. 2008;18(7):637-45.
124. Arias IM, Che M, Gatmaitan Z, Leveille C, Nishida T, St Pierre M. The biology of the bile canaliculus, 1993. *Hepatology*. 1993;17(2):318-29.

125. Ghibellini G, Leslie EM, Brouwer KL. Methods to evaluate biliary excretion of drugs in humans: an updated review. *Molecular pharmaceutics*. 2006;3(3):198-211.
126. Gabrielsson J, Weiner D. "Pharmacokinetic and Pharmacodynamic Data Analysis: Concepts and Applications"—4th edition. Fourth ed. Sweden 2010. 1254 p.
127. Saltelli A, Chan K, Scott EM: sensitivity analysis. Wiley. 2000;79:80.
128. Nestorov IA, Aarons LJ, Rowland M. Physiologically based pharmacokinetic modeling of a homologous series of barbiturates in the rat: a sensitivity analysis. *Journal of pharmacokinetics and biopharmaceutics*. 1997;25(4):413-47.
129. Gueorguieva I, Nestorov IA, Rowland M. Reducing whole body physiologically based pharmacokinetic models using global sensitivity analysis: diazepam case study. *Journal of pharmacokinetics and pharmacodynamics*. 2006;33(1):1-27.
130. Woodruff TJ, Bois FY. Optimization issues in physiological toxicokinetic modeling: a case study with benzene. *Toxicology Letters*. 1993;69(2):181-96.
131. Thomas RS, Yang RS, Morgan DG, Moorman MP, Kermani HR, Sloane RA, et al. PBPK modeling/Monte Carlo simulation of methylene chloride kinetic changes in mice in relation to age and acute, subchronic, and chronic inhalation exposure. *Environmental Health Perspectives*. 1996;104(8):858-65.
132. Thomas RS, Lytle WE, Keefe TJ, Constan AA, Yang RS. Incorporating Monte Carlo simulation into physiologically based pharmacokinetic models using advanced continuous simulation language (ACSL): a computational method. *Fundamental and applied toxicology : official journal of the Society of Toxicology*. 1996;31(1):19-28.
133. Natrella M. NIST/SEMATECH e-handbook of statistical methods. 2010.
134. Peters SA. Evaluation of a generic physiologically based pharmacokinetic model for lineshape analysis. *Clinical Pharmacokinetics*. 2008;47(4):261-75.
135. Ginsberg G, Hattis D, Russ A, Sonawane B. Physiologically based pharmacokinetic (PBPK) modeling of caffeine and theophylline in neonates and adults: Implications for assessing children's risks from environmental agents. *Journal of Toxicology and Environmental Health-Part a-Current Issues*. 2004;67(4):297-329.
136. Parrott N, Davies B, Hoffmann G, Koerner A, Lave T, Prinssen E, et al. Development of a Physiologically Based Model for Oseltamivir and Simulation of Pharmacokinetics in Neonates and Infants. *Clinical Pharmacokinetics*. 2011;50(9):613-23.
137. Poulin P, Theil FP. Prediction of pharmacokinetics prior to in vivo studies. II. Generic physiologically based pharmacokinetic models of drug disposition. *Journal of Pharmaceutical Sciences*. 2002;91(5):1358-70.
138. Obach RS. Prediction of human clearance of twenty-nine drugs from hepatic microsomal intrinsic clearance data: An examination of in vitro half-life approach and nonspecific binding to microsomes. *Drug Metabolism and Disposition*. 1999;27(11):1350-9.
139. Sager JE, Yu J, Ragueneau-Majlessi I, Isoherranen N. Physiologically Based Pharmacokinetic (PBPK) Modeling and Simulation Approaches: A Systematic Review of Published Models, Applications, and Model Verification. *Drug metabolism and disposition: the biological fate of chemicals*. 2015;43(11):1823-37.
140. Lin Z, Jaber-Douraki M, He C, Jin S, Yang RS, Fisher JW, et al. Performance Assessment and Translation of Physiologically Based Pharmacokinetic Models From acslX to Berkeley Madonna, MATLAB, and R Language: Oxytetracycline and Gold Nanoparticles As Case Examples. *Toxicological Sciences*. 2017;158(1):23-35.
141. Jamei M, Marciniak S, Edwards D, Wragg K, Feng K, Barnett A, et al. The simcyp population based simulator: architecture, implementation, and quality assurance. *In silico pharmacology*. 2013;1:9-.

142. Willmann S, Lippert J, Sevestre M, Solodenko J, Fois F, Schmitt W. PK-Sim®: a physiologically based pharmacokinetic ‘whole-body’ model. *Biosilico*. 2003;1(4):121-4.
143. Okumu A, DiMaso M, Löbenberg R. Computer simulations using GastroPlus™ to justify a biowaiver for etoricoxib solid oral drug products. *European Journal of Pharmaceutics and Biopharmaceutics*. 2009;72(1):91-8.
144. Agoram B, Woltosz WS, Bolger MB. Predicting the impact of physiological and biochemical processes on oral drug bioavailability. *Advanced Drug Delivery Reviews*. 2001;50:S41-S67.
145. Shi JG, Fraczekiewicz G, Williams WV, Yeleswaram S. Predicting Drug-Drug Interactions Involving Multiple Mechanisms Using Physiologically Based Pharmacokinetic Modeling: A Case Study With Ruxolitinib. *Clinical Pharmacology & Therapeutics*. 2015;97(2):177-85.
146. Wang J, Xia SM, Xue WF, Wang DW, Sai Y, Liu L, et al. A semi-physiologically-based pharmacokinetic model characterizing mechanism-based auto-inhibition to predict stereoselective pharmacokinetics of verapamil and its metabolite norverapamil in human. *European Journal of Pharmaceutical Sciences*. 2013;50(3-4):290-302.
147. Johnson TN, Zhou D, Bui KH. Development of physiologically based pharmacokinetic model to evaluate the relative systemic exposure to quetiapine after administration of IR and XR formulations to adults, children and adolescents. *Biopharmaceutics & Drug Disposition*. 2014;35(6):341-52.
148. Zhao P, Vieira MdLT, Grillo JA, Song P, Wu T-C, Zheng JH, et al. Evaluation of Exposure Change of Nonrenally Eliminated Drugs in Patients With Chronic Kidney Disease Using Physiologically Based Pharmacokinetic Modeling and Simulation. *Journal of Clinical Pharmacology*. 2012;52:91S-108S.
149. Sayama H, Takubo H, Komura H, Kogayu M, Iwaki M. Application of a Physiologically Based Pharmacokinetic Model Informed by a Top-Down Approach for the Prediction of Pharmacokinetics in Chronic Kidney Disease Patients. *Aaps Journal*. 2014;16(5):1018-28.
150. Lu G, Abduljalil K, Jamei M, Johnson TN, Soltani H, Rostami-Hodjegan A. Physiologically-based Pharmacokinetic (PBPK) Models for Assessing the Kinetics of Xenobiotics during Pregnancy: Achievements and Shortcomings. *Current Drug Metabolism*. 2012;13(6):695-720.
151. Leong R, Vieira MLT, Zhao P, Mulugeta Y, Lee CS, Huang SM, et al. Regulatory Experience With Physiologically Based Pharmacokinetic Modeling for Pediatric Drug Trials. *Clinical Pharmacology & Therapeutics*. 2012;91(5):926-31.
152. Zakaria Z, Badhan R. Development of a Region-Specific Physiologically Based Pharmacokinetic Brain Model to Assess Hippocampus and Frontal Cortex Pharmacokinetics. *Pharmaceutics*. 2018;10(1):14.
153. Jones HM, Chen Y, Gibson C, Heimbach T, Parrott N, Peters SA, et al. Physiologically Based Pharmacokinetic Modeling in Drug Discovery and Development: A Pharmaceutical Industry Perspective. *Clinical Pharmacology & Therapeutics*. 2015;97(3):247-62.
154. Chen Y, Jin JY, Mukadam S, Malhi V, Kenny JR. Application of IVIVE and PBPK modeling in prospective prediction of clinical pharmacokinetics: strategy and approach during the drug discovery phase with four case studies. *Biopharmaceutics & Drug Disposition*. 2012;33(2):85-98.

155. Shardlow CE, Generaux GT, Patel AH, Tai GY, Tran T, Bloomer JC. Impact of Physiologically Based Pharmacokinetic Modeling and Simulation in Drug Development. *Drug Metabolism and Disposition*. 2013;41(12):1994-2003.
156. Huang SM, Abernethy DR, Wang YN, Zhao P, Zineh I. The Utility of Modeling and Simulation in Drug Development and Regulatory Review. *Journal of Pharmaceutical Sciences*. 2013;102(9):2912-23.
157. European Medicines Agency. Draft Guideline on the qualification and reporting of physiologically based pharmacokinetic (PBPK) modelling and simulation [Guideline]. 2016 [21 July 2016]. Available from: [http://www.ema.europa.eu/docs/en\\_GB/document\\_library/Scientific\\_guideline/2016/07/WC500211315.pdf](http://www.ema.europa.eu/docs/en_GB/document_library/Scientific_guideline/2016/07/WC500211315.pdf).
158. European Medicines Agency. Concept paper on qualification and reporting of physiologically based pharmacokinetic (PBPK) modeling and analyses. EMA/CHMP/211243/2014 [Guidelines]. 2014 [26 June 2014]. Available from: [http://www.ema.europa.eu/docs/en\\_GB/document\\_library/Scientific\\_guideline/2014/06/WC500169452.pdf](http://www.ema.europa.eu/docs/en_GB/document_library/Scientific_guideline/2014/06/WC500169452.pdf).
159. U.S. Food and Drug Administration. Advancing Regulatory Science for Public Health—A Framework for FDA’s Regulatory Science Initiative 2010 [25 January 2018]. Available from: <https://www.fda.gov/downloads/ScienceResearch/SpecialTopics/RegulatoryScience/UCM228444.pdf>.
160. U.S. Food Drug Administration. Drug development and drug interactions 2011 [13 May 2016]. Available from: <https://www.fda.gov/Drugs/DevelopmentApprovalProcess/DevelopmentResources/DrugInteractionsLabeling/ucm080499.htm>.
161. U.S. Food and Drug Administration. Physiologically Based Pharmacokinetic Analyses — Format and Content. Guidance for Industry 2016 [28 January 2018]. Available from: <https://www.fda.gov/downloads/Drugs/GuidanceComplianceRegulatoryInformation/Guidances/UCM531207.pdf>.
162. European Medicines Agency. Visual identity of the European Medicines Agency. 2011 [19 January 2018]. Available from: [http://www.ema.europa.eu/ema/index.jsp?curl=pages/about\\_us/general/general\\_content\\_000221.jsp&murl=menus/news\\_and\\_events/news\\_and\\_events.jsp&mid=WC0b01ac058008a65a&jsenabled=true](http://www.ema.europa.eu/ema/index.jsp?curl=pages/about_us/general/general_content_000221.jsp&murl=menus/news_and_events/news_and_events.jsp&mid=WC0b01ac058008a65a&jsenabled=true).
163. Shepard T, Scott G, Cole S, Nordmark A, Bouzom F. Physiologically based models in regulatory submissions: output from the ABPI/MHRA forum on physiologically based modeling and simulation. *CPT: pharmacometrics & systems pharmacology*. 2015;4(4):221-5.
164. Jamei M. Recent advances in development and application of physiologically-based pharmacokinetic (PBPK) models: a transition from academic curiosity to regulatory acceptance. *Current pharmacology reports*. 2016;2(3):161-9.
165. Chang CC, Crane M, Zhou JL, Mina M, Post JJ, Cameron BA, et al. HIV and co-infections. *Immunol Rev*. 2013;254:114-42.
166. U.S. Food and Drug Administration. FDA's Origin 2009 [19 January 2018]. Available from: <http://www.fda.gov/AboutFDA/WhatWeDo/History/Origin/ucm124403.htm>.
167. U.S. Food and Drug Administration. Laws Enforced by FDA 2009 [19 January 2018]. Available from: <http://www.fda.gov/AboutFDA/WhatWeDo/Laws/default.htm>

168. Clewell HJ, 3rd, Andersen ME, Wills RJ, Latriano L. A physiologically based pharmacokinetic model for retinoic acid and its metabolites. *Journal of the American Academy of Dermatology*. 1997;36(3 Pt 2):S77-85.
169. Huang S-M, Lesko LJ. Authors' Response. *The Journal of Clinical Pharmacology*. 2009;49(3):370-.
170. U.S. Food Drug Administration. Guidance for industry clinical lactation studies—study design, data analysis, and recommendations for labeling. Federal Register. 2005;70(25):6697.
171. Zhang L, Reynolds KS, Zhao P, Huang S-M. Drug interactions evaluation: an integrated part of risk assessment of therapeutics. *Toxicology and applied pharmacology*. 2010;243(2):134-45.
172. Huang W, Lee SL, Lawrence XY. Mechanistic approaches to predicting oral drug absorption. *The AAPS journal*. 2009;11(2):217-24.
173. Davies NM, Takemoto JK, Brocks DR, Yáñez JA. Multiple Peaking Phenomena in Pharmacokinetic Disposition. *Clinical Pharmacokinetics*. 2010;49(6):351-77.
174. Rowland M, Peck C, Tucker G. Physiologically-based pharmacokinetics in drug development and regulatory science. *Annual review of pharmacology and toxicology*. 2011;51:45-73.
175. Huang SM, Strong JM, Zhang L, Reynolds KS, Nallani S, Temple R, et al. New era in drug interaction evaluation: US Food and Drug Administration update on CYP enzymes, transporters, and the guidance process. *The Journal of Clinical Pharmacology*. 2008;48(6):662-70.
176. Zhang L, Zhang YD, Zhao P, Huang S-M. Predicting drug–drug interactions: an FDA perspective. *The AAPS journal*. 2009;11(2):300-6.
177. Zhao P, Ragueneau-Majlessi I, Zhang L, Strong JM, Reynolds KS, Levy RH, et al. Quantitative evaluation of pharmacokinetic inhibition of CYP3A substrates by ketoconazole: a simulation study. *J Clin Pharmacol*. 2009;49(3):351-9.
178. Pharmaceuticals and Medical Devices Agency. About PMDA 2017 [25 January 2018]. Available from: <https://www.pmda.go.jp/english/about-pmda/index.html>.
179. Sato M, Ochiai Y, Kijima S, Nagai N, Ando Y, Shikano M, et al. Quantitative Modeling and Simulation in PMDA: A Japanese Regulatory Perspective. *CPT: Pharmacometrics & Systems Pharmacology*. 2017.
180. de Boer AG, Gaillard PJ. Drug targeting to the brain. *Annual Review of Pharmacology and Toxicology*. Annual Review of Pharmacology and Toxicology. 47. Palo Alto: Annual Reviews; 2007. p. 323-55.
181. Olesen J, Baker MG, Freund T, di Luca M, Mendlewicz J, Ragan I, et al. Consensus document on European brain research. *Journal of neurology, neurosurgery, and psychiatry*. 2006;77 Suppl 1:i1-49.
182. Pardridge WM. The blood-brain barrier: bottleneck in brain drug development. *NeuroRx : the journal of the American Society for Experimental NeuroTherapeutics*. 2005;2(1):3-14.
183. Wolburg H, Lippoldt A. Tight junctions of the blood-brain barrier: Development, composition and regulation. *Vascular Pharmacology*. 2002;38(6):323-37.
184. Ghose AK, Viswanadhan VN, Wendoloski JJ. A knowledge-based approach in designing combinatorial or medicinal chemistry libraries for drug discovery. 1. A qualitative and quantitative characterization of known drug databases. *Journal of combinatorial chemistry*. 1999;1(1):55-68.

185. Cecchelli R, Berezowski V, Lundquist S, Culot M, Renftel M, Dehouck M-P, et al. Modelling of the blood-brain barrier in drug discovery and development. *Nature Reviews Drug Discovery*. 2007;6(8):650-61.
186. Abbott NJ. Evidence for bulk flow of brain interstitial fluid: significance for physiology and pathology. *Neurochemistry International*. 2004;45(4):545-52.
187. Abbott NJ, Patabendige AAK, Dolman DEM, Yusof SR, Begley DJ. Structure and function of the blood-brain barrier. *Neurobiology of Disease*. 2010;37(1):13-25.
188. Abbott NJ, Ronnback L, Hansson E. Astrocyte-endothelial interactions at the blood-brain barrier. *Nature Reviews Neuroscience*. 2006;7(1):41-53.
189. Deli MA. Drug transport and the blood-brain barrier. (Eds) KTaMV, editor: Bentham Science; 2011.
190. Begley DJ, Brightman MW. Structural and functional aspects of the blood-brain barrier. Peptide transport and delivery into the central nervous system. 2003;Volume 61:39-78.
191. Hawkins BT, Davis TP. The blood-brain barrier/neurovascular unit in health and disease. *Pharmacological Reviews*. 2005;57(2):173-85.
192. Zlokovic BV. The blood-brain barrier in health and chronic neurodegenerative disorders. *Neuron*. 2008;57(2):178-201.
193. El-Bacha RS, Minn A. Drug metabolizing enzymes in cerebrovascular endothelial cells afford a metabolic protection to the brain. *Cellular and Molecular Biology*. 1999;45(1):15-23.
194. Dauchy S, Dutheil F, Weaver RJ, Chassoux F, Daumas-Duport C, Couraud P-O, et al. ABC transporters, cytochromes P450 and their main transcription factors: expression at the human blood-brain barrier. *Journal of Neurochemistry*. 2008;107(6):1518-28.
195. Dauchy S, Miller F, Couraud P-O, Weaver RJ, Weksler B, Romero I-A, et al. Expression and transcriptional regulation of ABC transporters and cytochromes P450 in hCMEC/D3 human cerebral microvascular endothelial cells. *Biochemical Pharmacology*. 2009;77(5):897-909.
196. Bauer B, Hartz AMS, Lucking JR, Yang X, Pollack GM, Miller DS. Coordinated nuclear receptor regulation of the efflux transporter, Mrp2, and the phase-II metabolizing enzyme, GST pi, at the blood-brain barrier. *Journal of Cerebral Blood Flow and Metabolism*. 2008;28(6):1222-34.
197. Minn A, Ghersiegea JF, Perrin R, Leininger B, Siest G. DRUG-METABOLIZING-ENZYMES IN THE BRAIN AND CEREBRAL MICROVESSELS. *Brain Research Reviews*. 1991;16(1):65-82.
198. Banks WA. Characteristics of compounds that cross the blood-brain barrier. *BMC neurology*. 2009;9 Suppl 1:S3-S.
199. Pardridge WM. Drug and gene targeting to the brain with molecular Trojan horses. *Nature Reviews Drug Discovery*. 2002;1(2):131-9.
200. Enerson BE, Drewes LR. The rat blood-brain barrier transcriptome. *Journal of Cerebral Blood Flow and Metabolism*. 2006;26(7):959-73.
201. Oldendorf WH. Brain uptake of radiolabeled amino acids, amines, and hexoses after arterial injection. *Am J Physiol*. 1971;221(6):1629-39.
202. Terasaki T, Ohtsuki S. Brain-to-blood transporters for endogenous substrates and xenobiotics at the blood-brain barrier: an overview of biology and methodology. *NeuroRx : the journal of the American Society for Experimental NeuroTherapeutics*. 2005;2(1):63-72.
203. Fricker G, Miller DS. Modulation of drug transporters at the blood-brain barrier. *Pharmacology*. 2004;70(4):169-76.

204. Loscher W, Potschka H. Drug resistance in brain diseases and the role of drug efflux transporters. *Nature Reviews Neuroscience*. 2005;6(8):591-602.
205. Banks WA. Physiology and pathology of the blood-brain barrier: implications for microbial pathogenesis, drug delivery and neurodegenerative disorders. *Journal of Neurovirology*. 1999;5(6):538-55.
206. Joo F. Endothelial cells of the brain and other organ systems: Some similarities and differences. *Progress in Neurobiology*. 1996;48(3):255-&.
207. Gumbleton M, Audus KL. Progress and limitations in the use of in vitro cell cultures to serve as a permeability screen for the blood-brain barrier. *Journal of Pharmaceutical Sciences*. 2001;90(11):1681-98.
208. Reichel A, Begley DJ, Abbott NJ. An overview of in vitro techniques for blood-brain barrier studies. *Methods in molecular medicine*. 2003;89:307-24.
209. Lundquist S, Renftel M. The use of in vitro cell culture models for mechanistic studies and as permeability screens for the blood-brain barrier in the pharmaceutical industry - Background and current status in the drug discovery process. *Vascular Pharmacology*. 2002;38(6):355-64.
210. Pardridge WM. Blood-brain barrier biology and methodology. *Journal of Neurovirology*. 1999;5(6):556-69.
211. Abbott NJ. Prediction of blood-brain barrier permeation in drug discovery from in vivo, in vitro and in silico models. *Drug discovery today Technologies*. 2004;1(4):407-16.
212. Liu X, Chen C, Smith BJ. Progress in brain penetration evaluation in drug discovery and development. *Journal of Pharmacology and Experimental Therapeutics*. 2008;325(2):349-56.
213. Syvänen S, Xie R, Sahin S, Hammarlund-Udenaes M. Pharmacokinetic consequences of active drug efflux at the blood-brain barrier. *Pharmaceutical research*. 2006;23(4):705-17.
214. Deguchi Y, Inabe K, Tomiyasu K, Nozawa K, Yamada S, Kimura R. Study on brain interstitial fluid distribution and blood-brain barrier transport of baclofen in rats by microdialysis. *Pharmaceutical research*. 1995;12(12):1838-44.
215. Bostrom E, Simonsson US, Hammarlund-Udenaes M. In vivo blood-brain barrier transport of oxycodone in the rat: indications for active influx and implications for pharmacokinetics/pharmacodynamics. *Drug Metab Dispos*. 2006;34(9):1624-31.
216. Marchand S, Chenel M, Lamarche I, Pariat C, Couet W. Dose ranging pharmacokinetics and brain distribution of norfloxacin using microdialysis in rats. *J Pharm Sci*. 2003;92(12):2458-65.
217. Marchand S, Forsell A, Chenel M, Comets E, Lamarche I, Couet W. Norfloxacin blood-brain barrier transport in rats is not affected by probenecid coadministration. *Antimicrob Agents Chemother*. 2006;50(1):371-3.
218. Doran A, Obach RS, Smith BJ, Hosea NA, Becker S, Callegari E, et al. The impact of P-glycoprotein on the disposition of drugs targeted for indications of the central nervous system: evaluation using the MDR1A/1B knockout mouse model. *Drug metabolism and disposition: the biological fate of chemicals*. 2005;33(1):165-74.
219. Elmquist WF, Sawchuk RJ. Application of microdialysis in pharmacokinetic studies. *Pharmaceutical research*. 1997;14(3):267-88.
220. Hammarlund-Udenaes M, Paalzow LK, de Lange EC. Drug equilibration across the blood-brain barrier--pharmacokinetic considerations based on the microdialysis method. *Pharmaceutical research*. 1997;14(2):128-34.

221. Kalvass JC, Maurer TS. Influence of nonspecific brain and plasma binding on CNS exposure: implications for rational drug discovery. *Biopharmaceutics & drug disposition*. 2002;23(8):327-38.
222. Liu X, Smith BJ, Chen C, Callegari E, Becker SL, Chen X, et al. Evaluation of cerebrospinal fluid concentration and plasma free concentration as a surrogate measurement for brain free concentration. *Drug metabolism and disposition: the biological fate of chemicals*. 2006;34(9):1443-7.
223. Becker S, Liu XR. Evaluation of the utility of brain slice methods to study brain penetration. *Drug Metabolism and Disposition*. 2006;34(5):855-61.
224. Summerfield SG, Stevens AJ, Cutler L, Osuna MD, Hammond B, Tang SP, et al. Improving the in vitro prediction of in vivo central nervous system penetration: integrating permeability, P-glycoprotein efflux, and free fractions in blood and brain. *Journal of Pharmacology and Experimental Therapeutics*. 2006;316(3):1282-90.
225. Jeffrey P, Summerfield SG. Challenges for blood-brain barrier (BBB) screening. *Xenobiotica; the fate of foreign compounds in biological systems*. 2007;37(10-11):1135-51.
226. Summerfield SG, Lucas AJ, Porter RA, Jeffrey P, Gunn RN, Read KR, et al. Toward an improved prediction of human in vivo brain penetration. *Xenobiotica; the fate of foreign compounds in biological systems*. 2008;38(12):1518-35.
227. Campbell J, Van Landingham C, Crowell S, Gentry R, Kaden D, Fiebelkorn S, et al. A preliminary regional PBPK model of lung metabolism for improving species dependent descriptions of 1,3-butadiene and its metabolites. *Chemico-biological interactions*. 2015;238:102-10.
228. Neuhoff S, Gaohua L, Burt H, Jamei M, Li L, Tucker GT, et al. Accounting for Transporters in Renal Clearance: Towards a Mechanistic Kidney Model (Mech KiM). In: Sugiyama Y, Steffansen B, editors. *Transporters in Drug Development: Discovery, Optimization, Clinical Study and Regulation*. New York, NY: Springer New York; 2013. p. 155-77.
229. Ball K, Bouzom F, Scherrmann JM, Walther B, Declèves X. A physiologically based modeling strategy during preclinical CNS drug development. *Molecular pharmaceutics*. 2014;11(3):836-48.
230. Ball K, Bouzom F, Scherrmann J-M, Walther B, Declèves X. Development of a physiologically based pharmacokinetic model for the rat central nervous system and determination of an in vitro–in vivo scaling methodology for the blood–brain barrier permeability of two transporter substrates, morphine and oxycodone. *Journal of Pharmaceutical Sciences*. 2012;101(11):4277-92.
231. Liu X, Smith BJ, Chen C, Callegari E, Becker SL, Chen X, et al. Use of a physiologically based pharmacokinetic model to study the time to reach brain equilibrium: an experimental analysis of the role of blood-brain barrier permeability, plasma protein binding, and brain tissue binding. *The Journal of pharmacology and experimental therapeutics*. 2005;313(3):1254-62.
232. Ball K, Bouzom F, Scherrmann J-M, Walther B, Declèves X. Development of a physiologically based pharmacokinetic model for the rat central nervous system and determination of an in vitro-in vivo scaling methodology for the blood-brain barrier permeability of two transporter substrates, morphine and oxycodone. *Journal of Pharmaceutical Sciences*. 2012;101(11):4277-92.
233. Ball K, Bouzom F, Scherrmann JM, Walther B, Declèves X. A Physiologically Based Modeling Strategy during Preclinical CNS Drug Development. *Molecular Pharmaceutics*. 2014;11(3):836-48.

234. Yamamoto Y, Väitalo PA, Wong YC, Huntjens DR, Proost JH, Vermeulen A, et al. Prediction of human CNS pharmacokinetics using a physiologically-based pharmacokinetic modeling approach. *European Journal of Pharmaceutical Sciences*. 2018;112(Supplement C):168-79.
235. Yamamoto Y, Väitalo PA, van den Berg D-J, Hartman R, van den Brink W, Wong YC, et al. A Generic Multi-Compartmental CNS Distribution Model Structure for 9 Drugs Allows Prediction of Human Brain Target Site Concentrations. *Pharmaceutical research*. 2017;34(2):333-51.
236. Yamamoto Y, Väitalo PA, Huntjens DR, Proost JH, Vermeulen A, Krauwinkel W, et al. Predicting Drug Concentration-Time Profiles in Multiple CNS Compartments Using a Comprehensive Physiologically-Based Pharmacokinetic Model. *CPT: Pharmacometrics & Systems Pharmacology*. 2017;6(11):765-77.
237. Yamamoto Y, Danhof M, de Lange ECM. Microdialysis: the Key to Physiologically Based Model Prediction of Human CNS Target Site Concentrations. *The AAPS Journal*. 2017;19(4):891-909.
238. Beal S, Sheiner L, Boeckmann A, Bauer R. *NONMEM User's Guides*.(1989–2009), Icon Development Solutions, Ellicott City, MD, USA, 2009. Book *NONMEM User's Guides*(1989–2009) Ellicott City, MD, USA: Icon Development Solutions. 2009.
239. Yamamoto Y, Väitalo PA, van den Berg D-J, Hartman R, van den Brink W, Wong YC, et al. A Generic Multi-Compartmental CNS Distribution Model Structure for 9 Drugs Allows Prediction of Human Brain Target Site Concentrations. *Pharmaceutical research*. 2016.
240. Walker MC, Alavijeh MS, Shorvon SD, Patsalos PN. Microdialysis study of the neuropharmacokinetics of phenytoin in rat hippocampus and frontal cortex. *Epilepsia*. 1996;37(5):421-7.
241. Sechi GP, Petrucci V, Rosati G, Tanca S, Monaco F, Formato M, et al. BRAIN INTERSTITIAL FLUID AND INTRACELLULAR-DISTRIBUTION OF PHENYTOIN. *Epilepsia*. 1989;30(2):235-9.
242. Van Belle K, Sarre S, Ebinger G, Michotte Y. Brain, liver and blood distribution kinetics of carbamazepine and its metabolic interaction with clomipramine in rats: a quantitative microdialysis study. *J Pharmacol Exp Ther*. 1995;272(3):1217-22.
243. Bouw R, Ederoth P, Lundberg J, Ungerstedt U, Nordström CH, Hammarlund-Udenaes M. Increased blood–brain barrier permeability of morphine in a patient with severe brain lesions as determined by microdialysis. *Acta Anaesthesiologica Scandinavica*. 2001;45(3):390-2.
244. Ederoth P, Tunblad K, Bouw R, Lundberg CJF, Ungerstedt U, Nordström C-H, et al. Blood–brain barrier transport of morphine in patients with severe brain trauma. *British Journal of Clinical Pharmacology*. 2004;57(4):427-35.
245. The MathWorks Inc. Natick, MA.2000.
246. Kalvass JC, Maurer TS, Pollack GM. Use of plasma and brain unbound fractions to assess the extent of brain distribution of 34 drugs: comparison of unbound concentration ratios to in vivo p-glycoprotein efflux ratios. *Drug Metab Dispos*. 2007;35(4):660-6.
247. Uchida Y, Ohtsuki S, Kamiie J, Terasaki T. Blood-Brain Barrier (BBB) Pharmacoproteomics: Reconstruction of In Vivo Brain Distribution of 11 P-Glycoprotein Substrates Based on the BBB Transporter Protein Concentration, In Vitro Intrinsic Transport Activity, and Unbound Fraction in Plasma and Brain in Mice. *Journal of Pharmacology and Experimental Therapeutics*. 2011;339(2):579-88.

248. Suzuki H, Sawada Y, Sugiyama Y, Iga T, Hanano M. Facilitated transport of benzylpenicillin through the blood-brain barrier in rats. *Journal of pharmacobio-dynamics*. 1989;12(3):182-5.
249. Tanaka H, Mizojiri K. Drug-protein binding and blood-brain barrier permeability. *J Pharmacol Exp Ther*. 1999;288(3):912-8.
250. Rapoport SI, Ohno K, Pettigrew KD. Drug entry into the brain. *Brain Res*. 1979;172(2):354-9.
251. Takasato Y, Rapoport SI, Smith QR. An in situ brain perfusion technique to study cerebrovascular transport in the rat. *Am J Physiol*. 1984;247(3 Pt 2):H484-93.
252. Liu X, Tu M, Kelly RS, Chen C, Smith BJ. Development of a computational approach to predict blood-brain barrier permeability. *Drug Metab Dispos*. 2004;32(1):132-9.
253. Summerfield SG, Read K, Begley DJ, Obradovic T, Hidalgo IJ, Coggon S, et al. Central nervous system drug disposition: the relationship between in situ brain permeability and brain free fraction. *J Pharmacol Exp Ther*. 2007;322(1):205-13.
254. Youdim KA, Qaiser MZ, Begley DJ, Rice-Evans CA, Abbott NJ. Flavonoid permeability across an in situ model of the blood-brain barrier. *Free radical biology & medicine*. 2004;36(5):592-604.
255. Zhao R, Kalvass JC, Pollack GM. Assessment of blood-brain barrier permeability using the in situ mouse brain perfusion technique. *Pharmaceutical research*. 2009;26(7):1657-64.
256. Summerfield SG, Read K, Begley DJ, Obradovic T, Hidalgo IJ, Coggon S, et al. Central nervous system drug disposition: the relationship between in situ brain permeability and brain free fraction. *J Pharmacol Exp Ther*. 2007;322(1):205-13.
257. Rodgers T, Leahy D, Rowland M. Physiologically based pharmacokinetic modeling 1: predicting the tissue distribution of moderate-to-strong bases. *Journal of pharmaceutical sciences*. 2005;94(6):1259-76.
258. Hansch CL, A.; Hoekman, D.. *Exploring QSAR.: . Fundamentals and applications in chemistry and biology: American Chemical Society; 1995.*
259. O'Neil MJ. *The Merck index : an encyclopedia of chemicals, drugs, and biologicals*. Whitehouse Station, N.J.: Merck; 2001.
260. Ullrich KJ, Rumrich G. Renal contraluminal transport systems for organic anions (paraaminohippurate, PAH) and organic cations (N1-methyl-nicotinamide, NMeN) do not see the degree of substrate ionization. *Pflugers Archiv : European journal of physiology*. 1992;421(2-3):286-8.
261. Martin AN. *Physical Pharmacy*, 2 ed: Philadelphia, Lea & Febiger,; 1969.
262. Sangster J. *Octanol-Water Partition Coefficients: Fundamentals and Physical Chemistry*. 1 ed. New York: Wiley; 1994.
263. McLure JA, Miners JO, Birkett DJ. Nonspecific binding of drugs to human liver microsomes. *Br J Clin Pharmacol*. 2000;49(5):453-61.
264. Deak K, Takacs-Novak K, Tihanyi K, Noszal B. Physico-chemical profiling of antidepressive sertraline: solubility, ionisation, lipophilicity. *Medicinal chemistry*. 2006;2(4):385-9.
265. Kodaira H, Kusuhara H, Fujita T, Ushiki J, Fuse E, Sugiyama Y. Quantitative evaluation of the impact of active efflux by p-glycoprotein and breast cancer resistance protein at the blood-brain barrier on the predictability of the unbound concentrations of drugs in the brain using cerebrospinal fluid concentration as a surrogate. *J Pharmacol Exp Ther*. 2011;339(3):935-44.

266. Ronfeld RA, Tremaine LM, Wilner KD. Pharmacokinetics of sertraline and its N-demethyl metabolite in elderly and young male and female volunteers. *Clin Pharmacokinet.* 1997;32 Suppl 1:22-30.
267. Lin JH. Applications and limitations of interspecies scaling and in vitro extrapolation in pharmacokinetics. *Drug Metab Dispos.* 1998;26(12):1202-12.
268. Scavone JM, Blyden GT, Greenblatt DJ. Lack of effect of influenza vaccine on the pharmacokinetics of antipyrine, alprazolam, paracetamol (acetaminophen) and lorazepam. *Clin Pharmacokinet.* 1989;16(3):180-5.
269. Scavone JM, Greenblatt DJ, Abernethy DR, Luna BG, Harmatz JS, Shader RI. Influence of oral contraceptive use and cigarette smoking, alone and together, on antipyrine pharmacokinetics. *J Clin Pharmacol.* 1997;37(5):437-41.
270. Thompson GA, St Peter JV, Heise MA, Horowitz ZD, Salyers GC, Charles TT, et al. Assessment of doxylamine influence on mixed function oxidase activity upon multiple dose oral administration to normal volunteers. *J Pharm Sci.* 1996;85(11):1242-7.
271. Birkett DJ, Miners JO. Caffeine renal clearance and urine caffeine concentrations during steady state dosing. Implications for monitoring caffeine intake during sports events. *Br J Clin Pharmacol.* 1991;31(4):405-8.
272. Hammarlund-Udenaes M, Friden M, Syvanen S, Gupta A. On the rate and extent of drug delivery to the brain. *Pharm Res.* 2008;25(8):1737-50.
273. Pardridge WM. Drug and gene delivery to the brain: the vascular route. *Neuron.* 2002;36(4):555-8.
274. Davies B, Morris T. PHYSIOLOGICAL-PARAMETERS IN LABORATORY-ANIMALS AND HUMANS. *Pharmaceutical research.* 1993;10(7):1093-5.
275. Spanswick SC, Dyck RH. Object/Context Specific Memory Deficits following Medial Frontal Cortex Damage in Mice. *Plos One.* 2012;7(8):7.
276. Ashbrook DG, Williams RW, Lu L, Stein JL, Hibar DP, Nichols TE, et al. Joint genetic analysis of hippocampal size in mouse and human identifies a novel gene linked to neurodegenerative disease. *BMC Genomics.* 2014;15:9.
277. Hong L, Jiang W, Pan H, Jiang Y, Zeng S, Zheng W. Brain regional pharmacokinetics of p-aminosalicylic acid and its N-acetylated metabolite: effectiveness in chelating brain manganese. *Drug Metab Dispos.* 2011;39(10):1904-9.
278. Syková E, Nicholson C. Diffusion in Brain Extracellular Space. *Physiological reviews.* 2008;88(4):1277-340.
279. Murtha LA, Yang Q, Parsons MW, Levi CR, Beard DJ, Spratt NJ, et al. Cerebrospinal fluid is drained primarily via the spinal canal and olfactory route in young and aged spontaneously hypertensive rats. *Fluids and barriers of the CNS.* 2014;11:12.
280. Hamberger A, Jacobson I, Nyström B, Sandberg M. Microdialysis sampling of the neuronal environment in basic and clinical research. *Journal of Internal Medicine.* 1991;230(4):375-80.
281. Poulin P, Theil FP. Prediction of pharmacokinetics prior to in vivo studies. 1. Mechanism-based prediction of volume of distribution. *Journal of Pharmaceutical Sciences.* 2002;91(1):129-56.
282. Harnish PP, Samuel K. REDUCED CEREBROSPINAL-FLUID PRODUCTION IN THE RAT AND RABBIT BY DIATRIZOATE - VENTRICULO-CISTERNAL PERFUSION. *Invest Radiol.* 1988;23(7):534-6.
283. Brinker T, Stopa E, Morrison J, Klinge P. A new look at cerebrospinal fluid circulation. *Fluids and barriers of the CNS.* 2014;11:10-

284. Lu G, Neuhoff S, Johnson TN, Rostami-Hodjegan A, Jamei M. Development of a permeability-limited model of the human brain and cerebrospinal fluid (CSF) to integrate known physiological and biological knowledge: Estimating time varying CSF drug concentrations and their variability using in vitro edata. *Drug Metabolism and Pharmacokinetics*. 2016;31(3):224-33.
285. Meno-Tetang GM, Li H, Mis S, Pyszczynski N, Heining P, Lowe P, et al. Physiologically based pharmacokinetic modeling of FTY720 (2-amino-2[2-(-4-octylphenyl)ethyl]propane-1,3-diol hydrochloride) in rats after oral and intravenous doses. *Drug Metab Dispos*. 2006;34(9):1480-7.
286. Lee T, Jarome T, Li S-J, Kim JJ, Helmstetter FJ. Chronic stress selectively reduces hippocampal volume in rats: a longitudinal MRI study. *Neuroreport*. 2009;20(17):1554-8.
287. Honeycutt NA, Smith CD. Hippocampal volume measurements using magnetic resonance imaging in normal young adults. *Journal of neuroimaging : official journal of the American Society of Neuroimaging*. 1995;5(2):95-100.
288. Dexter BC, Rahmouni K, Cushman T, Hermann GM, Ni C, Nopoulos PC, et al. Neonatal Leptin Deficiency Reduces Frontal Cortex Volumes and Programs Adult Hyperactivity in Mice. *Behav Brain Res*. 2014;263:115-21.
289. Semendeferi K, Lu A, Schenker N, Damasio H. Humans and great apes share a large frontal cortex. *Nature neuroscience*. 2002;5(3):272-6.
290. Bass NH, Lundborg P. Postnatal development of bulk flow in the cerebrospinal fluid system of the albino rat: clearance of carboxyl-( 14 C)inulin after intrathecal infusion. *Brain Res*. 1973;52:323-32.
291. Sakka L, Coll G, Chazal J. Anatomy and physiology of cerebrospinal fluid. *European Annals of Otorhinolaryngology, Head and Neck Diseases*. 2011;128(6):309-16.
292. Dale O, Nilsen T, Olaussen G, Tvedt KE, Skorpen F, Smidsrød O, et al. Transepithelial transport of morphine and mannitol in Caco-2 cells: the influence of chitosans of different molecular weights and degrees of acetylation. *Journal of Pharmacy and Pharmacology*. 2006;58(7):909-15.
293. Roy SD, Flynn GL. Solubility Behavior of Narcotic Analgesics in Aqueous Media: Solubilities and Dissociation Constants of Morphine, Fentanyl, and Sufentanil. *Pharmaceutical research*. 1989;6(2):147-51.
294. Illum L, Watts P, Fisher AN, Hinchcliffe M, Norbury H, Jabbal-Gill I, et al. Intranasal Delivery of Morphine. *Journal of Pharmacology and Experimental Therapeutics*. 2002;301(1):391-400.
295. Olsen GD. Morphine binding to human plasma proteins. *Clinical pharmacology and therapeutics*. 1975;17(1):31-5.
296. Reichel A. The role of blood-brain barrier studies in the pharmaceutical industry. *Curr Drug Metab*. 2006;7(2):183-203.
297. Tornqvist E, Annas A, Granath B, Jalkestén E, Cotgreave I, Oberg M. Strategic Focus on 3R Principles Reveals Major Reductions in the Use of Animals in Pharmaceutical Toxicity Testing. *Plos One*. 2014;9(7).
298. Suzuki H, Terasaki T, Sugiyama Y. Role of efflux transport across the blood-brain barrier and blood cerebrospinal fluid barrier on the disposition of xenobiotics in the central nervous system. *Advanced Drug Delivery Reviews*. 1997;25(2-3):257-85.
299. Dahlström BE, Paalzow LK. Pharmacokinetics of morphine in plasma and discrete areas of the rat brain. *Journal of Pharmacokinetics and Biopharmaceutics*. 1975;3(5):293-302.

300. Yokagawa K, Nakashima E, Ishizaki J, Hasegawa M, Kido H, Ichimura F. Brain regional pharmacokinetics of biperiden in rats. *Biopharmaceutics & drug disposition*. 1992;13(2):131-40.
301. Kamiie J, Ohtsuki S, Iwase R, Ohmine K, Katsukura Y, Yanai K, et al. Quantitative atlas of membrane transporter proteins: development and application of a highly sensitive simultaneous LC/MS/MS method combined with novel in-silico peptide selection criteria. *Pharmaceutical research*. 2008;25(6):1469-83.
302. Hoshi Y, Uchida Y, Tachikawa M, Inoue T, Ohtsuki S, Terasaki T. Quantitative atlas of blood-brain barrier transporters, receptors, and tight junction proteins in rats and common marmoset. *J Pharm Sci*. 2013;102(9):3343-55.
303. Adachi Y, Suzuki H, Sugiyama Y. Comparative studies on in vitro methods for evaluating in vivo function of MDR1 P-glycoprotein. *Pharmaceutical research*. 2001;18(12):1660-8.
304. Uchida Y, Ohtsuki S, Kamiie J, Terasaki T. Blood-brain barrier (BBB) pharmacoproteomics: reconstruction of in vivo brain distribution of 11 P-glycoprotein substrates based on the BBB transporter protein concentration, in vitro intrinsic transport activity, and unbound fraction in plasma and brain in mice. *J Pharmacol Exp Ther*. 2011;339(2):579-88.
305. O'Brien JS, Sampson EL. Lipid composition of the normal human brain: gray matter, white matter, and myelin. *Journal of lipid research*. 1965;6(4):537-44.
306. O'Brien JS, Sampson EL. Fatty acid and fatty aldehyde composition of the major brain lipids in normal human gray matter, white matter, and myelin. *Journal of lipid research*. 1965;6(4):545-51.
307. Lohmann C, Schachmann E, Dandekar T, Villmann C, Becker CM. Developmental profiling by mass spectrometry of phosphocholine containing phospholipids in the rat nervous system reveals temporo-spatial gradients. *J Neurochem*. 2010;114(4):1119-34.
308. Martinez M, Mougan I. Fatty acid composition of human brain phospholipids during normal development. *J Neurochem*. 1998;71(6):2528-33.
309. Pardridge WM. Blood-brain barrier drug targeting: the future of brain drug development. *Molecular interventions*. 2003;3(2):90-105, 51.
310. World Health Organization. World malaria report 2016 2016 [12 June 2016]. Available from: <http://www.who.int/malaria/publications/world-malaria-report-2016/report/en/>.
311. World Health Organisation WHO. Malaria in children under five 2016 [updated April 6, 2016; cited 2016 29th September]. Available from: [http://www.who.int/malaria/areas/high\\_risk\\_groups/children/en/](http://www.who.int/malaria/areas/high_risk_groups/children/en/).
312. World Health Organization: UNAIDS. AIDS epidemic update: December 2009: WHO Regional Office Europe; 2009 [13 June 2017]. Available from: [http://www.unaids.org/en/resources/documents/2009/20091124\\_jc1700\\_epi\\_update\\_2009\\_en.pdf](http://www.unaids.org/en/resources/documents/2009/20091124_jc1700_epi_update_2009_en.pdf).
313. Saito T, Kikuchi A, Kaneko A, Isozumi R, Teramoto I, Kimura M, et al. Rapid and sensitive multiplex single-tube nested PCR for the identification of five human Plasmodium species. *Parasitology international*. 2018;67(3):277-83.
314. White NJ, Pukrittayakamee S, Hien TT, Faiz MA, Mokuolu OA, Dondorp AM. Malaria. *Lancet (London, England)*. 2014;383(9918):723-35.
315. Bhatt S, Weiss DJ, Cameron E, Bisanzio D, Mappin B, Dalrymple U, et al. The effect of malaria control on Plasmodium falciparum in Africa between 2000 and 2015. *Nature*. 2015;526(7572):207-11.

316. Miller LH, Baruch DI, Marsh K, Doumbo OK. The pathogenic basis of malaria. *Nature*. 2002;415(6872):673-9.
317. Gardner MJ, Hall N, Fung E, White O, Berriman M, Hyman RW, et al. Genome sequence of the human malaria parasite *Plasmodium falciparum*. *Nature*. 2002;419(6906):498-511.
318. Tilley L, Dixon MW, Kirk K. The *Plasmodium falciparum*-infected red blood cell. *The international journal of biochemistry & cell biology*. 2011;43(6):839-42.
319. Bartoloni A, Zammarchi L. Clinical aspects of uncomplicated and severe malaria. *Mediterranean journal of hematology and infectious diseases*. 2012;4(1):e2012026.
320. Taylor WRJ, Hanson J, Turner GDH, White NJ, Dondorp AM. Respiratory manifestations of malaria. *Chest*. 2012;142(2):492-505.
321. Nadjm B, Behrens RH. Malaria: An Update for Physicians. *Infectious Disease Clinics of North America*. 2012;26(2):243-59.
322. Kokwaro G. Ongoing challenges in the management of malaria. *Malar J*. 2009;8 Suppl 1:S2.
323. Keating GM. Dihydroartemisinin/Piperaquine: a review of its use in the treatment of uncomplicated *Plasmodium falciparum* malaria. *Drugs*. 2012;72(7):937-61.
324. Organization WH. Guidelines for the treatment of malaria: World Health Organization; 2015.
325. Sinclair D, Donegan S, Isba R, Lalloo DG. Artesunate versus quinine for treating severe malaria. *The Cochrane database of systematic reviews*. 2012(6):Cd005967.
326. Kyu HH, Fernandez E. Artemisinin derivatives versus quinine for cerebral malaria in African children: a systematic review. *Bulletin of the World Health Organization*. 2009;87(12):896-904.
327. Weiss RA. How does HIV cause AIDS? *Science*. 1993;260(5112):1273-9.
328. Cunningham AL, Donaghy H, Harman AN, Kim M, Turville SG. Manipulation of dendritic cell function by viruses. *Current opinion in microbiology*. 2010;13(4):524-9.
329. Levy JA. HIV pathogenesis and long-term survival. *Aids*. 1993;7(11):1401-10.
330. Doitsh G, Galloway NL, Geng X, Yang Z, Monroe KM, Zepeda O, et al. Cell death by pyroptosis drives CD4 T-cell depletion in HIV-1 infection. *Nature*. 2014;505(7484):509-14.
331. Garg H, Mohl J, Joshi A. HIV-1 induced bystander apoptosis. *Viruses*. 2012;4(11):3020-43.
332. Kumar V. Robbins Basic Pathology. 2013.
333. Robertson DL, Hahn BH, Sharp PM. Recombination in AIDS viruses. *Journal of molecular evolution*. 1995;40(3):249-59.
334. Rambaut A, Posada D, Crandall KA, Holmes EC. The causes and consequences of HIV evolution. *Nature reviews Genetics*. 2004;5(1):52-61.
335. Perelson AS, Ribeiro RM. Estimating drug efficacy and viral dynamic parameters: HIV and HCV. *Statistics in medicine*. 2008;27(23):4647-57.
336. Gilbert PB, McKeague IW, Eisen G, Mullins C, Gueye NA, Mboup S, et al. Comparison of HIV-1 and HIV-2 infectivity from a prospective cohort study in Senegal. *Statistics in medicine*. 2003;22(4):573-93.
337. Reeves JD, Doms RW. Human immunodeficiency virus type 2. *The Journal of general virology*. 2002;83(Pt 6):1253-65.
338. Jmarchn. HIV replication cycle. 2017.
339. WHO Guidelines Approved by the Guidelines Review Committee. Consolidated Guidelines on the Use of Antiretroviral Drugs for Treating and Preventing HIV Infection: Recommendations for a Public Health Approach. Geneva: World Health Organization

Copyright (c) World Health Organization 2013.; 2013.

340. van der Kuyl AC, Cornelissen M. Identifying HIV-1 dual infections. *Retrovirology*. 2007;4:67.
341. May MT, Ingle SM. Life expectancy of HIV-positive adults: a review. *Sexual health*. 2011;8(4):526-33.
342. Korenromp EL, Williams BG, de Vlas SJ, Gouws E, Gilks CF, Ghys PD, et al. Malaria attributable to the HIV-1 epidemic, sub-Saharan Africa. *Emerging infectious diseases*. 2005;11(9):1410-9.
343. Seyler C, Anglaret X, Dakoury-Dogbo N, Messou E, Toure S, Danel C, et al. Medium-term survival, morbidity and immunovirological evolution in HIV-infected adults receiving antiretroviral therapy, Abidjan, Cote d'Ivoire. *Antiviral therapy*. 2003;8(5):385-93.
344. Holmes CB, Losina E, Walensky RP, Yazdanpanah Y, Freedberg KA. Review of human immunodeficiency virus type 1-related opportunistic infections in sub-Saharan Africa. *Clinical infectious diseases : an official publication of the Infectious Diseases Society of America*. 2003;36(5):652-62.
345. Hoglund RM, Byakika-Kibwika P, Lamorde M, Merry C, Ashton M, Hanpithakpong W, et al. Artemether-lumefantrine co-administration with antiretrovirals: population pharmacokinetics and dosing implications. *British Journal of Clinical Pharmacology*. 2015;79(4):636-49.
346. Flateau C, Le Loup G, Pialoux G. Consequences of HIV infection on malaria and therapeutic implications: a systematic review. *Lancet Infect Dis*. 2011;11(7):541-56.
347. Milton K, Edwards G, Ward S, Orme M, Breckenridge A. Pharmacokinetics of halofantrine in man: effects of food and dose size. *British journal of clinical pharmacology*. 1989;28(1):71-7.
348. Ezzet F, Mull R, Karbwang J. The population pharmacokinetics of CGP 56697 and its effects on the therapeutic response in malaria patients. *Br J Clin Pharmacol*. 1998;46:553-61.
349. Ezzet F, Van Vugt M, Nosten F, Looareesuwan S, White N. Pharmacokinetics and pharmacodynamics of lumefantrine (benflumetol) in acute falciparum malaria. *Antimicrobial agents and chemotherapy*. 2000;44(3):697-704.
350. White NJ, van Vugt M, Ezzet FD. Clinical Pharmacokinetics and Pharmacodynamics of Artemether-Lumefantrine. *Clinical Pharmacokinetics*. 1999;37(2):105-25.
351. Ogburn ET, Jones DR, Masters AR, Xu C, Guo Y, Desta Z. Efavirenz primary and secondary metabolism in vitro and in vivo: identification of novel metabolic pathways and cytochrome P450 2A6 as the principal catalyst of efavirenz 7-hydroxylation. *Drug Metab Dispos*. 2010;38(7):1218-29.
352. Shou M, Hayashi M, Pan Y, Xu Y, Morrissey K, Xu L, et al. Modeling, prediction, and in vitro in vivo correlation of CYP3A4 induction. *Drug Metab Dispos*. 2008;36(11):2355-70.
353. Hariparsad N, Nallani SC, Sane RS, Buckley DJ, Buckley AR, Desai PB. Induction of CYP3A4 by efavirenz in primary human hepatocytes: comparison with rifampin and phenobarbital. *Journal of clinical pharmacology*. 2004;44(11):1273-81.
354. Dybul M, Fauci AS, Bartlett JG, Kaplan JE, Pau AK. Guidelines for using antiretroviral agents among HIV-infected adults and adolescents. Recommendations of the Panel on Clinical Practices for Treatment of HIV. *MMWR Recommendations and reports: Morbidity and mortality weekly report Recommendations and reports*. 2002;51(RR-7):1-55.
355. Squibb BM. Efavirenz (Sustiva) product information. 2010.

356. European Medicines Agency. Sustiva (efavirenz) Scientific Discussion 2006 [12 June 2017]. Available from: [http://www.ema.europa.eu/docs/en\\_GB/document\\_library/EPAR\\_-\\_Scientific\\_Discussion/human/000249/WC500058308.pdf](http://www.ema.europa.eu/docs/en_GB/document_library/EPAR_-_Scientific_Discussion/human/000249/WC500058308.pdf).
357. Bharti PK, Shukla MM, Ringwald P, Krishna S, Singh PP, Yadav A, et al. Therapeutic efficacy of artemether-lumefantrine for the treatment of uncomplicated Plasmodium falciparum malaria from three highly malarious states in India. *Malar J*. 2016;15:9.
358. Maganda B, Minzi O, Ngaimisi E, Kamuhabwa A, Aklillu E. CYP2B6\* 6 genotype and high efavirenz plasma concentration but not nevirapine are associated with low lumefantrine plasma exposure and poor treatment response in HIV-malaria-coinfected patients. *The pharmacogenomics journal*. 2016;16(1):88.
359. Lefèvre G, Thomsen MS. Clinical pharmacokinetics of artemether and lumefantrine (Riamet®). *Clinical Drug Investigation*. 1999;18(6):467-80.
360. Thillainayagam M, Ramaiah S. Mosquito, Malaria and Medicines—A Review. *Research Journal of Pharmacy and Technology*. 2016;9(8):1368-276.
361. U.S. Food and Drug Administration. Coartem (artemether/lumefantrine) Tablets highlights of prescribing information [Package insert]. 2009 [30 October 2017]. Available from: [https://www.accessdata.fda.gov/drugsatfda\\_docs/label/2009/0222681bl.pdf](https://www.accessdata.fda.gov/drugsatfda_docs/label/2009/0222681bl.pdf).
362. Law V, Knox C, Djoumbou Y, Jewison T, Guo AC, Liu Y, et al. DrugBank 4.0: shedding new light on drug metabolism. *Nucleic acids research*. 2014;42(Database issue):D1091-7.
363. European Medicines Agency. Sustiva (efavirenz) European public assessment report [Report]. 2012 [20 December 2012]. Available from: [http://www.ema.europa.eu/ema/index.jsp?curl=pages/medicines/human/medicines/000249/human\\_med\\_001068.jsp&mid=WC0b01ac058001d124](http://www.ema.europa.eu/ema/index.jsp?curl=pages/medicines/human/medicines/000249/human_med_001068.jsp&mid=WC0b01ac058001d124).
364. Oswald S, Schwabedissen H, Nassif A, Modess C, Desta Z, Ogburn ET, et al. Impact of Efavirenz on Intestinal Metabolism and Transport: Insights From an Interaction Study With Ezetimibe in Healthy Volunteers. *Clinical Pharmacology & Therapeutics*. 2012;91(3):506-13.
365. Gericke NM, Hagberg M. Definition of historical models of gene function and their relation to students' understanding of genetics. *Science & Education*. 2007;16(7):849-81.
366. Pearson H. Genetics: what is a gene? *Nature*. 2006;441(7092):398-401.
367. Shafee T. 2015.
368. Eichelbaum M, Ingelman-Sundberg M, Evans WE. Pharmacogenomics and individualized drug therapy. *Annu Rev Med*. 2006;57:119-37.
369. Bertz RJ, Granneman GR. Use of in vitro and in vivo data to estimate the likelihood of metabolic pharmacokinetic interactions. *Clinical pharmacokinetics*. 1997;32(3):210-58.
370. Evans WE, Relling MV. Pharmacogenomics: translating functional genomics into rational therapeutics. *science*. 1999;286(5439):487-91.
371. Phillips KA, Veenstra DL, Oren E, Lee JK, Sadee W. Potential role of pharmacogenomics in reducing adverse drug reactions: a systematic review. *Jama*. 2001;286(18):2270-9.
372. Lauschke VM, Ingelman-Sundberg M. Requirements for comprehensive pharmacogenetic genotyping platforms. *Pharmacogenomics*. 2016;17(8):917-24.
373. Sim SC, Ingelman-Sundberg M. The human cytochrome P450 Allele Nomenclature Committee Web site: submission criteria, procedures, and objectives. *Cytochrome P450 Protocols*. 2006:183-91.
374. Eccles D. A Single Nucleotide Polymorphism. 2014.
375. Klein K, Lang T, Saussele T, Barbosa-Sicard E, Schunck W-H, Eichelbaum M, et al. Genetic variability of CYP2B6 in populations of African and Asian origin: allele frequencies,

- novel functional variants, and possible implications for anti-HIV therapy with efavirenz. *Pharmacogenetics and Genomics*. 2005;15(12):861-73.
376. Wang H, Tompkins LM. CYP2B6: New Insights into a Historically Overlooked Cytochrome P450 Isozyme. *Current drug metabolism*. 2008;9(7):598-610.
377. Xie HJ, Yasar U, Lundgren S, Giskevicius L, Terelius Y, Hassan M, et al. Role of polymorphic human CYP2B6 in cyclophosphamide bioactivation. *Pharmacogenomics J*. 2003;3(1):53-61.
378. Tsuchiya K, Gatanaga H, Tachikawa N, Teruya K, Kikuchi Y, Yoshino M, et al. Homozygous CYP2B6 \*6 (Q172H and K262R) correlates with high plasma efavirenz concentrations in HIV-1 patients treated with standard efavirenz-containing regimens. *Biochemical and biophysical research communications*. 2004;319(4):1322-6.
379. Zanger UM, Klein K. Pharmacogenetics of cytochrome P450 2B6 (CYP2B6): advances on polymorphisms, mechanisms, and clinical relevance. *Frontiers in Genetics*. 2013;4:24.
380. Lang T, Klein K, Fischer J, Nussler AK, Neuhaus P, Hofmann U, et al. Extensive genetic polymorphism in the human CYP2B6 gene with impact on expression and function in human liver. *Pharmacogenetics*. 2001;11(5):399-415.
381. Mehlotra RK, Bockarie MJ, Zimmerman PA. CYP2B6 983T>C polymorphism is prevalent in West Africa but absent in Papua New Guinea: implications for HIV/AIDS treatment. *Br J Clin Pharmacol*. 2007;64(3):391-5.
382. Guan S, Huang M, Li X, Chen X, Chan E, Zhou SF. Intra- and inter-ethnic differences in the allele frequencies of cytochrome P450 2B6 gene in Chinese. *Pharmaceutical research*. 2006;23(9):1983-90.
383. Ma Q, Okusanya OO, Smith PF, Dicenzo R, Slish JC, Catanzaro LM, et al. Pharmacokinetic drug interactions with non-nucleoside reverse transcriptase inhibitors. *Expert Opin Drug Metab Toxicol*. 2005;1(3):473-85.
384. Ngaimisi E, Mugusi S, Minzi OM, Sasi P, Riedel KD, Suda A, et al. Long-term efavirenz autoinduction and its effect on plasma exposure in HIV patients. *Clinical pharmacology and therapeutics*. 2010;88(5):676-84.
385. Habtewold A, Amogne W, Makonnen E, Yimer G, Riedel KD, Ueda N, et al. Long-term effect of efavirenz autoinduction on plasma/peripheral blood mononuclear cell drug exposure and CD4 count is influenced by UGT2B7 and CYP2B6 genotypes among HIV patients. *The Journal of antimicrobial chemotherapy*. 2011;66(10):2350-61.
386. Ward BA, Gorski JC, Jones DR, Hall SD, Flockhart DA, Desta Z. The Cytochrome P450 2B6 (CYP2B6) Is the Main Catalyst of Efavirenz Primary and Secondary Metabolism: Implication for HIV/AIDS Therapy and Utility of Efavirenz as a Substrate Marker of CYP2B6 Catalytic Activity. *Journal of Pharmacology and Experimental Therapeutics*. 2003;306(1):287-300.
387. Rodriguez-Novoa S, Barreiro P, Rendon A, Jimenez-Nacher I, Gonzalez-Lahoz J, Soriano V. Influence of 516G>T polymorphisms at the gene encoding the CYP450-2B6 isoenzyme on efavirenz plasma concentrations in HIV-infected subjects. *Clinical infectious diseases : an official publication of the Infectious Diseases Society of America*. 2005;40(9):1358-61.
388. Rotger M, Colombo S, Furrer H, Bleiber G, Buclin T, Lee BL, et al. Influence of CYP2B6 polymorphism on plasma and intracellular concentrations and toxicity of efavirenz and nevirapine in HIV-infected patients. *Pharmacogenet Genomics*. 2005;15(1):1-5.

389. Haas DW, Ribaldo HJ, Kim RB, Tierney C, Wilkinson GR, Gulick RM, et al. Pharmacogenetics of efavirenz and central nervous system side effects: an Adult AIDS Clinical Trials Group study. *Aids*. 2004;18(18):2391-400.
390. Habtewold A, Amogne W, Makonnen E, Yimer G, Nysten H, Riedel K, et al. Pharmacogenetic and pharmacokinetic aspects of CYP3A induction by efavirenz in HIV patients. *The pharmacogenomics journal*. 2013;13(6):484-9.
391. Mouly S, Lown KS, Kornhauser D, Joseph JL, Fiske WD, Benedek IH, et al. Hepatic but not intestinal CYP3A4 displays dose-dependent induction by efavirenz in humans. *Clinical Pharmacology & Therapeutics*. 2002;72(1):1-9.
392. King J, Aberg JA. Clinical impact of patient population differences and genomic variation in efavirenz therapy. *Aids*. 2008;22(14):1709-17.
393. Achan J, Kakuru A, Ikilezi G, Ruel T, Clark TD, Nsanjabana C, et al. Antiretroviral Agents and Prevention of Malaria in HIV-Infected Ugandan Children. *N Engl J Med*. 2012;367(22):2110-8.
394. Khoo S, Back D, Winstanley P. The potential for interactions between antimalarial and antiretroviral drugs. *Aids*. 2005;19(10):995-1005.
395. Barnes KI, Watkins WM, White NJ. Antimalarial dosing regimens and drug resistance. *Trends Parasitol*. 2008;24(3):127-34.
396. Drake AL, Wagner A, Richardson B, John-Stewart G. Incident HIV during Pregnancy and Postpartum and Risk of Mother-to-Child HIV Transmission: A Systematic Review and Meta-Analysis. *PLoS Medicine*. 2014;11(2):e1001608.
397. World Health Organisation WHO. Malaria: Fact sheets 2016 [updated January Available from: <http://www.who.int/mediacentre/factsheets/fs094/en/>.
398. Doolan DL, Dobano C, Baird JK. Acquired Immunity to Malaria. *Clinical Microbiology Reviews*. 2009;22(1):13-36.
399. Feng B, Varma MV. Evaluation and Quantitative Prediction of Renal Transporter-Mediated Drug-Drug Interactions. *J Clin Pharmacol*. 2016;56 Suppl 7:S110-21.
400. Johansson S, Lofberg B, Aunes M, Lunde H, Frison L, Edvardsson N, et al. In Silico Predictions and In Vivo Results of Drug-Drug Interactions by Ketoconazole and Verapamil on AZD1305, a Combined Ion Channel Blocker and a Sensitive CYP3A4 Substrate. *Clin Pharmacol Drug Dev*. 2016;5(5):364-73.
401. Olafuyi O, Coleman M, Badhan RKS. The application of physiologically-based pharmacokinetic modelling to assess the impact of antiretroviral-mediated drug-drug interactions on piperazine antimalarial therapy during pregnancy. 2017.
402. Salem F, Johnson TN, Barter ZE, Leeder JS, Rostami-Hodjegan A. Age related changes in fractional elimination pathways for drugs: assessing the impact of variable ontogeny on metabolic drug-drug interactions. *J Clin Pharmacol*. 2013;53(8):857-65.
403. Salem F, Rostami-Hodjegan A, Johnson TN. Do children have the same vulnerability to metabolic drug-drug interactions as adults? A critical analysis of the literature. *J Clin Pharmacol*. 2013;53(5):559-66.
404. Johnson TN, Zhou D, Bui KH. Development of physiologically based pharmacokinetic model to evaluate the relative systemic exposure to quetiapine after administration of IR and XR formulations to adults, children and adolescents. *Biopharmaceutics & drug disposition*. 2014;35(6):341-52.
405. Olafuyi O, Coleman M, Badhan RKS. Development of a paediatric physiologically based pharmacokinetic model to assess the impact of drug-drug interactions in tuberculosis co-infected malaria subjects: A case study with artemether-lumefantrine and the CYP3A4-inducer rifampicin. *Eur J Pharm Sci*. 2017;106:20-33.

406. Jamei M, Marciniak S, Feng K, Barnett A, Tucker G, Rostami-Hodjegan A. The Simcyp® population-based ADME simulator. *Expert opinion on drug metabolism & toxicology*. 2009;5(2):211-23.
407. Jamei M, Turner D, Yang J, Neuhoff S, Polak S, Rostami-Hodjegan A, et al. Population-based mechanistic prediction of oral drug absorption. *The AAPS journal*. 2009;11(2):225-37.
408. Parikh S, Kajubi R, Huang L, Ssebuliba J, Kiconco S, Gao Q, et al. Antiretroviral Choice for HIV Impacts Antimalarial Exposure and Treatment Outcomes in Ugandan Children. *Clinical infectious diseases : an official publication of the Infectious Diseases Society of America*. 2016;63(3):414-22.
409. Fillekes Q, Natukunda E, Balungi J, Kendall L, Bwakura-Dangarembizi M, Keishanyu R, et al. Pediatric underdosing of efavirenz: a pharmacokinetic study in Uganda. *Journal of acquired immune deficiency syndromes (1999)*. 2011;58(4):392-8.
410. Pressiat C, Amorissani-Folquet M, Yonaba C, Treluyer JM, Dahourou DL, Eboua F, et al. Pharmacokinetics of Efavirenz at a High Dose of 25 Milligrams per Kilogram per Day in Children 2 to 3 Years Old. *Antimicrob Agents Chemother*. 2017;61(7).
411. Viljoen M, Karlsson MO, Meyers TM, Gous H, Dandara C, Rheeders M. Influence of CYP2B6 516G>T polymorphism and interoccasion variability (IOV) on the population pharmacokinetics of efavirenz in HIV-infected South African children. *Eur J Clin Pharmacol*. 2012;68(4):339-47.
412. Xu C, Quinney SK, Guo YY, Hall SD, Li L, Desta Z. CYP2B6 Pharmacogenetics-Based In Vitro-In Vivo Extrapolation of Efavirenz Clearance by Physiologically Based Pharmacokinetic Modeling. *Drug Metabolism and Disposition*. 2013;41(12):2004-11.
413. Ke A, Barter Z, Rowland-Yeo K, Almond L. Towards a Best Practice Approach in PBPK Modeling: Case Example of Developing a Unified Efavirenz Model Accounting for Induction of CYPs 3A4 and 2B6. *CPT: Pharmacometrics & Systems Pharmacology*. 2016;5(7):367-76.
414. Huang L, Parikh S, Rosenthal PJ, Lizak P, Marzan F, Dorsey G, et al. Concomitant efavirenz reduces pharmacokinetic exposure to the antimalarial drug artemether-lumefantrine in healthy volunteers. *Journal of acquired immune deficiency syndromes (1999)*. 2012;61(3):310-6.
415. Colussi D, Parisot C, Legay F, Lefèvre G. Binding of artemether and lumefantrine to plasma proteins and erythrocytes. *European journal of pharmaceutical sciences*. 1999;9(1):9-16.
416. Zaloumis S, Humberstone A, Charman SA, Price RN, Moehrle J, Gamo-Benito J, et al. Assessing the utility of an anti-malarial pharmacokinetic-pharmacodynamic model for aiding drug clinical development. *Malar J*. 2012;11(1):303.
417. Kotila O, Olaniyi O, Adegoke A, Babalola C. Experimental determination of the physicochemical properties of lumefantrine. *African journal of medicine and medical sciences*. 2013;42(3):209-14.
418. Xu C, Quinney SK, Guo Y, Hall SD, Li L, Desta Z. CYP2B6 Pharmacogenetics-Based In Vitro-In Vivo Extrapolation of Efavirenz Clearance by Physiologically Based Pharmacokinetic Modeling. *Drug Metabolism and Disposition*. 2013;41(12):2004-11.
419. Mukonzo JK, Nanzigu S, Waako P, Ogwal-Okeng J, Gustafson LL, Aklillu E. CYP2B6 genotype, but not rifampicin-based anti-TB cotreatments, explains variability in long-term efavirenz plasma exposure. *Pharmacogenomics*. 2014;15(11):1423-35.
420. Maganda B, Minzi O, Ngaimisi E, Kamuhabwa A, Aklillu E. CYP2B6\* 6 genotype and high efavirenz plasma concentration but not nevirapine are associated with low

- lumefantrine plasma exposure and poor treatment response in HIV-malaria-coinfected patients. *The Pharmacogenomics Journal*. 2015;1:8.
421. Mukonzo JK, Nanzigu S, Waako P, Ogwal-Okeng J, Gustafson LL, Aklillu E. CYP2B6 genotype, but not rifampicin-based anti-TB cotreatments, explains variability in long-term efavirenz plasma exposure. *Pharmacogenomics*. 2014;15(11):1423-35.
422. Hayes DJ, van Buuren S, ter Kuile FO, Stasinopoulos DM, Rigby RA, Terlouw DJ. Developing regional weight-for-age growth references for malaria-endemic countries to optimize age-based dosing of antimalarials. *Bulletin of the World Health Organization*. 2015;93(2):74-83.
423. Critical Path to TB Drug Regimens. CPTR and SIMCYP launch models to evaluate exposure and efficacy of TB drugs in combination 2016 [Available from: <http://www.cptrinitiative.org/2016/10/01/cptr-and-simcyp-launch-models-to-evaluate-exposure-and-efficacy-of-tb-drugs-in-combination/>].
424. Gardner I. Using virtual populations to solve drug development problems, : Certara; 2016 [Available from: <http://www.cptrinitiative.org/wp-content/uploads/2016/05/4.5-Gardiner.pdf>].
425. Maganda BA, Minzi OM, Ngaimisi E, Kamuhabwa AA, Aklillu E. CYP2B6\*6 genotype and high efavirenz plasma concentration but not nevirapine are associated with low lumefantrine plasma exposure and poor treatment response in HIV-malaria-coinfected patients. *Pharmacogenomics J*. 2016;16(1):88-95.
426. Kwena A, Wakhisi J, Mambo F. Possible biochemical markers in *Plasmodium falciparum* malaria infected children with or without malnutrition at Webuye and Eldoret, Western Kenya. *Adv Biores*. 2012;3(2):49-54.
427. Friedman MJ. Control of malaria virulence by alpha 1-acid glycoprotein (orosomuroid), an acute-phase (inflammatory) reactant. *Proceedings of the National Academy of Sciences*. 1983;80(17):5421-4.
428. Muwonge H, Kikomeko S, Sembajjwe LF, Seguya A, Namugwanya C. How Reliable Are Hematological Parameters in Predicting Uncomplicated *Plasmodium falciparum* Malaria in an Endemic Region? *ISRN tropical medicine*. 2013;2013:1-9.
429. Muwonge H, Kikomeko S, Sembajjwe LF, Seguya A, Namugwanya C. How Reliable Are Hematological Parameters in Predicting Uncomplicated *Plasmodium falciparum* Malaria in an Endemic Region? *ISRN tropical medicine*. 2013;2013:1-9.
430. Holmes EG, Stanier MW, Thompson MD. The serum protein pattern of Africans in Uganda: relation to diet and malaria. *Transactions of the Royal Society of Tropical Medicine and Hygiene*. 1955;49:376-84.
431. Johnson TN, Rostami-Hodjegan A, Tucker GT. Prediction of the clearance of eleven drugs and associated variability in neonates, infants and children. *Clinical pharmacokinetics*. 2006;45(9):931-56.
432. Johnson TN. The problems in scaling adult drug doses to children. *Arch Dis Child*. 2008;93(3):207-11.
433. Ezzet F, van Vugt M, Nosten F, Looareesuwan S, White NJ. Pharmacokinetics and pharmacodynamics of lumefantrine (benflumetol) in acute *falciparum* malaria. *Antimicrob Agents Chemother*. 2000;44(3):697-704.
434. Hayes DJ, Buuren Sv, Ter Kuile FO, Stasinopoulos DM, Rigby RA, Terlouw DJ. Developing regional weight-for-age growth references for malaria-endemic countries to optimize age-based dosing of antimalarials. *Bulletin of the World Health Organization*. 2014;93:74-83.

435. Maganda BA, Ngaimisi E, Kamuhabwa AA, Aklillu E, Minzi OM. The influence of nevirapine and efavirenz-based anti-retroviral therapy on the pharmacokinetics of lumefantrine and anti-malarial dose recommendation in HIV-malaria co-treatment. *Malar J*. 2015;14(1):179.
436. Pearce RE, Gaedigk R, Twist GP, Dai H, Riffel AK, Leeder JS, et al. Developmental Expression of CYP2B6: A Comprehensive Analysis of mRNA Expression, Protein Content and Bupropion Hydroxylase Activity and the Impact of Genetic Variation. *Drug Metabolism and Disposition*. 2015.
437. Croom EL, Stevens JC, Hines RN, Wallace AD, Hodgson E. Human hepatic CYP2B6 developmental expression: The impact of age and genotype. *Biochemical Pharmacology*. 2009;78(2):184-90.
438. (UNAIDS). JUNPoHA. UNAIDS Gap Report. 2014.
439. Gonzalez R, Ataide R, Nanihe D, Menendez C, Mayor A. HIV and malaria interactions: where do we stand? Expert review of anti-infective therapy. 2012;10(2):153-65.
440. Omoti CE, Ojide CK, Lofor PV, Eze E, Eze JC. Prevalence of parasitemia and associated immunodeficiency among HIV-malaria co-infected adult patients with highly active antiretroviral therapy. *Asian Pacific journal of tropical medicine*. 2013;6(2):126-30.
441. Desai M, ter Kuile FO, Nosten F, McGready R, Asamo K, Brabin B, et al. Epidemiology and burden of malaria in pregnancy. *The Lancet infectious diseases*. 2007;7(2):93-104.
442. Seden K, Gibbons S, Marzolini C, Schapiro JM, Burger DM, Back DJ, et al. Development of an evidence evaluation and synthesis system for drug-drug interactions, and its application to a systematic review of HIV and malaria co-infection. *PLOS ONE*. 2017;12(3):e0173509.
443. World Health Organization. Global Health Observatory (GHO) data. 2016.
444. Puoane T, Steyn K, Bradshaw D, Laubscher R, Fourie J, Lambert V, et al. Obesity in South Africa: the South African demographic and health survey. *Obesity research*. 2002;10(10):1038-48.
445. Hanley MJ, Abernethy DR, Greenblatt DJ. Effect of obesity on the pharmacokinetics of drugs in humans. *Clin Pharmacokinet*. 2010;49(2):71-87.
446. Carasco CF, Fletcher P, Maconochie I. Review of commonly used age-based weight estimates for paediatric drug dosing in relation to the pharmacokinetic properties of resuscitation drugs. *British Journal of Clinical Pharmacology*. 2016;81(5):849-56.
447. Wagner C, Zhao P, Pan Y, Hsu V, Grillo J, Huang SM, et al. Application of Physiologically Based Pharmacokinetic (PBPK) Modeling to Support Dose Selection: Report of an FDA Public Workshop on PBPK. *CPT Pharmacometrics Syst Pharmacol*. 2015;4(4):226-30.
448. Ashley EA, Stepniewska K, Lindegardh N, McGready R, Annerberg A, Hutagalung R, et al. Pharmacokinetic study of artemether-lumefantrine given once daily for the treatment of uncomplicated multidrug-resistant falciparum malaria. *Tropical medicine & international health : TM & IH*. 2007;12(2):201-8.
449. Salem F, Johnson TN, Abduljalil K, Tucker GT, Rostami-Hodjegan A. A Re-evaluation and Validation of Ontogeny Functions for Cytochrome P450 1A2 and 3A4 Based on In Vivo Data. *Clinical Pharmacokinetics*. 2014;53(7):625-36.
450. Djimdé A, Lefèvre G. Understanding the pharmacokinetics of Coartem®. *Malar J*. 2009;8(1):S4.
451. Yeung S, White NJ. How do patients use antimalarial drugs? A review of the evidence. *Trop Med Int Health*. 2005;10(2):121-38.

452. Maganda BA, Minzi OMS, Kamuhabwa AAR, Ngasala B, Sasi PG. Outcome of artemether-lumefantrine treatment for uncomplicated malaria in HIV-infected adult patients on anti-retroviral therapy. *Malar J*. 2014;13:10.
453. Maganda BA, Ngaimisi E, Kamuhabwa AAR, Aklillu E, Minzi OMS. The influence of nevirapine and efavirenz-based anti-retroviral therapy on the pharmacokinetics of lumefantrine and anti-malarial dose recommendation in HIV-malaria co-treatment. *Malar J*. 2015;14:11.
454. World Health Organisation WHO. Number of malaria cases : Global Health Observatory (GHO) data 2015 [Available from: <http://www.who.int/gho/malaria/epidemic/cases/en/>].
455. Ho M. Current population estimates, Malaysia, 2014–2016. Malaysia: The Office of Chief Statistician Malaysia, Department of Statistics Malaysia. 2016.
456. National Pharmaceutical Regulatory Agency Ministry of Health Malaysia. National Centre for Adverse Drug Reaction Monitoring Annual Report 2018 [Available from: <http://npra.moh.gov.my/index.php/recent-updates/publication/national-centre-for-adverse-drug-reaction-monitoring-annual-report>].
457. Xie HG, B Kim R, Wood A, Michael Stein C. Molecular Basis of Ethnic Differences in Drug Disposition and Response 2001. 815-50 p.
458. Yusoff N, Saleem M, Nagaya D, Yahaya B, Rasmaizatul Akma R, Moosa N, et al. Cross-Ethnic Distribution of Clinically Relevant Cyp2c19 Genotypes and Haplotypes 2015.
459. Yang Y, Wong L, Lee T, Mustafa A, Mohamed Z, Lang CC. Genetic polymorphism of cytochrome P450 2C19 in healthy Malaysian subjects. *British journal of clinical pharmacology*. 2004;58(3):332-5.
460. Liew H, Rosli M, Wan WA, Robaayah Z, Sim K. The foundation of NCVI PCI Registry: the Malaysia's first multi-centre interventional cardiology project. *The Medical journal of Malaysia*. 2008;63:41-4.
461. Mendis S, Puska P, Norrving B, Organization WH. Global atlas on cardiovascular disease prevention and control: Geneva: World Health Organization; 2011.
462. Ross R. The pathogenesis of atherosclerosis—an update. *N Engl J Med*. 1986;314(8):488-500.
463. Perk J, De Backer G, Gohlke H, Graham I, Reiner Ž, Verschuren WM, et al. European Guidelines on cardiovascular disease prevention in clinical practice (version 2012): The Fifth Joint Task Force of the European Society of Cardiology and Other Societies on Cardiovascular Disease Prevention in Clinical Practice (constituted by representatives of nine societies and by invited experts). *Atherosclerosis*. 2012;223(1):1-68.
464. Musselman DL, Evans DL, Nemeroff CB. The relationship of depression to cardiovascular disease: epidemiology, biology, and treatment. *Archives of general psychiatry*. 1998;55(7):580-92.
465. Merz CNB, Shaw LJ, Reis SE, Bittner V, Kelsey SF, Olson M, et al. Insights from the NHLBI-Sponsored Women's Ischemia Syndrome Evaluation (WISE) Study: Part II: gender differences in presentation, diagnosis, and outcome with regard to gender-based pathophysiology of atherosclerosis and macrovascular and microvascular coronary disease. *Journal of the American College of Cardiology*. 2006;47(3 Supplement):S21-S9.
466. Bonow RO, Mann DL, Zipes DP, Libby P. Braunwald's Heart Disease E-Book: A Textbook of Cardiovascular Medicine: Elsevier Health Sciences; 2011.
467. Calonge N, Petitti DB, DeWitt TG, Gordis L, Gregory KD, Harris R, et al. Aspirin for the prevention of cardiovascular disease: US Preventive Services Task Force recommendation statement. *Annals of internal medicine*. 2009;150(6):396-404.

468. Kannel WB. Blood pressure as a cardiovascular risk factor: prevention and treatment. *Jama*. 1996;275(20):1571-6.
469. Lorenzo C, Williams K, Hunt KJ, Haffner SM. The National Cholesterol Education Program–Adult Treatment Panel III, International Diabetes Federation, and World Health Organization definitions of the metabolic syndrome as predictors of incident cardiovascular disease and diabetes. *Diabetes care*. 2007;30(1):8-13.
470. Cattaneo M. Response variability to clopidogrel: is tailored treatment, based on laboratory testing, the right solution? *Journal of Thrombosis and Haemostasis*. 2012;10(3):327-36.
471. Bhatt DL, Topol EJ. Scientific and therapeutic advances in antiplatelet therapy. *Nature Reviews Drug Discovery*. 2003;2(1):15.
472. Simon T, Bhatt DL, Bergougnan L, Farenc C, Pearson K, Perrin L, et al. Genetic polymorphisms and the impact of a higher clopidogrel dose regimen on active metabolite exposure and antiplatelet response in healthy subjects. *Clinical pharmacology and therapeutics*. 2011;90(2):287-95.
473. Mega JL, Close SL, Wiviott SD, Shen L, Hockett RD, Brandt JT, et al. Cytochrome p-450 polymorphisms and response to clopidogrel. *N Engl J Med*. 2009;360(4):354-62.
474. Kim K, Park P, Hong S, Park JY. The effect of CYP2C19 polymorphism on the pharmacokinetics and pharmacodynamics of clopidogrel: a possible mechanism for clopidogrel resistance. *Clinical Pharmacology & Therapeutics*. 2008;84(2):236-42.
475. Holmes DR, Jr., Dehmer GJ, Kaul S, Leifer D, O'Gara PT, Stein CM. ACCF/AHA clopidogrel clinical alert: approaches to the FDA "boxed warning": a report of the American College of Cardiology Foundation Task Force on clinical expert consensus documents and the American Heart Association endorsed by the Society for Cardiovascular Angiography and Interventions and the Society of Thoracic Surgeons. *J Am Coll Cardiol*. 2010;56(4):321-41.
476. Kazui M, Nishiya Y, Ishizuka T, Hagihara K, Farid NA, Okazaki O, et al. Identification of the human cytochrome P450 enzymes involved in the two oxidative steps in the bioactivation of clopidogrel to its pharmacologically active metabolite. *Drug Metab Dispos*. 2010;38(1):92-9.
477. Djebli N, Fabre D, Boulenc X, Fabre G, Sultan E, Hurbin F. Physiologically-based pharmacokinetic modeling for sequential metabolism: effect of CYP2C19 genetic polymorphism on clopidogrel and clopidogrel active metabolite pharmacokinetics. *Drug Metabolism and Disposition*. 2015:dmd. 114.062596.
478. Cappola TP, Margulies KB. Functional genomics applied to cardiovascular medicine. *Circulation*. 2011;124(1):87-94.
479. Wei YQ, Wang DG, Yang H, Cao H. Cytochrome P450 CYP 2C19\*2 Associated with Adverse 1-Year Cardiovascular Events in Patients with Acute Coronary Syndrome. *PLoS One*. 2015;10(7):e0132561.
480. Shuldiner AR, O'Connell JR, Bliden KP, Gandhi A, Ryan K, Horenstein RB, et al. Association of cytochrome P450 2C19 genotype with the antiplatelet effect and clinical efficacy of clopidogrel therapy. *Jama*. 2009;302(8):849-57.
481. Brandt JT, Close SL, Iturria SJ, Payne CD, Farid NA, Ernest CS, 2nd, et al. Common polymorphisms of CYP2C19 and CYP2C9 affect the pharmacokinetic and pharmacodynamic response to clopidogrel but not prasugrel. *Journal of thrombosis and haemostasis : JTH*. 2007;5(12):2429-36.
482. Teh L, Ismail R, Yusoff R, Hussein A, Isa M, Rahman A. Heterogeneity of the CYP2D6 gene among Malays in Malaysia. *J Clin Pharm Ther*. 2001;26(3):205-11.

483. Istana J, Indera B. CYP2C9 polymorphism: prevalence in healthy and warfarin-treated Malay and Chinese in Malaysia. *Singapore Med J.* 2009;50(5):490.
484. Moulin DE, Inturrisi CE, Foley KM. CEREBROSPINAL-FLUID PHARMACOKINETICS OF INTRATHECAL MORPHINE-SULFATE AND D-ALA2-D-LEU5-ENKEPHALIN. *Annals of Neurology.* 1986;20(2):218-22.
485. Yin T, Miyata T. Pharmacogenomics of clopidogrel: evidence and perspectives. *Thrombosis research.* 2011;128(4):307-16.
486. Amin AM, Sheau Chin L, Azri Mohamed Noor D, Sk Abdul Kader MA, Kah Hay Y, Ibrahim B. The Personalization of Clopidogrel Antiplatelet Therapy: The Role of Integrative Pharmacogenetics and Pharmacometabolomics. *Cardiol Res Pract.* 2017;2017:8062796.
487. Scott SA, Sangkuhl K, Stein CM, Hulot JS, Mega JL, Roden DM, et al. Clinical Pharmacogenetics Implementation Consortium guidelines for CYP2C19 genotype and clopidogrel therapy: 2013 update. *Clinical pharmacology and therapeutics.* 2013;94(3):317-23.
488. De Morais S, Wilkinson GR, Blaisdell J, Nakamura K, Meyer UA, Goldstein JA. The major genetic defect responsible for the polymorphism of S-mephenytoin metabolism in humans. *Journal of Biological Chemistry.* 1994;269(22):15419-22.
489. De Morais S, Wilkinson GR, Blaisdell J, Meyer UA, Nakamura K, Goldstein JA. Identification of a new genetic defect responsible for the polymorphism of (S)-mephenytoin metabolism in Japanese. *Molecular pharmacology.* 1994;46(4):594-8.
490. Desta Z, Zhao X, Shin J-G, Flockhart DA. Clinical significance of the cytochrome P450 2C19 genetic polymorphism. *Clinical pharmacokinetics.* 2002;41(12):913-58.
491. Xie H-G, Kim RB, Wood AJ, Stein CM. Molecular basis of ethnic differences in drug disposition and response. *Annual review of pharmacology and toxicology.* 2001;41(1):815-50.
492. Cacabelos R, Martinez-Bouza R, Carril JC, Fernandez-Novoa L, Lombardi V, Carrera I, et al. Genomics and pharmacogenomics of brain disorders. *Curr Pharm Biotechnol.* 2012;13(5):674-725.
493. Cacabelos R, Martinez R, Fernandez-Novoa L, Carril JC, Lombardi V, Carrera I, et al. Genomics of Dementia: APOE- and CYP2D6-Related Pharmacogenetics. *International journal of Alzheimer's disease.* 2012;2012:518901.
494. Mega JL, Simon T, Collet JP, Anderson JL, Antman EM, Bliden K, et al. Reduced-function CYP2C19 genotype and risk of adverse clinical outcomes among patients treated with clopidogrel predominantly for PCI: a meta-analysis. *Jama.* 2010;304(16):1821-30.
495. Mejin M, Tiong WN, Lai LY, Tiong LL, Bujang AM, Hwang SS, et al. CYP2C19 genotypes and their impact on clopidogrel responsiveness in percutaneous coronary intervention. *International journal of clinical pharmacy.* 2013;35(4):621-8.
496. Gurbel PA, Tantry US. Do platelet function testing and genotyping improve outcome in patients treated with antithrombotic agents?: platelet function testing and genotyping improve outcome in patients treated with antithrombotic agents. *Circulation.* 2012;125(10):1276-87; discussion 87.
497. Krishna V, Diamond GA, Kaul S. Do platelet function testing and genotyping improve outcome in patients treated with antithrombotic agents?: the role of platelet reactivity and genotype testing in the prevention of atherothrombotic cardiovascular events remains unproven. *Circulation.* 2012;125(10):1288-303; discussion 303.
498. Collins FS, Varmus H. A new initiative on precision medicine. *The New England journal of medicine.* 2015;372(9):793-5.

499. Jameson JL, Longo DL. Precision medicine--personalized, problematic, and promising. *The New England journal of medicine*. 2015;372(23):2229-34.
500. Olafuyi O, Coleman M, Badhan RKS. The application of physiologically based pharmacokinetic modelling to assess the impact of antiretroviral-mediated drug-drug interactions on piperazine antimalarial therapy during pregnancy. *Biopharm Drug Dispos*. 2017;38(8):464-78.
501. Hamzah AA, BAKAR Z, Sani NA, Tan J, Damanhuri MA, ARIPIN K, et al. Relationship between Education and Cognitive Performance among Healthy Malay Adults. *Sains Malaysiana*. 2016;45(9):1371-9.
502. Khor G, Duraisamy G, Loh S, Green T, Skeaff C. Dietary and blood folate status of Malaysian women of childbearing age. *Asia Pacific journal of clinical nutrition*. 2006;15(3):341.
503. Varma MVS, Lai Y, Kimoto E, Goosen TC, El-Kattan AF, Kumar V. Mechanistic Modeling to Predict the Transporter- and Enzyme-Mediated Drug-Drug Interactions of Repaglinide. *Pharmaceutical research*. 2013;30(4):1188-99.
504. T'jollyn H, Snoeys J, Vermeulen A, Michelet R, Cuyckens F, Mannens G, et al. Physiologically based pharmacokinetic predictions of tramadol exposure throughout pediatric life: an analysis of the different clearance contributors with emphasis on CYP2D6 maturation. *The AAPS journal*. 2015;17(6):1376-87.
505. Hatorp V. Clinical pharmacokinetics and pharmacodynamics of repaglinide. *Clinical pharmacokinetics*. 2002;41(7):471-83.
506. Hatorp V, Huang W-C, Strange P. Repaglinide pharmacokinetics in healthy young adult and elderly subjects. *Clinical therapeutics*. 1999;21(4):702-10.
507. Zhai X-j, Hu K, Chen F, Lu Y-n. Comparative bioavailability and tolerability of a single 2-mg dose of 2 repaglinide tablet formulations in fasting, healthy chinese male volunteers: an open-label, randomized-sequence, 2-period crossover study. *Current Therapeutic Research*. 2013;75:48-52.
508. Ruzilawati A, Gan S. CYP3A4 genetic polymorphism influences repaglinide's pharmacokinetics. *Pharmacology*. 2010;85(6):357-64.
509. Gan S, Ismail R, Adnan WW, Wan Z. Correlation of tramadol pharmacokinetics and CYP2D6\* 10 genotype in Malaysian subjects. *Journal of pharmaceutical and biomedical analysis*. 2002;30(2):189-95.
510. Karaźniewicz-Łada M, Danielak D, Burchardt P, Kruszyna Ł, Komosa A, Lesiak M, et al. Clinical pharmacokinetics of clopidogrel and its metabolites in patients with cardiovascular diseases. *Clinical pharmacokinetics*. 2014;53(2):155-64.
511. Simon T, Bhatt D, Bergougnan L, Farenc C, Pearson K, Perrin L, et al. Genetic polymorphisms and the impact of a higher clopidogrel dose regimen on active metabolite exposure and antiplatelet response in healthy subjects. *Clinical Pharmacology & Therapeutics*. 2011;90(2):287-95.
512. Administration UFaD. Summary Minutes of the Advisory Committee for Pharmaceutical

Science and Clinical Pharmacology 2012 [Available from: <https://wayback.archive-it.org/7993/20170403224110/https://www.fda.gov/AdvisoryCommittees/CommitteesMeetingMaterials/Drugs/AdvisoryCommitteeforPharmaceuticalScienceandClinicalPharmacology/ucm286697.htm>].

513. Wang H, Naghavi M, Allen C, Barber RM, Bhutta ZA, Carter A, et al. Global, regional, and national life expectancy, all-cause mortality, and cause-specific mortality for

- 249 causes of death, 1980&#x2013;2015: a systematic analysis for the Global Burden of Disease Study 2015. *The Lancet*. 2016;388(10053):1459-544.
514. Reddy KS, Yusuf S. Emerging epidemic of cardiovascular disease in developing countries. *Circulation*. 1998;97(6):596-601.
515. Khoo KL, Tan H, Liew YM. Serum lipids and their relationship with other coronary risk factors in healthy subjects in a city clinic. *Med J Malaysia*. 1997;52(1):38-52.
516. Department of Statistics M. Statistics on causes of death, Malaysia. 2018 [Available from: [https://www.dosm.gov.my/v1/index.php?r=column/cthemByCat&cat=401&bul\\_id=eTY2NWOOS3BLb1dldWJmVFNMWmphQT09&menu\\_id=L0pheU43NWJwRWVSZklWdzQ4TlhUUT09](https://www.dosm.gov.my/v1/index.php?r=column/cthemByCat&cat=401&bul_id=eTY2NWOOS3BLb1dldWJmVFNMWmphQT09&menu_id=L0pheU43NWJwRWVSZklWdzQ4TlhUUT09)].
517. Greving JP, Buskens E, Koffijberg H, Algra A. Cost-Effectiveness of Aspirin Treatment in the Primary Prevention of Cardiovascular Disease Events in Subgroups Based on Age, Gender, and Varying Cardiovascular Risk. *Circulation*. 2008;117(22):2875-83.
518. Luk HH, Pang J, Li LSW, Ng M. Use of antiplatelet drugs in the stroke unit of a Hong Kong hospital. *Pharmacy World and Science*. 2005;27(3):258-62.
519. Uchiyama S, Fukuuchi Y, Yamaguchi T. The safety and efficacy of clopidogrel versus ticlopidine in Japanese stroke patients: combined results of two Phase III, multicenter, randomized clinical trials. *Journal of neurology*. 2009;256(6):888-97.
520. Lee JB, Lee KA, Lee KY. Cytochrome P450 2C19 polymorphism is associated with reduced clopidogrel response in cerebrovascular disease. *Yonsei medical journal*. 2011;52(5):734-8.
521. Man M, Farmen M, Dumauual C, Teng CH, Moser B, Irie S, et al. Genetic variation in metabolizing enzyme and transporter genes: comprehensive assessment in 3 major East Asian subpopulations with comparison to Caucasians and Africans. *The Journal of Clinical Pharmacology*. 2010;50(8):929-40.
522. Gaedigk A. Interethnic differences of drug-metabolizing enzymes. *International journal of clinical pharmacology and therapeutics*. 2000;38(2):61-8.
523. Investigators CiUAAtPRET. Effects of clopidogrel in addition to aspirin in patients with acute coronary syndromes without ST-segment elevation. *New England Journal of Medicine*. 2001;345(7):494-502.
524. Steinhubl SR, Berger PB, Mann III JT, Fry ET, DeLago A, Wilmer C, et al. Early and sustained dual oral antiplatelet therapy following percutaneous coronary intervention: a randomized controlled trial. *Jama*. 2002;288(19):2411-20.
525. Pereira NL, Geske JB, Mayr M, Shah SH, Rihal CS. Pharmacogenetics of Clopidogrel: An Unresolved Issue. *Circulation: Genomic and Precision Medicine*. 2016;9(2):185-8.
526. Hulot J-S, Collet J-P, Silvain J, Pena A, Bellemain-Appaix A, Barthélemy O, et al. Cardiovascular risk in clopidogrel-treated patients according to cytochrome P450 2C19\* 2 loss-of-function allele or proton pump inhibitor coadministration: a systematic meta-analysis. *Journal of the American College of Cardiology*. 2010;56(2):134-43.
527. Sibbing D, Koch W, Gebhard D, Schuster T, Braun S, Stegherr J, et al. Cytochrome 2C19\* 17 allelic variant, platelet aggregation, bleeding events, and stent thrombosis in clopidogrel-treated patients with coronary stent placement. *Circulation*. 2010;121(4):512-8.
528. Gurbel PA, Shuldiner AR, Bliden KP, Ryan K, Pakyz RE, Tantry US. The relation between CYP2C19 genotype and phenotype in stented patients on maintenance dual antiplatelet therapy. *American heart journal*. 2011;161(3):598-604.

529. Umemura K, Furuta T, Kondo K. The common gene variants of CYP2C19 affect pharmacokinetics and pharmacodynamics in an active metabolite of clopidogrel in healthy subjects. *Journal of Thrombosis and Haemostasis*. 2008;6(8):1439-41.
530. Hochholzer W, Trenk D, Fromm MF, Valina CM, Stratz C, Bestehorn H-P, et al. Impact of cytochrome P450 2C19 loss-of-function polymorphism and of major demographic characteristics on residual platelet function after loading and maintenance treatment with clopidogrel in patients undergoing elective coronary stent placement. *Journal of the American College of Cardiology*. 2010;55(22):2427-34.
531. Siasos G, Oikonomou E, Vavuranakis M, Kokkou E, Mourouzis K, Tsalamandris S, et al. Genotyping, Platelet Activation, and Cardiovascular Outcome in Patients after Percutaneous Coronary Intervention: Two Pieces of the Puzzle of Clopidogrel Resistance. *Cardiology*. 2017;137(2):104-13.
532. Zakaria Z, Badhan RK. The impact of CYP2B6 polymorphisms on the interactions of efavirenz with lumefantrine: Implications for paediatric antimalarial therapy. *European Journal of Pharmaceutical Sciences*. 2018.
533. Bhindi R, Ormerod O, Newton J, Banning A, Testa L. Interaction between statins and clopidogrel: is there anything clinically relevant? *QJM: An International Journal of Medicine*. 2008;101(12):915-25.
534. Rolan P. Plasma protein binding displacement interactions—why are they still regarded as clinically important? *British journal of clinical pharmacology*. 1994;37(2):125-8.
535. Holford N, editor *The visual predictive check—superiority to standard diagnostic (Rorschach) Plots*. 2005. Abstract; 2005.
536. Karlsson MO, Holford N, editors. *A tutorial on visual predictive checks*. abstr; 2008.
537. Post TM, Freijer JI, Ploeger BA, Danhof M. Extensions to the visual predictive check to facilitate model performance evaluation. *Journal of pharmacokinetics and pharmacodynamics*. 2008;35(2):185.
538. T S, DL B, L B, C F, K P, L P, et al. Genetic Polymorphisms and the Impact of a Higher Clopidogrel Dose Regimen on Active Metabolite Exposure and Antiplatelet Response in Healthy Subjects. *Clinical Pharmacology & Therapeutics*. 2011;90(2):287-95.
539. Lim KG. A Review of Adult Obesity Research in Malaysia. *Med J Malaysia*. 2016;71(Suppl 1):1-19.
540. Wang X-q, Shen C-l, Wang B-n, Huang X-h, Hu Z-l, Li J. Genetic polymorphisms of CYP2C19\*2 and ABCB1 C3435T affect the pharmacokinetic and pharmacodynamic responses to clopidogrel in 401 patients with acute coronary syndrome. *Gene*. 2015;558(2):200-7.
541. Chan MY, Tan K, Tan H-C, Huan P-T, Li B, Phua Q-H, et al. CYP2C19 and PON1 polymorphisms regulating clopidogrel bioactivation in Chinese, Malay and Indian subjects. *Pharmacogenomics*. 2012;13(5):533-42.
542. Rosdi RA, Yusoff NM, Ismail R, Choon TS, Musa N, Yusoff S. A minireview of CYP2C9 and CYP2C19 single nucleotide polymorphisms (SNPs) among Malaysian populations. *Journal of Biomedical and Clinical Sciences (JBCS)*. 2017;2(1):47-52.
543. Wang H-y, Chen X, Jiang J, Shi J, Hu P. Evaluating a physiologically based pharmacokinetic model for predicting the pharmacokinetics of midazolam in Chinese after oral administration. *Acta Pharmacologica Sinica*. 2016;37(2):276-84.
544. Feng S, Cleary Y, Parrott N, Hu P, Weber C, Wang Y, et al. Evaluating a physiologically based pharmacokinetic model for prediction of omeprazole clearance and assessing ethnic sensitivity in CYP2C19 metabolic pathway. *Eur J Clin Pharmacol*. 2015;71(5):617-24.

545. Hasan MS, Basri HB, Hin LP, Stanslas J. Genetic polymorphisms and drug interactions leading to clopidogrel resistance: why the Asian population requires special attention. *International Journal of Neuroscience*. 2013;123(3):143-54.
546. Tang YD, Wang W, Yang M, Zhang K, Chen J, Qiao S, et al. Randomized Comparisons of Double-Dose Clopidogrel or Adjunctive Cilostazol Versus Standard Dual Antiplatelet in Patients With High Posttreatment Platelet Reactivity: Results of the CREATIVE Trial. *Circulation*. 2018;137(21):2231-45.
547. Bossard M, Granger CB, Tanguay JF, Montalescot G, Faxon DP, Jolly SS, et al. Double-Dose Versus Standard-Dose Clopidogrel According to Smoking Status Among Patients With Acute Coronary Syndromes Undergoing Percutaneous Coronary Intervention. *Journal of the American Heart Association*. 2017;6(11).
548. Chen S, Zhang Y, Wang L, Geng Y, Gu J, Hao Q, et al. Effects of Dual-Dose Clopidogrel, Clopidogrel Combined with Tongxinluo Capsule, and Ticagrelor on Patients with Coronary Heart Disease and CYP2C19\*2 Gene Mutation After Percutaneous Coronary Interventions (PCI). *Medical science monitor : international medical journal of experimental and clinical research*. 2017;23:3824-30.
549. Collet J-P, Hulot J-S, Anzaha G, Pena A, Chastre T, Caron C, et al. High Doses of Clopidogrel to Overcome Genetic Resistance. The Randomized Crossover CLOVIS-2 (Clopidogrel and Response Variability Investigation Study 2). 2011;4(4):392-402.
550. Wilffert B, Swen J, Mulder H, Touw D, Maitland-Van der Zee A-H, Deneer V, et al. From evidence based medicine to mechanism based medicine. Reviewing the role of pharmacogenetics. *International journal of clinical pharmacy*. 2013;35(3):369-75.
551. Stein W. *Transport and diffusion across cell membranes*: Elsevier; 2012.
552. Ong SW, Liu HL, Pidgeon C. Immobilized-artificial-membrane chromatography: Measurements of membrane partition coefficient and predicting drug membrane permeability. *Journal of Chromatography A*. 1996;728(1-2):113-28.
553. Reichel A, Begley DJ. Potential of immobilized artificial membranes for predicting drug penetration across the blood-brain barrier. *Pharmaceutical research*. 1998;15(8):1270-4.
554. Di L, Kerns EH, Fan K, McConnell OJ, Carter GT. High throughput artificial membrane permeability assay for blood-brain barrier. *European Journal of Medicinal Chemistry*. 2003;38(3):223-32.
555. Carrara S, Reali V, Misiano P, Dondio G, Bigogno C. Evaluation of in vitro brain penetration: Optimized PAMPA and MDCKII-MDR1 assay comparison. *International Journal of Pharmaceutics*. 2007;345(1-2):125-33.
556. Pardridge WM. Isolated brain capillaries: an in vitro model of blood-brain barrier research. *Introduction to the blood-brain barrier: methodology, biology and pathology* (Pardridge WM, ed). 1998:49-61.
557. Joo F. THE BLOOD-BRAIN BARRIER INVITRO - 10 YEARS OF RESEARCH ON MICROVESSELS ISOLATED FROM THE BRAIN. *Neurochemistry International*. 1985;7(1):1-25.
558. de Boer AG, Gaillard PJ. In vitro models of the blood-brain barrier: When to use which? *Current Medicinal Chemistry - Central Nervous System Agents*. 2002;2(3):203-9.
559. Feng MR. Assessment of blood-brain barrier penetration: In silico, in vitro and in vivo. *Current Drug Metabolism*. 2002;3(6):647-57.
560. Garberg P, Ball M, Borg N, Cecchelli R, Fenart L, Hurst R, et al. In vitro models for the blood-brain barrier. *Toxicology in vitro*. 2005;19(3):299-334.
561. Lohmann C, Huwel S, Galla HJ. Predicting blood-brain barrier permeability of drugs: Evaluation of different in vitro assays. *Journal of Drug Targeting*. 2002;10(4):263-76.

562. Collins JM, Dedrick RL. DISTRIBUTED MODEL FOR DRUG DELIVERY TO CSF AND BRAIN-TISSUE. *American Journal of Physiology*. 1983;245(3):R303-R10.
563. deLange ECM, Danhof M, deBoer AG, Breimer DD. Methodological considerations of intracerebral microdialysis in pharmacokinetic studies on drug transport across the blood-brain barrier. *Brain Research Reviews*. 1997;25(1):27-49.
564. Smith QR. A review of blood-brain barrier transport techniques. *Methods in molecular medicine*. 2003;89:193-208.
565. Ohno K, Pettigrew KD, Rapoport SI. LOWER LIMITS OF CEREBROVASCULAR PERMEABILITY TO NON-ELECTROLYTES IN CONSCIOUS RAT. *American Journal of Physiology*. 1978;235(3):H299-H307.
566. Lockwood AH. FUNCTIONAL-EVALUATION OF THE BLOOD-BRAIN-BARRIER USING POSITRON EMISSION TOMOGRAPHY. *Annals of Neurology*. 1984;15:S103-S6.
567. Tofts PS, Kermode AG. MEASUREMENT OF THE BLOOD-BRAIN-BARRIER PERMEABILITY AND LEAKAGE SPACE USING DYNAMIC MR IMAGING .1. FUNDAMENTAL-CONCEPTS. *Magnetic Resonance in Medicine*. 1991;17(2):357-67.
568. Li H, Yap CW, Ung CY, Xue Y, Cao ZW, Chen YZ. Effect of selection of molecular descriptors on the prediction of blood-brain barrier penetrating and nonpenetrating agents by statistical learning methods. *Journal of Chemical Information and Modeling*. 2005;45(5):1376-84.
569. Engkist O, Wrede P, Rester U. Prediction of CNS activity of compound libraries using substructure analysis. *Journal of Chemical Information and Computer Sciences*. 2003;43(1):155-60.
570. Chen Y, Zhu Q-J, Pan J, Yang Y, Wu X-P. A prediction model for blood-brain barrier permeation and analysis on its parameter biologically. *Computer Methods and Programs in Biomedicine*. 2009;95(3):280-7.
571. Obrezanova O, Csanyi G, Gola JMR, Segall MD. Gaussian processes: A method for automatic QSAR Modeling of ADME properties. *Journal of Chemical Information and Modeling*. 2007;47(5):1847-57.
572. Kortagere S, Chekmarev D, Welsh WJ, Ekins S. New predictive models for blood-brain barrier permeability of drug-like molecules. *Pharmaceutical research*. 2008;25(8):1836-45.
573. Konovalov DA, Coomans D, Deconinck E, Vander Heyden Y. Benchmarking of QSAR models for blood-brain barrier permeation. *Journal of Chemical Information and Modeling*. 2007;47(4):1648-56.
574. Katritzky AR, Kuanar M, Slavov S, Dobchev DA, Fara DC, Karelson M, et al. Correlation of blood-brain penetration using structural descriptors. *Bioorganic & Medicinal Chemistry*. 2006;14(14):4888-917.
575. Bendels S, Kansy M, Wagner B, Huwyler J. In silico prediction of brain and CSF permeation of small molecules using PLS regression models. *European Journal of Medicinal Chemistry*. 2008;43(8):1581-92.
576. Adenot M, Lahana R. Blood-brain barrier permeation models: Discriminating between potential CNS and non-CNS drugs including P-glycoprotein substrates. *Journal of Chemical Information and Computer Sciences*. 2004;44(1):239-48.
577. Levin VA. RELATIONSHIP OF OCTANOL-WATER PARTITION-COEFFICIENT AND MOLECULAR-WEIGHT TO RAT-BRAIN CAPILLARY-PERMEABILITY. *Journal of Medicinal Chemistry*. 1980;23(6):682-4.

578. Pajouhesh H, Lenz GR. Medicinal chemical properties of successful central nervous system drugs. *NeuroRx : the journal of the American Society for Experimental NeuroTherapeutics*. 2005;2(4):541-53.
579. Glave WR, Hansch C. RELATIONSHIP BETWEEN LIPOPHILIC CHARACTER AND ANESTHETIC ACTIVITY. *Journal of Pharmaceutical Sciences*. 1972;61(4):589-&.
580. Young RC, Mitchell RC, Brown TH, Ganellin CR, Griffiths R, Jones M, et al. DEVELOPMENT OF A NEW PHYSICOCHEMICAL MODEL FOR BRAIN PENETRATION AND ITS APPLICATION TO THE DESIGN OF CENTRALLY ACTING H-2-RECEPTOR HISTAMINE-ANTAGONISTS. *Journal of Medicinal Chemistry*. 1988;31(3):656-71.
581. Van Damme S, Langenaeker W, Bultinck P. Prediction of blood-brain partitioning: A model based on ab initio calculated quantum chemical descriptors. *Journal of Molecular Graphics & Modelling*. 2008;26(8):1223-36.
582. Liu XR, Tu MH, Kelly RS, Chen CP, Smith BJ. Development of a computational approach to predict blood-brain barrier permeability. *Drug Metabolism and Disposition*. 2004;32(1):132-9.
583. Hitchcock SA, Pennington LD. Structure-brain exposure relationships. *Journal of Medicinal Chemistry*. 2006;49(26):7559-83.
584. Ono A, Tomono T, Ogihara T, Terada K, Sugano K. Investigation of biopharmaceutical and physicochemical drug properties suitable for orally disintegrating tablets. *ADMET and DMPK*. 2016;4(4):335-60.

## APPENDIX A

### Calculating tissue partition coefficients

#### Mechanistic tissue partition equations

$$\text{One basic pKa} \quad K_{pu} = \left[ \left( \frac{1+X \cdot fw}{1+Y} \right) + f_{EW} + \left( \frac{K_{a,AP} \cdot [AP]_t \cdot X}{1+Y} \right) + \frac{P \cdot fnl + (0.3P + 0.7) \cdot fnp}{1+Y} \right]$$

$$\text{Other types} \quad K_{pu} = \left[ \left( \frac{1+X \cdot fw}{1+Y} \right) + f_{EW} + (K_{a,PR} \cdot [PR]_t) + \frac{P \cdot fnl + (0.3P + 0.7) \cdot fnp}{1+Y} \right]$$

#### Affinity constants

$$\text{Acidic phospholipids Extracellular albumin} \quad K_{a,AP} = \left[ K_{puBC} - \left( \frac{1+Z}{1+Y} \cdot fw_{BC} \right) - \left( \frac{P \cdot fnl_{BC} + (0.3P + 0.7) \cdot fnp_{BC}}{1+Y} \right) \right] \cdot \left( \frac{1+Y}{[AP]_{BC} \cdot Z} \right)$$

$$\text{Lipoproteins} \quad K_{a,PR} = \left[ \frac{1}{fu} - 1 - \left( \frac{P \cdot fnl_p + (0.3P + 0.7) \cdot fnp_p}{1+Y} \right) \right] \cdot \left( \frac{1}{[PR]_p} \right)$$

#### Drug ionisation

	X	Y	Z
Monoprotic base	$10^{pKa-pH_w}$	$10^{pKa-pH_p}$	$10^{pKa-pH_{BC}}$
Diprotic base	$10^{pKa2-pH_w} + 10^{pKa1+pKa2-2pH_w}$	$10^{pKa2-pH_p} + 10^{pKa1+pKa2-2pH_p}$	$10^{pKa2-pH_{BC}} + 10^{pKa1+pKa2-2pH_{BC}}$
Monoprotic acid	$10^{pH_w-pKa}$	$10^{pH_p-pKa}$	NA
Diprotic acid	$10^{pH_w-pKa1} + 10^{2pH_w-pKa1-pKa2}$	$10^{pH_p-pKa1} + 10^{2pH_p-pKa1-pKa2}$	NA
Zwitterion	$10^{pKa_{BASE}-pH_w} + 10^{pH_w-pKa_{ACID}}$	$10^{pKa_{BASE}-pH_p} + 10^{pH_p-pKa_{ACID}}$	$10^{pKa_{BASE}-pH_{BC}} + 10^{pH_{BC}-pKa_{ACID}}$
Neutral	0	0	NA

**P** is the n-octanol:water partition coefficient for unionised compound for all tissues except adipose (vegetable oil:water)

**f** is the fractional tissue volume

**IW** and **EW** refer to intra- and extra-cellular tissue water

**NL** and **NP** refer to tissue neutral lipids and neutral phospholipids

**AP<sub>t</sub>** and **PR<sub>t</sub>** refer to the tissue concentrations of acidic phospholipids and extra-cellular albumin (for acids and weak bases) or lipoprotein (for neutrals), respectively

**K<sub>a,AP</sub>** and **K<sub>a,PR</sub>** are affinity constants of the drug for acidic phospholipids and either extra-cellular albumin or lipoprotein, respectively;

**X**, **Y** and **Z** account for drug ionisation

Subscripts **BC** and **P** refer to red blood cells and plasma

**pH<sub>BC</sub>** is the intracellular pH of blood cells

**fu** is fraction unbound in plasma

**K<sub>puBC</sub>** can be calculated from the fu and blood-to-plasma ratio

## APPENDIX B

### *Advantages and disadvantages of in vitro models available for BBB permeability.*

MODEL	DESCRIPTION	ADVANTAGE/ DISADVANTAGE	REFERENCE
<b>NON CELL-BASED</b>			
Immobilized Artificial Membrane Chromatography (IAM)	<ul style="list-style-type: none"> <li>• Monolayer phosphatidylcholine that is bound covalently to inert silica support.</li> <li>• Simulates lipid phase of cell membrane.</li> </ul>	<ul style="list-style-type: none"> <li>• Ability to predict drug permeability across intestinal tissue, human skin, caco-2 cells, and BBB.</li> <li>• Poor predictive power whenever there is another factor affecting brain uptake occurs such as metabolism, active transport or protein binding.</li> <li>• Does not represent diffusion across membrane bilayer.</li> <li>• Does not represent fluid membranes dynamics, i.e., lateral diffusion.</li> </ul>	Stein (551), Ong, Liu (552), Reichel and Begley (553)
Parallel Artificial Permeability Assay (PAMPA)	<ul style="list-style-type: none"> <li>• Artificial membrane barrier derived from porcine brain lipid extract dissolved in 2% w/v n-dodecane.</li> </ul>	<ul style="list-style-type: none"> <li>• Good representation of passively permeating compounds.</li> <li>• Only useful for representation of BBB penetration without active transport.</li> </ul>	Di, Kerns (554), Carrara, Reali (555)
<b>CELL-BASED (CEREBRAL ORIGIN)</b>			
Isolated Brain Capillaries	<ul style="list-style-type: none"> <li>• Derived from animal and human sources using mechanical and/or enzymatic isolation procedures.</li> </ul>	<ul style="list-style-type: none"> <li>• Good representation of <i>in vivo</i> situation.</li> <li>• Not suitable for BBB permeability screening since it has limited accessibility at the luminal surface of microvessels.</li> </ul>	Pardridge (556), Joo (557)
Primary or Low Passage Brain Capillary Endothelial Cells (BCECs)	<ul style="list-style-type: none"> <li>• Isolated brain capillaries from human and animal brains.</li> <li>• Brain capillaries are then cultured and plated. The BCECs, which grows from the capillaries, are then isolated and cultured with or without</li> </ul>	<ul style="list-style-type: none"> <li>• Closest representation of <i>in vivo</i> situation.</li> <li>• Ethical constraints when using human BCECs.</li> <li>• Time and resource consuming to incubate, seed and isolate the cells.</li> </ul>	Reichel, Begley (208)

Immortalized Brain Endothelial Cells	<ul style="list-style-type: none"> <li>• Cell lines that form monolayers, resembling tight junctions.</li> <li>• Most frequently used are the immortalized rat brain endothelial cell line (RBE4).</li> </ul>	<ul style="list-style-type: none"> <li>• an astrocytes-cultured medium.</li> <li>• Difficult to standardize due to inter- and intra-batch reproducibility.</li> <li>• Useful for biochemical and mechanistic research.</li> <li>• Limited use in BBB transport studies due to the leakiness of the paracellular membranes.</li> </ul>	de Boer and Gaillard (558), Gumbleton and Audus (207)
--------------------------------------	---	---	---

---

**CELL-BASED (NON-CEREBRAL ORIGIN)**

---

Madin-Darby Canine Kidney (MDCK)	<ul style="list-style-type: none"> <li>• Commonly used cell line.</li> <li>• Low permeability to sucrose and relatively high TEER reproducibility with more than 2000 <math>\Omega\text{cm}^2</math>.</li> </ul>	<ul style="list-style-type: none"> <li>• High TEER reproducibility.</li> <li>• Easy to grow.</li> <li>• Better representation of P-gp transporter due to the ability of the cells transfecting with multidrug resistance gene (MDR1).</li> <li>• Best representation of BBB permeability compared to other <i>in vitro</i> models.</li> <li>• Important model in facilitating drug discovery.</li> <li>• Disregards other important transporters such as BCRP and MRP.</li> </ul>	Feng (559), Garberg, Ball (560)
Caco-2 Cell Line	<ul style="list-style-type: none"> <li>• Derived from human colon adenoma.</li> </ul>	<ul style="list-style-type: none"> <li>• Not a good representation of BBB permeability due to a significant difference found when compared with brain endothelial cells cocultured with rat astrocytes.</li> </ul>	Lundquist and Renftel (209), Lohmann, Huwel (561)

---

## APPENDIX C

### *In vivo methods used to determine BBB permeability of compounds.*

METHOD	PARAMETER	DESCRIPTION	REFERENCE
<b>INVASIVE</b>			
Sampling of the CSF	CSF free drug concentration, kinetic profile	Measurement of drug concentration from CSF samples	Collins and Dedrick (562)
Intracerebral microdialysis	Brain interstitial fluid free drug concentration, kinetic profile	Measurement of drug concentration from microdialysis samples	deLange, Danhof (563)
<i>In situ</i> brain perfusion	Permeability-surface area (PS or log PS), unidirectional uptake coefficient (K <sub>in</sub> )	Drug is infused directly via carotid artery. Brain and perfusate samples are taken to represent drug concentrations.	Smith (564)
Bolus injection	Brain/Plasma concentration ratio (K <sub>p</sub> or log BB)	Measurement of drug concentration from brain samples and plasma at single or multiple time points.	Ohno, Pettigrew (565)
<b>NON-INVASIVE</b>			
Positron emission tomography (PET)	Permeability-surface area (PS or log PS), uptake kinetics profile.	Drug labelled with positron emitting radiotracer is injected systemically and quantified by dynamic scanning at the brain.	Lockwood (566)
Magnetic resonance imaging (MRI)	Permeability-surface area (PS or log PS), uptake kinetics profile.	Drug labelled with paramagnetic spin or contrast media is injected systemically and quantified by dynamic MRI in the brain.	Tofts and Kermode (567)

## APPENDIX D

### *Molecular Approaches and Parameters involved in BBB Drug Penetrability in silico Models and Eligibility of Drugs Candidate.*

MODEL	DESCRIPTION	PARAMETER	REFERENCE
<b>QUANTITATIVE STRUCTURE-ACTIVITY RELATIONSHIP (QSAR)</b>			
Non-Linear	Predictive-based molecular descriptor	Bayesian Modelling Substructure Analysis Neural Networks Recursive Partitioning Gaussian Processes Support Vector Machine <i>k</i> Nearest Neighbour Method	Li, Yap (568), Engkist, Wrede (569), Chen, Zhu (570), Li, Yap (568), Obrezanova, Csanyi (571), Kortagere, Chekmarev (572), Konovalov, Coomans (573)
Linear	Predictive-based molecular descriptor	Linear Discriminant Analysis Multiple Linear Regression Comprehensive Descriptors for Structural and Statistical Analysis Partial Least-Squares Variable Selection and Modelling Method based on Prediction	Katritzky, Kuanar (574), Konovalov, Coomans (573), Bendels, Kansy (575), Li, Yap (568)
<b>MOLECULAR DESCRIPTORS</b>			
	P-glycoprotein substrate	Efflux transport through the BBB	Adenot and Lahana (576)
	Classic descriptors	Molecular weight Polar surface area Molecular size, shape, and flexibility Charge	Levin (577)
	logD	Lipophilicity ( $0 < \log D < 3$ )	Pajouhesh and Lenz (578)
	logP <sub>oct</sub>	H-bond donor potential, hydrophobicity	Glave and Hansch (579)
	$\Delta \log P$	Low overall H-bonding ability	Young, Mitchell (580)

	partition coefficients (LogP <sub>OCT</sub> -logP <sub>CYC</sub> )		
Quantum chemical descriptors	Calculations explaining geometric and electronic properties of compounds/molecules and its interactions	Molecular electronegativity, electrophilicity, molecular hardness/softness  Polarizability, dipole moment  Covalent H-bond acidity and basicity  Dipole moment, polarizability  Molecular electrostatic potential derived properties	Van Damme, Langenaeker (581)
<b>BRAIN PENETRABILITY PARAMETERS</b>			
logPS	BBB permeability surface area	Interrelated with QSAR data	Liu, Tu (582)
logBB	Brain to plasma ratio (logC <sub>brain</sub> /logC <sub>blood</sub> )	Interrelated with QSAR data	Konovalov, Coomans (573)
logCSF	Cerebrospinal fluid to plasma ratio (logC <sub>CSF</sub> /logC <sub>blood</sub> )	Interrelated with QSAR data	Bendels, Kansy (575)
<b>RULE-BASED MODELS</b>			
CNS active drugs	Predictive-based molecular descriptor	Molecular weight < 450 Da  H-bond donors < 3  Polar surface area < 90 Å <sup>2</sup>  2.0 < logP <sub>OCT</sub> < 5.0	Hitchcock and Pennington (583)
Hansch's rule of 2	Predictive-based octanol/water partition coefficient	Optimum brain penetration for molecules that have logP <sub>OCT</sub> ~ 2.0	Glave and Hansch (579)
Modified Lipinski's rules for CNS penetration	Predictive-based molecular descriptor	Molecular weight ≤ 400 Da  7.5 < pKa < 10.5  H-bond acceptors ≤ 7  H-bond donors ≤ 3  LogP <sub>OCT</sub> ≤ 5.0	Pajouhesh and Lenz (578)

## APPENDIX E

*Physicochemical and pharmacokinetic parameters used in Simcyp for repaglinide, tramadol, clopidogrel, 2-oxo-clopidogrel and clopi-H4 (active metabolite).*

	Parameters	Value	
<b>Repaglinide</b>			
<b>Physicochemical</b>	MW (g/mol)	452.6	
	Log P <sub>o:w</sub>	3.98	
	Compound type	Ampholyte	
<b>Absorption</b>	Pka	4.16; 6.01	
	Absorption model	ADAM	
	<i>fa</i> ; <i>Ka</i> (h <sup>-1</sup> )	0.984; 1.696	
	P <sub>eff, man</sub> (10 <sup>-4</sup> cm/s)	3.886	
	<i>fu</i> <sub>Gut</sub>	0.4	
<b>Distribution</b>	Distribution model	Full PBPK model	
	V <sub>ss</sub> (l/kg)	0.238	
	B/P ratio	0.62	
	<i>fu</i> <sub>p</sub>	0.023	
<b>Metabolism</b>	Clearance type	Enzyme kinetics	
	<i>In vitro</i> metabolic system	Human recombinant P450 isoforms	
	rhCYP3A4	V <sub>max</sub> (pmol/min per mol)	958.2
		K <sub>M</sub> (μM)	13.2
		<i>fu</i> <sub>mic</sub>	1
		CL <sub>int</sub>	137 <sup>a</sup>
	rhCYP2C8	V <sub>max</sub> (pmol/min per mol)	300.8
		K <sub>M</sub> (μM)	2.3
		<i>fu</i> <sub>mic</sub>	1
	<b>Tramadol</b>		
<b>Physicochemical</b>	MW (g/mol)	263.38	
	Log P <sub>o:w</sub>	1.35	
	Compound type	Monoprotic base	
<b>Absorption</b>	Pka	9.6	
	Absorption model	ADAM (oral); First order (IV)	
	<i>fa</i> ; <i>Ka</i> (h <sup>-1</sup> )	0.813; 0.568	
	P <sub>eff, man</sub> (10 <sup>-4</sup> cm/s)	1.3 <sup>a</sup>	
	<i>fu</i> <sub>Gut</sub>	1	
	PSA	33 <sup>b</sup>	
	HBD	1 <sup>b</sup>	
<b>Distribution</b>	Distribution model	Full PBPK model	
	V <sub>ss</sub> (l/kg)	2.842	
	B/P ratio	1.09	
	<i>fu</i> <sub>p</sub>	0.8	
<b>Metabolism</b>	Clearance type	Enzyme kinetics	
	<i>In vitro</i> metabolic system	Human recombinant P450 isoforms	
	rhCYP3A4	0.01538	

	rhCYP2B6	CL <sub>int</sub> (μl/min	0.02949	
	rhCYP2D6	per mg)	0.30114	
<b><i>Clopidogrel</i></b>				
<b>Physicochemical</b>	MW (g/mol)		321.8	
	Log P <sub>o:w</sub>		3.89	
	Compound type		Monoprotic acid	
<b>Absorption</b>	Pka		4.55	
	Absorption model		First order	
	<i>fa</i> ; <i>Ka</i> (h <sup>-1</sup> )		0.5; 0.5	
	P <sub>eff, man</sub> (10 <sup>-4</sup> cm/s)		0.466	
<b>Distribution</b>	<i>fu</i> <sub>Gut</sub>		0.02	
	Distribution model		Full PBPK model	
	<i>V<sub>ss</sub></i> (l/kg)		0.217	
	B/P ratio		0.72	
	<i>fu<sub>p</sub></i>		0.02	
<b>Metabolism</b>	K <sub>p</sub> scalar		2.67 <sup>a</sup>	
	Clearance type		Enzyme kinetics	
	<i>In vitro</i> metabolic system		Human recombinant P450 isoforms	
	rhCYP1A2	V <sub>max</sub> (pmol/min per mol)		2.27
		K <sub>M</sub> (μM)		1.58
		<i>fu<sub>mic</sub></i>		0.015
	rhCYP2B6	V <sub>max</sub> (pmol/min per mol)		7.66
		K <sub>M</sub> (μM)		2.08
		<i>fu<sub>mic</sub></i>		0.015
	rhCYP2C19	V <sub>max</sub> (pmol/min per mol)		7.52
		K <sub>M</sub> (μM)		1.12
<i>fu<sub>mic</sub></i>		0.015		
Additional systemic clearance (l/h)		600		
<b><i>2-Oxo-clopidogrel (primary metabolite)</i></b>				
<b>Physicochemical</b>	MW (g/mol)		337.8	
	Log P <sub>o:w</sub>		2.96	
	Compound type		Monoprotic acid	
<b>Distribution</b>	Pka		3.41	
	Distribution model		Minimal PBPK model	
	<i>V<sub>ss</sub></i> (l/kg)		0.10	
	B/P ratio		1	
<b>Metabolism</b>	<i>fu<sub>p</sub></i>		0.03	
	Clearance type		Enzyme kinetics	
	<i>In vitro</i> metabolic system		Human recombinant P450 isoforms	
	rhCYP2B6	V <sub>max</sub> (pmol/min per mol)		2.48
		K <sub>M</sub> (μM)		1.62
		<i>fu<sub>mic</sub></i>		0.18
rhCYP2C9	V <sub>max</sub> (pmol/min per mol)		0.855	

	$K_M$ ( $\mu\text{M}$ )	18.1
	$f u_{mic}$	0.18
rhCYP2C19	$V_{max}$ (pmol/min per mol)	9.06
	$K_M$ ( $\mu\text{M}$ )	12.1
	$f u_{mic}$	0.18
rhCYP3A4	$V_{max}$ (pmol/min per mol)	3.63
	$K_M$ ( $\mu\text{M}$ )	27.8
	$f u_{mic}$	0.18
	Additional clearance HLM $CL_{int}$ ( $\mu\text{l}/\text{min}$ per mg)	50
	$f u_{mic}$	0.18
	Active uptake into hepatocyte	2
<b><i>Clopi-H4 (secondary metabolite/active metabolite)</i></b>		
<b>Physicochemical</b>	MW (g/mol)	355.8
	Log $P_{o:w}$	3.60
	Compound type	Diprotic acid
	Pka 1; Pka 2	3.20; 5.10
<b>Distribution</b>	Distribution model	Minimal PBPK model
	$V_{ss}$ (l/kg)	0.23
	B/P ratio	0.82
	$f u_p$	0.018
<b>Metabolism</b>	Clearance type	<i>In vivo</i> clearance
	$CL_{po}$ (l/h)	500

<sup>a</sup>. Sensitivity analysis and parameter estimation

<sup>b</sup>. Ono *et al.* (2016) (584)

All values were from Simcyp (503) (repaglinide), T'jollyn *et al.* (504) (tramadol) and Djebli *et al.* (477) (clopidogrel and its metabolites) unless otherwise specified.